UNIVERSIDAD DE LAS PALMAS DE GRAN CANARIA
Facultad de Ciencias del Mar

UNDERSTANDING THE ZOOPLANKTON AMMONIUM EXCRETION: FROM BIOGEOCHEMICAL IMPLICATIONS TO INTRACELLULAR REGULATORY MECHANISMS

COMPRENDIENDO LA EXCRECIÓN DE AMONIO EN EL ZOOPLANCTON: DESDE SUS IMPLICACIONES BIOGEOQUÍMICAS A LOS MECANISMOS DE REGULACIÓN INTRACELULAR

Tesis doctoral presentada por Igor Fernández Urruzola
dentro del Programa de Doctorado en Oceanografía

Dirigida por Dr. Theodore T. Packard
y Dra. María M. Gómez Cabrera

UNIVERSIDAD DE LAS PALMAS DE GRAN CANARIA
Facultad de Ciencias del Mar

UNDERSTANDING THE ZOOPLANKTON AMMONIUM EXCRETION: FROM BIOGEOCHEMICAL IMPLICATIONS TO INTRACELLULAR REGULATORY MECHANISMS

COMPRENDIENDO LA EXCRECIÓN DE AMONIO EN EL ZOOPLANCTON: DESDE SUS IMPLICACIONES BIOGEOQUÍMICAS A LOS MECANISMOS DE REGULACIÓN INTRACELULAR

Tesis doctoral presentada por Igor Fernández Urruzola
dentro del Programa de Doctorado en Oceanografía

Dirigida por Dr. Theodore T. Packard
y Dra. María M. Gómez Cabrera

El doctorando | El/La director/a | El/La director/a

Las Palmas de Gran Canaria, noviembre de 2015

Understanding the zooplankton ammonium excretion: From biogeochemical implications to intracellular regulatory mechanisms

Author: Igor Fernández Urruzola

Advisor: Theodore T. Packard

Advisor: María M. Gómez Cabrera

Marine Ecophysiology Group (EOMAR),
Institute of Sustainable Aquaculture and Aquatic Ecosystems (ECOAQUA),
Marine Sciences Faculty, University of Las Palmas de Gran Canaria (ULPGC),
35017, Las Palmas, Spain.

This work is licensed under the Creative Commons Attribution-NonCommercial-NoDerivatives 4.0 International license.

The following web-page address contains up to date information about this dissertation and related topics:
http://hdl.handle.net/10553/14614
Text printed in Las Palmas de Gran Canaria
First edition, November 2015

A mis padres, por enseñarme que lo esencial
es invisible a los ojos.

Acknowledgements / Agradecimientos

Y por fin ha llegado el momento que todo doctorando ansía desde el instante en que comienza la tediosa travesía de su tesis doctoral: escribir los agradecimientos. Un efímero apartado en el que, excepcionalmente, el autor puede ser fiel a sí mismo, ajeno al incesante juicio del método científico. Un apartado no menos importante, que obliga a quien lo escribe a realizar un profundo ejercicio de reflexión para evitar la injusticia del olvido. Pido disculpas de antemano si mi frágil memoria comete tal error.

Quisiera comenzar agradeciendo a mis directores: Ted y May. Porque, sin vosotros, nada de esto hubiera sido posible. No solo habéis sido mis mentores en el campo de la investigación, sino que me habéis ofrecido todo a nivel personal. Y eso, cuando uno está lejos de su hogar, tiene especial relevancia. Ted, tú me has planteado un dilema que soy incapaz de resolver: no sé si te admiro como la gran persona que eres, o como el brillante investigador que todos conocen. Me siento privilegiado por haber compartido contigo todos estos años, en los que has fomentado mi curiosidad científica. Tu sana pasión por el conocimiento es, sin duda, el mejor ejemplo para alguien que se inicia en la investigación. Gracias también a ti, May. Porque siempre has peleado por ofrecerme las mejores oportunidades para progresar en mis investigaciones. Gracias por confiar en mi, por tener en cuenta mis opiniones, y por la paciencia que has tenido conmigo durante todo este tiempo. Gracias por darme la libertad de tomar mis propias decisiones, y por tu predisposición a ayudarme siempre que lo he necesitado, dentro y fuera del entorno académico. Contigo he aprendido lo importante que es formar parte de un grupo unido.

Gracias a mis compañeros de máster: JuanMa, Almu, Laia, Sabri y Mireya. Con vosotros comenzó todo, y esta tesis, en cierto modo, cierra una bonita etapa. Fuisteis un gran apoyo fuera del laboratorio y, aunque el tiempo nos haya guiado por caminos distintos, estoy seguro que, de alguna forma, volverán a unirse en el futuro.

Fede, contigo también compartí parte del máster, pero eso no tiene ningún mérito, pues varias generaciones lo hicieron. Así que te escribiré

como el gran amigo y compañero en el que te has convertido a lo largo de todos estos años. Polos opuestos en lo superficial, pero muy parecidos en lo importante. Por eso encajamos tan bien. Gracias por tu eterna generosidad y, sobre todo, gracias por sacarnos a todos una sonrisa incluso cuando no te apetecía hacerlo. Tu amistad es, sin duda, una de las cosas más valiosas que me llevo de este doctorado. Y esto lo hago también extensivo a ti, Yera. Juntos hemos vivido experiencias irrepetibles, pero lo que realmente importa es tener la certeza de que siempre podré contar contigo. En aquel camarote encontré un amigo para toda la vida.

Al resto de *Majalulos* y asociados: Ale, JuanCar, Iván, Nau y el fichaje estrella, Jose. Me resulta difícil escribiros, porque nada de lo que os diría debe incluirse en una tesis doctoral. Así que resumiré diciendo que con vosotros pasé los momentos más surrealistas y divertidos de todos estos años. No me cabe duda que se repetirán en el futuro.

A todos los compañeros con los que compartí momentos inolvidables en las campañas MALASPINA y SUCCESSION, en especial, a Ali y Gara. Descubriros en mitad del océano, aunque ya nos conociéramos, fue una grata sorpresa.

Gracias al resto de compañeros del laboratorio B-201. Especialmente, a las chicas EOMAR, Ico, Mayte y Vanesa, por ofrecerme vuestra ayuda siempre que la he necesitado. A Mine, Lidia, Isa y Cory, por tantos buenos momentos dentro y, sobre todo, fuera de la facultad. Y, por supuesto, a ese gran tándem de Paleontología-Teledetección-Vertebrados formado por los inigualables Tachi, Alex, Oscar y Raül. Fuisteis un soplo de aire fresco en el momento que más lo necesitaba.

Gracias también a todos aquellos que nos mostrasteis el camino a los que veníamos detrás, dejando vuestra impronta en el laboratorio: Fede, Marta, Claire, Valeria, Mar e Inma, entre otros.

I will switch briefly to English to thank Dr. Lutz Postel for inviting me to the SUCCESSION cruise and later, hosting me in your lab at IOW. I will always appreciate the relationship we developed during those productive months, as well as all the great moments we enjoyed together with Anneli out of the institute. I would also like to thank you, Benni, for the good time we shared together in Namibia, Warnemünde, and Las Palmas. You and Clau made my stay abroad much more enjoyable.

En el terreno institucional, creo justo recordar a todos los organismos que me brindaron el apoyo económico necesario para la realización de este trabajo. Principalmente, al Programa de Formación y Perfeccionamiento del Personal Investigador del Gobierno Vasco, que me dió la

oportunidad de disfrutar de una beca predoctoral, y me facilitó la movilidad a otros centros internacionales de investigación. Al Programa Innova Canarias 2020 de la Fundación Universitaria de Las Palmas, y por extensión, a la Obra Social "la Caixa", por patrocinar una parte del estudio. Finalmente, mencionar al Programa de Formación del Personal Investigador de la Universidad de Las Palmas de Gran Canaria, que financió mi asistencia a congresos científicos y mi participación en campañas oceanográficas.

Por último, quiero agradecer de una manera muy especial,

A mis padres, Charo e Iñaki, por haberme ofrecido todo lo necesario para llegar hasta aquí, por cuidarme desde la distancia y por echarme de menos cuando no estoy. Vuestro apoyo, en todos los sentidos, ha sido imprescindible para que esta tesis sea una realidad.

A mis hermanos, Gorka y Ghis, Nahi, y sobrinos, Samia y Adam, porque esta tesis me ha robado un tiempo precioso que debí haber compartido con todos vosotros. Algún día entenderéis por qué, igual que el Olentzero, el *tio Tato* solo volvía a casa por Navidad.

A mi segunda familia: Modes, LuisMi, Luis, Leyre, Ekaitz y Susana. Por vuestro cariño y constante preocupación porque todo saliera bien. Habéis hecho siempre que me sienta un hijo y un hermano más.

A mis amigos, los de toda la vida, los que nunca fallan. Porque con vosotros es como si no pasara el tiempo. Gracias por aguantar estoicamente el tipo en esas conversaciones en las que os explicaba los entresijos de mis investigaciones y que, a menudo, el erudito atajaba con un acertado: "En definitiva, lo que mean los bichos". Sois geniales.

Y sobre todo, a ti, Nat. Porque este logro también te pertenece, como pareja, amiga y compañera. Tus consejos, tu dedicación y tu cariño han hecho de esta tesis lo que hoy es. Gracias por haber estado a mi lado, incondicionalmente, en los buenos y en los malos momentos. Por compartir mis preocupaciones, y anteponerlas a las tuyas propias. Y gracias, principalmente, por hacer que mire el futuro con tanta ilusión.

Todos vosotros, consciente o inconscientemente, habéis sido una parte fundamental de esta tesis doctoral.

Eskerrik asko,

Igor.

Noviembre, 2015

Abstract

Zooplankton play a key role in marine ecosystems and their biogeochemical cycles. They exert control over the primary productivity through the consumption of organic matter and, at the same time, the release of nutrients that sustains the phytoplankton growth. This thesis focuses on the NH_4^+ excretion processes related to these heterotrophic organisms that support, at a global scale, about the 80 % of the phytoplankton requirements. However, there is no clear constant pattern in the zooplankton contribution to the NH_4^+ regeneration throughout the different pelagic ecosystems, so continuous monitoring of this metabolic process is essential at wide temporal and spatial scales.

In its more oceanographic facet, this study elucidates the role of the mesozooplankton community in the consumption and regeneration of the primary productivity in the northern Benguela upwelling ecosystem. Despite the complex interplay between mesoscale structures that caused short-term changes in the mesozooplankton community, the impact of their metabolism on the primary producers was always limited ($\sim$ 5 - 10 %). Furthermore, the vertical nitrogen flux was calculated in two stations from the transition zone by adjusting a mathematical function to the NH_4^+ excretion rates ($R_{NH_4^+}$) that were measured in the water column. The nitrogen fluxes calculated through modeling were compared to those measured with sediment traps. Estimates from both methodologies were close to each other when big phytoplanktonic cells such as diatoms dominated in a high-productivity scenario. In the less productive conditions, the small flagellates and coccolitophores took importance, and the differences between the fluxes calculated by the two techniques became larger. The model was also used to determine the capacity of the ecosystem to retain its nutrients, as well as to calculate the active flux driven by the vertical migrators. These organisms constituted an important component of the biological pump, as they actively transported, below 150 m, about the 5 % of what was produced.

At the physiological level, this work examines the relationship between the NH_4^+ excretion and its associated biochemistry. The enzyme glutamate dehydrogenase (GDH) is primarily responsible of the

NH_4^+ synthesis in the zooplankton, so it has been routinely used in oceanography as an index of the NH_4^+ released by these heterotrophic organisms. Using data analyzed from several oceanographic cruises and data from the literature, it was demonstrated that the GDH/$R_{NH_4^+}$ ratio cannot be explained through a single universal equation. Among the most important biological factors that explain such variability in that relationship were the taxonomic composition of the sample, the allometric behaviour of both rates with biomass and the changes in the trophic conditions. The latter two factors were studied in greater detail within a cohort of the marine mysid *Leptomysis lingvura*. Assuming the substrate availability as the critical factor in controlling the velocity of NH_4^+ production, a bisubstrate kinetic model was developed to predict the actual $R_{NH_4^+}$ in two species of marine zooplankton. This model based in the Michaelis-Menten equations as the best explanation for $R_{NH_4^+}$ time-courses during starvation, was better at predicting $R_{NH_4^+}$ than a model based on a constant GDH/$R_{NH_4^+}$ and the potential NH_4^+ excretion. Overall, this research provides knowledge about the control that the zooplankton exert over the primary productivity in the northern Benguela ecosystem, proposes a novel approach to calculate nitrogen fluxes from zooplankton $R_{NH_4^+}$, and introduces new insights into the study of the NH_4^+ excretion from enzymatic measurements.

Resumen

El zooplancton desempeña un papel fundamental en los ecosistemas marinos y en los ciclos biogeoquímicos. Ejerce un control sobre la productividad primaria mediante el consumo de materia orgánica y, al mismo tiempo, libera nutrientes que sustentan el crecimiento del fitoplancton. Esta tesis se centra en los procesos de excreción de NH_4^+ ligados a estos organismos heterótrofos y que, a escala global, proveen alrededor del 80 % de los requerimientos fitoplanctónicos. No existe, sin embargo, un patrón que determine la contribución del zooplancton a la regeneración de NH_4^+ en los distintos ecosistemas pelágicos, de manera que es imprescindible la continua monitorización de este proceso metabólico a escalas temporales y espaciales amplias.

En su faceta más oceanográfica, este estudio dilucida el rol que juega la comunidad de mesozooplancton en el consumo y la regeneración de la producción primaria en el sistema del afloramiento de Benguela. La complejidad mesoescalar del ecosistema provocó cambios drásticos a corto plazo en la estructura de la comunidad mesozooplanctónica, si bien el impacto de su metabolismo sobre los productores primarios fue siempre limitado (~ 5 - 10 %). Además, se ajustó un modelo matemático a las tasas de excreción de NH_4^+ ($R_{NH_4^+}$) encontradas en la columna de agua con el fin de determinar el flujo vertical de nitrógeno en dos estaciones localizadas en la zona de transición del afloramiento. Los flujos estimados se compararon con los medidos mediante trampas de sedimento. Ambas metodologías arrojaron resultados similares en un escenario de alta productividad, dominado por células fitoplanctónicas de gran tamaño tales como las diatomeas. En condiciones menos productivas, donde adquirieron mayor importancia los pequeños flagelados y los cocolitofóridos, las discrepancias entre los flujos calculados mediante las distintas técnicas se hicieron más evidentes. El modelo propuesto se utilizó adicionalmente para inferir la capacidad del ecosistema para retener nutrientes, así como para calcular el flujo activo debido a los migradores verticales. Estos organismos constituyeron un importante componente de la bomba biológica al transportar activamente, por debajo de 150 m, alrededor del 5 % de la producción primaria.

Desde un punto de vista fisiológico, este trabajo examina la relación que existe entre la excreción de NH_4^+ y el proceso bioquímico asociado. La enzima glutamato deshidrogenasa (GDH) es la mayor responsable de la síntesis de NH_4^+ en el zooplancton, de manera que ha sido frecuentemente utilizada en la oceanografía como un índice del NH_4^+ que es liberado por estos organismos heterótrofos. A partir de datos analizados en diversas campañas oceanográficas y una recopilación de valores publicados en la literatura, se demostró que la relación GDH/$R_{NH_4^+}$ no puede explicarse a partir de una ecuación universal. Dentro de los factores biológicos más relevantes para explicar la variabilidad encontrada en dicha relación destacaron la composición taxonómica de la muestra, el comportamiento alométrico de ambas tasas con respecto a la biomasa y los cambios en las condiciones tróficas. Estas dos últimas causas de variabilidad se estudiaron más detalladamente en una cohorte del misidáceo marino *Leptomysis lingvura*. Finalmente, asumiendo la disponibilidad de los sustratos como el factor fundamental que determina la velocidad de la reacción catalizada por la enzima GDH, se aplicó un modelo cinético bisustrato basado en los principios fundamentales de Michaelis-Menten para predecir la $R_{NH_4^+}$. Este modelo fue capaz de estimar los patrones de $R_{NH_4^+}$ medidos en dos especies de zooplancton a lo largo de un periodo de inanición, de una forma más precisa que si se aplicase un valor GDH/$R_{NH_4^+}$ a las medidas enzimáticas. En general, esta tesis aporta resultados novedosos acerca del control que la comunidad de mesozooplancton ejerce sobre la productividad primaria en las aguas de Benguela, introduce nuevas herramientas con las que estudiar su contribución a los ciclos biogeoquímicos y abre nuevas perspectivas en el estudio de la excreción de NH_4^+ debida al zooplancton desde un punto de vista enzimático.

Thesis preview

This thesis, entitled *Understanding the zooplankton ammonium excretion: From biogeochemical implications to intracellular regulatory mechanisms*, was conducted under the supervision of Dr. Theodore T. Packard and Dr. María M. Gómez Cabrera, at the Department of Biology of the Universidad de Las Palmas de Gran Canaria (ULPGC), within the Doctoral Program of Oceanography with a quality mention (MCD 2005-00179). The thesis compiles five original research works, published in peer-reviewed journals or under revision, in the frame of the projects EXZOME (CTM 2008-01616/MAR), CAMVALEX (CTM 2010-09515E) and BIOMBA (CTM 2012-32729), granted to Dr. May Gómez. Furthermore, this study has benefited from the active participation in oceanographic cruises that resulted from the research projects MALASPINA-2010 (CSD 2008-00077) and SUCCESSION (MSM18/5, DFG), headed by Dr. Carlos M. Duarte and Dr. Lutz Postel, respectively, as well as from a research stay in the Leibniz Institute for Baltic Sea Research (Germany).

The thesis is organized according to the typical structure of any academic text: A general introduction provides the essential background information, and outlines the objectives and hypothesis to be examined in the study; then, the five scientific contributions validate the stated hypothesis, each following the conventional structure of the research articles; finally, the results are synthesised in a general discussion, giving rise to the main conclusions and the future lines of research. All these sections are entirely written in English to comply with the valid regulation for obtaining the Doctor Europeus Mention (BOULPGC, Art. 1, Chap. IV, November 5th, 2008), which dictates that at least the abstract and conclusions must be presented in a language other than Spanish. Likewise, it has been included a final section summarizing in Spanish the general aspects of the thesis, as required from the PhD Thesis Regulations from the Universidad de Las Palmas de Gran Canaria (BOULPGC, Art. 2, Chap. I, November 5th, 2008).

Presentación de la Tesis

Esta tesis doctoral, titulada *Comprendiendo la excreción de amonio en el zooplancton: desde sus implicaciones biogeoquímicas a los mecanismos de regulación intracelular*, se ha desarrollado bajo la supervisión del Dr. Theodore T. Packard y la Dra. María M. Gómez Cabrera, en el Departamento de Biología de la Universidad de las Palmas de Gran Canaria (ULPGC), dentro del programa de Doctorado en Oceanografía con mención de calidad (MCD 2005-00179). La tesis consta principalmente de cinco trabajos de investigación originales, publicados en revistas internacionales con índice de impacto o en proceso de revisión, que se enmarcan dentro de los proyectos EXZOME (CTM 2008-01616/MAR), CAMVALEX (CTM 2010-09515E) y BIOMBA (CTM 2012-32729), concedidos a la Dra. May Gómez. Además, este estudio se ha beneficiado de la participación en campañas oceanográficas derivadas de los proyectos de investigación MALASPINA-2010 (CSD 2008-00077) y SUCCESSION (MSM18/5, DFG), dirigidos por los doctores Carlos M. Duarte y Lutz Postel, respectivamente, así como de una estancia realizada en el Leibniz Institute for Baltic Sea Research (Alemania).

La tesis se organiza siguiendo la estructura típica de un texto académico: una introducción general donde se presentan los antecedentes de la investigación, y se plantean los objetivos e hipótesis a estudiar; a continuación, las cinco contribuciones científicas desarrollan las hipótesis planteadas, respetando cada una de ellas la estructura convencional de un artículo de investigación; por último, se sintetizan los resultados en una discusión general, de la que se desprenden las principales conclusiones y líneas futuras de investigación. Todas estas secciones se han redactado íntegramente en inglés con el objetivo de cumplir con la normativa para la obtención de la Mención Internacional en el Título de Doctor (BOULPGC, Art. 1, Cap. IV, 5 de Noviembre de 2008), según la cual el resumen y las conclusiones deben presentarse en un idioma distinto a la lengua Española. Asimismo, se ha incluido un apartado final donde se resumen en castellano los aspectos generales de la tesis, tal y como exige el Reglamento de Elaboración, Tribunal, Defensa y Evaluación de Tesis Doctorales de la Universidad de Las Palmas de Gran Canaria (BOULPGC, Art. 2, Cap. I, 5 de Noviembre de 2008).

Contents

List of Figures

Page

List of Tables

Page

Symbols and Abbreviations

ADH	Alcohol dehydrogenase
ADP	Adenosine-5'-diphosphate
ANOVA	Analysis of variance
ATP	Adenosine-5'-triphosphate
BM_z	Zooplankton biomass
BSA	Bovine serum albumin
BU	Benguela upwelling
CI-LWB	Canary Islands, during the so-called late winter bloom
CI-ST	Canary Islands, during the stratification period
***CI*s**	Confidence intervals
CTD	Conductivity, temperature and depth sensor
CV	Coefficient of variation
CF	Correction factor
DIN	Dissolved inorganic nitrogen
DM	Dry mass
DON	Dissolved organic nitrogen
E_a	Activation energy
E_z	Euphotic zone
EBUS	Eastern boundary upwelling system
EC	Enzyme commission number
EI	Enzyme-inhibitor complex
ES	Enzyme-substrate complex
ESACW	East South Atlantic Central Waters
ESD	Espherical diameter
ETS	Electron transport system

F_N	Nitrogen flux
GDH	Glutamate dehydrogenase
GF/F	Glass microfiber filter
GLU	Sodium glutamate
GPP	Gross primary production
GTP	Guanosine-5'-triphosphate
HPLC	High performance liquid chromatography
IAEA	International atomic energy agency
INT	2-p-iodophenyl-3-p-nitrophenyl-5-phenyltetrazolium chloride
IO	Indian Ocean
IOW	Leibniz Institute for Baltic Sea Research
K_a	Activation constant
K_i	Inhibition constant
K_{ia}	Dissociation constant
K_m	Michaelis half-saturation constant
K_A	Michaelis half-saturation constant for substrate A
***LOQ*s**	Limits of quantification
MTT	Thiazolyl blue
MW	Molecular weight
N	North
NA	North Atlantic
NAD^+	Nicotinamide adenine dinucleotide oxidized
NADH	Nicotinamide adenine dinucleotide reduced
$NADP^+$	Nicotinamide adenine dinucleotide phosphate
NADPH	Nicotinamide adenine dinucleotide phosphate reduced
NPP	Net primary production
NRE	Nutrient retention efficiency
NW	North west
ODV	Ocean data view
PCA	Principal component analysis
PES	Phenazine ethosulfate
PN	Pyridine nucleotides
POC	Particulate organic carbon
POM	Particulate organic matter
PON	Particulate organic nitrogen
PSU	Practical salinity units

$\boldsymbol{R_{NH_4^+}}$	Ammonium excretion rate
$\boldsymbol{R_{O_2}}$	Respiration rate
RQ	Respiratory quotient
RSD	Relative standard deviation
RV	Research vessel
S	South
SACW	South Atlantic Central Waters
SD	Standard deviation
SEE	Standard error of estimate
spc-($\boldsymbol{R_{NH_4^+}}$)	Biomass-specific ammonium excretion rate
SPSS	Statistical package for the social sciences
SST	Sea surface temperature
ST	Sediment trap
SWA	Southwest Atlantic cruise
TCA	Tricarboxilic acid cycle
$\boldsymbol{T_{eff}}$	Transfer efficiency
U	Enzymatic units
UHPLC	Ultra high performance liquid chromatography
ULPGC	Universidad de Las Palmas de Gran Canaria
UNESCO	United nations educational, scientific and cultural organization
$\boldsymbol{v}$	Volume
$\boldsymbol{V_{max}}$	Apparent maximum enzyme reaction rate
$\boldsymbol{V_{NH_4^+}}$	Modeled enzyme reaction rate of NH_4^+ production
VPDB	Vienna pee dee belemnite
VPR	Video plankton recorder
W	West
$\boldsymbol{z_f}$	Any given depth in the water column
$\boldsymbol{z_m}$	Depth at maximum metabolic rate
$\boldsymbol{z_s}$	Seafloor depth
$\boldsymbol{z_t}$	Top of the water column
$\boldsymbol{\alpha}$	Factor by which the Michaelis half-saturation constant changes in the presence of either an inhibitor or activator
$\boldsymbol{\beta}$	Factor by which the apparent maximum enzyme reaction rate decreases in the presence of either an inhibitor or activator
$\boldsymbol{\Delta}$	Difference or change in a certain quantity
$\boldsymbol{\delta}$	Difference in isotope ratio to a standard
$\boldsymbol{\varepsilon}$	Molar absorption coefficient
$\boldsymbol{\lambda}$	Wavelength

The beginning is the most important part of the work.

Plato

CHAPTER

1

CAPÍTULO

General introduction

1.1 Background and rationale of the study

Zooplankton play a pivotal role in the biogeochemical cycles of the world oceans. They are a key component of the biological pump as they consume organic matter to satisfy their energetic demands and, on the other hand, release nutrients that result from catabolic processes. Depending on the size, these heterotrophic organisms are categorized into nanozooplankton (2 - 20 μm), microzooplankton (20 - 200 μm), mesozooplankton (0.2 - 2 mm) and macrozooplankton (> 2 mm). This thesis studies the metabolic activity in all these size fractions, although most of the investigation focuses on the mesozooplankton. These organisms regulate the mass and energy flow through the food web and consequently, they are the main trophic link between the primary producers and the top predators (Moloney, 1992).

Apart from predation, which controls phytoplankton growth and determines the particle flux to the deep sea, the zooplankton regenerate nutrients that are utilized by the primary producers in the carbon fixation (see Fig. 1.1). In this sense, nitrogen is one of the most limiting nutrient elements controlling phytoplankton growth in the oceans. Its availability depends on the remineralization processes that occur in the sunlit layer, as well as in the introduction of new nutrients via upwelling, diazotrophic nitrogen fixation or terrestrial runoff. Among all the nitrogen species, NH_4^+ is the primary compound released by heterotrophs in the water column (Ikeda and Skjoldal, 1989; Regnault,

nault, 1987), and constitutes the most reduced form of nitrogen, and thereby, the most efficient in terms of assimilation. At a global scale, NH_4^+ regeneration satisfies about the 80 % of the phytoplankton requirements (Harrison, 1992), which reflects the importance of this nitrogen source in the nutrient fluxes of marine ecosystems. In general, microzooplankton, and more particularly the flagellates and small ciliates, are considered to be the main regenerators of NH_4^+ in epipelagic waters (Bronk and Steinberg, 2008; Probyn, 1987), even

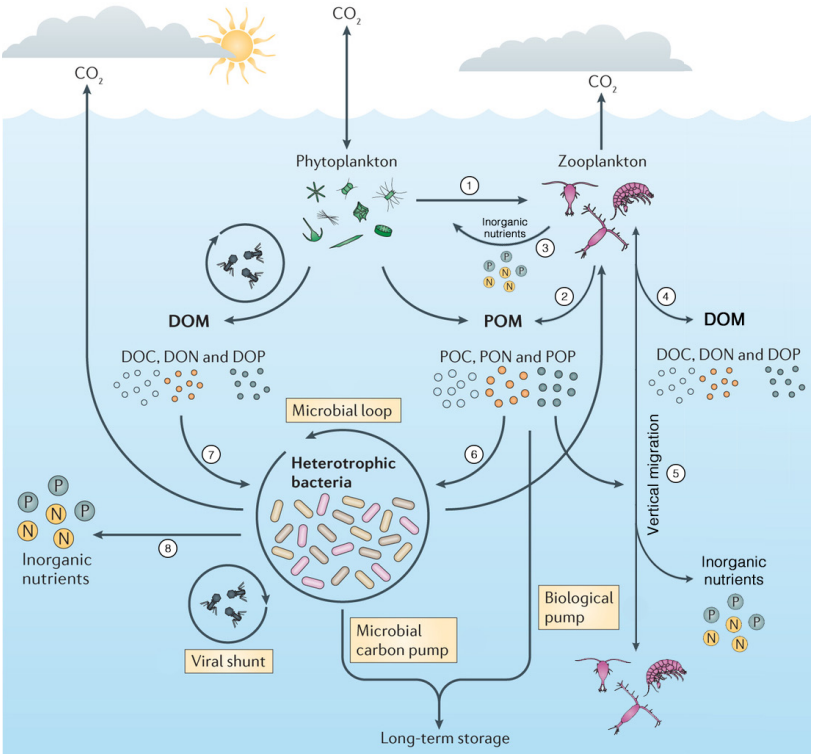

Figure 1.1: A schematic of the processes affecting the nutrient cycling in the ocean water columns. Zooplankton consume phytoplankton cells and POM (1), while producing POM (2) and releasing nutrients through excretion processes in both their inorganic (3) and organic forms (4). These dissolved nutrients can be used by phytoplankton in the sunlit layer, or transported to the mesopelagic zone either by vertical mixing and diffusion, or actively by migrant zooplankton (5). The microbial loop also utilizes POM (6) and DOM (7) for growth and respiration, and provides an important nutrient regeneration pathway (8). Figure adapted and modified from Buchan et al. (2014).

though mesozooplankton also contribute significantly to the nutrient recycling (Steinberg and Saba, 2008). In fact, mesozooplankton release an average of 12 - 33 % of the NH_4^+ required by autotrophs (Atkinson and Whitehouse, 2001; Hernández-León et al., 2008). However, there is no spatial pattern that defines the the role of mesozooplankton NH_4^+ excretion in the regeneration of the primary production. This metabolic process is expected to meet most of the phytoplankton needs in waters where there are low inputs of new nitrogen (i.e., NO_3^- and N_2), such as in open ocean and oligotrophic seas, and to have a minor role in coastal and upwelling systems. Thus, it has been found that mesozooplankton regenerate up to 90 % of primary production in oligotrophic gyres (Isla et al., 2004b), while it barely accounts for the 4 % of the phytoplankton nitrogen demands in upwelling ecosystems (Bode et al., 2004; Isla et al., 2004a). The same general trend was confirmed by Hernández-León et al. (2008), who studied the latitudinal potential contribution of mesozooplankton NH_4^+ excretion to the primary production. From existing data in the literature, these latter authors estimated a major importance of this metabolic process in tropical waters, where it would supply about the 47 % of the NH_4^+ required by the phytoplankton, and a decline in its contribution to the total pool of nitrogen with increasing latitude, thus having the least recycling ability in the polar areas ($\sim$ 6 %). But comparing individual studies of NH_4^+ excretion in communities of mixed mesozooplankton, it can be noticed that these trends are not so obvious. For instance, the percentages of the primary production regenerated by these organisms have been found to range from a low of 4 % (Bode et al., 2004; Isla et al., 2004a) to a high of 44 % (Smith and Whitledge, 1977) in different upwelling ecosystems.

Despite the many studies of zooplankton NH_4^+ excretion in a wide variety of marine environments (see data compilation –Table 8.4– in Bronk and Steinberg, 2008), the data of zooplankton metabolism in waters between 20 - 40° S are still scarce (Hernández-León et al., 2008). In particular, the role that the mesozooplankton community play in the nutrient cycling of the Benguela upwelling system is unknown. This thesis fills this knowledge gap by providing new data that elucidates the impact of mesozooplankton metabolism in the biogeochemical cycles from the northern Benguela (21° S). This coastal upwelling is one of the most productive ecosystem worldwide (Nelson and Hutchings, 1983). The wind-driven divergence allows the entrance of rich-nutrient deep waters into the surface, where both nutrient and light availability

provide a suitable environment for sustaining high biological productivity. According to Boyd et al. (1987), the physical processes intensify the upwelling pulses during the austral winter and spring. The upwelled waters favor the phytoplankton growth near the coast (Mitchell-Innes and Walker, 1991), which results in a rapid nutrient decline as the water mass matures on its way towards the open ocean. During this seawater ageing process, there occur successional events within the plankton community (Vinogradov et al., 1972), whereby the small flagellates and coccolithophorides give rise to a bloom of diatoms which, in turn, stimulates the mesozooplankton growth. However, eddies and filaments emerging from the upwelling center disrupt this specific successional pattern. In a scenario where diverse water masses with different origins and hydrographical characteristics converge (see Fig. 1.2), and the physical complexity is further increased by mesoscale processes, the plankton population dynamics may be altered in the order of days. These oceanographic instabilities also affect the zooplankton metabolism, whose role in the ecosystem biogeochemistry may vary in the short-term both in the temporal and spatial scales.

Furthermore, upwelling ecosystems such as the Benguela represent an interesting scenario for vertical nutrient exchange (Longhurst and Harrison,

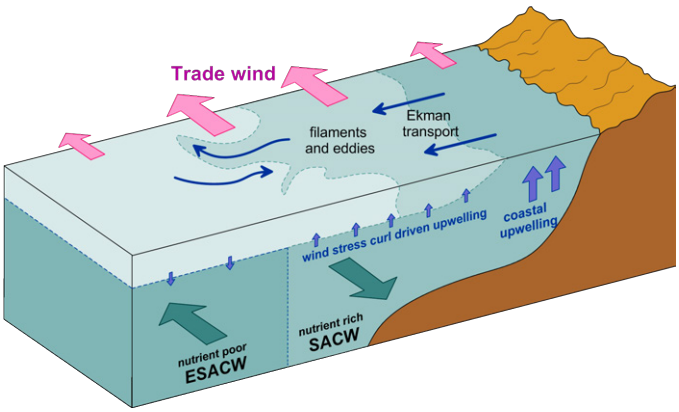

Figure 1.2: Graphical representation of the water mass distribution recorded in the northern Benguela upwelling system (20° S) during the SUCCESSION cruise (Aug.-Sep. 2011). Note that the mesoscale structures disrupt the general pattern of upwelled waters ageing with distance from the shore. Figure taken from Mohrholz et al. (2014).

1989). Within the sunlit layer, phytoplankton convert the carbon dioxide and dissolved nutrients into organic mater, which can be either regenerated or, in the most productive ecosystems, exported into the deep ocean. On average, about the 5 - 25 % of the primary production enter the mesopelagic zone, and only the 3 % reach the bathypelagic zone (De La Rocha and Passow, 2007). It is expected that these percentages were higher in upwelling ecosystems as compared to oligotrophic waters (Martin et al., 1987; Buesseler, 1998). Most of the sinking particles undergo a suite of biologically-mediated chemical transformations while falling down through the ocean water column, which cause the speciation of organic elements (mainly carbon, nitrogen and phosphorous) into their inorganic forms. In general, the bacterial community are responsible for remineralizing about the 15 % of the sinking particles (Ducklow, 2000), while the microzooplankton transform between 30 - 70 % (Calbet and Landry, 2004), and the mesozooplankton, the 20 - 35 % (Hernández-León and Ikeda, 2005) of the sinking particles. In addition to the gravitational flux, the mixing of dissolved organic matter along isopycnals and the active downward transport by migrating zooplankton (see Fig. 1.1) act as a complex network collectively known as the "biological pump" (Volk and Hoffert, 1985). All these processes together constrain the upper limit of the dark ocean metabolism (Arístegui et al., 2009), and set the capacity of the ecosystem to retain its nutrients (Packard et al., 1988; Ridgwell et al., 2011).

Surface primary productivity, vertical flux and heterotrophic consumption below the photic layer have been traditionally related by means of direct measurements of trap-collected particles. In a balanced ecosystem, the gravitational flux should satisfy the metabolic demands in the water column. On the basis of this rationale, Packard and Christensen (2004) employed enzyme activity measurements of electron transport system, which is responsible for respiration, to model vertical carbon flux from the mix-layer to the seabed. A similar concept is applied in this thesis to estimate vertical nitrogen flux in the Benguela waters from NH_4^+ regeneration in the water column. This model assumes that the zooplankton and the small microheterotrophs consume, among other non-conservative elements, the sinking particulate nitrogen for metabolism (Fig. 1.1). As a result, organisms release inorganic dissolved nitrogen (NH_4^+), as well as other organic compounds either in their dissolved (urea and amino acids) or particulate (fecal pellets) forms. Despite the possibility that the pool of organic nitrogen may represent a significant proportion of the re-

lease (Steinberg et al., 2002), the nitrogen flux calculations only consider the NH_4^+ excretion processes because they account for 60 - 100 % of the total nitrogen excreted by marine zooplankton (Regnault, 1987). Paradoxically, several studies have found the heterotrophic activity to be about 2 - 3 orders of magnitude greater than the sinking particulate matter available for consumption (Baltar et al., 2009; Steinberg et al., 2008). The reasons for this imbalance may stem either on the low efficiency of sediment traps to collect particles (Gardner, 2000), or on conversion factors that could overestimate the metabolism of the heterotrophic community. The origin of this mismatch is still a subject of discussion within the scientific community (Burd et al., 2010). In this context, this thesis proposes a novel approach to study nitrogen fluxes in the water column, and compares these estimates with the particulate nitrogen trapped in two sediment traps deployed in the Namibian waters.

Oceanographic studies such as those raised in the first two chapters of this research require rapid data acquisition rate for monitoring, at a high spatial resolution, the impact that zooplankton metabolism exert on the biogeochemical cycles (in both the horizontal and vertical axes). A detailed study of metabolic activities becomes even more relevant when it comes to marine ecosystems characterized by a complex interplay of mesoscale structures. Unfortunately, direct measurements of metabolism, such as the water-bottle incubations, are tedious and time-consuming, so their spatial coverage is limited. Furthermore, these techniques are complicated by methodological artifacts introduced during organism manipulation, overcrowding or even starvation events that may occur during long incubation times (Bidigare, 1983). All together these factors may result in excretion rates that are, to some extent, different from normal rates in seawater. In order to circumvent all these methodological constraints, Bidigare and King (1981) introduced, into the oceanographic field, the enzymatic assay of glutamate dehydrogenase (GDH) as a proxy for NH_4^+ excretion in zooplankton. This enzyme has been found in nearly every organism, and its reaction is a reference for many other biochemical reactions that occur in the mitochondrial matrix of eukaryotic cells. The enzyme GDH (EC 1.4.1.3) is an hexameric protein of 320 000 daltons, whose general architecture has remained relatively unchanged throughout evolution. The 6 subunits are basically organized in 3 dimers, each containing 2 binding domains, that undergo conformational changes during each catalytic cycle (Peterson and Smith, 1999). This structure provides specific binding sites for each substrate of the

reaction (glutamate and $NAD(P)^+$), as well as for effector molecules that allosterically regulate the enzymatic activity. Although reversible, the GDH reaction has low affinity for NH_4^+, which suggests that the main function of GDH in heterotrophs consists of the glutamate deamination (Fig. 1.3). In addition to NH_4^+, this biochemical pathway produces α-ketoglutarate, feeding the tricarboxylic (TCA) acid cycle, which generates electron donors (NADH and $FADH_2$) that are involved in the energy synthesis (ATP). The catalytic activity of the GDH is allosterically regulated, among others, by the adenosine-5'-diphosphate (ADP) and guanosine-5'-triphosphate (GTP), both related with the energy charge of organisms (Frieden and Colman, 1967). Accordingly,

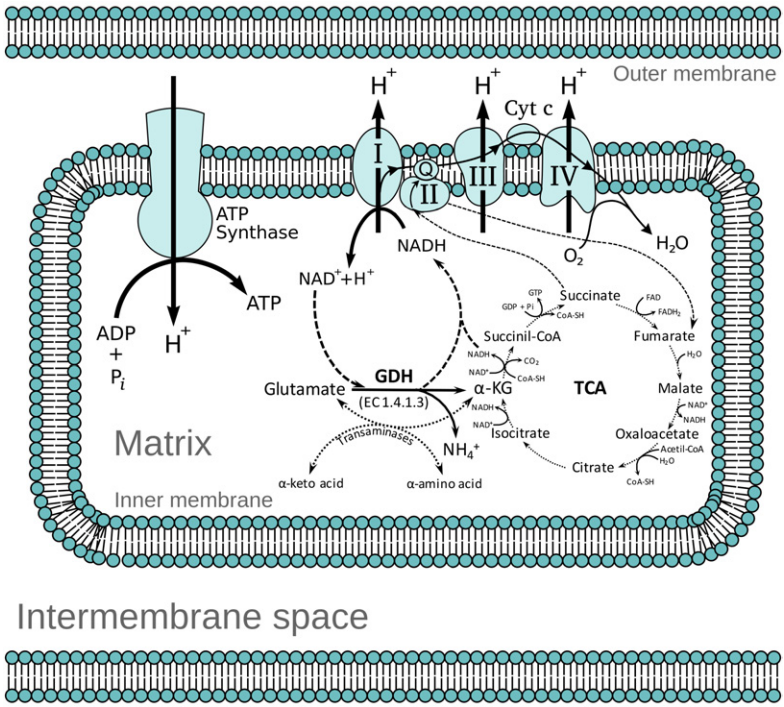

Figure 1.3: Schematic describing the NH_4^+ synthesis from glutamate deamination, catalyzed by the glutamate dehydrogenase (GDH –EC 1.4.1.3–), in the mitochondrial matrix. The reaction feeds the tricarboxylic acid cycle (TCA) by producing α-ketoglutarate (α-KG), which generates electron carriers (NADH) that are utilized by the electron transport system (complexes I - IV, embedded in the inner membrane) for energy. Note that the high-energy molecules of GTP and ATP inhibit the NH_4^+ production, while ADP molecules stimulate it.

GDH may indirectly regulate the energy production and biosynthesis processes, i.e., growth. Despite some transaminases that may also produce NH_4^+ as a product of their catalyzed reactions, the enzyme GDH is responsible for most of the NH_4^+ synthesis in marine organisms. In fact, it has been found that the GDH activity is sufficient to explain all the NH_4^+ release in several species of zooplankton (Batrel and Regnault, 1985; Bidigare and King, 1981). On this basis, the measurement of GDH activity has been routinely used in oceanography to infer NH_4^+ excretion rates in mixed zooplankton communities (Bidigare et al., 1982; Hernández-León and Torres, 1997; Hernández-León et al., 2001; Park et al., 1986, among others). The value of the enzymatic assays lies in the fact that they do not experience those methodological constraints that are intrinsic to the water-bottle incubations and, in addition, they foster a high data acquisition rate. Moreover, once captured, samples can be stored for subsequent analyses in the laboratory. However, these techniques require the addition of saturating levels of substrates to ensure the specificity and the reproducibility of the reaction (Segel, 1993), resulting in a potential measurement which gives the maximum rate instead of the actual one. The latter would be most likely much lower because substrates are hardly at saturating levels *in vivo*. Accordingly, it is necessary to calibrate the GDH measurements through an empirically determined factor that relates the GDH activities with the actual NH_4^+ excretion rates ($R_{NH_4^+}$). Many studies have demonstrated a significant relationship between both rates (Bidigare and King, 1981; Park et al., 1986), even though this may be altered by several factors. For instance, Berges et al. (1993) pointed out the necessity of considering that enzyme activities scale allometrically with body mass in order to avoid erroneous interpretation of data when size structure of population is different. Both variables should scale to the same exponent because otherwise it would lead to misleading interpretations in populations that contain a wide size spectra. To date, there is no study that addresses this issue, so this thesis presents the first equations that explain the influence of body mass over the GDH/$R_{NH_4^+}$ ratio. On the other hand, Bamstedt (1980) demonstrated that the activity of certain enzymes are inherently less responsive to environmental changes than the physiological rates. If this was the case for GDH, its relationship with the $R_{NH_4^+}$ would vary as the trophic conditions change in the marine environment. It was probably for this reason that Hernández-León and Torres (1997) found large fluctuations in the GDH/$R_{NH_4^+}$ ratio in mixed zooplankton samples from the Canary waters, when

the so-called late-winter bloom modified the trophic situation in the plankton community. These authors suggested that the substrate availability would constitute the main factor in explaining the variability between the GDH activities and the $R_{NH_4^+}$. The relationship that both rates maintain with each other in natural samples of mixed zooplankton from different marine systems, as well as in cultured marine zooplankton subjected to changing food conditions, is studied throughout this thesis. In this light, the appropriateness of using a single universal GDH/$R_{NH_4^+}$ for assessing NH_4^+ excretion from GDH measurements is discussed. Likewise, the bisubstrate kinetics of the GDH, and the intracellular pool of substrates involved in the enzymatic reaction (i.e., glutamate and NAD^+) are studied for the first time in marine organisms. Assuming the substrate availability as the critical factor in controlling the velocity of the GDH reaction, a kinetic model based on the first-principles of enzymology was built in order to predict the actual velocity of NH_4^+ production. This model assumes that the GDH activity controls the NH_4^+ synthesis, the concentration of intracellular substrates regulates the enzyme activity, and the reaction follows the Michaelian kinetics. The same concept has been already applied to other biochemical pathways of the respiratory metabolism, and demonstrated their ability to succesfully predict the oxygen consumption (Aguiar-González et al., 2012; Packard et al., 1996b) and CO_2 production (Roy and Packard, 2001) rates in several species of marine bacterium. The pioneering results from this thesis reinforce the utility of kinetic models in the study of NH_4^+ excretion in zooplankton, as they circumvent most of the constraints that entails the use of a constant ratio GDH/$R_{NH_4^+}$ for assessing the NH_4^+ release from measurements of the GDH activity. Furthermore, they constitute the first attempt to elucidate, on a kinetic basis, the allosteric control mechanisms of both GTP and ADP. Overall, this investigation introduces new insights in the study of NH_4^+ excretion in zooplankton, and establishes a baseline for future research of more complex GDH kinetics in zooplankton.

In oceanography, where nearly all of the observations have to be indirect ones, within a world we cannot see, the experimental research in the laboratory is of paramount importance. To deepen knowledge in the biochemical mechanisms that regulate the velocity of the GDH reaction will allow improvement of the appraisal of zooplankton NH_4^+ excretion and hence a derivation of a more precise conclusions about its role in the biogeochemical cycles.

1.2 Thesis objectives and outline

Given the current state of scientific knowledge about the zooplankton metabolism and its implication in the nutrient fluxes in marine ecosystems, this research provides novel results that reveal the role of mesozooplankton community in an important upwelling ecosystem, and define the biochemical mechanisms that control the NH_4^+ excretion in zooplankton.

Thus, the general objective of this thesis consists of determining the role of zooplankton metabolism, in particular the NH_4^+ excretion, in the biogeochemical cycles of the Benguela system, as well as studying those factors that cause variability in the relationship between the *in vivo* NH_4^+ excretion rates ($R_{NH_4^+}$) and the potential activity of the enzyme responsible for this process (glutamate dehydrogenase, GDH). These physiological studies use both natural samples from marine ecosystems characterized by different productivities, and cultured organisms subjected to variable nutritional conditions. In this sense, the thesis is aimed to test the ability of a kinetic model, which assumes substrate availability as the critical factor in regulating the GDH reaction velocity, to predict the $R_{NH_4^+}$ in a changing environment.

Understanding the control mechanisms of the GDH activity would allow more accurate determinations of $R_{NH_4^+}$, and thus obtain more reliable conclusions from field oceanographic investigations such as those presented in the first two chapters of this thesis. In this context, some specific objectives are proposed to answer a number of questions:

1. *Which is the role of the mesozooplankton metabolism in a productive ecosystem such as the Benguela upwelling, and how do the mesoscale structures influence its distribution?*

   These questions are answered in *Chapter* 2, which describes the results from an oceanographic cruise that surveyed the northern Benguela waters during the active upwelling season in 2011. Applying a Eulerian approach, the biomass and metabolism dynamics of mesozooplankton along a cross-shelf transect in waters off Namibia were analyzed. The starting hypothesis assumes the development of succession of zooplankton populations in the ageing advected waters, and little impact of the mesozooplankton metabolism on the primary productivity as compared to that found in oligotrophic systems.

2. *How does the NH_4^+ excretion determine the vertical nitrogen fluxes in*

this upwelling ecosystem? Are the modeled nitrogen fluxes comparable with the sediment trap measurements of particulate nitrogen? What is the importance of the active flux driven by the diel-migrant mesozooplankton?

Once the role of mesozooplankton metabolism in controling the primary productivity of the Benguela waters is known, the implications of the $R_{NH_4^+}$ in the vertical nitrogen fluxes are elucidated. All these concerns are met in *Chapter* 3 by applying a potential function to the zooplankton $R_{NH_4^+}$ profiles to calculate the gravitational nitrogen flux in this upwelling ecosystem. The modeled nitrogen fluxes are compared to the particulate nitrogen trapped by the sediment traps deployed at two stations of the transect. As suggested by previous work, an imbalance between the metabolic requirements of nitrogen in the water column and the sinking particulate nitrogen was expected. Furthermore, the $R_{NH_4^+}$ profiles are utilized for studying the active flux driven by diel-migrant mesozooplankton. Attending to the high biomass of these organisms in upwelling environments, the active flux may constitute an important component of the biological pump.

3. *Is there a general equation that explains the relationship between the $R_{NH_4^+}$ and the GDH activities in all oceanographic situations? Which are the factors that affect such relationship, and how do they modify it?*

The $R_{NH_4^+}$ determined in previous chapters was necessarily obtained from the enzymatic measurements of GDH. These are measurements that are related to $R_{NH_4^+}$ through an empirically determined factor. The relationship between the actual $R_{NH_4^+}$ and the GDH activities measured in several marine ecosystems in size-fractionated zooplankton is addressed in *Chapter* 4. These values are further compared with those published in the literature. The appropriateness of using a general GDH/$R_{NH_4^+}$ factor to infer the actual $R_{NH_4^+}$ from the enzymatic measurements is discussed. If biological variables such as biomass and trophic condition affect both rates in the same way, the relationship with each other would be constant. The influence of these two factors on the GDH/$R_{NH_4^+}$ ratio is studied in more detail on a monospecific culture of the marine mysid *Leptomysis lingvura* (*Chapter* 5).

4. *Is a kinetic model of GDH able to predict the actual $R_{NH_4^+}$ patterns in*

zooplankton? In which circumstances does the allosteric regulation become stronger?

To answer these biochemical concerns, a bisubstrate kinetic model based on the Michaelis-Menten equations is tested in two species of marine zooplankton along a starvation time-course (*Chapter 6*). As suggested by the results of preceding chapters, the model assumes the substrate availability as the most critical mechanism in enzyme regulation. Both the allosteric inhibition and activation by purine nucleotides are separately studied using monosubstrate kinetic models. It is expected that allosterism gains importance in organisms with a high energy charge.

What we know is a drop, what we ignore, the ocean.

Sir Isaac Newton

CHAPTER

2

CAPÍTULO

Distribution of zooplankton biomass and potential metabolic activities across the northern Benguela upwelling system

I. Fernández-Urruzola, N. Osma, T. Packard, M. Gómez and L. Postel (2014), Journal of Marine Systems 140 (B), 138 - 149.

http://dx.doi.org/10.1016/j.jmarsys.2014.05.009

ABSTRACT: The distribution of zooplankton biomass and potential metabolic rates, in terms of electron transport system (ETS) and glutamate dehydrogenase (GDH), were analyzed along a cross-shelf transect in waters off Namibia. The highly variable dynamics of upwelling filaments promoted short-term fluctuations in the zooplankton biomass and metabolism. Maximum values were characteristically found over the shelf-break, where zooplankton biomass as dry mass (DM) reached peaks of 64.5 mg m^{-3} within the upper 200 m in late August. Two weeks later, the zooplankton-DM decreased by more than a third (19 mg DM m^{-3}). Zooplankton potential respiration and NH_4^+ excretion averaged 234 µmol O_2 m^{-3} d^{-1} and 169 µmol NH_4^+ m^{-3} d^{-1} in the Namibian shelf, respectively. High protein-specific ETS activities even in the low-chlorophyll waters outside the filament suggested a shift into greater omnivory seaward. In this light, zooplankton elemental and isotopic compositions were used to investigate the pelagic food web interactions. They evidenced spatial changes

in the carbon resource for zooplankton as well as changes in the form of nitrogen that fueled the biological production in ageing advected waters. Overall, both aspects of zooplankton metabolism impacted the primary productivity at a level less than 10 % under all the different oceanographic conditions.

Keywords: Zooplankton; Biomass; Electron transport system (ETS); Glutamate dehydrogenase (GDH); Benguela upwelling system.

2.1 Introduction

Upwelling ecosystems are among the most productive areas worldwide. They mainly occur along the eastern boundaries of an ocean where the wind-driven divergence forces deep cold waters, rich in nutrients, into the sunlit layer. Both nutrient enrichment and light availability together, provide a suitable environment for sustaining high biological productivity. One of the major eastern boundary current systems of the world is the Benguela, which is divided in two sub-systems by a permanent upwelling cell located around 27 - 28° S (Boyer et al., 2000). Here, the northern part is the focus of investigation. It is limited by the warm water of the Angola-Benguela Front (Shannon, 2001) and exhibits important instabilities at short temporal and spatial scales in addition to the well-documented interannual fluctuations (Shannon and Nelson, 1996; Hutchings et al., 2009). Both oceanographic and atmospheric forces intensify the upwelling pulses during the austral winter and spring, and relax them in autumn (Boyd et al., 1987). Other processes such as jets and filaments emerging from the perennial cell also promote the variability in the northern Benguela ecosystem. These mesoscale structures will ultimately impact the plankton populations dynamics.

In this and in all upwelling systems, mesozooplankton play a key role in the mass and energy flows through the food web (Moloney, 1992). They are the primary food resource for fish larvae and consequently, the main trophic link to the top predators. In recognizing the importance of zooplankton in the Benguela system, several studies have paid attention to its spatial distribution (Verheye and Hutchings, 1988; Olivar and Barangé, 1990; Hansen et al., 2005; Postel et al., 2007, among others), as well as to the long-term trends in the zooplankton abundance (Verheye et al., 1998) and biomass (Huggett et al.,

2009). Changes in the community composition (Gibbons and Hutchings, 1996; Verheye et al., 2001), ecology (Gibbons et al., 1992; Verheye et al., 1992) and secondary production (Hutchings et al., 1991; Richardson and Verheye, 1999) in relation to physical and biological forcings have also been described in the last decades. However, these studies have not considered the short-term zooplankton structural dynamics caused by successive upwelling-relaxation events, filaments or eddies which take place in a particular region. Wind-driven offshore advection, for instance, causes the stratified plankton-rich waters to be rapidly replaced by deeper waters, which introduce a new batch of nutrients into the photic layer, but little plankton. Accordingly, the inherent variability of these chemical and physical phenomena constrains the integrity of biological communities on the order of days.

Furthermore, the instability of the oceanographic setting also affect the physiological dynamics of zooplankton (Langford and Youssara, 2003). Respiration and NH_4^+ excretion are important processes in marine ecology, as the balance between synthesis and demand of both carbon and nitrogen controls the efficiency of the net production (Margalef, 1982). In this context, Chapman et al. (1994) measured electron transport system (ETS) activities in microplankton to broadly estimate the carbon requirements and the nutrient regeneration in the waters south of Walvis Bay. Few studies have directly dealt, however, with mesozooplankton metabolism in this upwelling ecosystem. Recently, Huenerlage and Buchholz (2013) demonstrated variations in the physiological behavior of *Euphausia hanseni* under changeable trophic conditions in the Angola-Benguela frontal waters. The respiration in terms of ETS activity was also determined, but only on the dominant copepod species from Benguela (Timonin et al., 1992; Bode et al., 2013). Indeed, from respiration measurements, Schukat et al. (2013b) assessed an important daily phytoplankton removal by copepods. Here we elucidate the magnitude of the respiration and NH_4^+ excretion rates by the total mesozooplankton community in a cross-shelf transect off Namibia. We used the enzymatic approach because direct measurements of physiology such as the water-bottle procedures give low spatial resolution and are additionally complicated by artifacts derived from organism manipulation, overcrowding and even starvation when long incubation times are needed (Bidigare, 1983). Enzymatic assays in turn, require the addition of saturating levels of substrates to ensure the specificity of the reaction (Segel, 1993; Maldonado et al., 2012), resulting in a potential

measurement which gives the maximum rate (V_{max}) instead of the actual one. Nevertheless, studies have demonstrated the utility of enzymes as an accurate index of metabolic rates, especially when they are previously calibrated for the surveyed system (e.g., Packard, 1985; Hernández-León et al., 1999; Bode et al., 2013).

This field study is embedded in an interdisciplinary research of the ageing process of a coastal upwelling system. We aimed to characterize how the physical structuring processes affect the biomass of zooplankton, as well as to describe the impact that zooplankton metabolism has on the primary productivity from the northern Namibian cell. Elemental composition and stable isotopes of zooplankton were additionally used to infer spatial changes in the pelagic food web of this ecosystem. Since continuous monitoring is required to understand the structure and functioning of the plankton community, we applied a Eulerian approach by sampling a cross-shelf transect four times during a month of intense wind-forcing. The irruption of eddies and filaments will affect the maturation pattern of the fresh upwelled waters along its pathway seaward. This influences the successional developments in these ageing advected waters, promoting the heterogeneity in zooplankton populations towards the open ocean. In this scenario, our research illustrates the dynamics of zooplankton biomass and potential metabolism in face of the different oceanographic situations recorded in the northern Benguela.

2.2 Material and methods

Four consecutive transects were made to collect zooplankton samples and hydrographic data at 20° S off Namibia during the SUCCESSION cruise onboard RV Maria S. Merian from August 27th to September 15th, 2011. Three of the transects sampled 12 stations to a distance of 230 km from the coast, while the fourth one was extended seaward by 9 stations to 500 km (Fig. 2.1). Stations from NAM001 to NAM018 were sampled during both day and night in order to minimize the effect of the vertical migrations by the large zooplankton. Salinity, temperature, chlorophyll-a fluorescence and dissolved oxygen profiles were obtained at each station by deployment of a CTD SBE 911+, equipped with a WETlab FLRT-1754 fluorometer, and mounted on a rosette sampler with twenty-four 10-L Niskin bottles. Nutrients (NO_2^-, NO_3^-, PO_4^-, NH_4^+ and SiO_4^{4-}) as well as chlorophyll-a concentrations were also measured at different

depths (Mohrholz et al., 2014; Nausch and Nausch, 2014).

2.2.1 **Zooplankton sampling**

Zooplankton was collected by Multinet vertical hauls (Hydrobios GmbH, Kiel, Germany). The equipment consisted of a net frame with an opening of 0.25 m^2, fitted alternatively with 100 and 500 μm meshed nets (L = 2.5 m, diameter at the end = 0.11 m) and stabilized by V-fin depressor. Each net ended in a cod-end consisting of a plastic bucket with side windows covered by gauze. The two flowmeters, mounted inside and outside of the frame, measured the amount of water filtered by the net during each haul, and a pressure sensor recorded the depth in real-time. The multiple open/closing system enabled the collection of stratified zooplankton samples in a single deployment. Three depth layers were sampled: from 200 to 75 m (or 10 m from the bottom in the shallower stations), 75 to 25 m and 25 m to the sea surface. Net sets with the two mesh sizes sampled each strata, so two samples per depth layer were

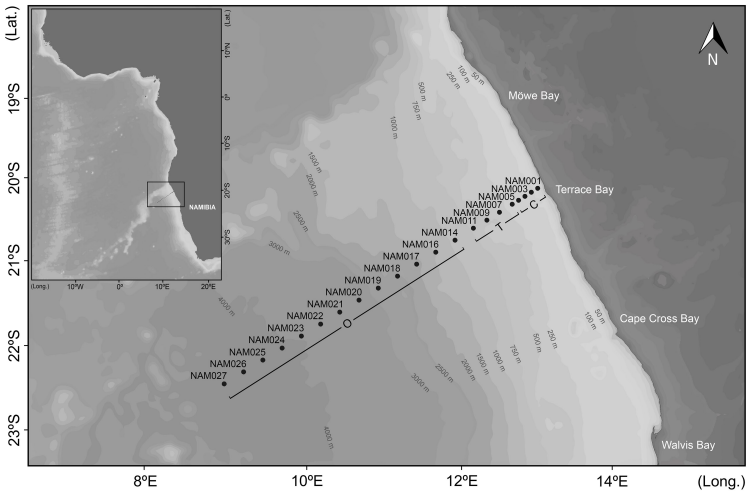

Figure 2.1: Map of the study area showing the cross-shelf transect of the Namibian upwelling where zooplankton samples were collected during the SUCCESSION cruise. Stations from NAM001 to NAM018 were sampled four times, while samples from NAM019 to NAM027 were collected only once. The transect was divided into coastal (C), transition (T) and offshore (O) areas according to the geological and oceanographical properties of the stations.

recovered. We used the 100 μm mesh size for the zooplankton fractions below 500 μm, and the 500 μm mesh size for the larger ones. This approach ensured a quantitative sampling for size fractions below 10 mm.

Once on deck, the net was rinsed with seawater and the samples were maintained at 4 °C while awaiting the processing. First, we split the samples by the beaker technique (Van Guelpen et al., 1982). One half was fractionated for the 100 - 200, 200 - 500, 500 - 1000 and > 1000 μm size classes, and immediately frozen in liquid nitrogen before being stored in the freezer (−80 °C) for subsequent enzymatic analyses. The other was split into two new subsamples: one was frozen at −20 °C for biomass and isotopic determinations; the other was stored in plastic bottles filled with buffered formaldehyde (4 % final concentration) for taxonomic analysis. Size fractionation was made in both cases as well. Organisms over 5000 μm such as jellyfish were not included in our calculations. However, they were counted and the diameter of the umbrella was measured with a calibrated rule in order to convert them into dry mass (DM) using the equation $DM = 0.03\, Diameter^{2.3}$ given in Møller and Riisgrd (2007) for the genus *Aquarea*.

Chains of diatoms were found in a few 100 μm meshed net hauls in the surface layer from NAM005 to NAM009, mainly during the first two transects. Despite the samples being carefully washed with filtered seawater, some diatoms still remained in them. This contamination was noticeable in only 18 % of the samples. In order to quantify the biomass due to phytoplankton in these samples, the amount of chlorophyll-a (Chl-a) was first determined by spectrophotometry (Parsons et al., 1984). Then, chlorophyll-a values were converted into organic carbon with a factor of 27 (μg C/μg Chl-a) calculated from the relationship: $C = 24.3\, Chl\text{-}a + 29.3$ ($n = 29$, $r^2 = 0.75$, $p < 0.05$) given in Schlüter and Havskum (1997) with the intercept forced through zero. This factor agrees with others reported for marine phytoplankton communities in an exponential growth phase (Banse, 1977; Smetacek and Hendrikson, 1979). For communities in senescence with high detrital presence, the relationship between carbon and chlorophyll-a can rise up to 200. This was not the case here. Since the samples in question were found in mature waters rich in nutrients, suitable for a bloom of diatoms, the lower limit of the C/Chl-a ratio (ranging from 22 to 200) was used. Accordingly, these should be considered as conservative estimates. The phytoplankton-associated carbon value was subtracted from the total

organic carbon of each contaminated sample. On average, these zooplankton samples contained 35 ± 24 % phytoplankton biomass. Afterwards, our own ratios (see *Results* section) were applied to Ricker's concept based on the sum of the least products (Ricker, 1973) so as to recalculate the biomass of zooplankton in terms of DM, organic nitrogen and protein in these samples.

2.2.2 **Biomass analyses and stable isotopes measurements**

Frozen samples were dried at 60 °C in the land-based laboratory. The isotope, particulate organic carbon (POC) and particulate organic nitrogen (PON) samples were ground to fine powder and weighed in tin capsules. Measurements were made by means of Flash combustion in a CE Instruments Flash EA 1112 at 1020 °C in a Finnigan Delta S isotope ratio mass-spectrometer via a Conflow III open split interface. Calibration for the total POC and PON determinations was done daily with an acetanilide standard. The stable nitrogen and carbon isotope ratios measured for each sample were corrected with the values obtained from standards with defined nitrogen and carbon element and isotopic compositions (International Atomic Energy Agency IAEA: IAEA-N1, IAEA-N2, IAEA-N3, NBS 22, IAEA-C3 and IAEA-CH-6) by mass balance. Values are reported relative to atmospheric N_2 (^{15}N) and VPDB (^{13}C-Vienna Peedee belemnite). The analytical precision for both stable isotope ratios was 0.2 ‰. Carbon and nitrogen contents were calculated by the percentages of the initial dry masses in relation to the total. Then, considering the split part and the amount of water filtered, the carbon and nitrogen concentrations were given in mg m^{-3}. C/N ratios were calculated on a molar basis. Samples were not generally acidified prior to combustion in order to remove inorganic carbon. An experiment using 45 samples selected by chance served as a data base to estimate the effect. The average of non acidified samples amounted to 25.1 ± 6.9 % as compared to 22.4 ± 7.1 % after acidifying them. The difference amounted to a maximum of 7.5 %, but was not significant ($p > 0.05$). None of the zooplankton samples contaminated with phytoplankton were considered for isotope characterization. In addition, biomass in terms of protein content was determined from the samples kept for enzyme activities by using the method of Lowry et al. (1951) modified by Rutter (1967).

2.2.3 **Zooplankton community composition**

Taxonomic analysis was done with great deliberation on all size classes and all depth levels down to 200 m from five transect II stations. The distance to shore was 10, 20, 110, 200, and 230 km or a "pseudo-age" (Mohrholz et al., 2014) of 4.0, 3.7, 48.9, 46.4 and 44.5 days respectively. Transect II was chosen to facilitate a later comparison with the results obtained by the Video-Plankton-Recorder VPR II, which produces the same taxonomic resolution, but at higher sampling frequency. Samples were taken at night except for NAM001, which was taken at dawn. As a result, the vertical profiles were not affected by daily vertical migration and consequently, are comparable.

The species analysis of the larger zooplankton required a stereomicroscope (Leica, MZ 8) with a magnification between 16 and 80×. The smaller size classes were analyzed by an inverted microscope (Labovert FS, Leitz) usually with a magnification of 50×. In both cases, Bogorov trays of suitable sizes were used for counting. The total samples were first surveyed for rare specimens. High sample concentrations often required the analysis of sub-samples. The entire procedure and the discussion of errors have been described in detail in Postel et al. (2000). Taxonomic determinations were performed to different levels, often down to genera, using the literature for the Angolan-South African region (Gibbons, 1997), the South Atlantic (Boltovskoy, 1999), the northern hemisphere (ICES, 2001) and the Mediterranean (Trégouboff and Rose, 1978; Riedl, 1983).

2.2.4 **Indices of metabolism**

Electron transport system (ETS) and glutamate dehydrogenase (GDH) activities were measured on the same homogenate that was used for protein determination. During the whole procedure, the samples were kept in ice in order to prevent a decline in the enzymatic activities. The supernatant fluid was assayed for ETS activity following the Owens and King (1975) methodology, and for GDH activity using the procedure of Bidigare and King (1981) modified according to Fernández-Urruzola et al. (2011) –*Chapter* 5, this thesis–. Both analyses were carried out kinetically at 18 °C and then corrected for temperature. This recalculation assured an accurate estimation of the *in situ* respiration and NH_4^+ excretion by employing the Arrhenius equation with activation energies of 15 Kcal mol^{-1} (Packard et al., 1975) and 10 Kcal mol^{-1} (calculated from Park et al. 1986), respectively. The phytoplankton associated-ETS activities

in the aforementioned samples were subtracted from the total ETS by means of an ETS to zooplankton-protein ratio equal to 61.6 μmol O_2 mg protein^{-1} d^{-1}. This factor was obtained by regression analysis of non-contaminated zooplankton smaller than 500 μm, and sampled from the same area (*ETS activity* = 61.6 *protein*, $n = 91$, $r^2 = 0.93$, $p < 0.001$). However, it was not necessary to correct the GDH activities since the deamination function for NAD^+-specific GDH in phytoplankton is negligible (King, 1984; Park et al., 1986).

Additionally, water-bottle incubations for respiration (R_{O_2}) and NH_4^+ excretion ($R_{NH_4^+}$) were conducted on board in order to calibrate the enzymatic measurements with specific R_{O_2}/ETS and GDH/$R_{NH_4^+}$ ratios for the Benguela system. Zooplankters were collected by WP-2 net hauls and after fractionation, maintained in filtered seawater at sea surface temperature (14 - 16 °C). After an hour acclimation period, the healthiest organisms were incubated in filtered seawater at 14 °C for 2 hours in glass-capped bottles. All the experiments included at least one control flask. Oxygen consumption was estimated by the continuous measurement of dissolved O_2 with a 6-channel Strathkelvin 928 Oxygen System® respirometer. Once the incubation was finished, a sample of seawater (10 mL) was siphoned off from each bottle for NH_4^+ determinations in accordance with the phenol-hypochlorite method (Solorzano, 1969). Afterwards, the zooplankters were removed and frozen at −80 °C in order to analyze the enzyme activities as described above. The mean R_{O_2}/ETS value for zooplankton was 0.48 ± 0.29 ($n = 19$), while for GDH/$R_{NH_4^+}$ it was 16.4 ± 12.2 ($n = 26$). Although the standard deviations were high, these ratios are close to the reported R_{O_2}/ETS ratio by Bode et al. (2013) for the same region, and in the middle of the range of GDH/$R_{NH_4^+}$ ratios from the literature (see *Chapter* 4, this thesis). The errors caused by these ratios have been discussed by King and Packard (1975), and Hernández-León and Gómez (1996). Furthermore, del Giorgio (1992) found that these errors were not greater than those of other methods used in standard ecological procedures for plankton metabolic processes, such as the thymidine and ^{14}C uptake techniques (Richardson, 1991). As a result, the average ratios measured here were used to estimate the community respiration and NH_4^+ excretion throughout this study. Oxygen consumption rates were converted into carbon from the respiratory quotient of 0.86, assuming a mixed diet (Omori and Ikeda, 1984). The C/N uptake ratio of 6.1 (μg C/μg N) given by Dugdale and Goering (1967) was used to assess the carbon regenerated by the zooplankton NH_4^+ excretion rates. Gross primary

production (GPP) was estimated from chlorophyll-a and ^{14}C uptake measurements made on board; the calculations followed the procedure described in Brown et al. (1991) for the Benguela system, with the regression model (best fit to the data): $^{14}C = 3.75\ Chl\text{-}a^{0.653}$ ($n = 24$, $r^2 = 0.60$, $p < 0.001$). The difference between GPP and the daily phytoplankton respiration (assumed to be 10 % of hourly production multiplied by night hours) equaled the net primary production (NPP).

2.3 Results

Mohrholz et al. (2014) describe in detail the hydrographic conditions during the SUCCESSION cruise. Different water masses were present in the study area, most of them with a northern origin. Additionally, a cold water filament was found extending offshore from the coastal upwelling center. This filament influenced the near-shore stations, while the ones over 140 km from coast were mainly under the influence of warmer water masses, especially at the end of the cruise. The phytoplankton development was coupled with the presence of the cold water filament, reaching a maximum peak of chlorophyll at the beginning of September. Ekman divergence dominated near coast, whereas around the outer shelf curl-driven upwelling introduced nutrient-rich South Atlantic Central Waters (SACW) into the euphotic zone with a maximum vertical velocity of 0.35 m d^{-1}. These differences in hydrology allowed us to distinguish three regions within the transect (Fig. 2.1). The coastal stations (NAM001 - NAM004) were characterized by the Ekman transport that brings deep central waters to the surface with high vertical velocities. The transition zone (NAM005 - NAM011) occurred over the shelf-break and was strongly influenced by both the filaments and the curl driven upwelling. The offshore stations over the continental slope (NAM014 - NAM027) were mainly affected by warm water masses and by the ocasional occurrence of younger waters arising from the filaments. The selection of these limits was strengthened by cluster analysis of physical and chemical properties of the stations (see *Appendix* section, Fig. A.1).

2.3.1 Zooplankton biomass and community structure

The pattern of water masses at 20° S promoted great temporal variability in zooplankton biomass along the transect (Fig. 2.2). Accordingly, peaks of zooplankton were found coinciding with maximum values of chlorophyll-a

in late August. At that time, a nearly stable cold water filament sustained high primary productivity, even at the outer stations such as NAM017 (see Hansen et al., 2014). Afterwards, the filament was dispersed to the northwest, which led to a decrease in the chlorophyll-a concentration as well as a 3-fold decrease in the zooplankton biomass. In order to reduce the impact of these mesoscale structures, the measurements of the four transects were averaged for some analyses.

Despite the fact that the zooplankton and more particularly the size fractions over 500 µm showed higher biomass during the night (Fig. 2.3), the non-parametric Mann-Whitney U test did not reveal a significant day-night difference ($p > 0.05$). This means that only a small percentage of the larger zooplankton migrated out of the upper 200 m during the day. Nonetheless, the schedule of the sample collection during the cruise minimized those vertical differences by sampling two days and two nights at each station and averageing results over time. Larger horizontal differences of the biomass were observed

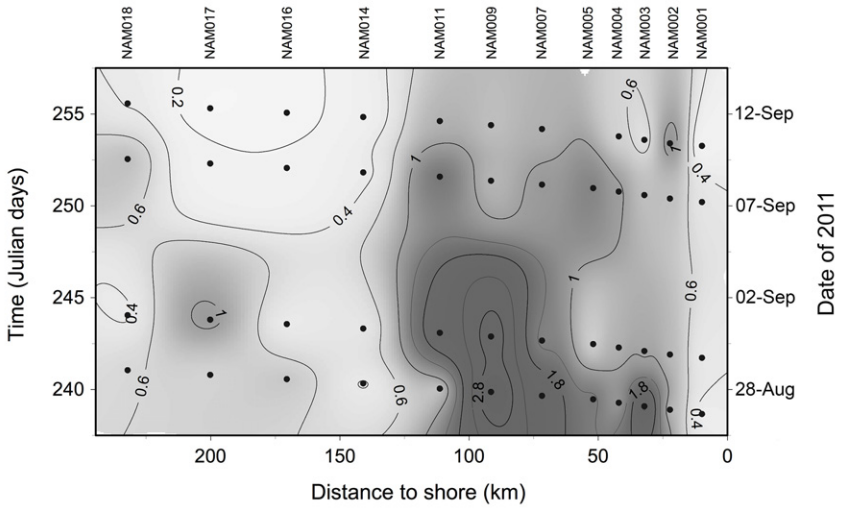

Figure 2.2: Temporal variability of zooplankton biomass (g DM m^{-2}) along the SUCCESSION transect. Only the first 25 m of the water-column is considered because this layer contains most of the variability. The secondary axis (right) shows the corresponding sampling-dates. Ocean Data View (ODV) software was used to generate interpolated values using the weighted averaged gridding method option.

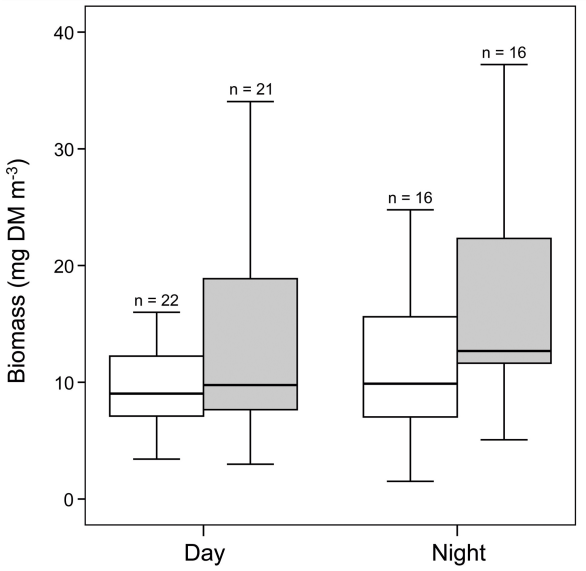

Figure 2.3: Differences in zooplankton biomass distribution between day and night in the upper 75 m of the water-column. The gray boxes represent the zooplankton > 500 µm and the white boxes, the 100 - 500 µm size fraction. The lower and upper boundaries of the boxes represent the first and third quartile of the data distribution respectively, with the dark line in the middle as the median. Error bars indicate the 95 % confidence intervals (*CI*s).

among the areas (one-way ANOVA, $F_{2,48} = 20.22$, $p < 0.001$). The DM-values averaged 51 mg m^{-3} in the upper 75 m of the transition zone, a value much higher than those measured at the other two zones (Table 2.1). The development of salp blooms in the mature waters from the transition area during the first half of the cruise resulted in high biomass deviations in the largest size class.

The total zooplankton biomass peaked at all three depth layers at 90 km from the coast (Fig. 2.4). The maximum mean value in the surface layer was 81 mg DM m^{-3}. This occurred slightly displaced offshore from the diatom bloom that was found at 70 km from the coast. Then, the zooplankton biomass diminished seaward down to 3 mg DM m^{-3}, although an unexpected peak in the upper 25 m was found 380 km from the shore owing to the high abundance in the largest size fraction. The highest densities of zooplankton

Table 2.1: Cross-shelf distribution of averaged (± *SD*) zooplankton biomass for the three regions in terms of dry mass (DM), organic carbon (C), organic nitrogen (N) and protein (all in mg m^{-3}) measured on four size fractions in the upper 75 m. The relative contribution (%) of each fraction to the total protein biomass is also given.

Area	Size (μm)	*n*	DM	C	N	Protein	%
Coastal	100 - 200	16	3.60 ± 1.54	1.08 ± 0.45	0.26 ± 0.11	0.63 ± 0.21	13.7
	200 - 500	16	6.61 ± 4.20	1.71 ± 0.94	0.46 ± 0.24	1.24 ± 0.60	27.1
	500 - 1000	16	3.50 ± 2.58	1.17 ± 0.89	0.33 ± 0.24	0.75 ± 0.54	16.3
	> 1000	16	9.34 ± 8.94	2.89 ± 3.03	0.89 ± 0.85	1.97 ± 2.11	42.9
	TOTAL	64	23.05 ± 10.32	6.85 ± 3.32	1.94 ± 0.92	4.59 ± 2.27	100
Transition	100 - 200	14	3.96 ± 3.00	0.67 ± 0.41	0.16 ± 0.09	0.67 ± 0.50	6.4
	200 - 500	14	16.44 ± 12.32	2.60 ± 1.71	0.57 ± 0.38	3.74 ± 3.12	35.8
	500 - 1000	16	4.12 ± 2.77	1.36 ± 0.94	0.36 ± 0.25	1.28 ± 1.02	12.3
	> 1000	14	26.38 ± 34.18	7.01 ± 5.04	1.71 ± 1.16	4.75 ± 3.29	45.5
	TOTAL	58	50.90 ± 36.56	11.64 ± 5.42	2.80 ± 1.24	10.44 ± 4.67	100
Offshore	100 - 200	23	1.87 ± 1.44	0.41 ± 0.29	0.10 ± 0.07	0.29 ± 0.18	10.4
	200 - 500	24	4.86 ± 4.58	1.03 ± 0.80	0.26 ± 0.20	0.68 ± 0.58	24.3
	500 - 1000	23	2.64 ± 1.82	0.84 ± 0.61	0.24 ± 0.18	0.47 ± 0.34	16.8
	> 1000	24	8.51 ± 5.32	2.07 ± 1.39	0.57 ± 0.39	1.36 ± 1.14	48.6
	TOTAL	92	17.88 ± 7.39	4.35 ± 1.74	1.17 ± 0.48	2.80 ± 1.34	100

were always found in the upper 25 m, where the chlorophyll-a concentration was about 2-fold greater than the one measured from 25 to 75 m, and almost one order of magnitude greater in comparison with the deepest layer. In general, our zooplankton biomass results were of similar magnitude to those registered in 1979 along the same transect (Southwest Atlantic cruise, SWA; see details in Postel, 1995). However, peaks of zooplankton during our cruise were displaced inshore compared to the earlier expedition (Fig. 2.4). Throughout the entire transect, cyclopoid copepods were the most abundant taxa within the size fractions below 500 μm (Fig. 2.5*a*). At the inner stations, the relative abundance of meroplanktonic larvae (ophioplutei) was also high (∼ 30 %). They decreased further offshore, while the presence of other groups such as calanoids, harpacticoids and tintinnids increased. In the larger zooplankton there appeared more variability in the dominant species (Fig. 2.5*b*). Thaliaceans predominated at the shelf-break and calanoids were more important inshore and offshore. Jellyfish were not considered here, although we noted their presence mainly confined to the inner shelf (Fig. 2.6).

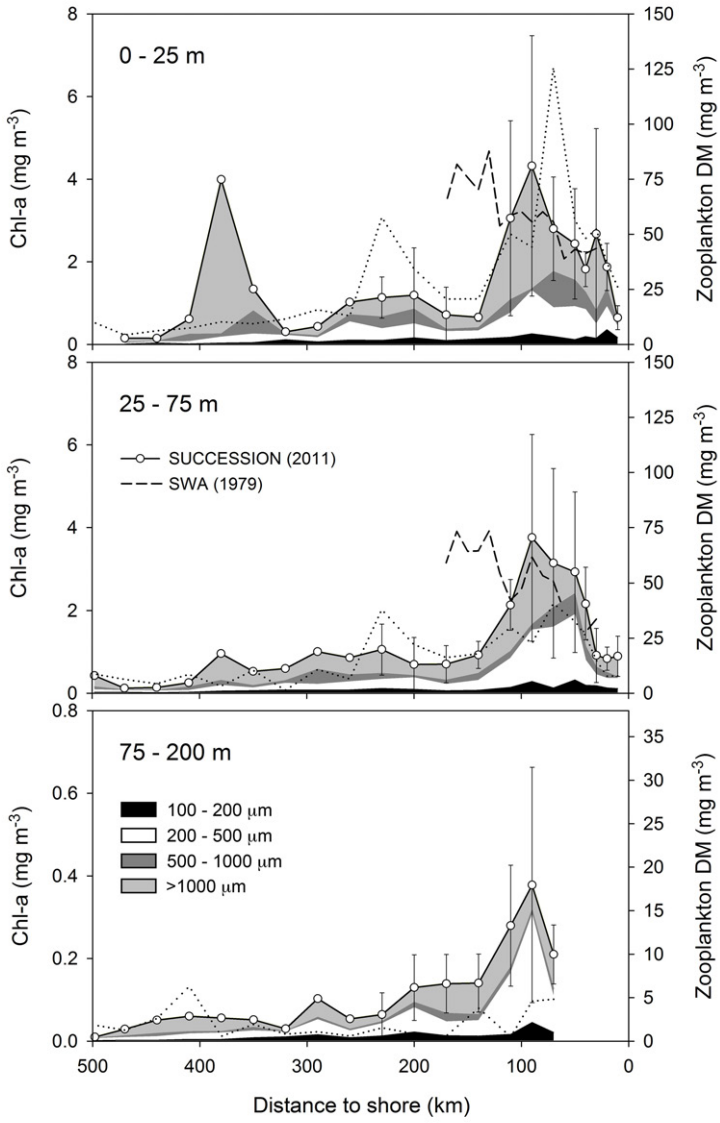

Figure 2.4: Mean zooplankton biomass at different depth levels with the contribution of each size fraction. Dotted line stands for the chlorophyll-a concentration. Zooplankton biomass data for the SUCCESSION cruise are compared (top two panels) with data from the same transect made 32 years before (1979), during the Southwest Atlantic cruise (SWA). No data are shown for the shallow stations along the first 70 km in the bottom panel. Note that the scale for both chlorophyll-a and zooplankton is smaller in the 75 - 200 m layer. Error bars indicate the 95 % *CI*s, but not for the data seaward of 230 km where only one measurement was made.

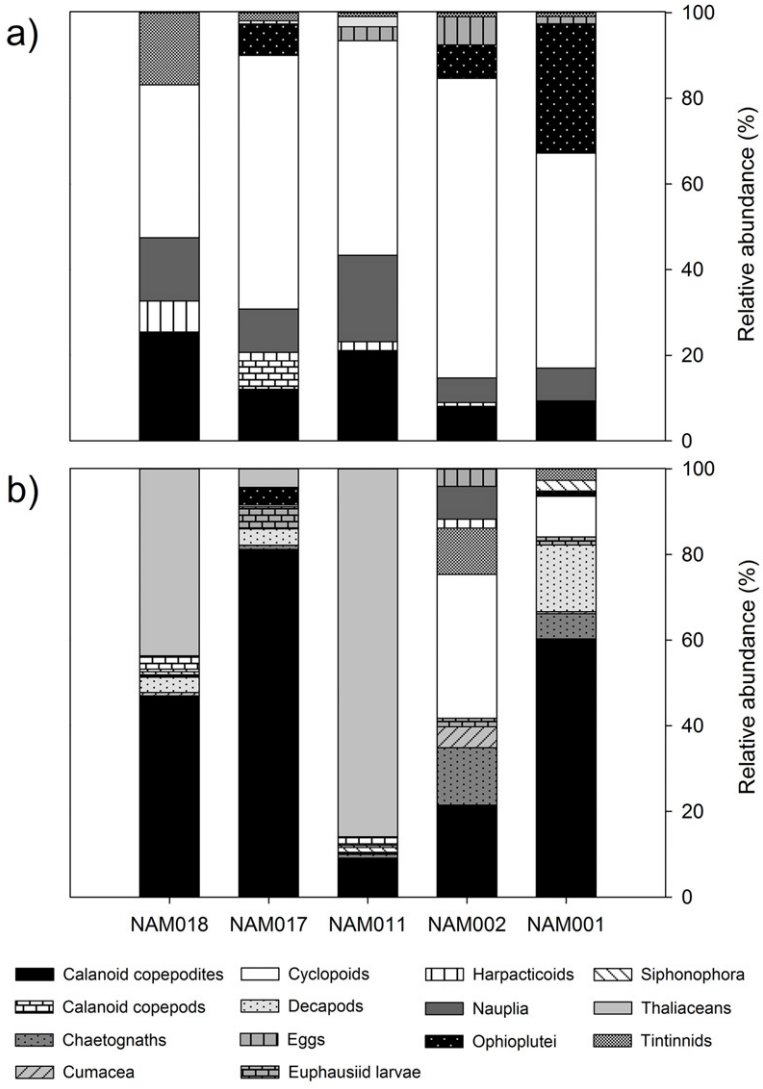

Figure 2.5: Relative abundances of the taxa which contributed to more than 2 % of the zooplankton community abundance in both the 100 - 500 μm (a) and the > 500 μm (b) size classes. Only the upper 25 m of the water-column was considered.

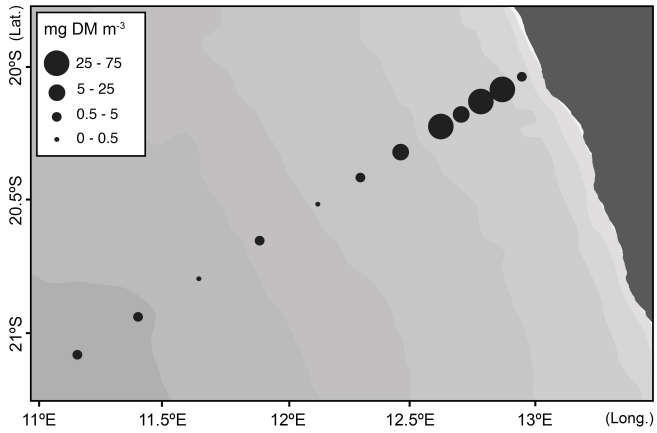

Figure 2.6: Cross-shelf distribution of jellyfish biomass in the upper 200 m of the water-column, except for the five near-shore stations where the bottom depth was shallower.

2.3.2 **Body composition and stable isotopes in zooplankton**

The relationship between organic carbon and DM varied from 0.11 to 0.33, while protein and DM were related by a factor of 0.18 ± 0.05. Nitrogen content averaged 36 % of the protein (see Table 2.1). Furthermore, the resulting C/N atomic ratios of zooplankton ranged between 4.2 and 6.4 (Fig. 2.7), with the values being significantly higher in the transition area (one-way ANOVA, $F_{2,210} = 11.16$, $p < 0.0001$; post hoc Tukey's HSD, $p < 0.0001$). Only the C/N ratios of the microzooplankton (100 - 200 μm) were invariant throughout the transect (one-way ANOVA, $F_{2,50} = 0.27$, $p = 0.765$). Overall, the smaller size classes (100 - 200 μm and 200 - 500 μm) tended to have C/N ratios above 5.2, whereas the larger size classes (500 - 1000 μm and > 1000 μm) tended to have ratios below 5.2.

The averaged zooplankton-δ^{13}C (ranging from −21.3 to −18.9 ‰) revealed variability in the carbon source along the transect (Fig. 2.8). More negative δ^{13}C values were mainly found in the inner stations (Kruskal-Wallis test, $p < 0.005$). In the case of δ^{15}N, the averaged zooplankton-values showed a more pronounced decrease from 11.0 to 4.8 ‰ within the first 100 km (Kruskal-Wallis test, $p < 0.0001$). The individual patterns of the different size categories followed the same shape (data not shown). In addition, with increasing size, the zooplankton exhibited an enrichment in ^{15}N and a depletion in ^{13}C.

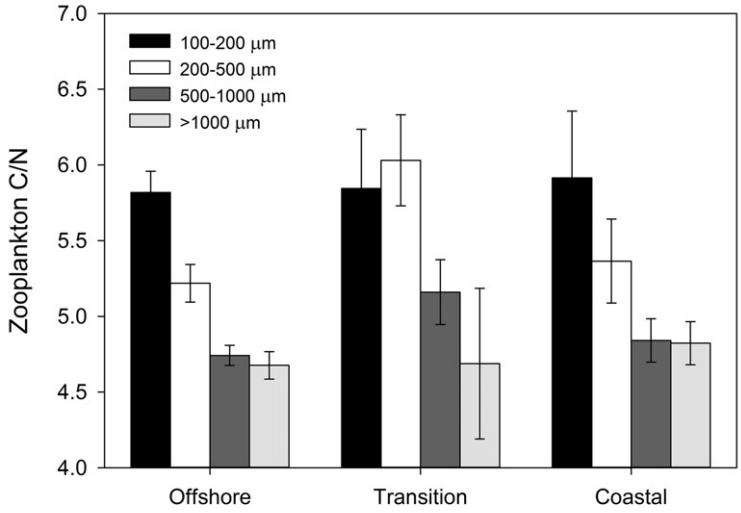

Figure 2.7: Averaged atomic C/N ratios for each size fraction in the different zones. Error bars indicate the 95 % *CI*s.

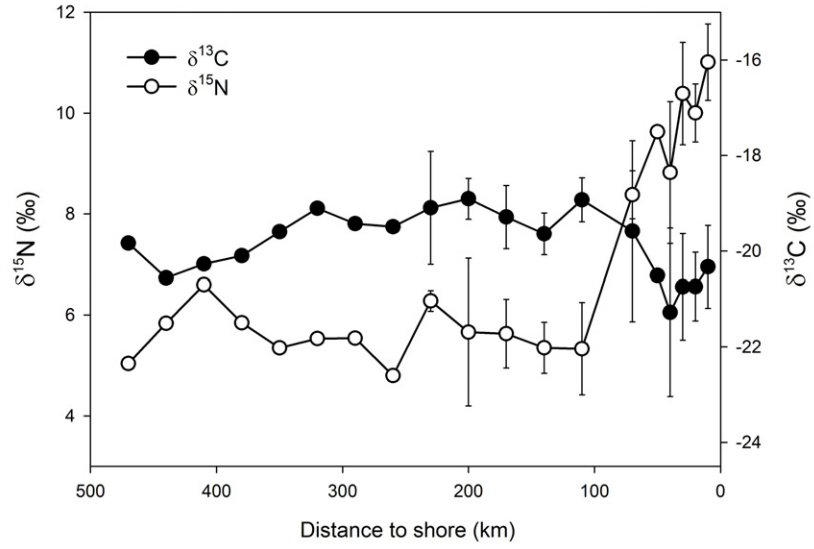

Figure 2.8: Spatial variation of averaged zooplankton δ^{15}N and δ^{13}C values along the transect. Note that each value in the first 230 km comes from the average of the four sections. Error bars indicate the 95 % *CI*s.

2.3.3 **Zooplankton metabolism**

The zooplankton potential respiratory (ETS activity) and potential excretory (GDH activity) rates for the four transects are presented in Fig. 2.9. The highest metabolic activities were measured in late August (i.e., transects 1 and 2), which concurs with the pattern described for the zooplankton biomass. Thus, during the first two transects, the zooplankton enzyme activities exceeded by almost 2-fold the ones measured in mid September (transect 4). A strong gradient in the ETS and GDH activities was also found with distance to shore. Highest metabolic rates were displaced further offshore by the filament during the transects 1 and 2. Accordingly, both enzyme activities peaked between NAM007 and NAM011. Afterwards, these peaks moved inward as the system became more stable and therefore, the zooplankton exhibited higher potential respiration and potential NH_4^+ excretion rates from NAM002 to NAM005. Here in the upper 75 m, the averaged ETS activity was 360 ± 240 μmol O_2 m^{-3} d^{-1}, and the averaged GDH activity was 320 ± 155 μmol NH_4^+ m^{-3} d^{-1}. A second maximum appeared in the surface of NAM023 (transect 4) due to a patch particularly rich in large zooplankton, with values of 490 μmol O_2 m^{-3} d^{-1} and 316 μmol NH_4^+ m^{-3} d^{-1} for ETS and GDH, respectively (Fig. 2.9). The contribution of the smaller zooplankton (100 - 200 μm) to the total NH_4^+ excretion was significantly greater in the near-shore stations (one-way ANOVA, $F_{1,51} = 26.42$, $p < 0.0001$). On the contrary, the high metabolic rates found in the transition waters were mainly associated with the largest size fraction.

Measurable differences in the protein-specific ETS activities were found between regions (one-way ANOVA, $F_{11,196} = 8.53$, $p < 0.001$). GDH activities per unit of biomass displayed similar variability (one-way ANOVA, $F_{11,188} = 15.97$, $p < 0.001$). In general, the zooplankton from the transition area had lower specific rates (Table 2.2). Here, the specific ETS activity of the largest size fraction dropped from 2.72 to 1.28 μmol O_2 mg $protein^{-1}$ h^{-1} (post hoc Tuckey's HSD, $p < 0.001$). This coincided with blooms of salps (Fig. 2.5*b*), which have a lower specific-metabolism. In contrast, the main decrease in the GDH activity was observed in the smaller size classes (100 - 200 μm and 200 - 500 μm), as their rates declined by half to values of around 1.2 μmol NH_4^+ mg $protein^{-1}$ h^{-1} over the transition zone shelf-break (post hoc Tuckey's HSD, $p < 0.001$). The slopes of the regression of log-transformed data for both ETS and GDH scaled to exponents of 1.04 and 0.88 with protein mass, respectively

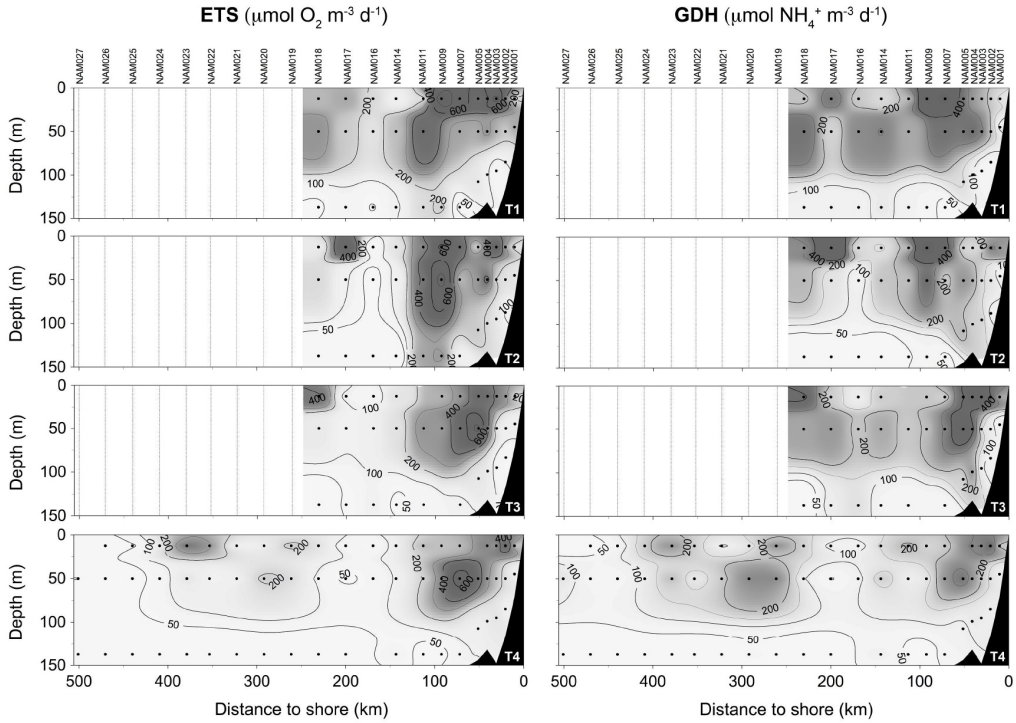

Figure 2.9: Depth-profiles of zooplankton ETS activites (µmol O_2 m^{-3} d^{-1}) and GDH activities (µmol NH_4^+ m^{-3} d^{-1}) for each transect. Sampling dates in 2011 were as follows: 27 Aug. - 30 Aug. (T1), 31 Aug. - 02 Sep. (T2), 08 Sep. - 10 Sep. (T3) and 11 Sep. - 15 Sep. (T4). ODV software was used to generate interpolated values using the weighted averaged gridding method option.

Table 2.2: Mean values (± *SD*) of biomass-specific ETS and GDH activities of size-fractionated zooplankton in coastal (C), transition (T) and offshore (O) stations, averaged over the 200 m water-column.

	Specific ETS (µmol O_2 mg protein^{-1} h^{-1})			Specific GDH (µmol NH_4^+ mg protein^{-1} h^{-1})		
Size (µm)	C	T	O	C	T	O
100 - 200	1.95 ± 0.65	1.98 ± 0.52	2.07 ± 0.45	2.99 ± 0.87	1.16 ± 0.74	2.68 ± 1.16
200 - 500	2.36 ± 0.66	2.23 ± 0.59	2.46 ± 0.46	2.88 ± 1.00	1.58 ± 0.79	3.77 ± 0.87
500 - 1000	2.96 ± 1.14	2.12 ± 0.60	2.61 ± 0.74	2.63 ± 1.01	2.25 ± 1.02	3.41 ± 0.82
> 1000	2.72 ± 0.79	1.28 ± 0.39	1.66 ± 0.60	1.15 ± 0.61	1.15 ± 0.57	2.09 ± 0.81

(Fig. 2.10). These relationships showed positive correlations with a Pearson coefficient of 0.92 for ETS and a non-parametric Spearman coefficient of 0.81 for GDH (in both cases, $p < 0.0001$).

Estimations of the physiological rates of the zooplankton community reflected higher respiration and NH_4^+ excretion at those stations where the primary productivity attained its maximum values (Table 2.3), with the largest size class contributing most (data not shown). However, the phytoplankton carbon which was respired in the upper 75 m by mesozooplankton (from 0.73 to 16.90 mmol C m^{-2} d^{-1}) barely amounted to 1.1 - 10.6 % of what was produced. It is noteworthy that the range of these percentages was wider in mature waters (from 15 to 39 days). Likewise, the potential contribution of the excreted nitrogen (global average = 0.97 mmol NH_4^+ m^{-2} d^{-1}) did not exceed more than the 4.8 ± 2.3 % of the primary producers' requirements. This percentage remained fairly constant irrespective of the system productivity, although zooplankton seemed to fulfill more of the phytoplankton demands in aged waters (see Table 2.3). Overall, the relationship between respiration and NH_4^+ excretion ($R_{O_2}/R_{NH_4^+}$

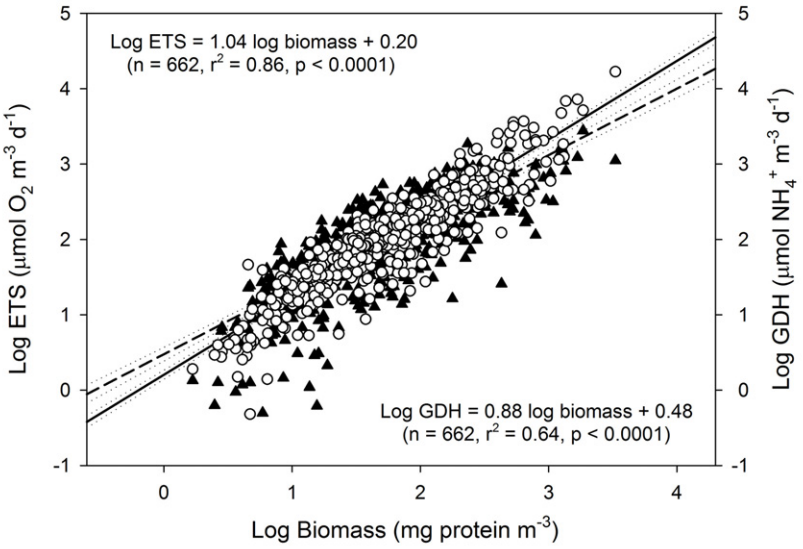

Figure 2.10: Log-transformed ETS activities (open dots and solid line) and GDH activities (black symbols and dashed line) *versus* Log-transformed protein mass. Dotted lines limit the 95 % confidence intervals for each regression line.

Table 2.3: Averaged (± *SD*) net primary production (NPP) for each station, and the respiration and NH_4^+ excretion of zooplankton in the upper 75 m of the water-column. The resultant $R_{O_2}/R_{NH_4^+}$ ratios as well as the range of NPP (%) both respired and regenerated by zooplankton are also presented. Pseudo-age stands for the estimated age of the waters (mean ± *SD*), as detailed in Mohrholz et al. (2014). Note that no *SD*s are given from NAM019 to NAM027 as these stations were sampled just once. A dash indicates data not determined.

Station	Pseudo-age (d)	NPP (mmol C m^{-2} d^{-1})	R_{O_2} (mmol C m^{-2} d^{-1})	% $NPP_{Resp.}$	$R_{NH_4^+}$ (mmol NH_4^+ m^{-2} d^{-1})	% $NPP_{Regen.}$	$R_{O_2}/R_{NH_4^+}$
NAM001	5.3 ± 2.9	64.4 ± 24.2	4.60 ± 1.81	6.9 - 7.2	0.45 ± 0.09	3.7 - 5.5	11.0 ± 8.7
NAM002	7.3 ± 3.4	123.0 ± 14.3	7.24 ± 2.41	4.4 - 7.0	1.01 ± 0.11	5.0 - 5.1	10.3 ± 7.6
NAM003	11.0 ± 1.8	123.7 ± 50.8	10.19± 6.14	5.6 - 9.4	0.95 ± 0.34	4.5 - 5.1	10.3 ± 7.4
NAM004	15.5 ± 4.2	169.7 ± 37.3	12.76± 2.55	7.4 - 7.7	1.60 ± 0.60	4.6 - 6.5	12.2 ± 10.4
NAM005	23.3 ±10.7	184.2 ± 50.4	14.32±10.54	2.8 - 10.6	1.74 ± 0.74	4.6 - 6.4	12.1 ± 7.2
NAM007	31.5 ±16.1	215.2 ± 49.0	14.22± 4.87	5.6 - 7.2	1.44 ± 0.58	3.2 - 4.7	14.5 ± 11.1
NAM009	38.9 ±10.8	210.8 ± 66.7	16.90±11.30	3.9 - 10.2	1.55 ± 1.44	0.5 - 6.6	19.9 ± 13.2
NAM011	70.1 ±18.6	196.4 ± 27.1	9.64 ± 2.79	4.0 - 5.6	0.82 ± 0.19	2.3 - 2.8	15.1 ± 10.8
NAM014	78.2 ± 8.0	109.4 ± 27.0	4.64 ± 1.29	4.1 - 4.3	0.98 ± 0.14	5.0 - 6.2	5.8 ± 2.0
NAM016	74.9 ±11.2	113.7 ± 16.0	3.23 ± 2.18	1.1 - 4.2	0.79 ± 0.35	2.7 - 5.4	4.5 ± 2.5
NAM017	62.5 ±22.9	154.1 ± 53.7	4.65 ± 3.44	1.2 - 3.9	0.93 ± 0.56	2.2 - 4.4	6.6 ± 3.8
NAM018	62.1 ±15.9	110.0 ± 39.4	6.25 ± 2.56	5.2 - 5.9	1.06 ± 0.43	5.4 - 6.1	7.1 ± 2.7
NAM019	68.9	86.3	7.06	8.2	1.60	11.3	5.3
NAM020	68.7	111.0	6.39	5.8	1.12	6.2	6.3
NAM021	67.4	94.1	2.27	2.4	0.61	4.0	4.8
NAM022	82.8	106.1	5.20	4.9	0.47	2.7	12.7
NAM023	85.6	87.7	8.99	10.3	1.25	8.7	8.6
NAM024	86.8	74.1	1.97	2.7	0.59	4.9	4.5
NAM025	100.3	68.1	0.77	1.1	0.22	2.0	5.6
NAM026	104.6	72.9	0.73	1.0	0.16	1.3	6.9
NAM027	104.3	87.8	-	-	-	-	-

ratios) showed higher values in the transition area (from 12 to 20); then, they decreased towards the open ocean to a range of 5 to 13. This means that zooplankton metabolism relied on more protein offshore.

2.4 Discussion

2.4.1 Zooplankton biomass and community structure

The signature of several water masses such as the South Atlantic Central Water (SACW), the East South Atlantic Central Water (ESACW) and the cold filament intrusions from the fresh upwelled waters coexisted in the northern Namibian cell during the study. This coincides with previous findings of Boyd et al. (1987) in the same area. As a result, zooplankton biomass was not distributed uniformly throughout the transect (Fig. 2.2), but displayed strong temporal and spatial gradients caused by the physical forcing. For instance, the upwelling of deep waters rapidly disrupts the structure of the resident biota, and generates an ecological succession in the ageing advected waters. In our study, mature waters rich in nutrients predominated at the end of August over most of the transect, and promoted the enhancement of phytoplankton (Hansen et al., 2014) and eventually of zooplankton, just as the model of Vinogradov et al. (1972) predicted. At this time, zooplankton biomass reached peaks of 65 mg DM m^{-3} in the upper 200 m of the transition area, which agreed with the values reported in Postel (1995) and Postel et al. (2007) in the upwelled waters north of Walvis Bay, but not with the estimates of zooplankton standing stock recorded in quiescent periods (Verheye and Hutchings, 1988; Olivar and Barangé, 1990). The latter research sampled the northern Benguela during the austral autumn, when the upwelling activity is the most sluggish, resulting in a mean biomass of only 26 mg DM m^{-3} for the entire shelf area. This value falls in the range observed in other less productive upwelling systems (Hernández-León et al., 2002; Bode et al., 2005). Here, similar values were measured in September, when filaments were not strongly influencing the transect and thereby, the less productive aged waters dominated in the study area. In general, the low zooplankton biomass found in the newly upwelled waters, increased as it moved seaward to a maximum over the shelf-break. This coincided with the offshore edge of the chlorophyll maxima. Further offshore, the zooplankton biomass decreased dramatically. Such a pattern is in accordance with the spatial trend described in Shannon and Pillar (1986) and Olivar and Barangé (1990). One

exception, however, was found in the surface waters 380 km from the coast (NAM023) in mid September (Fig. 2.4). The extraordinarily high concentration of large organisms (> 1000 μm) at this oceanic station (70 mg DM m^{-3}) was explained by the introduction of SACW waters via the filament (see Fig. 6*e* in Mohrholz et al., 2014). This water still maintained some of its original properties. Accordingly, a successional development in this water mass resulted in a mature plankton community (*sensu* Vinogradov and Shushkina, 1978) dominated by predatory zooplankton in a low chlorophyll environment.

Overall, the zooplankton correlated with the diatom distribution (Fig. 2.11), which argues for a "bottom-up" control over the trophic chain as usually occurs in productive ecosystems (Cury and Shannon, 2004). The dominance of chain-forming diatoms in the transition area might entail, however, a food particle size limitation to the microzooplankton (100 - 200 μm), whose diet relies primarily on both individual phytoplanktonic cells and small microheterotrophs (Irigoien, 2005). Accordingly, their contribution to the total biomass dropped at the shelf edge (Table 2.1). Unfortunately, the coarse taxonomic resolution (Fig. 2.5) constrains our discussion of how the biological forcing, as well as the highly advective environment, disrupted the zooplankton assemblages. In general, the numerical prevalence of copepods that we observed (Fig. 2.5) concurs with investigations of Timonin (1997) and Loick et al. (2005) for the Benguela ecosystem. However, in our study the pelagic copepods peaked near the coast (6751 ind m^{-3}), contrary to the previous findings of maximum densities developing at the outer shelf resulting from advection by Ekman transport (Verheye et al., 1992). Indeed, this offshore transport via filaments together with the inshore upwelling cells, may explain the oceanic occurrence of organisms normally common in neritic waters such as chaetognaths (Gibbons et al., 1992), tintinnids (Dolan et al., 2012) and the benthic harpacticoids that we have documented. Still, other processes such as biological competition may be controlling the pelagic copepod population. With a plentiful food supply, salps can take immediate advantage of their high filtering rates and rapid growth (Ikeda, 1977), so swarms of these tunicates could easily exclude other planktonic grazers over the shelf-break. Thus, the spatial pattern of zooplankton from the Benguela upwelling seems to be determined in the short-term not only by the complex interplay between mesoscale structures, as the satellite images show (Mohrholz et al., 2014), but also by the interspecific relationships linked to the successional development of the water masses.

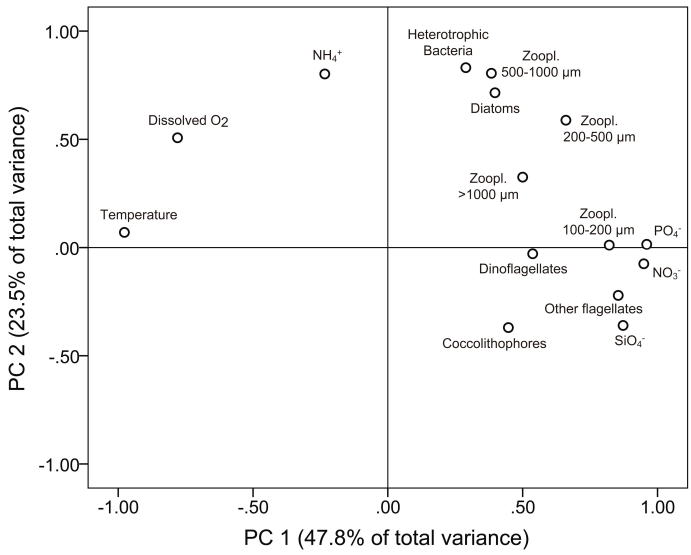

Figure 2.11: Correlation matrix-based principal component analysis plotted according to the hydrographic characteristics (PC 1) and the occurrence of different biological communities (PC 2). Both axes together explained 71.3 % of the total variance. Chemical variables were given in µM units, while the biological ones were correlated in terms of biomass (mg C m^{-3}). Non-normal data sets were previously normalized through the log (x + 1) transformation.

2.4.2 **Body composition and stable isotopes in zooplankton**

The data on elemental composition (Table 2.1) are comparable to DM, carbon and nitrogen content reported for the zooplankton community from the NW Spanish upwelling (Bode et al., 1998). Differences between the three zones were not marked, although a shift in both nutritional source and zooplankton assemblages might explain a slightly higher carbon and nitrogen contribution to the total mass in the transition area. Nonetheless, low carbon content (ranging from 11 to 33 % of DM) in comparison to that measured in polar regions (e.g., from 23.5 to 61.0 % in Ikeda and Skjoldal, 1989) suggests minor lipid storage by the zooplankton in Benguela. In fact, protein is often the dominant metabolic reserve in areas with abundant and constant food supply (Postel et al., 2000). Likewise, atomic C/N ratios were in a range consistent with those found in several groups of mesozooplankton from the northern Benguela (Schukat et al., 2014), and in marine crustaceans in general (Bode et al., 1998).

The larger values in the C/N relationship at the transition zone, however, may reflect a shift in the zooplankton diet (Fig. 2.7). This enhancement, jointly with lower specific-GDH activities (Table 2.2), would result in reduced NH_4^+ excretion rates per unit of biomass in the transition waters (Anderson, 1992). Furthermore, C/N ratios resembled the trend set by the $R_{O_2}/R_{NH_4^+}$ ratios (see Table 2.3), which provide an indicator of the metabolic substrate oxidized for energy. Depending on the amino-acid and the fatty acid involved in the catabolic pathways, the $R_{O_2}/R_{NH_4^+}$ ratio can theoretically range from 3 to infinity (Mayzaud and Conover, 1988). Accordingly, pure protein catabolism is assumed to yield $R_{O_2}/R_{NH_4^+}$ ratios below 13, while a value of around 24 indicates a reliance on both protein and lipids. In our study, offshore, outside of the filament, the $R_{O_2}/R_{NH_4^+}$ ratios were characteristically between 4 and 6, indicating protein-dominated catabolism. This was likely caused by higher indices of carnivory within this area. On the contrary, at the transition zone the $R_{O_2}/R_{NH_4^+}$ ranged between 12 and 20, which would correspond to a more lipid-rich diet.

Additional ecological understanding is achieved through a study of the zooplankton isotopic composition, since the stable isotopes constitute a useful tool to describe the structure of the food web and nutrient dynamics of a given ecosystem. Thus, $\delta^{15}N$ sheds light on the trophic position of organisms as well as on the contribution of isotopically distinct nitrogen sources entering the base of the food chain (Montoya, 2008). $\delta^{13}C$ provides insight into the character of the zooplankton carbon source (Koppelmann et al., 2009). Here we use both isotopes in order to determine potential changes in dietary relationships in the study area. The significance in the spatial variability in $\delta^{13}C$ that we observed was likely caused by changes in food resources from the diverse water masses found along the transect (Fig. 2.8). For instance, zooplankton with small lipid reserves would explain lower $\delta^{13}C$ at the inner shelf (Saupe et al., 1989). Preying more on diatoms, which are enriched in ^{13}C compared to the small flagellates (Fry and Wainright, 1991), would led to less negative zooplankton-$\delta^{13}C$ values in transition waters. On the other hand, the differences in $\delta^{15}N$ signatures were remarkably greater than the corresponding differences in the $\delta^{13}C$ signatures. This likely originated in the source of the nitrogen utilised by phytoplankton rather than in species succession processes, since the same trend was followed by all the size fractions. Thus, upwelled nitrate near the coast is expected to be enriched in ^{15}N through bacterial remineralization in deep waters. This resulted in a progressive phyto-

plankton enrichment in ^{15}N as the primary producers removed dissolved nitrate over the shelf waters (O'Reilly et al., 2002; Bode and Álvarez-Ossorio, 2004). Farther offshore, $\delta^{15}N$-depleted nitrogen-species, such as N_2 fixed by diazotrophs or NH_4^+ excreted by heterotrophs, could become dominant in supporting the primary production and therefore, lower $\delta^{15}N$ signatures would be propagated into the other components of the trophic chain. Differences in the number of intermediary trophic levels which are channeling the mass transfer through the food web could also explain such a variability, but isotope reference values for phytoplankton would be necessary for confirmation.

2.4.3 **Zooplankton metabolism**

In seeking an understanding of the carbon balance it is important to know whether the heterotrophs consume all the primary productivity or whether there is some fixed carbon left over to be exported to the bottom (Ducklow and Doney, 2013). This will depend on the level of primary productivity which will be limited by nitrogen, among other elements. In this scenario, zooplankton metabolism impacts both carbon and nitrogen cycles, with environment, season and taxonomy modulating its biogeochemical role. Compared to shelf waters of other upwelling case studies where zooplankton respiration and NH_4^+ excretion in the upper 200 m varied from 7.5 to 103.1 μmol O_2 m^{-3} d^{-1} and from 0.2 to 5.4 μmol NH_4^+ m^{-3} d^{-1}, respectively (Packard et al., 1974; Hernández-León et al., 2002; Isla and Anadón, 2004; Pérez-Aragón et al., 2011), here zooplankton consumed on average more oxygen (112.4 μmol O_2 m^{-3} d^{-1}) and released more NH_4^+ (10.3 μmol NH_4^+ m^{-3} d^{-1}). In spite of this elevated respiration and NH_4^+ excretion, when compared to the net primary productivity (NPP), the relative values of these two processes were consistent with those measured in NW Africa (Packard, 1979) and in Benguela (Chapman et al., 1994).

The respiratory carbon demand of zooplankton averaged 7.1 ± 4.7 mmol C m^{-2} d^{-1} in the whole transect (Table 2.3). According to the energy budget approach given in Ikeda and Motoda (1978), the ingestion rate can be derived from the respiration by a factor of 2.5. This means that the zooplankton would remove between 6.0 and 29.5 mmol C m^{-2} d^{-1} in the upper 75 m of the water-column, i.e., about 14 % of mean daily (net) production if we assume major herbivory and an assimilatory efficiency of 70 % (Kiørboe et al., 1985). These estimates are slightly higher than the average copepod consumption rates re-

ported by Schukat et al. (2013b) for the northern Benguela (1.8 - 6.5 mmol C m^{-2} d^{-1}). Even though Hernández-León and Ikeda (2005) calculated a mesozooplankton carbon demand ranging from 34 to 63 % of the global primary productivity, the percentage drops more than three times in eutrophic ecosystems (Calbet, 2001), which encompasses our approximations. It is known that microheterotrophs' grazing often accounts for most of the phytoplankton production, but will these organisms be able to consume the remaining carbon in such a productive system? Parallel research with bacteria during the same cruise (Bergen et al., 2015) calculated that a consumption of around 29 % of the net production was necessary to sustain their metabolic carbon requirements in the upper 75 m (43 mmol C m^{-2} d^{-1}). In addition, estimations of Chapman et al. (1994) suggested that microplankton would double the carbon losses attributable to zooplankton (i.e., ~ 28 % of the NPP in our case study). Considering the top predators and large gelatinous zooplankton as minor sinks for phytoplankton biomass, it seems reasonable to presume that the system was autotrophic during the active upwelling season. In other words, there was a surplus of net production to be exported. In support of this, estimates by Osma et al. (2014) revealed that an average of about 23 % of the NPP was either respired in the water column below 75 m or deposited in the sediments. Some of the remaining NPP was likely exported by the filament towards the open ocean.

The contribution of zooplankton NH_4^+ excretion to the phytoplankton productivity (Table 2.3) was also limited (0.5 - 11.3 %). Although a secondary role might be expected for remineralization in areas with large inputs of new nitrogen, there is no obvious pattern about the importance of zooplankton in fueling the primary productivity throughout different ecosystems (Bronk and Steinberg, 2008). Here, the zooplankton did not seem to be a key component of the total NH_4^+ regeneration via excretion processes. Our results were comparable with the mesozooplankton regeneration in the upwelling off NW Spain (Bode et al., 2004; Isla et al., 2004a). Accordingly, dissolved NH_4^+ displayed a weak correlation with zooplankton distribution (Fig. 2.11), although some caution about this interpretation is needed as the NH_4^+ has a very rapid turnover. In fact, remineralized nitrogen (Benavides et al., 2014) and phosphorus (Nausch and Nausch, 2014) were found necessary to support the large phytoplankton biomass at 20° S. This may reveal a major remineralization pathway through microheterotrophs as Probyn (1987) found for the southern Benguela. Despite

the dynamics of zooplankton metabolism in both the time and space domain, we conclude that it had little impact on the NPP in all the different productivity regimes within the Namibian system.

On a physiological basis, the indices of metabolism did not sharply respond to the patterns of chlorophyll-a and productivity. While phytoplankton biomass declined in the transition area, likely due to the grazing pressure and nutrient depletion, high values of specific-ETS activities remained relatively constant from the rich upwelled waters to the oceanic ones (Table 2.2). Longer life cycles allow zooplankton to reside longer in the water-column than the phytoplankton, so they are more intensely subjected to both advection and active transport seaward. During this process, the zooplankton diet shifts gradually into omnivory (Hernández-León et al., 2002), which would sustain a highly active metabolism even offshore. Indeed, more carnivory would explain the decrease in zooplankton biomass and a more protein-based metabolism (as denoted by lower $R_{O_2}/R_{NH_4^+}$ ratios) towards the ocean. In contrast, specific-GDH activities fell in the highly productive transition waters, similar to the findings of Hernández-León et al. (2001) in Canary Islands waters. Those authors showed negative correlations between GDH and both zooplankton gut content and chlorophyll-a. In fact, GDH activity not only depends on the intracellular substrate availability, but also on the energy charge of the organisms. As the guanosine-5'-triphosphate (GTP) levels increase in response to the nutrient-sufficient metabolic states, GDH should be inhibited and, rather than being deaminated, amino acids such as glutamate could be used for growth and protein biosynthesis (Bidigare and King, 1981). Thus, the enhanced $R_{O_2}/R_{NH_4^+}$ ratios over the shelf-break implied a decrease in protein catabolism. Independently of these internal adjustments in zooplankton biochemistry, both enzymatic indices showed good correlations with biomass, reflecting their constitutive nature as permanent components of living cells. Scaling exponents of 1.04 and 0.88 (Fig. 2.10) revealed nearly isometric relationships between the potential respiration or NH_4^+ excretion and protein-biomass, which appears to be a common feature in the metabolism of pelagic organisms (Glazier, 2006). This means that both ETS and GDH activities covary linearly with biomass. However, short-term fluctuations in the environmental conditions might force the physiology to diverge from biomass more rapidly than do the potential rates, resulting in different scaling exponents. This would impact both R_{O_2}/ETS and GDH/$R_{NH_4^+}$ ratios (Berges et al., 1993; Fernández-Urruzola

et al., 2011), but its influence would not be great enough to deter the use of these enzymes as ecological indices.

2.5 Conclusions

The distribution of zooplankton biomass as well as the impact of its metabolism on the northern Namibian phytoplankton community during active upwelling have been described here. Our results are in broad agreement with previous findings from this system. Zooplankton biomass and metabolic rates fluctuated highly with the upwelling filaments, but their maxima were characteristically observed over the outer shelf. Thus, there was a horizontal zonation determined by the hydrographic and hydrochemical conditions. The pelagic copepods dominated the zooplankton in all parts of the transect. Nevertheless, the structure of the community was strongly altered by salp blooms over the shelf-break. On average, the elemental composition of zooplankton indicated low lipid storage in the study area. This was more noticeable in neritic waters, where plankton with lower $\delta^{13}C$ such as flagellates constituted the main carbon resource for zooplankton. In addition, the spatial pattern of zooplankton-$\delta^{15}N$ in the ageing advected waters revealed a progressive substitution of the nitrogen-species that sustained the biological production.

The zooplankton respiration and NH_4^+ excretion rates in the highly productive waters of the northern Benguela exceeded those measured in other upwelling systems. Still, this respiration consumed just a small proportion of the daily primary production (1.1 - 10.6 %). Accordingly, the northern Benguela ecosystem acted as an autotrophic system during the intense wind-forcing season. High protein-specific respiration rates over the entire transect suggested an enhancement in omnivory over herbivory in the low-chlorophyll offshore area. This also explains the decrease in zooplankton biomass and the increase in protein-catabolism towards the open ocean. Parallel with the respiration, zooplankton NH_4^+ excretion only contributed 0.5 to 11.3 % of primary production's nitrogen requirements. Therefore, most of the organic matter produced in these Namibian waters should be recycled through the microbial food web.

Acknowledgements. We wish to thank the crew of the RV Maria S. Merian for their assistance during the cruise, and the researchers involved in collecting the samples. We are also grateful to I. Martínez for the protein determinations, to A. Herrera for her collaboration in ETS measurements, to I. Liskow for the isotopic analyses as well as to S. Rubin for the taxo-

nomic characterization. Furthermore, N. Wasmund kindly lent us his ^{14}C data. Comments from anonymous referees also contributed in improving the manuscript. This work was funded by the German Research Foundation (DFG) cruise support and by the BIOMBA project (CTM2012-32729/MAR). The latter was granted to M. Gómez by the Spanish Economy and Competitiveness Ministry. I. Fernández-Urruzola and N. Osma received financial support from the Formation and Perfection of the Researcher Personal Program from the Basque Government. T.T. Packard was partially supported by a grant from the Leibniz Institute for Baltic Sea Research.

If I have seen further it is only by standing on the shoulders of giants.

Sir Isaac Newton

CHAPTER

3

CAPÍTULO

Modeling downward particulate organic nitrogen flux from zooplankton ammonium regeneration in the northern Benguela

I. Fernández-Urruzola, N. Osma, M. Gómez, F. Pollehne, L. Postel and T.T. Packard, Submitted to Progress in Oceanography.

Submission ID: PROOCE-2015-42. ***Major revisions.***

ABSTRACT: The vertical fluxes of particulate organic matter play a crucial role in the distribution of nutrients throughout the oceans. Although they have been the focus of intensive research, little effort has been made to explore alternative approaches that quantify the particle export at a high spatial resolution. In this study, we assess the downward nitrogen flux (F_N) in the northern Benguela from ocean depth profiles of zooplankton NH_4^+ excretion ($R_{NH_4^+}$) during the active upwelling season. The reduction of $R_{NH_4^+}$ as a function of depth was described by a power law fit, $R_{NH_4^+} = (R_{NH_4^+})_m\ (z/z_m)^b$, whereby the b-value determines the net particulate nitrogen loss with increasing depth. Integrating these excretory functions from the base of the euphotic zone to the ocean bottom, we calculated F_N at two stations located over the Namibian outer shelf. Estimates of F_N (ranging between 0.68 - 1.18 mmol N m^{-2} d^{-1}) were compared with the sinking rates of particles collected in sediment traps (0.15 - 1.01 mmol N m^{-2} d^{-1}) 50 m over the seafloor. We found a reasonable agreement

between the two approaches when fast-sinking particles dominated the ecosystem, but the F_N was somewhat at odds with the measured gravitational flux during a low-sedimentation regime. Applying our conceptual model to the mesozooplankton $R_{NH_4^+}$ we further constructed a section of F_N along a cross-shelf transect at 20° S, and estimated the efficiency of the epipelagic ecosystem to retain nutrients. Finally, we address the impact of the active flux driven by the migrant mesozooplankton to the total nitrogen export. Depending on the sedimentation regime, the downward active flux (1.01 mmol N m^{-2} d^{-1} at 150 m) accounted for between 59 - 361 % of the gravitational flux.

Keywords: Zooplankton; Dissolved inorganic nitrogen (DIN); Glutamate dehydrogenase (GDH); Ammonium excretion; Benguela upwelling system.

3.1 Introduction

Particulate organic matter (POM) export down to the deep ocean is a critical mechanism in understanding the carbon balance across the air-sea interface. Carbon and inorganic nutrient salts are converted in the epipelagic ocean into organic matter mainly by phytoplankton, and rapidly regenerated through heterotrophic processes. This fuels the biological production by direct feedback loops within the relatively thin sunlit layer. In productive ecosystems such as the Benguela upwelling system, the phytoplankton growth rates often exceed the grazing pressure and as a result, either advection or gravitational settling processes gain importance in the biogenic material loss. Indeed, some authors have demonstrated an export flux out of the euphotic zone as high as 25 % in coastal upwellings (Martin et al., 1987; Buesseler, 1998; Osma et al., 2014). Most of these sinking particles undergo a suite of biologically-mediated chemical transformations while falling down through the ocean water column, which cause the speciation of carbon and associated elements (i.e., nitrogen and phosphorus) into their inorganic forms. Factors such as particle composition, community structure and ambient temperature will determine the decline of this downward POM flux with increasing depth. In addition to the rain of POM, the mixing of dissolved organic matter along isopycnals and the active downward transport by migrating zooplankton act as a complex network collectively known as the "biological pump" (Volk and Hoffert, 1985). All these processes together constrain the upper limit of the dark ocean metabolism (Arístegui et al., 2009) as well as the capacity to sequester elements in the

ocean interior (Packard et al., 1988; Ridgwell et al., 2011).

Surface primary productivity, vertical flux and heterotrophic consumption below the photic layer have been traditionally related by means of direct measurements of trap-collected particles, despite the recognition that some biases affect the sediment traps efficiency (Gardner, 2000). These methodological uncertainties may partially explain the apparent carbon budget imbalances (Burd et al., 2010), and foster efforts to explore complementary approaches to estimate global export fluxes. Oceanic depth profiles of both plankton respiration, as principal component involved in POM attenuation, and thorium-234 radionuclide have also been fruitfully applied to trace particle utilization through the ocean water columns (e.g. Packard et al., 1988; Buesseler, 1991; Steinberg et al., 2008; Maiti et al., 2010). In this line, Packard and Christensen (2004) employed enzyme activity measurements of electron transport system (ETS) to model vertical carbon flux by integrating plankton respiration from the bottom of the mixed layer to the seabed. Both processes are closely related, mathematically described by a potential function, and therefore each can be calculated from the other. This approach based on enzymology was subsequently used to assess the carbon transference by zooplankton down to 3000 m in waters from Canary islands (Packard and Gómez, 2013), and compared with sediment-trap measurements in the mesopelagic zone from the northern Benguela (Osma et al., 2014, –see *Appendix* AIII.1, this thesis–). It was precisely on a plankton respiration basis that Packard et al. (2015) modeled a synoptic section of carbon flux in the Peru upwelling system, and demonstrated the utility of this approach to quantify the ability of an ocean layer to retain its nutrients. Here we extrapolate this concept into nitrogen metabolism in a first attempt to perform similar nitrogen flux calculations. In order to achieve this goal, we assayed glutamate dehydrogenase (GDH), a widespread enzyme in nature whose role in the oxidative deamination of glutamate argues for its control over a great proportion of ammonium (NH_4^+) production in marine ecosystems. The rationale behind this conceptual model is the assumption that the resident deep-sea zooplankton and smaller microheterotrophs consume sinking particulate organic nitrogen (PON), among other non-conservative elements, to satisfy their metabolic requirements. As a result, these organisms release NH_4^+ as part of the dissolved inorganic nitrogen (DIN) pool, as well as other organic nitrogenous compounds either in the dissolved (urea and amino acids) or particulate (fecal pellets) forms. Although these organic end-products may represent

a significant budget in the nitrogen export (Steinberg et al., 2002), we focus on NH_4^+ excretion processes because they account for 60 - 100 % of the total nitrogen excreted by marine zooplankton (Regnault, 1987). At the intracellular biochemical level, NAD^+-specific GDH activity is thought to be responsible for most of the NH_4^+ synthesis in heterotrophs and consequently, it should provide a good index of NH_4^+ regeneration in seawater. Furthermore, such an enzymatic technique would allow a high data acquisition rate and enough sensitivity to detect excretion processes even in the deep ocean, while obviating methodological artifacts associated with direct metabolic analyses involving water-bottle incubations (Bidigare, 1983).

In the present study we calculate downward particulate nitrogen flux from the integration of nano/micro- and mesozooplankton NH_4^+ excretion depth profiles, and compare our modeled flux with *in situ* measurements of nitrogen collected by two sediment traps moored in waters off Namibia. Previously, we investigated in that same region the carbon losses from the water column respiration and demonstrated the influence of particle composition on the carbon attenuation efficiency (Osma et al., 2014). Changes in the flux attenuation, i.e., in the curvature of either respiration or NH_4^+ excretion depth profiles, will ultimately affect the capacity of epipelagic ecosystems to retain their nutrients (Packard et al., 2015, –see *Appendix* AIII.2, this thesis–) and thereby, to maintain a high regenerated production. Further, we address the relevance of zooplankton diel migrations at 20° S as important drivers of active nitrogen flux relative to the vertical export of PON. The research was conducted in the northern Benguela current since these waters represent an interesting scenario for the vertical nutrient exchange, which should result in a balance between the downward transference of PON and the upwelling flux of DIN (Longhurst and Harrison, 1989). Nevertheless, the nitrogen transfer down to the seafloor will vary in the short-term according to the fluctuations in the upwelling pulses. In this context, we show how the different productivity regimes impact the vertical recycling of PON off the Namibian coast.

3.2 Material and methods

3.2.1 Zooplankton sampling

Sampling was carried out in waters off Terrace Bay (Namibia) onboard RV Maria S. Merian during the austral winter from August 24th to September

17th, 2011. Nano/microzooplankton (0.7 - 100 μm) and large zooplankton (>100 μm) GDH profiles were performed at those stations in which sediment-traps were placed. Accordingly, two traps were successively moored for 13 days at an inshore station (NAM006), and 10 days over the shelf-break at an offshore station (NAM011) (see Fig. 3.1). Both locations were, in any case, situated under the influence of mesoscale structures such as upwelling pulses and filaments emerging from the southern perennial cell. Water column samples for GDH activities were first taken as the shallower sediment-trap was recovered (NAM006r) and then, during the outer trap deployment (NAM011d) and subsequent recovery (NAM011r). In addition, mesozooplankton was collected in four consecutive surveys throughout a cross-shelf transect at 20° S, which covered 12 stations along 230 km from the shore (broadly described by Fernández-Urruzola et al., 2014, –*Chapter* 2, this thesis–). NAM011 was sampled during both day (07:06 - 18:54 h) and night (18:55 - 07:05 h) in order to quantify the magnitude of diel vertical migrations.

Hydrographic data (salinity, temperature and dissolved oxygen concentration) were recorded by casting a CTD SBE 911+ equipped with a WETlab FLRT-1754 fluorometer. Chlorophyll-a concentrations were likewise determined in water samples taken by 10-L Niskin bottles mounted on a rosette. Seawater from eight (NAM006r) to nine (NAM011d/r) discrete depths were collected for nano/microzooplankton (below 100 μm) GDH activities. After sieving through a 100 μm mesh size, 4 - 6 L of seawater (depending on organism densities at each depth) were filtered at room temperature by GF/F glass fiber filters. Phytoplankton would not interfere in our measurements as their NAD^+-specific GDH activity is negligible (King, 1984; Park et al., 1986). Furthermore, large zooplankton were sampled for vertical distribution using a Multinet (Hydrobios GmbH, Kiel, Germany), fitted with 100 and 500 μm meshed nets which ensured a quantitative zooplankton sampling between 0.1 - 0.5 mm and 0.5 - 10 mm sizes, respectively. Two flowmeters installed on the net-frame quantified the volume of water filtered during each haul. In this case, five (NAM006r) to six (NAM011d/r) depth layers were considered to calculate zooplankton GDH vertical profiles, whereas three depth intervals were used to assess active transport in the upper 200 m along the transect. Once on deck, the samples were immediately fractionated for the 100 - 200, 200 - 500, 500 - 1000 and > 1000 μm size classes, frozen in liquid nitrogen and stored at −80 °C awaiting enzymatic analyses in the land based laboratory.

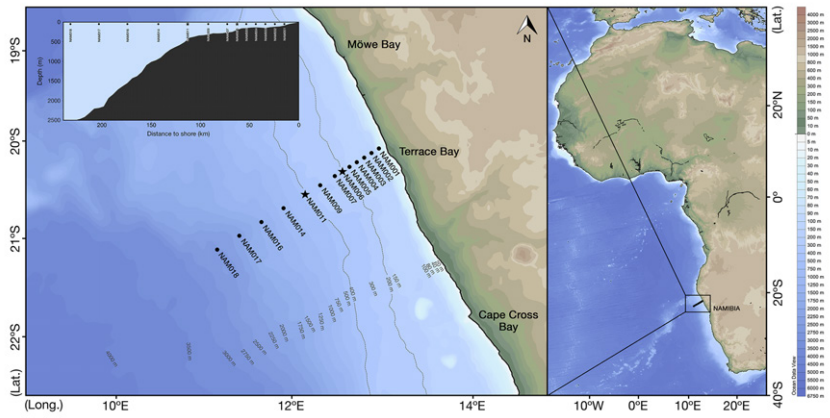

Figure 3.1: Cross-shelf transect off the northern Namibian coast surveyed during the SUCCESSION cruise (2011). 13 stations were considered over a distance of 230 km from the Terrace Bay. Dots represent the stations where only zooplankton was collected by Multinet vertical hauls. Stations NAM006 and NAM011 (depicted by star symbols) were sampled for nano/microzooplankton and mesozooplankton. Sediment trap moorings were deployed at these two stations, which coincided with the outer limit of the inner shelf and the shelf-break (NAM006 and NAM011, respectively –see dashed lines–).

3.2.2 NH_4^+ excretion rates in terms of GDH activity

GDH activities were measured kinetically following the procedure of Bidigare and King (1981), slightly modified by applying spectrofluorometry as described in Fernández-Urruzola et al. (2011). This change improved the sensitivity at depths where nano/microzooplankton densities were extremely low (< 8 µg protein L^{-1}). Accordingly, the linear increase of fluorescence linked to the enzymatic NADH production was monitored during 4 minutes. Some samples were assayed in duplicate to check the possible contribution of $NADP^+$-specific GDH isozyme that has been found in certain protozoa (Santero et al., 2012). We added 0.25 mM $NADP^+$ to the assay, but no more GDH activity was detected as compared to the correspondent samples without $NADP^+$. The assay was carried out at 18 °C, so an activation energy of 10 Kcal mol^{-1} (calculated from Park et al., 1986) was used to recalculate *in situ* potential activities by Arrhenius equation. The protein content of each sample was then analyzed following the procedure described by Lowry et al. (1951). Biomass in terms of N was derived from protein using a factor of 0.36 provided

by Fernández-Urruzola et al. (2011) for the same pelagic community.

Water-bottle incubations were additionally conducted on board in order to assess actual NH_4^+ excretion rates from a specific GDH/$R_{NH_4^+}$ ratio for the northern Benguela Current. Zooplankters were collected by 200 μm meshed WP-2 net vertical hauls, fractionated into the aforementioned size classes and maintained at sea surface temperature (15 ± 1°C) for acclimation. Afterwards, 6 - 8 healthy organisms were transferred into capped glass bottles (60 mL each) filled with filtered seawater, and incubated at 14 °C for 2 h. Such a short incubation-time avoids artifacts derived from starvation. All the experiments included one control flask without zooplankters. Water samples (10 mL) were siphoned off from each bottle at the end of the incubation so as to determine NH_4^+ concentrations in accordance with the phenol-hypochlorite method (Solorzano, 1969). Dissolved NH_4^+ concentrations measured in the control flasks were subtracted from the NH_4^+ in the experimental ones. Organisms were then removed from the bottles and frozen at −80 °C to assay GDH activities as described above. As a result, an averaged GDH/$R_{NH_4^+}$ ratio of 16.7 (r^2 = 0.49, n = 26, $p < 0.0001$, *SEE* = ± 23.3 %) was used to estimate $R_{NH_4^+}$ in the large zooplankton (size classes over 100 μm) from potential GDH measurements through the water column. An additional GDH/$R_{NH_4^+}$ relationship of 4.43 (r^2 = 0.66, n = 11, $p < 0.01$, *SEE* = ± 17.9 %) was applied to assess $R_{NH_4^+}$ associated with the smaller nano/microzooplankton, as was found in an early study on organisms below 100 μm collected in waters from the North Atlantic and identically assayed (see *Chapter 4*, this thesis). The errors associated with these ratios have been widely discussed in previous works (King and Packard, 1975; Hernández-León and Gómez, 1996), and are comparable with the errors found in other standard techniques for metabolic processes (del Giorgio, 1992). Furthermore, our ratios fall in the range of those reported in the literature (see Table 3.2 in Fernández-Urruzola et al., 2011).

The $R_{NH_4^+}$ determined at different depths from the GDH activities served to generate modeled profiles of heterotrophic $R_{NH_4^+}$ by fitting the power function to the original values. In fact, the power function that takes in the form of,

$$R_{NH_4^+} = (R_{NH_4^+})_m \, (z/z_m)^b \tag{3.1}$$

not only explains the measured $R_{NH_4^+}$ at a significant level ($p < 0.001$), but it is also consistent with previous descriptions of the vertical distribution of particle attenuation and plankton metabolism (e.g. Martin et al., 1987; Packard

and Christensen, 2004; Buesseler et al., 2007; Osma et al., 2014; Packard et al., 2015). Note that depth-normalization is necessary to keep the equation units balanced.

3.2.3 Nitrogen flux calculations from nano/microzooplankton and mesozooplankton $R_{NH_4^+}$ profiles

The basis of this approach lies in modeling vertical profiles of heterotrophic $R_{NH_4^+}$ as a continuous function of depth (z). Here, one must consider that nano/microzooplankton jointly with the mesozooplankton play a key role in transforming sinking PON mainly into NH_4^+, and assume that the NH_4^+ excreted at a certain depth should equal the difference between the particulate nitrogen entering from above ($F_{N_{Z_1}}$) and the remaining PON which is still available for the metabolism of deeper layers ($F_{N_{Z_2}}$) under steady state conditions (*sensu* Sverdrup et al., 1942). This can be mathematically expressed as,

$$(R_{NH_4^+})_{z_1-z_2} = F_{N_{Z_1}} - F_{N_{Z_2}} \tag{3.2}$$

in the one-dimensional vertical flow case study. Note that the lateral advection of PON compared to the downward PON flux should not be relevant in this scenario. Accordingly, the minimum vertical PON flux needed to support all the NH_4^+ regeneration in the water column, could be calculated by integrating a depth-normalized $R_{NH_4^+}$ profile from the surface (z_t) down to the seafloor (z_s), as represented in Eq. 3.2:

$$F_N = \int_{z_t}^{z_s} R_{NH_4^+}\, dz = \int_{z_t}^{z_s} (R_{NH_4^+})_m\, (z_t/z_m)^b\, dz \tag{3.3}$$

where $(R_{NH_4^+})_m$ stands for the hypothetical NH_4^+ being excreted per unit time at the surface, and the exponent b determines the curvature of the power function of best fit to each $R_{NH_4^+}$ vertical profile (see results). That is to say the more negative b-value, the greater is the decrease of $R_{NH_4^+}$ with depth. Thus, one may apply these continuous mathematics to calculate the vertical F_N from any given depth in the water column (z_f) to the bottom, as follows:

$$F_{N_{f-s}} = \{(R_{NH_4^+})_m / [(b+1)\, z_m^b]\}\, (z_s^{b+1} - z_f^{b+1}) \tag{3.4}$$

Nevertheless, equation 3 would be only representative of F_N at depths

without photosynthetic production (i.e., below the euphotic zone), as phytoplankton generate large amount of PON from the assimilation of inorganic nitrogen in the sunlit layer. This is the same restriction that applies to the carbon flux models of Packard and Gómez (2013), Osma et al. (2014) and Packard et al. (2015).

From the calculated F_{N} one can also derive other biogeochemical parameters such as the nutrient retention efficiency (NRE) (Packard et al., 2015), which stands for the capacity of each depth layer to retain nutrients. It is mathematically defined as,

$$NRE_{z_1-z_2} = \left(\int_{z_2}^{z_1} R_{\mathrm{NH_4^+}} \, \mathrm{d}z \right) / F_{\mathrm{N}_{z_1}} \tag{3.5}$$

3.2.4 Active F_{N} driven by diel migrators

Downward F_{N} out of the 150 m driven by the migratory fraction of the community was studied at station NAM011. According to Postel et al. (2007), we assume that most of the migrant zooplankton in the northern Benguela reside in the uppermost 150 m for 12 h during the night. The active F_{N} was calculated by two alternative approaches for comparison: First, we calculated the active flux following our modeling approach ($F_{\mathrm{N_M}}$). As described previously, we fitted a power function to the measured $R_{\mathrm{NH_4^+}}$, and integrated that depth-normalized profile to the bottom (Eq. 3.3). The difference between the F_{N} at $\mathrm{E_z}$ depth and 150 m equals the PON (mmol N $\mathrm{m^{-2}\ d^{-1}}$) that is consumed within that layer (N_{M}). The $F_{\mathrm{N_M}}$ would result from subtracting the daytime N_{M} from the correspondent nighttime value. Secondly, we used the mesozooplankton biomass and the specific metabolism, measured at *in situ* temperature, to calculate the PON consumption (N_{B}) at both day- and nighttime. This approach is based in the concept explained by Dam et al. (1995):

$$N_{\mathrm{B}} = BM_{\mathrm{z}} \times \text{ spc-}(R_{\mathrm{NH_4^+}}) \times 12\,(\mathrm{h}) \tag{3.6}$$

where N_B is the nitrogen consumption rate by the mesozooplankton (mmol N $\mathrm{m^{-2}\ d^{-1}}$), BM_{z} is the biomass of the mesozooplankton (g N $\mathrm{m^{-2}}$), and spc-($R_{\mathrm{NH_4^+}}$) is the biomass specific-$R_{\mathrm{NH_4^+}}$ (mmol $\mathrm{NH_4^+}$ g $\mathrm{N^{-1}\ h^{-1}}$). To determine the equivalent active flux as a function of the migratory biomass ($F_{\mathrm{N_B}}$), we subtracted the N_{B} during daytime from the nighttime N_{B}.

Active flux was then compared to trap flux at 150 m. For this purpose, we extrapolated the measured PON flux from 320 m to 150 m after Martin et al. (1987), where

$$\mathrm{PON}_{flux_{150\,\mathrm{m}}} = \mathrm{PON}_{flux_{320\,\mathrm{m}}} \times (150\,\mathrm{m} / 320\,\mathrm{m})^{-0.858} \tag{3.7}$$

3.2.5 **Sediment trap measurements**

Sinking particles were collected at 150 m (NAM006) and 320 m (NAM011) using automatic sediment traps (Kiel Multitrap K/MT 234) with 0.5 m^2 sample area. Each sediment trap was equipped with 21 collecting glasses, programmed to sample every 24 h. The sampling vials contained a salt brine of 70 ‰, and were filled with a preserving solution consisting of 2 % formaldehyde. Once the traps were recovered, an aliquot of the samples was filtered through pre-combusted Whatman GF/F filters for the analysis of particulate carbon and nitrogen. Filters were frozen at −20 °C until analyses in the land-based laboratory, by means of a Carlo Erba/Fisons 1108 elemental analyzer.

3.2.6 **Statistical analyses**

Statistical analyses were performed using SPSS (Statistical Package for the Social Sciences), version 22.0. Data distribution was analyzed by the Kolmogorov-Smirnov test. A one-way ANOVA was applied to determine statistical differences between logarithmic, exponential and potential functions fitted to the NH_4^+ excretion data in Sigmaplot v12.5. Statistical differences between the settling rates of organic matter and the calculated F_N, as well as the significance between the active F_N calculated by the two approaches were analyzed through a Student *t*-test.

3.3 **Results**

3.3.1 **Ocean setting**

The oceanographic properties at 20° S during the SUCCESSION cruise are fully described in Mohrholz et al. (2014). Hydrological and hydrochemical data revealed an irregular pattern in the water masses distribution, rather than a continuous flow of the newly upwelled waters towards the open ocean. Accordingly, there was a short-term spatio-temporal variability of the chlorophyll-

a concentration along the transects (Fig. 3.2*a*). Remote sensed sea surface temperature data (Fig. 8*a-e* in Mohrholz et al., 2014) evidenced the influence of a stable filament structure, colder and more productive than the surrounding waters, on most of the stations from 24th August to 3rd September. This filament generated a peak of chlorophyll-a further offshore during the transect 1 (T1), with a high of 13.5 mg m^{-3} in the near surface waters from NAM017 (Fig. 3.2*a*). Afterwards, the highest phytoplankton biomass was characteristically found in the upper 40 m over the outer shelf, where the fertilized waters promoted a high productivity that reached 15.9 mg chlorophyll-a m^{-3} at NAM007 during the transect 2 (T2). As the wind forcing strengthened, the filament was dispersed allowing warm aged waters to occupy most of the transect. This led the chlorophyll-a to decrease almost 3-fold while moving inward to a maximum of 6.2 mg m^{-3} at the end of the cruise (T4). Similar variability was found at those stations where the sediment traps were deployed (Fig. 3.2*b*). Indeed, the sampling date was more critical to explain the oceanographic properties at each station than the distance to the upwelling center, so that the vertical profiles between NAM006 and NAM011d were closer to one another than between the two samplings conducted at NAM011 (i.e., NAM011d and NAM011r).

These dynamics of the physical setting and primary productivity could be seen in the variability of the euphotic zone (E_z) depth. Averaged E_z depths, defined as the 1% light-level, ranged from a low of 23 m at station NAM007 to 58 m at the offshore station NAM009 (see Table 6 in Osma et al., 2014). The deepest E_z were found during transect 4 due to the low plankton biomass present in the nutrient-depleted waters that occupied the transect at that time. The E_z depth recorded at each station was considered to calculate F_N, except for those stations sampled between dawn and dusk. In this latter case, we set the E_z depth according to the one measured in adjacent stations that presented similar chlorophyll-a profile.

3.3.2 Vertical F_N from heterotrophic $R_{NH_4^+}$ throughout the water column

In all the cases, $R_{NH_4^+}$ for nano/microzooplankton and mesozooplankton were maxima in the upper 50 m (Fig. 3.3). Similarly to the hydrographycal properties, the $R_{NH_4^+}$ profiles were closer between NAM006 and NAM011d. Nano/microzooplankton sea surface $R_{NH_4^+}$ ranged about 2-fold from a high of 53.2

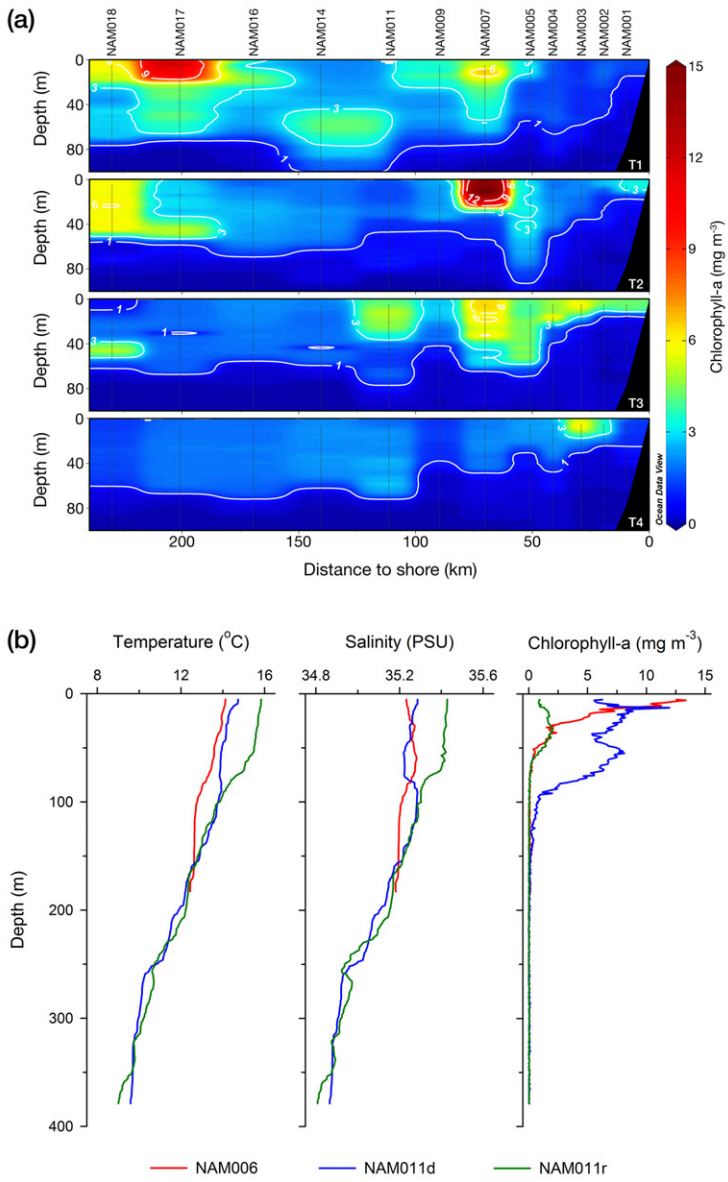

Figure 3.2: (a) Distribution of chlorophyll-a in the upper 100 m at the SUCCESSION transect. Sampling dates in 2011 were as follows: 27 Aug. - 30 Aug. (T1), 31 Aug. - 02 Sep. (T2), 08 Sep. - 10 Sep. (T3) and 11 Sep. - 15 Sep. (T4). (b) Temperature, salinity and chlorophyll-a depth-profiles for stations NAM006 and NAM011, where the sediment traps were deployed. NAM006 was sampled on Sep 06 (NAM006), while NAM011 was sampled on two separate days: Sep. 07 (NAM011d) and 10 days later, on Sep. 17 (NAM011r).

Table 3.1: $R_{NH_4^+}$ models for nano/microzooplankton and mesozooplankton, normalized by the depth at maximum $R_{NH_4^+}$ (z_m). They are described by power functions in the form of $R_{NH_4^+} = (R_{NH_4^+})_m\ (z/z_m)^b$, where $R_{NH_4^+}$ is the NH_4^+ excreted at any depth, $(R_{NH_4^+})_m$ is the $R_{NH_4^+}$ maximum (μmol NH_4^+ m^{-3} d^{-1}), and b-value is the curvature of the function (unitless). The least-square regression analysis (r^2) for each $R_{NH_4^+}$ model, and the number of samples (n) used to fit the models are also presented. Both the modeled and the calculated values were then compared to check the reciprocity.

Station	Group	Depth	z_m	Modeled $R_{NH_4^+}$ (μmol NH_4^+ m^{-3} d^{-1})				Modeled *vs.* Calculated $R_{NH_4^+}$		
		(m)	(m)	$(R_{NH_4^+})_m$	b-value	r^2	n	Slope	Intercept	r^2
NAM006	Nano/Microzoo.	206	10	34.64	−0.45	0.92 *	8	0.93	1.23	0.81 **
	Mesozoo.	206	25	25.67	−0.68	0.96 *	5	0.97	0.28	0.99 *
NAM011d	Nano/Microzoo.	395	5	80.87	−0.63	0.70 **	9	1.25	−5.31	0.83 **
	Mesozoo.	395	25	32.31	−0.82	0.92 *	5	1.09	−2.02	0.84 **
NAM011r	Nano/Microzoo.	395	50	13.01	−0.50	0.67 **	8	0.79	2.44	0.49 **
	Mesozoo.	395	25	35.06	−0.71	0.74 **	5	0.62	4.59	0.90 **

* Significant at a level $p < 0.001$.

** Significant at a level $p < 0.05$.

μmol NH_4^+ m^{-3} d^{-1} at NAM011d to a low of 29.6 μmol NH_4^+ m^{-3} d^{-1} at NAM011r. Interestingly, sea surface $R_{NH_4^+}$ of mesozooplankton showed the opposite pattern. It rose from 26.7 μmol NH_4^+ m^{-3} d^{-1} to reach a peak of 49.3 μmol NH_4^+ m^{-3} d^{-1} at NAM011r, which coincided with the decrease in the chlorophyll-a concentration (Fig. 3.2*b*). It is however noticeable that this enhanced $R_{NH_4^+}$ at NAM011r was mainly due to the NH_4^+ excreted by the large migrant zooplankton (i.e., > 1000 μm, in Fig. 3.3). In general, nano/microzooplankton seem to regenerate more NH_4^+ throughout the water column than did the mesozooplankton. Among this latter group, the 100 - 200 μm size fraction contributed the least to the total NH_4^+ regeneration, while the 200 - 500 μm and > 1000 μm size fractions were the most important remineralizers, specially at NAM006 and NAM011d (Fig. 3.3). Both together accounted for more than the 85% of the total NH_4^+ excreted by the mesozooplankton. The PON consumption at NAM011r was, as stated above, almost exclusively dominated by the > 1000 μm zooplankters.

These vertical $R_{NH_4^+}$ profiles for nano/microzooplankton and mesozooplankton were then fitted to a power function. Each parameter of the equation is shown in Table 3.1. Power functions were selected not only for consistency with previous works, but also because they explain the vertical data distribution meaningfully. The exponent b, always negative, explain the decrease of

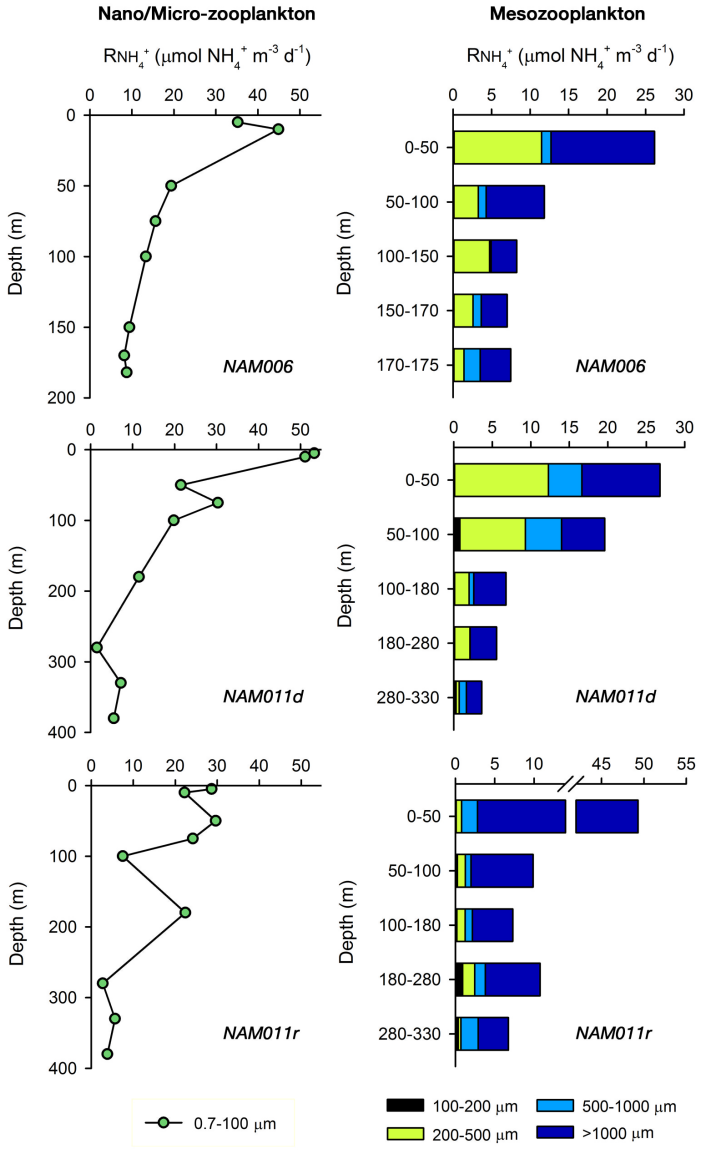

Figure 3.3: $R_{NH_4^+}$ (µmol NH_4^+ m^{-3} d^{-1}) of nano/microzooplankton (left side) and size-fractionated mesozooplankton (right side) at the three stations where the sediment traps were deployed. Note that the $R_{NH_4^+}$ profiles for nano/microzooplankton were determined at discrete depths, while the $R_{NH_4^+}$ for mesozooplankton were calculated from integrated values at different depth-intervals.

$R_{NH_4^+}$ with increasing depth. The most negative *b*-values were found for the mesozooplankton $R_{NH_4^+}$ profiles (Table 3.1), which corresponded to a higher release of $R_{NH_4^+}$ at the surface layer. All the $R_{NH_4^+}$ models were tested for reciprocity by comparing the predicted $R_{NH_4^+}$ with the measured $R_{NH_4^+}$ at the same depth. There was a high significance in all the cases except for the nano/-microzooplankton $R_{NH_4^+}$ at NAM011r. The modeled $R_{NH_4^+}$ were subsequently integrated from any considered depth below the E_z to the bottom, resulting in the F_N at discrete depths. The models fitted to these values of F_N are presented in Fig. 3.4. In this case, the logarithmic functions were the best fit to the F_N data as compared to the exponential and power functions (one-way ANOVA, $F_{2,6} = 74.47$, $p < 0.001$). The PON flux related to the NH_4^+ excretion in the water column followed a similar pattern at NAM011d and NAM011r, despite the latter's deeper E_z . This PON utilization below the E_z depth ranged from 6.59 mmol N m^{-2} d^{-1} at NAM011d to 5.47 mmol N m^{-2} d^{-1} at NAM011r, 10 days latter. Similarly, 5.46 mmol m^{-2} d^{-1} of nitrogen were regenerated through the water column at the shallower NAM006 station. The calculated F_N at the mooring depths which represented the minimum PON necessary for sustaining NH_4^+ excretion processes below 150 m and 320 m in NAM006 and NAM011d/r, respectively, was compared with the gravitational sinking rates measured by sediment traps at those depths (Fig. 3.5). Since the vertical PON consumption and the particles collection at the bottom are inherently uncoupled in time, we compare the vertical F_N with the mean gravitational rate measured during the correspondent productivity regime, rather than on a daily basis. Osma et al. (2014) explain the characteristics defining high- and low-sedimentation periods. Thus, high levels of primary productivity at NAM006 (30.17 mmol N m^{-2} d^{-1}) and NAM011d (33.31 mmol N m^{-2} d^{-1}), mainly due to a bloom of diatoms, allowed rapid sinking velocities of the particulate matter from the surface waters to the deep sea. The sinking rates during this regime of high-sedimentation was 1.01 mmol N m^{-2} d^{-1} at NAM006, and 0.90 mmol N m^{-2} d^{-1} at NAM011d. These sinking PON values did not differ significantly from the correspondent F_N calculations ($p > 0.05$ in both cases, Student *t*-test), that were 1.18 mmol N m^{-2} d^{-1} at NAM006 and 0.68 mmol N m^{-2} d^{-1} at NAM011d. This scenario changed at NAM011r as the diatom-dominated population gave way to a coccolithphorid-dominated one. Accordingly, the POM shifted to mainly smaller-sized particles in the water column, although the primary productivity decreased only about 16 % to 25.31

mmol N m^{-2} d^{-1}. This led to a low-sedimentation regime with PON sinking rates of about 0.15 mmol N m^{-2} d^{-1}. The modeled F_N however remained fairly constant at NAM011r (0.77 mmol N m^{-2} d^{-1}), so the difference between the calculated PON flux and the measured sinking PON amounted to 5-fold. Here the mesozooplankton contributed more to the total F_N.

Following the same calculations, but focused exclusively on the $R_{NH_4^+}$ of mesozooplankton, we constructed a synoptic section of F_N along the cross-shelf transect off the Namibian coast (Fig. 3.6*a*). In order to include the greatest number of stations, the F_N in Fig. 3.6*a* only consists of that part of the flux that supports the $R_{NH_4^+}$ of mesozooplankton throught the water column,

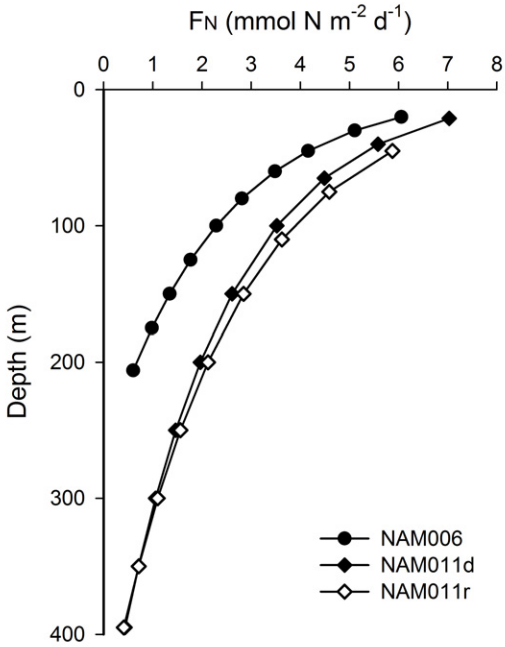

Figure 3.4: Inorganic nitrogen flux depth profiles calculated at the onshore and offshore limits of the outer Namibian shelf (Fig. 3.1, inset upper left). Each of these fluxes represents the total PON remineralization to NH_4^+ driven by the nano/microzooplankton and mesozooplankton from the base of the euphotic zone to the bottom, and comes from the measurement of their GDH activities. The logarithmic functions were: $F_N = -2.34\ \mathrm{Ln}\,(z/E_z) + 6.07$ (at NAM006); $F_N = -2.25\ \mathrm{Ln}\,(z/E_z) + 7.03$ (at NAM011d); $F_N = -2.52\ \mathrm{Ln}\,(z/E_z) + 5.87$ (at NAM011r). Note that NAM006 was shallower (206 m) than NAM011d/r (395 m).

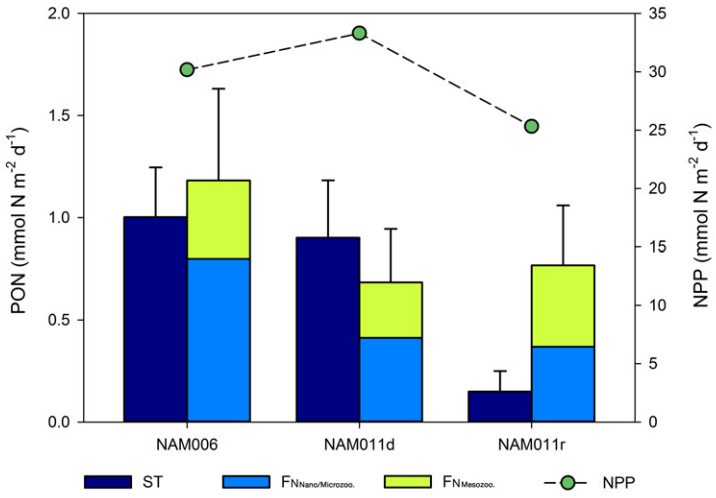

Figure 3.5: Comparison between the sinking PON (mmol N m^{-2} d^{-1}) collected by sediment traps (ST), and the PON flux calculated from NH_4^+ excretion models for nano/microzooplankton ($F_{N_{Nano/microzoo.}}$) and mesozoplankton ($F_{N_{Mesozoo.}}$). According to the accumulated error that was found by Packard et al. (1988) for a similar enzymatic technique, we considered an uncertainty of 38 % for the F_N flux calculations. Sinking PON rates were calculated from the average daily ST values. Note the difference between the high-sedimentation regime (NAM006 and NAM011d), and the low-sedimentation regime (NAM011r). Daily sinking rates of the trapped particles, and the criteria for setting each oceanographic regime are given in Osma et al. (2014). Net primary production (NPP) as mmol N m^{-2} d^{-1} is also presented for each sampling day. Calculations of the NPP are fully described in Fernández-Urruzola et al. (2014).

while obviates the nitrogen burial. We do consider this part of the nitrogen flux in Fig. 3.6*b* and c for those stations that allow integrating $R_{NH_4^+}$ from the surface to infinity because their exponents b are more negative than -1. The stations in Fig. 3.6*a* were averaged over two periods in order to detect temporal differences in the F_N magnitude. In both cases, we only considered those stations that had significant $R_{NH_4^+}$ models at a level $p < 0.01$. The earlier section of F_N (i.e., from 28th Aug. to 02th Sep.) showed peaks of about 1.7 mmol m^{-2} d^{-1} at the base of the E_z depth, that were displaced offshore as compared to the following period (07th - 12th Sep). The latter section presented a F_N maxima (2.1 mmol m^{-2} d^{-1}) 60 km from the shore. Nevertheless, most of the PON recycling always occurred in the epipelagic zone. The PON utilization

by mesozooplankton throughout the different depth-layers is indeed compared in Fig. 3.6*b* and *c*. The nutrient retention efficiency (NRE) concept, that was introduced by Packard and Gómez (2013) for the first time, stands for the ratio of nutrient regeneration within a given layer to the nutrients introduced into that layer. This NRE demonstrates that the deeper layers were the most efficients in recycling the available PON (up to 36.7 % for the bathypelagic domain in NAM017). The fate of F_N, in turn, reflects the amount of PON that is transformed into DIN by the mesozooplankton metabolism as compared to the total PON fluxing out the E_z depth (Fig. 3.6*c*). By integrating to infinity, we can calculate the remaining PON that is not recycled throughout the water column, i.e., the PON that is either buried or remineralized in the benthos. Accordingly, the Fig. 3.6*c* shows that most of the PON was consumed in the epipelagic zone, with the nitrogen burial being higher at the inshore stations.

3.3.3 Active F_N driven by diel migrators

Day-night differences in the vertical F_N driven by mesozooplankton were studied at the station NAM011 from September 7th to September 17th, 2011 (Table 3.2). The first night (07-Sep.) and day (09-Sep.) samplings corresponded to a higher productivity regime (33.3 - 36.8 mmol N m^{-2} d^{-1}), dominated by diatoms, with shallower E_z depths, and peaks of chlorophyll-a over 5 mg m^{-3}. The productivity changed thereafter as the ocean became more oligotrophic, and the maximum values of chlorophyll-a dropped to about 2.5 mg m^{-3} for the next two sampling dates. Nevertheless, the time of the day seemed to be more critical to explain the vertical distribution of mesozooplankton at NAM011 than the ocean dynamics. Thus, the averaged mesozooplankton biomass (BM_z) was 3.5-fold higher during the night (0.93 g N m^{-2}) than during the day (0.26 g N m^{-2}). The biomass specific-$R_{NH_4^+}$ (spc-[$R_{NH_4^+}$]) ranged from 0.08 to 0.31 mmol NH_4^+ g N^{-1} h^{-1} depending on the structure of the mesozooplankton community: a major presence of gelatinous zooplankton (such as the salp bloom recorded on 17-Sep) would result in a lower spc-($R_{NH_4^+}$). The modeled-$R_{NH_4^+}$ profiles showed maximum values at night, ranging between 32.3 - 35.1 µmol NH_4^+ m^{-3} d^{-1} in the surface waters (Table 3.2). These maxima decreased during the daytime to 27.9 µmol NH_4^+ m^{-3} d^{-1} in September 9th, and to less than half that value four days later (14.2 µmol NH_4^+ m^{-3} d^{-1}). Accordingly, the F_N at the bottom of the E_z was higher during the night (from 3.16 to 3.29 mmol N m^{-2} d^{-1}), decreasing more rapidly down to 150 m as compared to the

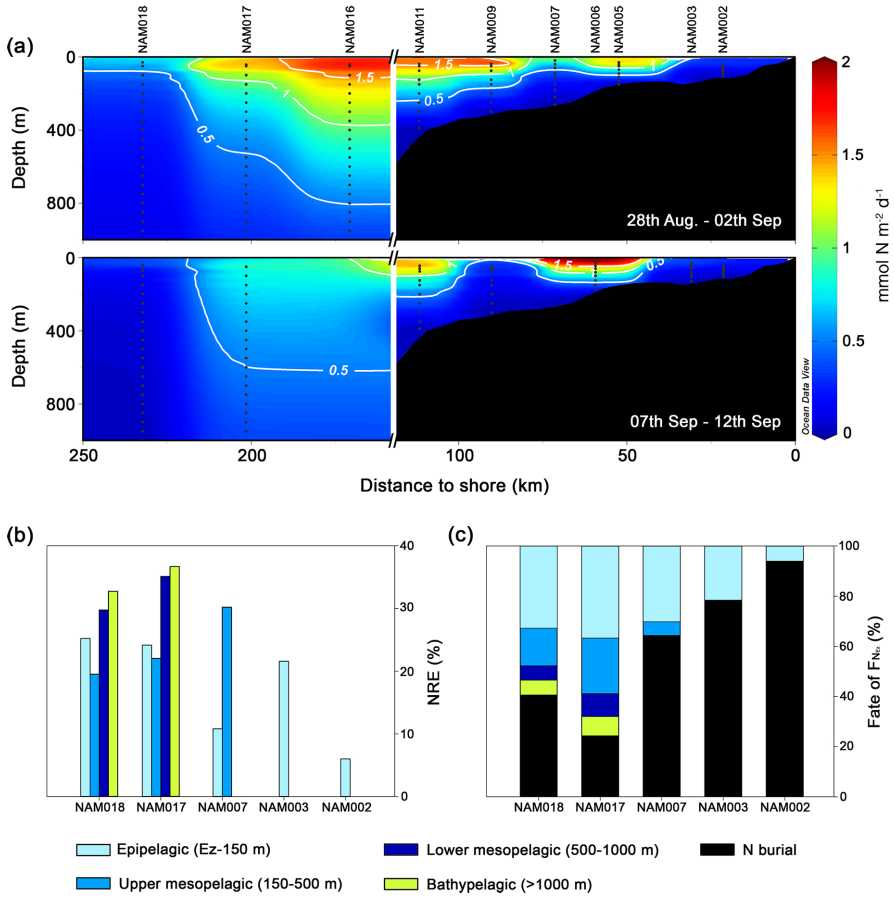

Figure 3.6: (a) F_N sections calculated by the definite integral from the E_z depth to the ocean bottom, at two different time periods, (b) the nutrient retention efficiency (NRE) through the different depth-layers, and (c) the fate of the nitrogen fluxing out the E_z depth. All these calculations consider only mesozooplankton $R_{NH_4^+}$.

daytime F_N profiles. As a result, the mesozooplankton required 1.58 mmol N m^{-2} d^{-1} to satisfy their metabolic demands at night, while only 0.57 mmol N m^{-2} d^{-1} were necessary during the day. It means that 1.01 mmol N m^{-2} d^{-1} were actively transported below 150 m by the migrant zooplankton. This modeled active flux (F_{N_M}) agreed ($p > 0.05$, Student t-test) with the classical calculations of active flux that are based on differences in zooplankton biomass between day and night (F_{N_B} = 0.91 mmol N m^{-2} d^{-1}). The averaged day and

night F_N profiles, as well as the resultant F_{N_M}, are illustrated as a continuous function of depth in Fig. 3.7. As expected, there is a significant difference between day and night fluxes of excreted NH_4^+ ($p < 0.001$, Student t-test) that is most apparent in the epipelagic zone. In other words, the mesozooplankton consume more PON in the surface during the night, and transport it to deeper layers during the day. Thus, 4.7 % of the net primary production (NPP) was actively transported below 150 m (e-ratio, Table 3.2). Comparing F_{N_M} (1.01 mmol N m^{-2} d^{-1}) to the trap flux at 150 m (see *Section* 3.2.4 for calculations) shows that the active transport of inorganic nitrogen accounted for an important proportion of the sinking PON flux. During a high-sedimentation regime (sinking PON = 1.72 mmol N m^{-2} d^{-1}), F_{N_M} averaged 59 % of the PON flux. But, when small particles with slower sinking velocities dominated in the water column, the potential F_N due to diel migrators could become 3.6 times (i.e., 361 % of) the gravitational PON flux (sinking PON = 0.28 mmol N m^{-2} d^{-1}). These percentages doubled when compared with the measured trap flux at 320 m.

3.4 Discussion

3.4.1 Modeling F_N from zooplankton-$R_{NH_4^+}$ profiles

In this study we present a novel approach to quantify downward F_N from measurements of GDH activity in nano/microzooplankton and mesozooplankton within the Namibian cell. This procedure facilitates the derivation of useful parameters concerning the nutrient cycling and the calculation of the spatial variability of F_N at a rate that is difficult to achieve by other methods used to estimate biogeochemical variables. Of course, a one-dimensional model, such as the one we propose here, has assumptions and limitations, but none of them would invalidate the whole concept. One could rightly claim that the neglected lateral inputs may be relevant in an eastern boundary upwelling ecosystem (EBUS) (Alonso-González et al., 2009). But even in upwellings, the vertical dynamics dominate the horizontal ones given the fact that each one operates at a different scale (from hundred meters to several km, respectively). Moreover, the estimated offshore velocity of advected water during our cruise was 0.06 m s^{-1}, and the current velocities in the inertial frequency band ranged between 0.02 - 0.06 m s^{-1} (Mohrholz et al., 2014). Relatively slow currents with velocities below 0.2 m s^{-1} result in little dispersal that allows the

Table 3.2: Downward F_N driven by migrant zooplankton out of 150 m at NAM011 (bottom row, in bold). Night-time was considered the time between dusk and dawn (i.e., from 18:54 h to 07:06 h). E_z depth for the night samplings was estimated by comparing the chlorophyll-a profiles with profiles of similar magnitude recorded during the day in adjacent stations. Net primary production (NPP) calculations are fully described in Fernández-Urruzola et al. (2014). The biomass of mesozooplankton (BM_z) in terms of N, and the biomass specific-excretory metabolism (spc-[$R_{NH_4^+}$]) are shown. PON consumption down to 150 m are given as a function of mesozooplankton-biomass (N_B), as well as on a $R_{NH_4^+}$ modeling basis (N_M). Note that there are not *SD*s for the mean day and night values of the modeled approach since they come from a new fit of the averaged $R_{NH_4^+}$ data. Active flux (F_{N_B} and F_{N_M}, also in bold) equals the difference between the mean night and day values in either the N_B or the N_M, respectively. The last column (*e*-ratio) stands for the export to production ratio, i.e., the proportion of NPP which is actively transported below 150 m.

Sampling date	Time	E_z depth	NPP	BM_z	spc-($R_{NH_4^+}$)	N_B	Modeled-$R_{NH_4^+}$ (µmol NH_4^+ m^{-3} d^{-1})			F_N (mmol N m^{-2} d^{-1})			N_M	*e*-ratio
	(h)	(m)	(mmol N m^{-2} d^{-1})	(g N m^{-2})	(mmol NH_4^+ g N^{-1} h^{-1})	(mmol N m^{-2} d^{-1})	($R_{NH_4^+}$)$_m$	*b*-value	r^2	E_z	150 m	320 m	(mmol N m^{-2} d^{-1})	(%)
07-Sep.	5:10	21	33.31	0.46	0.31	1.71	32.3	−0.82	0.92 *	3.16	1.11	0.32	2.05	6.2
09-Sep.	16:10	33	36.88	0.36	0.17	0.73	27.9	−0.76	0.98 *	1.57	0.65	0.19	0.92	2.5
12-Sep.	16:40	45	32.01	0.15	0.28	0.50	14.2	−0.75	0.99 *	0.73	0.34	0.10	0.39	1.2
17-Sep.	2:15	45	25.31	1.39	0.08	1.33	35.1	−0.71	0.76**	3.29	1.55	0.45	1.74	6.9
Mean day (± SD)	-	45†	-	0.26 (± 0.15)	0.19 (± 0.03)	0.62 (± 0.16)	21.1	−0.76	0.99 *	1.07	0.50	0.14	0.57	1.9 (± 0.9)
Mean night (± SD)	-	45†	-	0.93 (± 0.66)	0.14 (± 0.03)	1.52 (± 0.27)	35.2	−0.77	0.94 *	2.96	1.38	0.38	1.58	6.6 (± 0.5)
Active flux (± SD)	-	-	-	-	-	**0.91 (± 0.31)**	-	-	-	-	-	-	**1.01**	**4.7 (± 1.0)**

† The deepest E_z was considered for conservative estimations.

* Significant at a level $p < 0.001$.

** Significant at a level $p < 0.05$.

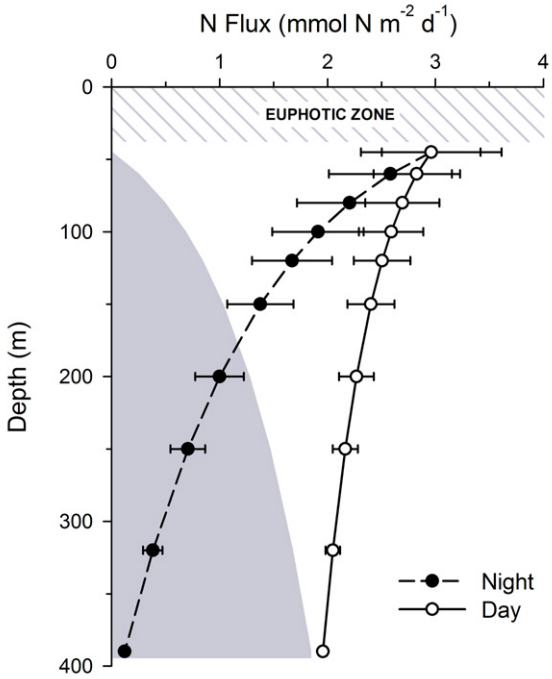

Figure 3.7: Active nitrogen flux driven by diel migrant zooplankton at the edge of the outer shelf (NAM011). The active F_N is defined as the difference between the day and night F_N profiles generated from the models in Table 3.2 (shaded area). To facilitate the comparison, the vertical F_N during the daytime was forced to start from the same level than did the night F_N profile.

particles to reach the seabed close to the point at which they left the surface (Jaeger et al., 1996). In such a situation, these authors demonstrated the validity of a one-dimensional model to predict particle accumulation rates in the Ross Sea. On the other hand, our modeled F_N rates must be considered conservative estimates, since not all the PON is necessarily transformed into DIN through zooplankton metabolism. Still, NH_4^+ is the primary nitrogenous excretory product in both microzooplankton (Caron and Goldman, 1990) and mesozooplankton (Bidigare, 1983; Ikeda et al., 2000), and usually accounts for more than the 70 % of the total released nitrogen. Dissolved organic nitrogenous compounds, such as urea and amino acids, contribute least to the total dissolved nitrogen that is excreted. The proportion of the dissolved organic nitrogen (DON) relative to the inorganic form of NH_4^+ depends on the quality and

quantity of the food that is consumed (Miller and Roman, 2008), as well as on the involved taxa (Steinberg and Saba, 2008). But, in general, the unaccounted release of DON would impact our modeled F_N less than 32 % (Steinberg et al., 2002). This percentage should also be applied to most of the oceanographic research on F_N that commonly disregards the contribution of the DON fraction to the total flux (e.g., Dam et al., 1995; Longhurst and Harrison, 1988, 1989).

3.4.2 Downward F_N in the northern Benguela

The complex interplay between mesoscale structures in the northern Benguela region during the period of maximum upwelling (i.e., from August to October according to Boyd et al., 1987) altered the general pattern of waters that strictly age with distance from shore. Accordingly, abrupt changes in the biomass were described for the phytoplankton (Hansen et al., 2014) and the zooplankton (Fernández-Urruzola et al., 2014) communities, rather than a continuous and homogenous successional development in the ageing advected waters. A mature upwelling filament moving to the northwest with a high nutrient-load stimulated a diatom bloom that extended farther offshore in late August (see satellite images in Mohrholz et al., 2014). The filament weakened afterwards, and began to mix with the warmer and more oligotrophic Eastern South Atlantic Central Water (ESCWA). This led to a decrease in the chlorophyll-a concentration rather than in the phytoplankton cell abundance (Hansen et al., 2014), which suggests a shift from large cells (diatoms) to small ones (nanoflagellates and coccolithophorids). All these physical and biological constraints in the surface mixed layer determined the pattern of vertical particle export, as will be later discussed.

In this study, the sediment traps were moored at the onshore (NAM006) and offshore (NAM011) limits of the outer shelf. These stations were located in a transitional zone that, in general terms, separated the cold nearshore upwelled waters, poor in plankton, from the nutrient-depleted aged waters. The temporal variability was thus more important in explaining the differences in the vertical $R_{NH_4^+}$ profiles between the two stations, than the distance to shore. The samples at NAM006 and NAM011d were taken on consecutive days, so these stations were similar not only in the magnitude of the $R_{NH_4^+}$ through the water column, but also in the contribution of each size fraction to the total NH_4^+ release (Fig. 3.3). In the uppermost 180 m of the two stations, the nan-

o/microzooplankton excreted 22.9 (± 4.7) μmol NH_4^+ m^{-3} d^{-1}, whereas the mesozooplankton excreted 15.1 (± 1.2) μmol NH_4^+ m^{-3} d^{-1}. Although these rates are higher than those measured in other EBUS, ranging between 0.2 - 5.4 μmol NH_4^+ m^{-3} d^{-1} in the case of mesozooplankton (Pérez-Aragón et al., 2011; Isla and Anadón, 2004; Hernández-León et al., 2002), the heterotrophic NH_4^+ release fuelled only a small proportion of the phytoplankton that was produced in the northern Benguela (Fernández-Urruzola et al., 2014). Here the nano/microzooplankton were the main regenerators of NH_4^+, which is consistent with estimates made throughout several marine systems that argue for a major role of microzooplankton in the regeneration of nitrogen (Bronk and Steinberg, 2008). Both the small protozoa and nanoflagellates were indeed found to be crucial in nutrient recycling in the waters of Southern Benguela (Probyn, 1987). Later, as the filament dispersed over the shelf-break, the new nutrients become limited and the system transformed into a late temporal phase of the upwelling. In general, the $R_{NH_4^+}$ decreased in all the size fractions at the late NAM011r, except in the largest zooplankton (> 1000 μm), that precisely showed its maximum (49.3 μmol NH_4^+ m^{-3} d^{-1} in the uppermost 50 m, Fig. 3.3). This pattern fits into the general scheme of succession of the ecosystem (Vinogradov et al., 1972), where the biological community is dominated by the large zooplankton, salps in our case study, in a late succession stage. Such a variability has been also described in other upwelling systems, with the relative contribution of mesozooplankton to the total NH_4^+ regeneration becoming more relevant in the low productivity situations (Bode et al., 2004).

All these changes in the structure of the zooplankton community had, in any case, little impact on the F_N. The nitrogen required to sustain the heterotrophic metabolism in the whole water column below de E_z was thus similar in NAM006, NAM011d and NAM011r (ranging from 5.5 to 6.6 mmol N m^{-2} d^{-1}, Fig. 3.4), and the modeled PON fluxing out the sediment trap depth at NAM011d was akin to the one calculated at NAM011r (Fig. 3.5). But the picture differs when viewed from the perspective of the sediment traps, since the rates of settling nitrogen changed dramatically from NAM011d to NAM011r (Fig. 3.5). The discrepancy between the estimated flux from ecosystem modeling and the flux from sediment trap data has long been the focus of controversy (Burd et al., 2010; Steinberg et al., 2008), and it may lay in the basis of each approach. The modeled F_N gives a high-depth resolution snapshot of the biological interactions that occur in the vertical one-dimension. The sediment

traps, however, integrate the sinking particles over time but cannot provide information on the processes that affect the PON transformation in the water column. Both approaches complement each other, as the weakness in one is the strength in the other. It must be considered that the PON that is modeled from the vertical $R_{NH_4^+}$ profiles may deposit in the sediments at different velocities depending on the size and composition of the particles (Alonso-González et al., 2010) and therefore, be out of phase with the traps record. So the comparison between the two approaches should not be made on a daily basis, but according to the productivity regime and the character of biogenic particle production. High-density aggregates and big recalcitrant particles would result in relatively fast-sinking velocities that allow them to reach the seafloor in the close proximity to its origin; by contrast, small labile cells are more prone either to attenuation or advection (Alonso-González et al., 2010; Iversen and Ploug, 2010; McDonnell et al., 2015). Here, the large diatoms dominated the phytoplankton community at NAM006 and NAM011d. That, combined with a high concentration of biogenic and lithogenic minerals that may promote a ballasting effect, resulted in a high-sedimentation regime (Osma et al., 2014). In this scenario, the modeled F_N (1.18 mmol N m^{-2} d^{-1} at 150 m in NAM006, and 0.68 mmol N m^{-2} d^{-1} at 320 m in NAM011d) compared well with the PON accumulation rates in the corresponding sediment traps (1.01 mmol N m^{-2} d^{-1} and 0.91 mmol N m^{-2} d^{-1}, respectively, Fig. 3.5). But the system aged afterwards, and both the productivity and the diatom to dinoflagellate ratio declined (Hansen et al., 2014). Lower phytoplankton biomass and a reduced load of lithogenic material, resulted in little aggregations of the small dominant cells, as shown by microscopic observations (Fig. 7*c* in Osma et al., 2014). Furthermore, zooplankton fecal pellets produced on a nanoflagellate diet were found to sink slower and be more labile as compared to those pellets produced on a diatom diet (Ploug et al., 2008). Altogether, these data reflected a characteristic low-sedimentation regime at NAM011r that may explain the imbalance between the modeled F_N (0.77 mmol N m^{-2} d^{-1}) and the nitrogen deposited in the traps (0.15 mmol N m^{-2} d^{-1}). While slow sinking particles enhance the heterotrophic metabolism through the water column and are easily remineralized (McDonnell et al., 2015), they tend to be underestimated by the sediment traps (Trull et al., 2008). Nevertheless, the PON measured during this low-sedimentation regime was still higher than the particle flux measured by Giraudeau et al. (2000) farther south, off Walvis Bay, during a quiescent

period (mean value from December to January = 0.06 ± 0.01 mmol N m^{-2} d^{-1}, extrapolated from 544 m to 320 m using the Martin curve).

By means of our modeling approach it was possible to draw an ocean section of F_N from GDH activity measurements (Fig. 3.6). This would not be feasible by the stationary trap approach given its narrow spatial coverage in both the vertical and horizontal axes. Here the temporal and spatial variability of mesozooplankton $R_{NH_4^+}$ revealed a high F_N along the whole transect at late August, with the maximum displaced offshore likely due to the influence of the filament structure (Fig. 3.6*a*). In fact, the chlorophyll-a peaked in the oceanic station NAM017 at this stage of upwelling (Fig. 3.2*a*). During mid September, the flux maximum moved inward over the outer shelf (NAM006) in parallel with the chlorophyll-a pattern. From these F_N we calculated the nutrient retention efficiency (NRE) of each ocean zone by applying Eq. 3.5. The NRE defines the capacity of a given depth-layer to remineralize the available POM, and it could be considered, in practical terms, the inverse of the so-called transfer efficiency (T_{eff}, *sensu* Buesseler et al., 2007). Mathematically, if expressed as a percentage, it equals 100 × (1- T_{eff}). It is therefore inversely related to F_N, and as such, high $R_{NH_4^+}$ to F_N ratio should result in high NRE (Fig. 3.6*b*). We further calculated the fate of the nitrogen (Fig. 3.6*c*), not only in the pelagic environment but also considering the nitrogen burial and benthic remineralization, that equals the difference between integrating Eq. 3.4 to infinity, and integrating it to the ocean bottom. Due to mathematical restrictions, this can only be made on those stations that have a *b*-value more negative than -1. We estimated a high level of PON burial in the coastal stations, decreasing seaward. This predicted burial would be much lower if the remineralization rates associated with the small nano/microzooplankton would have been included. In contrast, the epipelagic zone was more efficient in retaining nutrients in the oceanic stations, but always to a lesser extent than the mesopelagic and bathypelagic realms. Buesseler and Boyd (2009) already highlighted the importance of the twilight zone in the flux attenuation. The NRE is ultimately controlled by the shape of $R_{NH_4^+}$ as a function of depth (Packard et al., 2015); if depicted by a power law fit, as in the present case, the flux attenuation is defined by the *b*-value. The higher the *b*-value is (in absolute terms), the greater will be the curvature of the function, i.e., the more flux will be attenuated in the upper layers. So the study of this parameter is of particular interest as it will determine

the nutrient distribution throughout the ocean water columns (Marsay et al., 2015).

3.4.3 Active F_N driven by diel migrators

Here the F_N equations have been additionally used to calculate the active flux due to zooplankton vertical migration. The active transport of nitrogen to deeper waters is an important component of the PON flux (Longhurst and Harrison, 1988), and it is usually presented relative to the gravitational flux to facilitate the comparison among regions. The most traditional way to assess active nitrogen flux has been to subtract daytime zooplankton biomass from nighttime values in the euphotic zone (assuming that the migrants reside in this layer for 12 h at night), and multiply the resultant biomass by the biomass-specific excretion rate (Dam et al., 1995). This is fine, but it serves to calculate the active flux only at a discrete depth, e.g., the euphotic zone. We have applied our equations, and integrated day and night $R_{NH_4^+}$ depth-profiles at NAM011 to model the active flux in the entire water column below the photosynthetic zone (Fig. 3.7). Comparing our modeled value at 150 m, which presumably contains most of the diel migrators during the night, with the correspondent value calculated from the difference in the migrant biomass, we confirm that there is a reasonable agreement between the two approaches (see Table 3.2). The active nitrogen flux driven by the mesozooplankton fraction out of 150 m was thus estimated at 1.01 mmol N m^{-2} d^{-1} for the northern Benguela (20° S). The resultant migratory flux to gravitational flux ratio at that same depth varied from 59 % to 361 % depending on wether it was considered a high- or a low-sedimentation regime, respectively. This range encompasses the respiratory flux to POC flux ratio of 79 % estimated by Schukat et al. (2013a) for the pelagic decapods in the Angola-Benguela Front. By contrast, the migratory NH_4^+ to sinking PON ratios reported in the oligotrophic waters of Bermuda (Dam et al., 1995; Steinberg et al., 2002) and Hawai (Al-Mutairi and Landry, 2001) were about three- to fivefold lower as compared to our ratio. This is not surprising since the migrant biomass that we measured in the northern Benguela exceeds by more than an order of magnitude the one found by the authors in those oligotrophic gyres. Moreover, it should be noted that salps dominated the migrant fraction at NAM011. These opportunistic organisms have the capacity to bloom under appropriate conditions and are highly active migrants that produce fecal pellets enriched in nitrogen (Andersen, 1998), playing a key role in

transporting nitrogen to the deep sea (Wiebe et al., 1979). In total, about 5 % of the NPP was actively transported below 150 m by the mesozooplankton.

In the study of active flux it is generally assumed that organisms feed exclusively in the nighttime layer. However, during the day, some migrant zooplankton groups such as salps (Phillips et al., 2008) and adult chaetognaths (Stuart and Verheye, 1991) may also feed in the deep waters either upon sedimented POM or other zooplankters and therefore, there could be an upward transport of nitrogen that it is not being accounted for. Still, the inclusion of both macrozooplankton and micronekton in our calculations would increase the estimated downward active flux as it has been reported to be important contributors to particle export (Ariza et al., 2015; Hidaka et al., 2001; Schukat et al., 2013a).

3.5 Conclusions

In this research we propose an original mode of calculating nitrogen fluxes from the analysis of the GDH activity in marine heterotrophs. Our model serves to approximate biogeochemical fluxes, and provides information about the biological interactions occurring in the water column. It further allows to construct ocean sections of F_{N} that would otherwise be unachievable, as well as to derive the NRE as a metric that defines the capacity of the system to retain nutrients at a given depth layer. Here we demonstrate that a combination of F_{N} calculations and sediment trap data best illustrates the general picture of the downward nitrogen flux in a highly dynamic marine ecosystem such as the Benguela upwelling. In this scenario, both the particle size and production history are critical factors to explain any imbalance between the sinking PON and the metabolic requirements in the water column. Finally, we use day-night $R_{\mathrm{NH_4^+}}$ depth profiles to model the active transport of nitrogen to the deep sea driven by diel migrators. The downward active flux by the mesozooplankton fraction accounted for between 59 - 361 % of the gravitational flux at 150 m, depending on the sedimentation regime. These organisms were thus responsible for actively transporting about 5 % of the NPP below 150 m. This implies that, given the high biomass of migrant zooplankton found in the Benguela waters, the active flux constitutes an important component of the biological pump in this upwelling ecosystem.

Acknowledgements. We wish to thank the crew of the RV Maria S. Merian, as well as the

scientific researchers involved in the field sampling effort. Funding was provided by the German Research Foundation (DFG), and the BIOMBA project (CTM2012-32729/ MAR) granted to M.G. by the Spanish Economy and Competitiveness Ministry. I.F-U. and N.O. were supported by postgraduate grants from the Formation and Perfection of the Researcher Personal Program from the Basque Government.

The most exciting phrase to hear in science, the one that heralds new discoveries, is not "Eureka" but "That's funny..."

Isaac Asimov

CHAPTER

4

CAPÍTULO

Spatio-temporal variability in the GDH activity to ammonium excretion ratio in epipelagic marine zooplankton

I. Fernández-Urruzola, N. Osma, T.T. Packard, F. Maldonado and M. Gómez,
Submitted to Deep-Sea Research I.

Submission ID: DSR1-2015-166. ***Under review*.**

ABSTRACT: Glutamate dehydrogenase (GDH) activities have been widely used in oceanographic research as an index of *in situ* NH_4^+ excretion rates ($R_{NH_4^+}$) in zooplankton. Here we study the variability in the relationship between the enzymatic rates and the actual rates measured in epipelagic marine zooplankton throughout several marine ecosystems. Although both measures were significantly correlated across zooplankton assemblages, the regression models yielded different GDH/$R_{NH_4^+}$ ratios among ecosystems. Accordingly, the error of a general equation increased up to ± 42.5 % when regressing all our data together. Aside from possible interspecific differences, some of the variability was explained by the unequal allometric relation that each rate maintained with protein. Scaling exponents were 1.38 for GDH activities and 0.87 for $R_{NH_4^+}$, which would induce uncertainties in the GDH/$R_{NH_4^+}$ ratios when organisms with different sizes were considered. Nevertheless, the main factor causing divergence between GDH activities and $R_{NH_4^+}$ was the trophic situation. We compared the excretory metabolism of the zooplankton community at different productivity periods in waters off Gran Canaria, and observed an important

decrease in the $R_{NH_4^+}$ during stratification. Similar decrease was found in the internal pool of glutamate, which may be critical in the regulation of *in vivo* rates. Strengthening our knowledge of the relationship between GDH activities and the $R_{NH_4^+}$ will lead to more meaningful predictions of phytoplankton regeneration and community nitrogen fluxes at a large spatial scale.

Keywords: Zooplankton; Glutamate dehydrogenase (GDH); Ammonium excretion; Allometry; Intracellular glutamate.

4.1 Introduction

Nitrogen is one of the most limiting nutrient elements controlling phytoplankton growth throughout the world's oceans. The dissolved inorganic nitrogen availability may come either from remineralization processes in the sunlit layer or from introduction of new nutrients via upwelling, dinitrogen fixation and terrestrial run-off. Among all the inorganic nitrogen species, the recycling of the reduced form of ammonium (NH_4^+) satisfies a global mean of about 80 % of the primary production requirements (Harrison, 1992). It is therefore an outstanding source of nitrogen to be considered when assessing nutrient fluxes in any aquatic ecosystem.

The regeneration of NH_4^+ is mainly the result of both bacterial remineralization of dissoled organic matter and excretion processes in zooplankton (Bronk and Steinberg, 2008). Here we focus on this latter component of the nitrogen cycle. The importance of NH_4^+ excretion by zooplankton is closely related to the trophic character of the ecosystem and it is, in general terms, more important in oligotrophic than in eutrophic waters. Accordingly, mesozooplankton NH_4^+ excretion has been found to be responsible from a high of about 90 % of the primary production in oligotrophic gyres (Isla et al., 2004b) to a low of 5 % in upwelling environments (Bode et al., 2004; Fernández-Urruzola et al., 2014). However, the NH_4^+ excretion rates ($R_{NH_4^+}$) are also affected by the temperature, taxa, body size and nutritional level (Steinberg and Saba, 2008), so their potential contribution to the marine biogeochemical cycles varies widely in both the time and space domains. Such a variability in the $R_{NH_4^+}$ highlights the need for monitoring the zooplankton physiology in order to understand the basis of the phytoplankton growth. Unfortunately, measuring $R_{NH_4^+}$ on live zooplankton is, not only burdened by unavoidable uncertainties, but so time consuming that rarely can enough incubations be made to obtain a high-resolution spatial coverage of $R_{NH_4^+}$. This becomes even more complicated if

different size fractions of zooplankton are to be studied. Aside from the effort investment, *in vitro* measurements of zooplankton metabolism are subjected to several sources of error. Factors such as crowding, stress caused during manipulation, and starvation in the ongoing experiments would promote a rapid fall in the $R_{NH_4^+}$ (Bidigare, 1983; Ikeda et al., 2000). Conversely, injured organisms either during collection or handling are prone to release more nutrients than do the healthy specimens (Ikeda et al., 1982). All this together results in excretion rates that are, to some extent, different from normal $R_{NH_4^+}$ in seawater.

As part of the biochemical machinery, enzymes catalyze the synthesis of many metabolic end-products and therefore, they have been extensively used in oceanography to infer rates of particular physiological processes such as, for example, respiration (Packard et al., 1971), nitrate uptake (Eppley, 1978) or NH_4^+ excretion (Bidigare and King, 1981). Enzymatic assays constitute a relatively straightforward way to study the plankton metabolism that circumvents all the methodological constraints associated with the water-bottle incubations. Moreover, enzyme activities can be measured quickly, either on-board or at a later time as long as the biological samples were properly stored. This confers on the enzymatic assays an advantage for oceanographic research over the more direct incubation techniques. Prompted by these arguments, Bidigare and King (1981) introduced the analysis of the glutamate dehydrogenase (GDH) activity as a proxy for $R_{NH_4^+}$ in zooplankton. Since then, the GDH assay has been used to obtain a detailed $R_{NH_4^+}$ distribution, both in the vertical and horizontal axes, at sampling rates that otherwise would not have been attainable (e.g., Bidigare et al., 1982; King et al., 1987; Fernández-Urruzola et al., 2014). More recently, Fernández-Urruzola et al. (unpublished data) modeled downward nitrogen fluxes in the northern Benguela from GDH measurements through the water column (*Chapter* 3, this thesis). But enzymatic assays, such as the one for GDH, are not exempt from some methodological biases. They are potential measurements that reflect the maximum rate at which the reaction may occur, not the actual one, so they have to be converted into *in situ* rates through an empirical factor. However, the relationship between enzymatic and *in vivo* rates is not universal, but may be affected by the ambiental conditions. In fact, Bamstedt (1980) demonstrated that enzymes respond to the environmental changes with a certain delay as compared to the physiological response. This was subsequently corroborated on different metabolic pathways when varying food availability in cultures of marine mysids (Herrera et al.,

2011b; Fernández-Urruzola et al., 2011).

During a year (2011), we conducted on-board incubations of mixed epipelagic zooplankton throughout different marine systems: North Atlantic, Benguela Upwelling and Indian Ocean. Here we present both the $R_{NH_4^+}$ and GDH activities measured at each province, and provide the most complete GDH/$R_{NH_4^+}$ data set published to date for marine zooplankton. We compare our ratios with those found in the literature either for natural mixed zooplankton or cultured organisms, and discuss the advisability of using a generalized GDH/$R_{NH_4^+}$ ratio for routinely assessing *in vivo* $R_{NH_4^+}$ from GDH measurements. Furthermore, oceanic mixing events may induce trophic shifts that would locally impact the relationship between GDH activity and $R_{NH_4^+}$ in the resident zooplankton community. For this reason, we chose a station off Gran Canaria (28° N) to evaluate the magnitude of the seasonal changes in the biomass-specific rates from the same spot in comparison to those fluctuations found between different oceanic systems. In this light, we measured the intracellular levels of the main substrate for the GDH reaction, i.e., glutamate, to explore the correlation between physiological rates and substrate concentration. If the latter controls the former, then both should follow the same trend in response to the environmental changes.

4.2 Material and methods

4.2.1 Data sources

The spatial variability of both $R_{NH_4^+}$ and GDH activities in zooplankton were analyzed from five cruises that were carried out during 2011. These cruises surveyed tropical and temperate waters of the Indian Ocean (IO), North Atlantic (NA), Canary islands (CI), and Benguela upwelling (BU) system (Fig. 4.1). The temporal variability in the zooplankton metabolism was also assessed by sampling the same station off the Taliarte coast of Gran Canaria Island (28°00'03" N, 15°19'30" W) during the so-called "late winter bloom" (CI-LWB, characterized by the nutrient-enrichment of surface waters through mixing processes), and during the period of maximum stratification (CI-ST, with higher temperatures and a lower nutrient load in the sunlit layer that is expected to limit the phytoplankton growth). In all the cases we followed the same experimental procedure in order to minimize the bias associated with the methodology. Zooplankton was collected by vertical tows with a UNESCO

WP-2 net (60 cm diameter ring, fitted with either 100 μm or 200 μm mesh sizes depending on the cruise) from 200 m to the surface (i.e., the epipelagic zone). Additionally, a Hansen-Egg plankton net with a mouth opening of 20 cm, and fitted with a 50 μm mesh size, was used during the CI-LWB cruise to extend our study into the 50 - 100 μm size fraction. The hauling speed was always about 0.2 - 0.3 m s^{-1}, as recommended for physiological studies in live zooplankton (Sameoto et al., 2000). Once on deck, organisms were carefully fractionated for 50 - 100 μm, 100 - 200 μm, 200 - 500 μm, 500 - 1000 μm and > 1000 μm size categories. This fractionation varied according to the mesh size of the sampling-net, and how much zooplankton was gathered in the net. Each size fraction was then transferred by siphoning into 2-L bottles filled with GF/F filtered seawater, and maintained at *in situ* temperature. During the time the organisms were awaiting for incubation, the bottles were gently aerated with an air pump, taking care not to damage the organisms with the bubbles. They were thus acclimated for about an hour before being used in the NH_4^+ excretion experiments in order to reduce the stress incurred during the course of sampling.

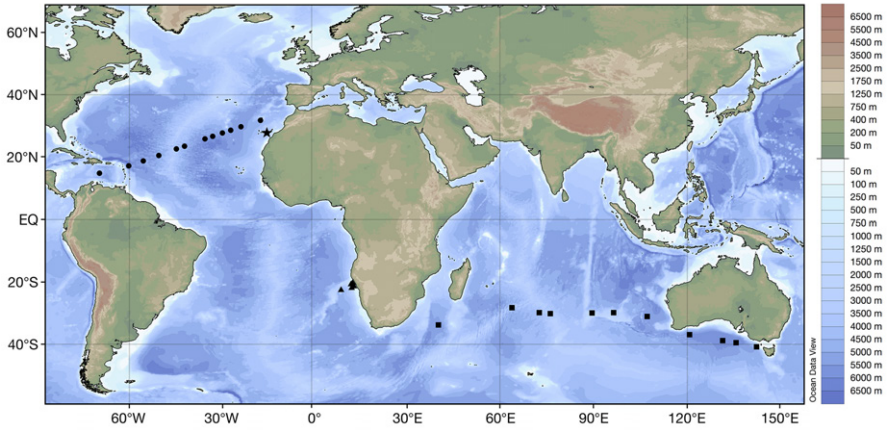

Figure 4.1: Stations sampled during the *CAMVALEX* (★), *SUCCESSION* (▲), and *MALASPINA-2010* –legs 3/4 (■) and leg 7 (●)– research cruises. All samples were taken from Feb-2011 to Oct-2011. To compare seasonal differences in the zooplankton NH_4^+ excretory metabolism, *Camvalex* cruise was conducted twice off Taliarte (Canary islands): during the so-called late winter bloom (Apr-2011), and during the period of maximum stratification (Oct-2011).

4.2.2 **Chlorophyll-a determinations**

Chlorophyll-a (Chl-a) was measured for each oceanic system as an estimator of phytoplankton biomass. Seawater was filtered through GF/F and, in some cases, stored at −20 °C for subsequent analyses. Pigments were extracted in acetone, and their concentration was determined according to two different methods depending on the cruise. Those Chl-a samples from the NA and the IO were measured onboard using their fluorescence properties as described by Yentsch and Menzel (1963), while the Chl-a concentration in the CI-LWB, CI-ST and BU was spectrophotometrically analyzed in the land-based laboratory following the protocol of Parsons et al. (1984).

4.2.3 **Water-bottle incubations**

After acclimation, the most healthy and active swimming zooplankters were washed in GF/F filtered seawater and siphoned into 60 mL gas-tight glass bottles. Each experimental batch included, at least, one control flask without organisms. Little effect of container size on the oxygen consumption rates was found when varying the experimental bottles from 30 mL to 160 mL (Ikeda et al., 2000), so we chose a volume in the lower range in order to reduce the incubation time. Thus, we obtained a significant signal of NH_4^+ release in less than 1.5 h. This achieved a compromise between those effects that density and starvation may produce on the physiological rates and which are fairly constant over 1.5 h of experimentation (see *Chapter* 6 in this thesis). Shortly before the incubation began, we took three replicates (10 mL each one) of filtered seawater to determine the dissolved NH_4^+ concentrations (μM) at the starting point. Then, we incubated the organisms at *in situ* temperature and in the dark for 1 - 1.5 h, depending on the density of the experimental population. Darkness prevented any autotrophic activity that could use the dissolved NH_4^+ available in the bottles. Afterwards, 10 mL of seawater were siphoned off from each bottle for NH_4^+ determinations. Dissolved NH_4^+ was spectrofluorometrically measured according to the Holmes et al. (1999) method, except in the "SUCCESSION" cruise where it was determined through the phenol-hypochlorite method (Solorzano, 1969) due to the inability to measure fluorescence on board. We used a standard curve from 0.04 to 10.24 μM to calibrate both the fluorescence and absorbance measurements. For the calculations of NH_4^+ excretion rates, we subtracted the NH_4^+ concentration quantified in the control flasks from those concentrations measured in the experimental flasks.

4.2.4 Enzymatic measurements

Once the seawater was sampled for NH_4^+ excretion analyses, the zooplankters were immediately frozen in liquid nitrogen (−196 °C) and stored at −80 °C awaiting enzyme analyses in the land-based laboratory. Organisms were then thawed, and sonicated for 45 s in 0.1 M Tris-buffer medium, made up to pH 8.6 with acetic acid. The resultant homogenate was centrifuged for 8 min at 4000 rpm. The whole process prior to the enzymatic assay never exceeded 20 min, with the samples being kept at 0 °C at all times. The supernatant was then assayed for glutamate dehydrogenase (GDH) activity following the method published in Bidigare and King (1981), slightly modified by applying the principles of fluorometry as explained in Fernández-Urruzola et al. (2011) to detect the NADH production rate in the reaction. To ensure the achivement of the maximum velocity (V_{max}) of the reaction, i.e., the potential enzymatic rate, we saturated the enzyme with 50 mM glutamate and 1.2 mM nicotinamide adenine dinucleotide (NAD^+). Furthermore, 2 mM adenosine-5'-diphosphate (ADP) was added to favor the glutamate deamination that could be inhibited to some degree by guanosine-5'-triphosphate (GTP) molecules present in the homogenate. In addition, for those samples collected off the Canary Islands, an aliquot of the supernatant fluid was simultaneously assayed for electron transport system (ETS) activity according to the Owens and King's (1975) protocol. This allowed us to evaluate seasonal changes in the $R_{O_2}/R_{NH_4^+}$ ratios. The two enzyme reactions were kinetically measured for 4 min at *in situ* temperature, so no correction through Arrhenius equation was needed.

4.2.5 Intracellular concentration of glutamate

We further studied the intracellular levels of the main substrate of the reaction (glutamate) in order to relate any temporal variation in the NH_4^+ excretion rates at the CI station with biochemical adjustments of the GDH. Among other factors, the concentration of available glutamate will be critical to determine the rate at which the GDH can operate. Accordingly, we analyzed the intracellular concentration of free glutamate by applying the method of Hans-Otto and Michal (1974), which uses diaphorase, tetrazolium salts and pure GDH from bovine liver (EC 1.4.1.3) to determine the glutamate concentration in the sample. This method overcomes the equilibrium of the GDH reaction by the continuous reoxidation of the NADH formed from the glutamate deamination

(Eq. 4.1), through coupling a second enzyme reaction catalyzed by diaphorase (Eq. 4.2):

$$\text{Glutamate} + \text{NAD}^+ + \text{H}_2\text{O} \overset{\text{GDH}}{\rightleftharpoons} \alpha - \text{Ketoglutarate} + \text{NADH} + \text{NH}_4^+ \quad (4.1)$$

$$\text{NADH} + \text{INT} + \text{H}^+ \overset{\text{Diaphorase}}{\rightleftharpoons} \text{NAD}^+ + \text{Formazan} \quad (4.2)$$

Since the reaction proceeds stoichiometrically, we derive the intracellular glutamate concentration from quantifying the total formazan production, whose extinction coefficient is measured at 492 nm.

4.2.6 **Statistics**

Statistical analyses were performed using SPSS for Macintosh (v 22, Inc., Chicago, USA). The normal distribution of data and the variance homogeneity were confirmed by the Shapiro-Wilk and the Levene's tests, respectively. An ANCOVA test was applied to check significant differences between the $R_{NH_4^+}$-protein and the GDH activities-protein slopes. Differences in the $R_{NH_4^+}$ and GDH activities between locations and size categories were determined by one-way ANOVA tests. When necessary, Box-Cox analyses were applied to look for the best transformations of the protein-specific data in order to achieve normality and homoscedasticity. All the regression equations and confidence intervals (*CI*s) were calculated using Sigmaplot (v 12.5, Systat Software Inc., California, USA).

4.3 **Results**

4.3.1 **Ocean setting from the study sites**

Sampling dates and oceanographic properties from the different provinces studied during 2011 are presented in Table 4.1, along with the number of experiments conducted at each marine system. Mean sea surface temperature (SST) values ranged from a low of 14.6 °C in the BU to a high of 25.1 °C in the NA. The opposite trend observed in the averaged chlorophyll-a values, with their maximum in the BU (3.18 mg m^{-3}) and the minimum in the NA (0.08 mg m^{-3}). Both variables reflected the features typical of upwelling and oligotrophic environments, respectively. There were less, but still noticeable, seasonal differences in the hydrographical properties in the Canary Islands waters.

Thus, during the late winter bloom period (CI-LWB) the waters were colder and had more phytoplankton biomass than during October (Table 4.1).

Table 4.1: Marine areas sampled during 2011 for NH_4^+ excretion and GDH analyses in zooplankton. SST and SSS stand for the sea surface temperature and salinity, respectively. The range min - max (mean) is given for each physical or biological variable. The last column (exp. number) indicates the number of incubations performed at each cruise.

Cruise	Region	Study season (in 2011)	SST (°C)	SSS (PSU)	Chl-a (mg m^{-3})	Exp. number
Malaspina 2010	Indian Ocean	Feb. - Mar.	16.5 - 25.9 (21.5)	34.8 - 36.0 (35.5)	0.04 - 0.52 (0.18)	23
	North Atlantic	Jun. - Jul.	21.1 - 28.8 (25.1)	34.5 - 35.4 (34.9)	0.04 - 0.27 (0.08)	57
Camvalex	Canary Islands	Apr.	18.2 - 20.8 (19.3)	36.6 - 38.8 (36.7)	0.33 - 0.36 (0.34)	83
		Oct.	20.6 - 23.3 (22.1)	36.8 - 36.9 (36.9)	0.22 - 0.26 (0.24)	52
Succession	Northern Benguela	Aug. - Sep.	12.8 - 16.2 (14.6)	34.4 - 35.8 (34.8)	0.75 - 14.34 (3.18)	32

4.3.2 NH_4^+ excretory metabolism of zooplankton throughout different marine systems

Fig. 4.2 shows the relationship between protein content in the sample and both $R_{NH_4^+}$ and GDH activities from the different marine systems surveyed, disregarding the potential effect of *in situ* temperature. Both variables were significantly correlated with the biomass ($p < 0.0001$), even though the variance in the GDH activities that was explained by the protein content (62 %) doubled that for $R_{NH_4^+}$ (29 %). On the other hand, the slopes from the regression analyses were significantly different from each other (ANCOVA test, $F_{1,243} = 16.39$, $p < 0.01$), which would cause variability in the GDH/$R_{NH_4^+}$ ratio with biomass.

$R_{NH_4^+}$ and GDH activities were then standardized by protein for comparison between areas and size fractions (Fig. 4.3). It is noteworthy that no large zooplankton (> 1000 μm) was captured in the net during CI-LWB. This was not the case in BU, where only the zooplankton between 500 - 1000 μm was considered due to methodological problems in the other size categories. Biomass specific-$R_{NH_4^+}$ indicated some allometry as they were, in general, higher in the smaller size fraction (Table 4.2). Considering the study area, the most significant differences in $R_{NH_4^+}$ were found at CI-ST and BU, where the NH_4^+ release per unit of protein showed the lowest rates (Table 4.2). This variability was attributed mainly to the smaller size fractions, since the $R_{NH_4^+}$ in the largest zooplankton (> 1000 μm) was relatively invariant along the marine systems (ANOVA test, $F_{2,28} = 1.55$, $p = 0.231$). As expected for potential meas-

urements, the protein specific-GDH activities were always higher than their correspondent $R_{NH_4^+}$ (Fig. 4.3*b*). GDH activities depicted, however, a different pattern than that observed in $R_{NH_4^+}$. In fact, the differences with size fraction followed the opposite trend, with the GDH activities being higher in the largest organisms (Table 4.2). The variability in the GDH between regions was not so

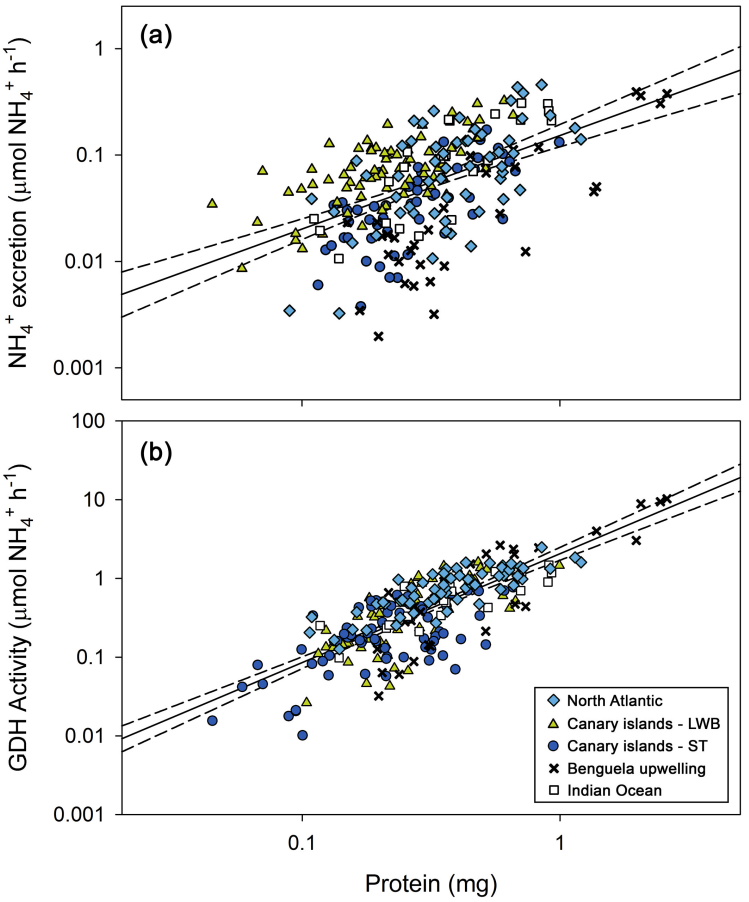

Figure 4.2: Log-scale scatterplot showing the relationship between protein content and NH_4^+ excretion rates (a), and between protein content and GDH activities (b). Each data point represents a mixed zooplankton sample incubated at *in situ* temperature (ranging from 12.8 to 28.8° C). The least-square linear regressions were: log $R_{NH_4^+}$ = 0.87 log *protein* − 0.82 (r^2 = 0.29, n = 243, $p < 0.0001$) for NH_4^+ excretion rates, and log *GDH* = 1.38 log *protein* + 0.31 (r^2 = 0.62, n = 247, $p < 0.0001$) for GDH activities. Dashed lines stand for the 95 % *CI*s.

marked although, paradoxically, CI-LWB presented the lowest GDH activities. Nevertheless, considering the zooplankton between 100 - 1000 µm, the GDH activities between CI-LWB and CI-ST were comparable (Student t-test, $p > 0.05$).

The relationships between GDH activities and $R_{NH_4^+}$ at each location and size fraction, in terms of µmol NH_4^+ mg protein^{-1} h^{-1}, are presented in Table 4.3. Both variables were linearly related in all the cases, so no transformations were applied to the data. Furthermore, each data set were normally distributed

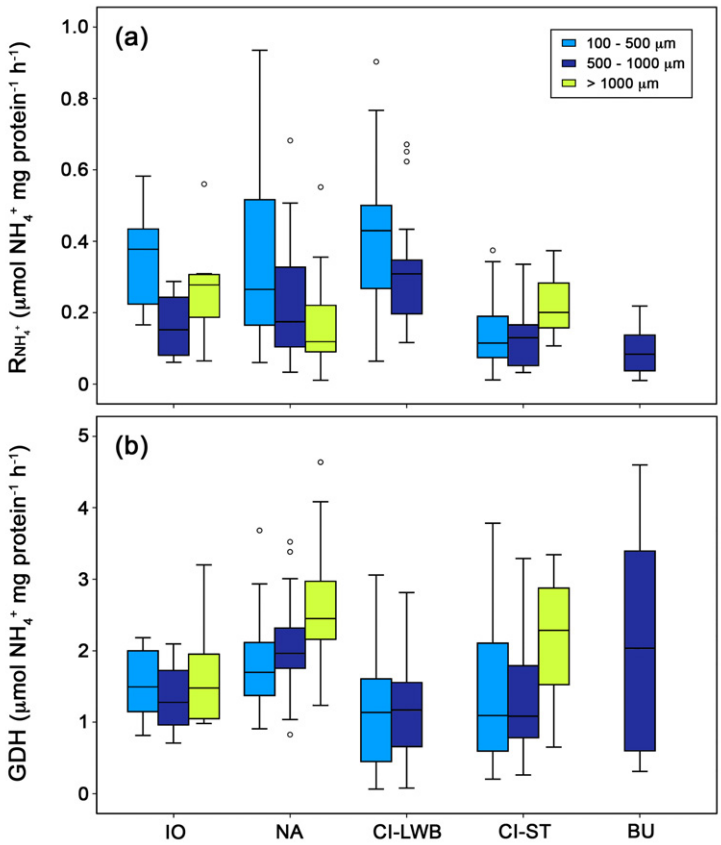

Figure 4.3: Boxplot showing the biomass-specific NH_4^+ excretion rates (a), and the biomass-specific GDH activities (b) in three size categories of zooplankton throughout different marine ecosystems. The lower and upper boundaries of the boxes represent the first and third quartiles of the data distribution, respectively, with the dark line in the middle as the median. Error bars indicate the 95 % *CI*s.

Table 4.2: One-way ANOVA analyses for both $R_{NH_4^+}$ and GDH activities. The factors, *location* and *size*, were applied separately, since not all the size categories were available in the five locations. Box-Cox analysis was applied wherever variable transformation was necessary to make ANOVA valid. Accordingly, the square root was found to be the best transformation of the data.

$R_{NH_4^+}$	*df*	*MS*	*F*	*p*-value	Pairwise comparison (Tukey's test)
Location	4	0.50	27.06	*	CI-LWB > [IO***, NA**, (CI-ST, BU)*];
Residual	219	0.02			[IO, NA] > [CI-ST***, BU*]
Size	2	0.32	13.00	**	100 μm > [1000 μm***, 500 μm*]
Residual	221	0.02			
GDH					
Location	4	5.60	7.77	*	NA > [CI-LWB*, CI-ST**];
Residual	216	0.72			BU > CI-LWB***
Size	2	5.61	7.33	*	1000 μm > [500 μm***, 100 μm*]
Residual	218	0.77			

* Significant at a level $p < 0.001$, ** $p < 0.01$, and *** $p < 0.05$.

(Shapiro-Wilk test, $p > 0.05$), and their variance was significantly constant across observations (Levene's test, $p > 0.05$). This allowed us to extract meaningful regression statistics and compare our slopes, which define the GDH to $R_{NH_4^+}$ ratio, with other published GDH/$R_{NH_4^+}$ means. These slopes were similar between the NA, IO and CI-LWB, ranging from 1.7 (NA) to 2.3 (IO) for the whole community. Furthermore, the ratio measured at the CI-LWB compared well with those reported in the literature for the same area and season (Fernández-Urruzola et al., 2011; Hernández-León and Torres, 1997). However, the GDH to $R_{NH_4^+}$ relationship increased dramatically up to 6-fold during the stratification period, at the CI-ST (= 13.27, $p < 0.0001$). Zooplankters from other ecosystems were characterized by a higher GDH/$R_{NH_4^+}$ ratio, with a maximum of 43.8 in the marine mysid *Praunus flexuosus* (Bidigare and King, 1981). In general, the error of estimates (*SEE*) was lower in the monospecific experiments than in those samples of mixed zooplankton. Seeking a common relationship for all the study areas, we pooled all our experimental data in Fig. 4.4. In this case, both rates (in μmol NH_4^+ sample^{-1} h^{-1} units) were logarithmically transformed to reduce heteroscedasticity of the residuals. The general

equation was:

$$\begin{gathered}\log GDH = 0.64\ \log R_{NH_4^+} + 0.36 \\ (r^2 = 0.37,\ n = 235,\ p < 0.0001,\ SEE = \pm 42.6\,\%)\end{gathered} \tag{4.3}$$

The values from the five cruises were distributed uniformly along the regression line, but all together generated a higher dispersion as compared to the one observed for each individual cruise. Accordingly, the standard error of the estimate in Eq. 4.3 doubled the errors found when regressing each cruise separately. Still, the linear model for the whole data set was significant at $p < 0.0001$. Considering a multivariate regression in the form of

$$\begin{gathered}\log GDH = -2.25 + 0.72\ \log R_{NH_4^+} + 0.12\ T + 0.42\ Chl\text{-}a \\ (r^2 = 0.59,\ n = 235,\ p < 0.0001,\ SEE = \pm 34.5\,\%)\end{gathered} \tag{4.4}$$

which includes other factors such as *in situ* temperature (T) and chlorophyll-a (*Chl-a*), we improved the prediction of GDH activities to 59 %. Similarly, the error associated with Eq. 4.4 decreased by 8.1 % with respect to the simple regression model.

4.3.3 **Temporal variability in the zooplankton excretory metabolism**

We chose a station located off the eastern coast of Gran Canaria to explore the temporal variability in the GDH/$R_{NH_4^+}$ ratios of zooplankton, as well as in other biochemical factors that are in some way related to the excretory metabolism. Fig. 4.5 shows the averaged $R_{NH_4^+}$, GDH activities, intracellular glutamate concentrations and the potential respiration to $R_{NH_4^+}$ relationships during the two sampling-times. While GDH activities increased slightly from 1.21 µmol NH_4^+ mg protein^{-1} h^{-1} during the mixing period (CI-LWB) to 1.58 µmol NH_4^+ mg protein^{-1} h^{-1} during the stratification (CI-ST), some other variables decreased sharply. Thus, the $R_{NH_4^+}$ declined by half from April to October, and the averaged intracellular glutamate was 4-times less concentrated in the latter period. There was therefore a positive correlation between the $R_{NH_4^+}$ and the internal pool of glutamate, as seen in Fig. 4.6. During the whole study, the $R_{O_2}/R_{NH_4^+}$ ratio remained relatively stable within the range of protein catabolism (i.e., below 13, see Fig. 4.5).

Table 4.3: Regression analyses between $R_{NH_4^+}$ and GDH activities in different marine ecosystems. The relationship between the two variables is defined by the equation $GDH = a + b\,R_{NH_4^+}$, where a is the intercept and b, the slope. For comparison, all the regressions relate both rates in terms of μmol NH_4^+ mg protein^{-1} h^{-1}. The column n stands for the number of data computed in each analysis, while the *SEE* represents the standard error of estimates.

Area	Group	Size (μm)	n	Slope	Intercept	r^2	F	p-value (F-test)	*SEE* (±%)	Reference
North Atlantic	Mixed zooplankton	100 - 500	25	2.2 **	0.66	0.41	16.1	0.0005	18.9	This study
		500 - 1000	25	1.6 ***	1.20	0.29	9.3	0.0056	21.4	This study
		> 1000	9	3.9 n.s.	1.8	0.19	1.6	0.2422	21.8	This study
		Total (> 100)	59	1.7 *	1.01	0.29	21.4	< 0.0001	15.0	This study
Canary Islands - LWB	Mysid (*Leptomysis lingvura*)	$> 2 \times 10^4$	41	4.7 *	0.58	0.81	124.1	< 0.0001	7.5	Fernández-Urruzola et al. (2011)†
	Mixed zooplankton	100 - 1000	59	3.8 **	1.09	0.20	14.3	0.0004	16.9	Hernández-León and Torres (1997)†
		50 - 100	11	4.4 ***	−0.05	0.66	17.5	0.0023	17.9	This study
		100 - 200	21	2.1 *	0.29	0.56	24.3	< 0.0001	18.5	This study
		200 - 500	29	2.3 *	0.24	0.45	22.1	< 0.0001	27.0	This study
		500 - 1000	15	3.0 ****	0.45	0.34	6.7	0.0230	18.9	This study
		Total (50 - 1000)	76	2.1 *	0.38	0.44	58.4	< 0.0001	18.5	This study
Canary Islands - ST	Mixed zooplankton	100 - 200	14	13.3**	−0.48	0.61	18.5	0.0010	18.0	This study
		200 - 500	18	13.9***	0.45	0.44	12.5	0.0028	23.4	This study
		500 - 1000	15	18.4**	−0.32	0.59	18.8	0.0008	16.8	This study
		> 1000	8	11.3***	−0.01	0.72	15.6	0.0076	16.1	This study
		Total (> 100)	55	13.3*	−0.20	0.56	62.1	< 0.0001	14.1	This study
Gulf of Maine	Mysid (*Praunus flexuosus*)	$> 4 \times 10^4$	8	43.8**	0.96	0.92	64.2	0.0002	3.7	Bidigare and King (1981)†
	Copepod (*Calanus finmarchicus*)	> 6000	10	16.8	-	-	-	-	15.5	Bidigare and King (1981)‡
	Mixed zooplankton	> 132	8	23.4	-	-	-	-	17.1	King et al. (1987)‡
Gulf of Mexico	Mixed zooplankton	> 333	11	18.7	-	-	-	-	23.0	Bidigare et al. (1982)‡
Great South Bay	Mixed zooplankton	> 200	10	24.3*	−0.52	0.98	436.3	< 0.0001	4.1	Park et al. (1986)†
Benguela upwelling system	Mixed zooplankton	500 - 1000	26	16.7*	0.40	0.49	23.4	< 0.0001	23.3	This study
Indian Ocean	Mixed zooplankton	100 - 500	8	2.9 ****	0.33	0.59	8.5	0.0270	14.9	This study
		500 - 1000	5	3.4 ****	0.48	0.88	24.2	0.0161	9.1	This study
		> 1000	6	2.2 n.s.	0.49	0.31	1.8	0.2487	28.5	This study
		Total (> 100)	19	2.3 **	0.56	0.47	15.2	0.0010	17.1	This study
East Sea of Korea	Mixed zooplankton	> 350	6	17.9****	0.12	0.71	9.89	0.0347	13.8	Park (1986b)†
Strait of Georgia	Copepod (*Neocalanus plumchrus*)	> 4000	4	15.3	-	-	-	-	28.1	Campbell et al. (2004)‡

* Significant at a level $p < 0.0001$, ** $p < 0.001$, *** $p < 0.01$, and **** $p < 0.05$. n.s. stands for not significant slope ($p > 0.05$).

† The regression equation between $R_{NH_4^+}$ and GDH activity (both in μmol NH_4^+ mg protein^{-1} h^{-1}) has been calculated from the published data.

‡ Only the averaged GDH/$R_{NH_4^+}$ ratio and the correspondent coefficient of variation are provided in the original work.

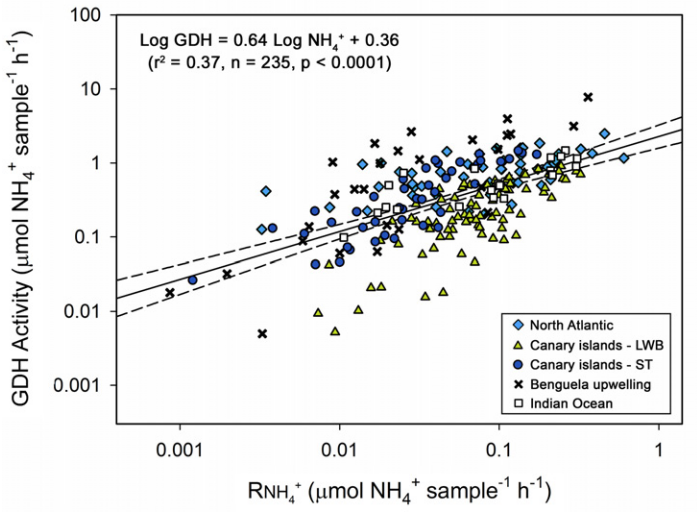

Figure 4.4: Log-transformed relationship between $R_{NH_4^+}$ and GDH activities. The regression includes all the experiments conducted during this research. Dashed lines stand for the 95 % *CI*s. The standard error of estimate (*SEE*) amounts to ± 42.5 %. The correction factor (*CF*, *sensu* Sprugel, 1983) to convert the equation into an arithmetic scale was 1.62.

4.4 Discussion

4.4.1 Zooplankton excretory metabolism throughout different marine systems

Providing universal equations for ecological processes has long been a challenge in marine sciences (e.g., Arístegui and Montero, 1995; Ikeda et al., 2001), but there are so many factors involved in modulating the biological rates that rarely a single mathematical function can explain any given variable in all the circumstances. Still, understanding the sources of variability in the plankton metabolism will help to predict nutrient fluxes in the oceans. Since Bidigare and King (1981) introduced the GDH assay as an index of heterotrophic NH_4^+ release, it has been extensively used in oceanographic research to assess both nitrogen regeneration within aquatic ecosystems (Fernández-Urruzola et al., 2014; Hernández-León et al., 1999, among others) and vertical nitrogen fluxes (*Chapter* 3, this thesis). However, there is little knowledge of the variability in the GDH to $R_{NH_4^+}$ ratio that results from the large spatial and temporal heterogeneity in the marine environments. A proper calibration of

this ratio throughout the world's oceans will lead to more meaningful estimations of $R_{NH_4^+}$ from GDH measurements.

Metabolic rates are known to vary as a function of body mass. In order to evaluate any potential effect of biomass in the relationship between the physiology ($R_{NH_4^+}$) and the enzymology (GDH), both rates were regressed against protein in Fig. 4.2. As Berges et al. (1993) pointed out, there would be no mass-specific influence in the GDH/$R_{NH_4^+}$ ratio if both variables follow the same allometric principles, i.e., scale to the same exponent. Here, the slope for $R_{NH_4^+}$ was 0.87, which means that smaller amounts of zooplankton excrete more NH_4^+ per unit protein than do larger amounts. This exponent falls in the range between 0.7 - 0.9 typical for marine planktonic metazoans (Ikeda et al., 2000). In addition to the size dependence, our value could be also explained by a bottle effect in the physiological rates, since high zooplankton densities would produce lower $R_{NH_4^+}$ (Bidigare, 1983). Conversely, GDH activities showed the opposite trend, with their slope being above 1.0 (b = 1.38). This dissimilarity in the scaling exponents would impact the relationship between

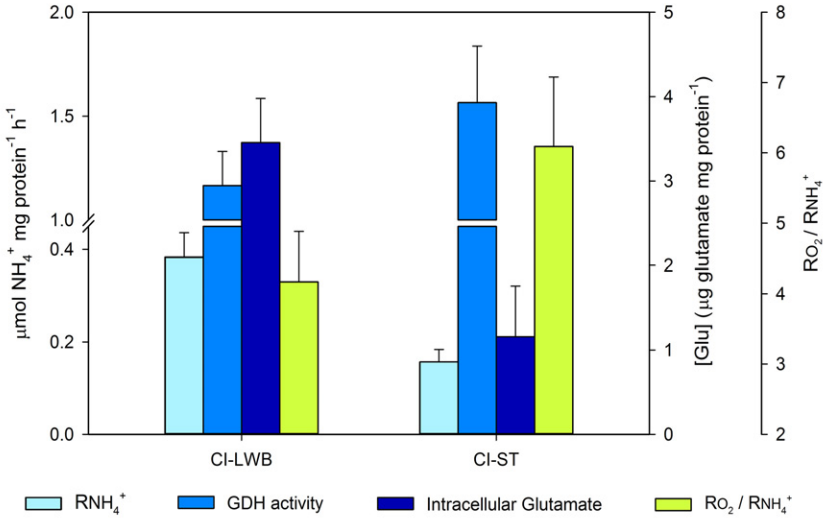

Figure 4.5: $R_{NH_4^+}$ (µmol NH_4^+ mg protein^{-1} h^{-1}), GDH activities (µmol NH_4^+ mg protein^{-1} h^{-1}), intracellular glutamate concentration (µg glutamate mg protein^{-1}) and $R_{O_2}/R_{NH_4^+}$ ratios measured in the zooplankton from the Canary islands during the so-called "late winter bloom" (CI-LWB), and during the stratification period (CI-ST). Error bars indicate the 95 % *CI*s.

GDH and $R_{NH_4^+}$ when analyzing samples with different biomass. Although organisms were fractionated in size categories, one should note that each mixed zooplankton sample was considered as a whole, and therefore there may be some biases according to the taxonomic composition and the size spectrum of organisms in the samples. Still, the scaling exponent for the GDH activities surpassed the correspondent value for the $R_{NH_4^+}$ by a similar magnitude in individual marine mysids with different protein content (Fernández-Urruzola et al., 2011 –see *Chapter* 5 in this thesis for details–). All this suggests that size fractionation of zooplankton samples is recommendable for reducing the mass effect when comparing metabolic measurements in populations with different size structures. Likewise, the use of particular GDH/$R_{NH_4^+}$ ratios for each size fraction should improve the prediction of actual $R_{NH_4^+}$. On the other hand, it is noteworthy that the dispersion in the $R_{NH_4^+}$ was considerably higher as compared to the one measured with the enzymatic rates. As has already been stated, water-bottle incubations are subjected to many methodological constraints that may lead to experimentally determined $R_{NH_4^+}$ values to be different from *in situ* rates in a hardly predictable manner. Furthermore, differences in the trophic conditions between oceanic systems could also affect more the physiological than the enzymatically determined potential rates, as the latter are inherently less responsive to environmental changes (Bamstedt, 1980).

The size-fractionated comparison of protein-specific excretory metabolism between marine ecosystems yielded similar conclusions (Fig. 4.3). $R_{NH_4^+}$ per unit protein was generally higher in the smallest size fraction (100 - 500 μm), which concurs with the mass-specific $R_{NH_4^+}$ given in Steinberg and Saba (2008) over a wide body mass range of marine zooplankton. However, as heralded by the scaling exponents, this pattern contrasted with the mass-specific GDH activities (Fig. 4.3*b*). Averaged specific $R_{NH_4^+}$ varied from a low of 0.09 μmol NH_4^+ mg protein^{-1} h^{-1} in the BU region to a high of 0.38 μmol NH_4^+ mg protein^{-1} h^{-1} in the CI-LWB. These values fitted reasonably well with the specific $R_{NH_4^+}$ range (0.13 - 0.27 μmol NH_4^+ mg protein^{-1} h^{-1}) predicted by the equations of Ikeda (1985). They were also close to the lower limit of the range provided in Hernández-León et al. (2008) for subtropical and temperate waters. This range varied between 0.43 - 0.67 μmol NH_4^+ mg protein^{-1} h^{-1} after a nitrogen to protein conversion factor of 0.52 (Postel et al., 2000). Nevertheless, these rates are not static, but fluctuate seasonally according to the different feeding and temperature scenarios. In fact, the metabolic rates are highly de-

pendent on the environmental temperature and as such, the $R_{NH_4^+}$ reached their minimum in the coldest waters from the BU despite being the most productive system in this study (see Table 4.1). Applying a Q_{10} of 3.60 (Hernández-León et al., 2008) and standardizing by the highest temperature (25.1 °C), the specific rates in the BU would become as high as in the NA (0.35 μmol NH_4^+ mg protein^{-1} h^{-1}). A similar temperature dependency should be considered for the catalytic activity of enzymes (Packard et al., 1975; Park et al., 1986). Particularly interesting was the wide range of protein-specific GDH activities found in the BU (Fig. 4.3*b*). Upwellings are complex ecosystems that give rise to a variety of metabolic states in heterogenous plankton communities that result from the interplay of water masses with different age and production histories (see Fernández-Urruzola et al., 2014, –*Chapter* 2, this thesis–, and the Chl-a range in Table 4.1). These waters hold exponential growing populations with net anabolic processes, as well as non-growing mature populations characterized largely by catabolism. All this may led to different levels of intracellular GTP across assemblages that would produce an uneven inhibition in the GDH activities. Furthermore, studies have shown great variability in the mass-specific metabolism when comparing multiple taxa (Steinberg and Saba, 2008). The balance between gelatinous and crustacean zooplankton in the samples could thus explain some differences in the metabolic rates among oceanic systems. On a dry mass basis, $R_{NH_4^+}$ has been found to be an order of magnitude lower in gelatinous zooplankton, even though such a difference becomes smaller when using carbon as a reference (Schneider, 1990). This means that the mass unit used for standardization largely determines both the specific $R_{NH_4^+}$ and GDH activities. Accordingly, any metabolic rate should be compared on the same mass basis, which also should be applied to comparisons between dimensionless variables such as the aforementioned scaling exponents and the GDH/$R_{NH_4^+}$ ratios. Enzymatic rates are usually scaled to protein because it is a relatively straightforward measure to assay in the same homogenate and therefore, our size fractionated GDH to $R_{NH_4^+}$ ratios were compared with those from literature in terms of protein (Table 4.3). Nevertheless, mass standardization assumes that body size is not a factor (Berges et al., 1993), so we pooled all our rates without standardizing in Fig. 4.4.

Previous studies on the respiratory metabolism suggested that the regression models between enzymatic and physiological rates would produce lower errors than averaging individual ratios (Arístegui and Montero, 1995; Packard

and Williams, 1981). Here, the mean standard error of the regression analyses that were applied to each data set amounted to ± 17.6 % (Table 4.3), while the mean coefficient of variation ($CV = 100 \times SD \div \overline{x}$) of the averaged ratios rose to ± 60.4 %. This evidences the superiority of the earlier approach. Its error, however, increased up to ± 42.6 % when regressing all data together (Eq. 4.3). Still, these uncertainties associated with the GDH/$R_{NH_4^+}$ ratios were on the same order than those produced by other standard techniques used in ecological procedures for plankton metabolism (King and Packard, 1975; Richardson, 1991). In general, GDH activities correlated well with $R_{NH_4^+}$ in all the marine ecosystems, with the analyses being significant mostly at a level $p < 0.01$. The highest coefficient of determination (r^2) was obtained in those monospecific cultures of mysids that were maintained under laboratory controlled conditions (Bidigare and King, 1981; Fernández-Urruzola et al., 2011). Working with natural mixed zooplankton assemblages, only Park et al. (1986) achieved a better correlation between GDH activities and $R_{NH_4^+}$. The relationship between the two rates was highly variable across marine ecosystems, and ranged from 1.7 in the whole community from the NA to 43.8 in the mysid *Praunus flexuosus* (Bidigare and King, 1981) from the Gulf of Maine. As discussed above, multiple factors that are inherent in the zooplankton communities such as biomass, growth, feeding and taxonomy, determine how the biochemistry and the physiology are related. Thus, physiological rates have been found to be closer to their potential rates in non-gelatinous zooplankton than in gelatinous zooplankters (King and Packard, 1975); the same is expected for small, growing and well-fed zooplankton (Fernández-Urruzola et al., 2011). Aside from these biological constraints, one assumes that other methodological artifacts derived from manipulation (e.g., stress, injury or crowding) and analytical procedures influence equally over all the measurements, but this is probably not the case. Therefore, an unique function can hardly consider all these sources of variability, so its ability to predict $R_{NH_4^+}$ in various ecosystems and zooplankton communities would be limited (Eq. 4.3). Nevertheless, its accuracy seems to be improved to some extent if environmental parameters such as temperature and chlorophyll-a are considered in the function (Eq. 4.4). In the less complex case of prokaryotes and nanozooplankton, a general equation may yield more accurate predictions of $R_{NH_4^+}$ from GDH measurements, as demonstrated by Arístegui and Montero (1995) in the respiratory metabolism case study.

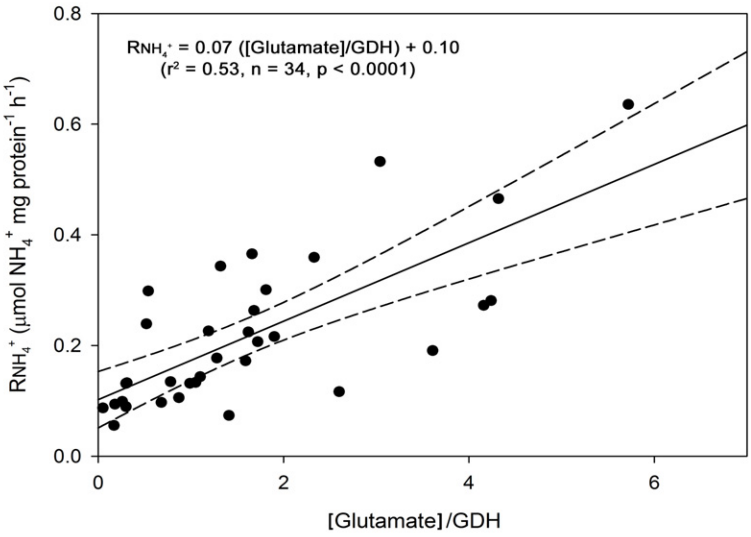

Figure 4.6: Relationship between the $R_{NH_4^+}$ and the glutamate concentrations (µg glutamate mg protein^{-1}) standardized by the GDH activities (µmol NH_4^+ mg protein^{-1} h^{-1}) in waters off Gran Canaria. Dashed lines stand for the 95 % *CI*s.

4.4.2 **Temporal variability in the zooplankton excretory metabolism**

Table 4.3 shows that seasonal changes in the GDH/$R_{NH_4^+}$ ratios at the same spot can be higher than the variation measured between oceans. During the late winter bloom (CI-LWB), which usually occurs from January to April in the Canary waters, the erosion of the thermocline allows the entrance of nutrients into the sunlit layer and consequently, an increased primary productivity (De León and Braun, 1973). This was reflected in the higher chlorophyll-a concentration during CI-LWB as compared to the stratification period, CI-ST (Table 4.1). At that time, zooplankton released an average of 0.39 µmol NH_4^+ mg protein^{-1} h^{-1}, which doubled the protein-specific $R_{NH_4^+}$ during CI-ST (Fig. 4.5). Hernández-León and Torres (1997) monitored the mesozooplankton $R_{NH_4^+}$ from November to May off Gran Canaria island, and also found great variability in the rates according to the trophic fluctuations (ranging between 0.02 - 0.71 µmol NH_4^+ mg protein^{-1} h^{-1}). Similar to our findings, their GDH activities did not follow the $R_{NH_4^+}$ pattern, which originated different GDH/$R_{NH_4^+}$ ratios during the study period. In fact, several studies have found

that the specific GDH activities did not peak in the chlorophyll-a maximum, but rather it was attenuated (Fernández-Urruzola et al., 2014; Hernández-León et al., 2001; Park et al., 1986). A plausible biochemical explanation was given by Park et al. (1986), who suggested a strong inhibition through the high GTP concentration that was being generated via the tricarboxilic acid cycle in those organisms that were actively growing under favourable trophic conditions. In such a situation, GDH activities may be underestimated by the standard assay, since it would require higher levels of ADP to counteract the GTP effect. This could explain the lower GDH/$R_{NH_4^+}$ ratios during well-fed conditions, as well as differences in the values of the *y*-intercepts observed in Table 4.3. Similar behavior in the ratio was observed when zooplankters were exposed to starvation in laboratory experiments (Fernández-Urruzola et al., 2011; Park, 1986a). In addition to the allosterism associated with GTP, GDH is known to be controlled by the internal pool of glutamate. As in all enzymes, the substrate concentrations determine the actual rate at which the reaction can operate (Bisswanger, 2008). However, few attempts have been made to relate them through direct measurements in marine sciences. Park et al. (1986) calculated the effective glutamate concentration from kinetic parameters in macrozooplankton, and showed an increase of the glutamate pool linked with those periods of food availability. Similar findings have been made in the respiratory metabolism, since Osma et al. (in press) measured a decrease in the levels of pyridine nucleotides in the marine dinoflagellate *Oxyrrhis marina* as organisms starved. Here, internal glutamate decreased dramatically from April to October, which supports the hypothesis of substrate levels as a key mechanism in the regulation of $R_{NH_4^+}$ (Hernández-León and Torres, 1997). Accordingly, the higher glutamate availability may lead the organisms to excrete more NH_4^+ per unit protein during the late winter bloom. The significant correlation between these two variables (Fig. 4.6) reinforces the utility of kinetic-based models in the study of zooplankton metabolism (Packard and Gómez, 2008). The measurement of biochemical parameters such as the Michaelis constant (K_m), jointly with the intracellular levels of both the substrates and allosteric regulators, would therefore open new avenues in the approximation of the *in vivo* $R_{NH_4^+}$ from GDH activities. Furthermore, we studied the relationship between the respiration rates (R_{O_2}) and the $R_{NH_4^+}$ because it serves as an index of the metabolized food (Mayzaud and Conover, 1988). In effect, this ratio is a remineralization scale. Although it was slightly higher during CI-ST, the low values reflec-

ted a protein-based catabolism during the two sampling periods. This is not surprising since the small microheterotrophs, poor in fatty acids, constitute the 35 - 80 % of the diet of mesozooplankton in these waters (Hernández-León et al., 2004). So rather than a shift in the diet, changes in the density of prey seem to be responsible for the variability measured in the zooplankton excretory metabolism.

4.5 Conclusions

GDH is an essential tool for mapping zooplankton $R_{NH_4^+}$ throughout the oceans. Unfortunately, the statistical relationship as measured by GDH/$R_{NH_4^+}$, the ratio between the enzymatic and physiological rates, is not universal. In this research we found that temporal variability in the GDH/$R_{NH_4^+}$ ratios from the same ecosystem could be higher than that found between oceans. Both GDH activities and $R_{NH_4^+}$ maintained different allometric relation with biomass, which has to be considered when comparing communities with different sizes. Still, this effect should be approached on specific taxa and controlled culturing conditions in order to avoid any interference from other sources of variability. On the other hand, the trophic situation is known to be a key factor in modulating the metabolic rates of zooplankton. Here we observed fluctuations in the internal glutamate pool according to the productivity regime, and parallel to the $R_{NH_4^+}$ trends. How this variation affects the actual enzymatic rates needs to be further investigated. Given the variability in the GDH activity to $R_{NH_4^+}$ relationship, we encourage a field calibration of this ratio for each specific community being studied.

Acknowledgements. We wish to thank the crews of the BIO Hespérides, BIO Atlantic Explorer, and RV Maria S. Merian for their expertise and enthusiastic support during the cruises. We thank L. Postel and C. M. Duarte for their invitation to participate in the "SUCCESSION" (I. F.-U.) and "MALASPINA 2010" (F. M., N. O., I. F.-U.) cruises. We are also grateful to M. Estrada and P. Mozetic for providing the chlorophyll data from the MALASPINA 2010 cruise. Funding was provided, in part, by the German Research Foundation (DFG), and by the MALASPINA 2010 (CSD2008-00077) and the BIOMBA (CTM2012-32729/MAR) projects granted to C. M. Duarte and M. G., respectively. I.F.-U. and N.O. were supported by postgraduate grants from the Formation and Perfection of the Researcher Personal Program from the Basque Government. T.T. P. was largely supported by TIAA-CREF and Social Security (USA).

Research is to see what everybody else has seen, and to think what nobody else has thought.

Albert Szent-Gyorgyi

CHAPTER

5

CAPÍTULO

GDH activity and ammonium excretion in the marine mysid, *Leptomysis lingvura*: Effects of age and starvation

I. Fernández-Urruzola, T.T. Packard and M. Gómez (2011), Journal of Experimental Marine Biology and Ecology 409 (1 - 2), 21 - 29.

http://dx.doi.or/10.1016/j.jembe.2011.07.035

ABSTRACT: NH_4^+ release by bacterial remineralization and heterotrophic grazers is the largest recycled nitrogen source in the euphotic zone. It determines the regenerated fraction of phytoplankton productivity, so the measurement of NH_4^+ excretion in marine organisms is necessary to characterize both the magnitude and the efficiency of the nitrogen cycle. Glutamate dehydrogenase (GDH) is largely responsible for NH_4^+ formation in crustaceans and consequently should be useful in estimating NH_4^+ excretion by marine zooplankton. Here, we study the physiological rate of NH_4^+ excretion and the GDH activity in an important North Atlantic mysid, *Leptomysis lingvura*. We address body size and starvation as sources of variability on the GDH to NH_4^+ excretion ratio (GDH/$R_{NH_4^+}$). We found a strong correlation between the $R_{NH_4^+}$ and the GDH activity ($r^2 = 0.87$) during growth. Both variables were regressed against protein in order to obtain the allometric scaling exponent. Since GDH activity maintained a linear relation ($b = 0.93$) and $R_{NH_4^+}$ scaled exponentially

(b = 0.55) in well fed mysids, the GDH/$R_{NH_4^+}$ ratio increased with size. However, the magnitude of its variation increased even more when adult mysids were starved. In this case, the GDH/$R_{NH_4^+}$ ratio ranged from 11.23 to 102.41.

Keywords: GDH; NH_4^+ regeneration; *L. lingvura*; Starvation; Body size.

5.1 Introduction

Nitrogen is essential for life. It is constituent to many biological structures and in all enzymatic reactions, but its availability is frequently limited in ocean ecosystems. As a result, nitrogen plays a critical role in biogeochemical cycles (Falkowski et al., 1998). Despite its existence in multiple oxidation states and in many chemical compounds in the ocean, the nitrogen which supports primary production occurs mainly in the forms of ammonium and nitrate (Bronk et al., 1994; Yool et al., 2007). The availability of these compounds determines the productivity of the ocean and thus, the capacity of this huge ecosystem to act as a carbon dioxide sink. Ammonium (NH_4^+) excretion from glutamate deamination in heterotrophic organisms constitutes an important recycled nitrogen source in the euphotic zone (Harrison et al., 1987; Steinberg and Saba, 2008), even though the nitrate remineralized in the near-surface mixed layer also sustains the regenerated production (Beckmann and Hense, 2009; Zehr and Ward, 2002). However, the nitrate produced in deep waters via nitrification, once it reaches the surface by vertical transport, is largely responsible for new production (Dugdale and Goering, 1967; Eppley and Peterson, 1979).

The relevance of the regenerated nitrogen to the phytoplanktonic growth rate and biomass has been widely addressed in the literature. The heterotrophic NH_4^+ release, on average, supplies around 80 % of the primary producers' requirements (Harrison, 1992), which reflects the significance of this metabolic process at a global scale. Factors such as temperature (Ikeda, 1985), nutritional composition of ingested food (Glibert, 1993; Miller and Roman, 2008; Saba et al., 2009) and the interaction between the different trophic levels (Glibert, 1998), among others, can modify locally this percentage. As a consequence, ammonium recycling efficiencies range from 50 % in coastal waters to about 95 % in the less productive areas of tropical latitudes (Eppley and Peterson, 1979), with the mesozooplankton responsible for 12 % to 33 % (Atkinson and Whitehouse, 2001; Hernández-León et al., 2008). Quantifying this physiological process in the oceans is then, necessary to characterize the efficiency of

the nitrogen cycle and to understand the basis of an aquatic ecosystem's productivity.

In order to assess the NH_4^+ excretion in zooplankton, water bottle-incubations and the more sensitive ^{15}N-isotope dilution technique have been used by oceanographers (Alcaraz et al., 2010; Glibert et al., 1982; Steinberg and Saba, 2008). However, although direct, these delicate methods are complicated by artifacts derived from organism manipulation, overcrowding or starvation that may occur during long incubation times (Bidigare, 1983). On a physiological scale such measurements can be made, but at a low data acquisition rate. This is fine for physiology, but oceanography requires many measurements made over large time and space scales and so a high data acquisition rate is needed. In recognizing these requirements of oceanography, Bidigare and King (1981) introduced a biochemical approach by proposing the enzyme glutamate dehydrogenase (GDH) as an index for NH_4^+ formation in the marine systems. They chose GDH because it is found in high levels in planktonic crustaceans and because its role in amino acid catabolism argues for its control over a great proportion of NH_4^+ excretion. In these ammoniotelic organisms, proteins are decomposed to amino acids and then, transaminated with α-ketoglutarate to produce α-ketoacids and glutamate. The glutamate is oxidized by NAD-dependent GDH (EC 1.4.1.3) into NH_4^+, NADH, α-ketoglutarate and one proton. Thus, the potential NH_4^+ excretion can be calculated from the rate of the GDH reaction (i.e., GDH activity).

The interest in GDH persists in spite of the problems associated with using enzyme assays to predict the physiology of the organisms. First of all, enzyme analyses are classically designed to measure the potential enzymatic activity (V_{max}) of an enzyme reaction. Accordingly, an enzyme assay requires the addition of externally added substrate, which insures that the assay determines the V_{max} instead of some undefinable other level of activity. It would be desirable to measure the actual rate of activity in the sample, the *in vivo* rate, but the technology is just not available now. Thus, any enzyme, under unlimited substrates, operates at its maximum rate, and the product generated over time is simply a function of the amount of enzyme present. In addition, there is variability in the ratios of GDH activity to NH_4^+ excretion due to changes in specific composition, body size and trophic conditions (see *Chapter* 4). How these parameters impact the biochemistry and physiology of NH_4^+ excretion is part of this investigation. In spite of these uncertainties, at an operational

level, the GDH analysis is a simple, fast and inexpensive proxy for heterotrophic NH_4^+ release. Strengthening our knowledge of the relationship between GDH activities and the NH_4^+ excretion rates ($R_{NH_4^+}$) under different conditions, would lead to more meaningful interpretations of the mesoscale variations in planktonic NH_4^+ excretion.

Working with the marine mysid *Praunus flexuosus*, Bidigare and King (1981) established a high correlation between GDH activity and the production of the main nitrogenous waste of crustaceans, NH_4^+ (Regnault, 1987; Ikeda et al., 2000). However, this ratio is expected to vary according to the body size, growth and nutritional status since GDH is a regulatory enzyme which is modulated by substrate availability, as well as by allosteric effectors such as adenosine-5'-diphosphate (ADP) and guanosine-5'-triphosphate (GTP). As a consequence, Park (1986a) obtained substantial fluctuations in the GDH/$R_{NH_4^+}$ for two species of copepods, when food availability conditions were modified during the experimentation. Similar behavior on that relationship was described by Hernández-León and Torres (1997) on mixed zooplankton from waters around Gran Canaria, where the so-called "late winter bloom" changes the trophic situation. These authors demonstrated a significant correlation between the GDH/$R_{NH_4^+}$ and respiration to excretion ($R_{O_2}/R_{NH_4^+}$) ratios, since the amount of NH_4^+ excreted is determined by the nitrogen content of the metabolized matter required for energy. In addition, Berges et al. (1993) pointed out the necessity of considering that enzyme activities scale allometrically with body mass in order to avoid erroneous interpretation of data when size structure of population is different. However, no attempt has been made to determine the influence of biomass scaling in both GDH and NH_4^+ excretion. If GDH is used as NH_4^+ excretion proxy, then it should follow equivalent size dependence. Here, we address the issue of age and starvation as sources of variation in the relationship between GDH activity and NH_4^+ excretion in the mysid shrimp *Leptomysis lingvura*. We chose this mysid specie because of its widespread distribution in shallow marine waters around Canary Islands, which implies a significant role in the nitrogen cycle of the coastal ecosystem. Furthermore, our choice is strengthened by the arguments that mysids are critical in nutrient cycling and selective grazing in the near coastal environments (Lindén and Kuosa, 2004). The main objective of this research is to provide better biochemical insight into *L. lingvura*'s nitrogen metabolism, which might be controlled under different physiological conditions by fluctu-

ations in the glutamate pool and by allosteric regulation of GDH. Furthermore, we introduce spectrofluorometry as a technique for increasing the sensibility of the GDH assay in zooplankton and hence, decreasing the biomass needed for a successful analysis.

5.2 Material and methods

5.2.1 Location and sampling

Marine mysids were sampled by diving off the Risco Verde coast (27°51'26" N, 15°23'11" W), located in the south-east of Gran Canaria island. The zooplankters were collected over shallow sandy bottoms, between 8 - 12 m depth. Along with each sample, *in situ* temperature was recorded (19.5 ± 1 °C). Scuba diving equipment, a 500 μm mesh size plankton net and plastic containers for storing the animals were used for sampling. Three species of mysids were identified: *Paramysis nouveli*, *Siriella armata* and *Leptomysis lingvura*. However, only *L. lingvura* was used for experimentation because its survival and fertility rates are high in culture (Herrera et al., 2011a).

5.2.2 Culture conditions

Once the mysids were captured, they were immediately transferred in 10-L buckets to a culture system constituted by six plastic trays (20 L each) suspended in a circulating water bath. Mysids were cultured as described in Herrera et al. (2011a), under a 14:10 ligth:dark cycle and a thermostated temperature (21 ± 0.5 °C) within the range registered in the sea. Except for starvation experiments, mysids were fed twice daily with 48 h nauplii of *Artemia* sp., enriched with Easy-DHA Selco® (INVE, Belgium). Since other studies (Domingues et al., 1998; Lussier et al., 1988) observed cannibalism of the smallest sizes if food became limiting, we provided *ad libitum* conditions by offering 100 *Artemia* organism^{-1} twice per day.

After an acclimation period of 24 h, the healthiest mature mysids were selected and separated in new tanks in order to spawn. The hatchlings collected after one day were used to study the effect of age on physiological rates and GDH activity. For starvation experiments, however, male adults were required, but otherwise the procedures were the same.

5.2.3 The influence of age on NH_4^+ excretion and GDH activity in *L. lingvura*

(i) Excretory metabolism. We assessed the impact of body mass on NH_4^+ excretion and GDH activity during the first thirty days of a mysid cohort, before these organisms became adults. In all the cases, animals were fed prior to experimentation. After feeding on *Artemia* for an hour, mysids were acclimated for half an hour in Whatman GF/F filtered seawater. Afterwards, two to six mysids, depending on the biomass, were placed carefully in glass-capped bottles (60 mL each) filled with filtered seawater at 21 °C and incubated in the dark. All the experiments included one control and three experimental flasks. After 30 minutes, the organisms were immediately transferred to new bottles and the water was siphoned off for NH_4^+ determination. NH_4^+ was measured spectrofluorometrically according to the Holmes et al. method (1999). It was optimized for the NH_4^+ concentrations expected in this study. The mysid excretion rates were quantified by subtracting the NH_4^+ concentration in control flasks from the NH_4^+ concentration in experimental flask at the end of each incubation period. The procedure was replicated with the same mysids four times over a period of two hours, which revealed the behavior of these rates. This procedure demonstrated that the rates were constant over these two hours. Furthermore, the short experimental time minimized induction and repression of the mysid's enzyme system as well as minimizing the potential effects of starvation.

(ii) GDH assay. Once the incubation experiments ended, mysids were immediately frozen in liquid N and stored in the freezer (−80 °C) for subsequent GDH analysis and protein determination. Later, the samples were thawed and kept on ice while awaiting analysis in order to prevent a decline in the protein activity. The mysids were placed in 2 mL of sonication medium composed of 100 mM Tris buffer, made up to pH 8.6 with acetic acid. Mysids were then sonicated for 50 seconds at 70 % amplitude in a VXC 130 Sonics device and centrifuged (0 - 2 °C) for 8 min at 4000 rpm. The supernatant fluid was assayed for GDH activity following a slightly modified Bidigare and King (1981) methodology. This modification consisted of using fluorometry rather than spectrophotometry to detect the NADH produced in the GDH reaction. The assay was run on an aliquot of the centrifuged extract (200 µL) that was mixed with NAD^+ and ADP solutions (300 µL and 250 µL, respect-

ively). Each reagent was made fresh daily and added separately to the mixture, prior to acclimation to the assay temperature. The resultant solution was incubated for a few minutes in a 1 cm path-length quartz cuvette until no fluctuations in NADH fluorescence were detected. Then, following the addition of glutamate (500 µL), the increase of fluorescence was monitored during 2 minutes with a Horiba Jobin Ybon Fluoromax® 4 spectrofluorometer, at 360 nm excitation and 460 nm emission wavelengths. The final volume of the reaction mixture was 1.25 mL. It contained 1.2 mM NAD^+, 2 mM ADP and 50 mM glutamate. Assay temperature was controlled to the *in situ* temperature (21 °C) by a thermostated multi-cell holder attached to a refrigerated recirculator. The fluorescence units were converted to activities (µmol NH_4^+ h^{-1}) from the NADH-fluorescence standard curve, which was prepared from pure GDH (1.4.1.3) extracted from bovine liver (from Sigma-Aldrich®) for each batch of work. This curve was determined over a range of 0.07 - 2.9 $\times$ 10^{-4} international units (U) of GDH activity per mL, where one U equals the amount of enzyme that converts one µmol NAD^+ min^{-1} (Fig. 5.1). This fluorometric

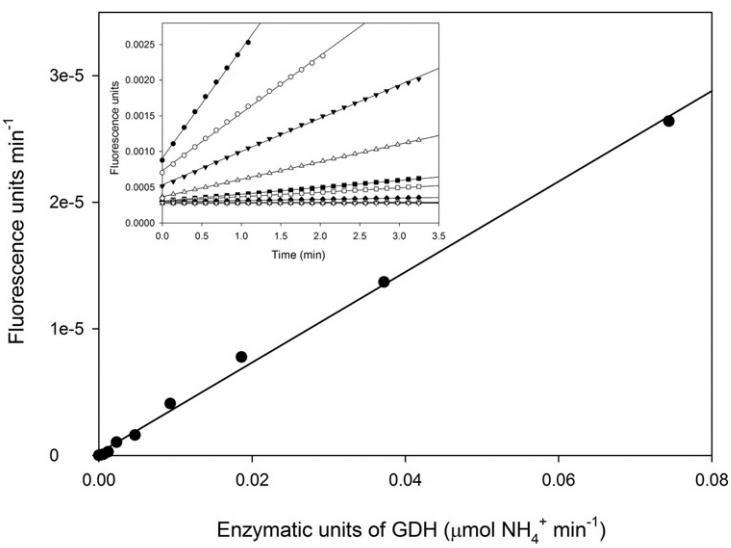

Figure 5.1: Construction of the standard curve for the GDH determination. Each data point represents the slope NADH production rate per minute obtained at the different GDH concentrations (inset). The resultant regression line is used to estimate the GDH activity in the mysids.

modification was compared with the spectrophotometric assay of Bidigare and King (1981), which is not directly calibrated against GDH activity. It is, instead, based on the specific absorptivity for NADH (ε = 6220 M^{-1} cm^{-1}) and Beers-Law. This leads to an apparent overestimation of GDH activity by the spectrophotometric assay as is shown in Fig. 5.2*a*, but does not affect its linear relationship with the fluorometric assay 5.2*b*.

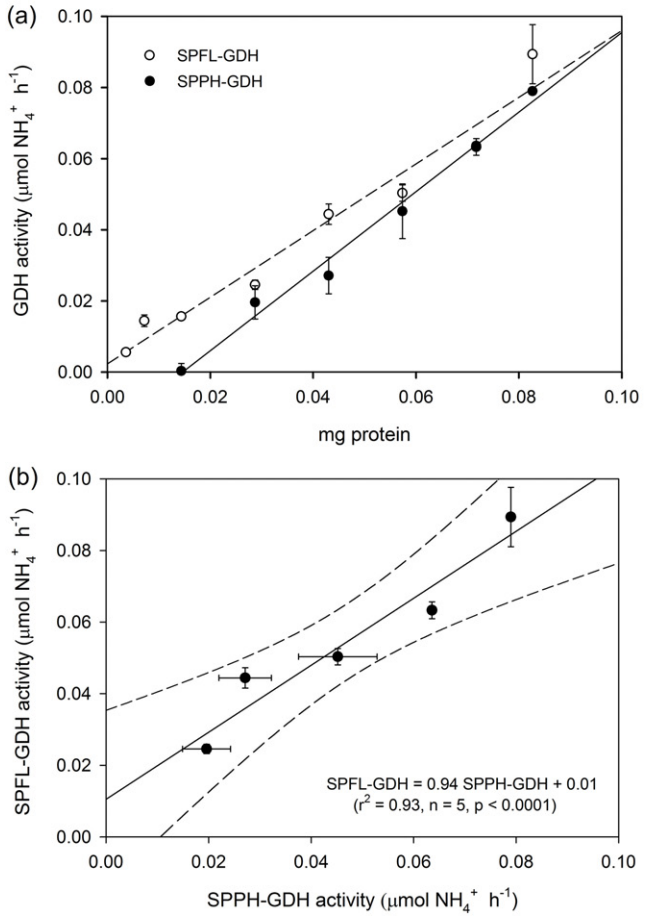

Figure 5.2: (a) Effect of enzyme concentration (mg protein per assay) on GDH activities measured spectrophotometrically (SPPH-GDH) and spectrofluorometrically (SPFL-GDH). (b) The correspondence between the SPPH-GDH (x-axis) and the SPFL-GDH (y-axis). None of the slopes are significantly different from 1 ($p > 0.05$). Each data point represents the mean of triplicates, with the standard deviations calculated for both techniques.

(iii) Biomass and protein determination. Biomass was estimated as protein in the samples using the Lowry et al. method (1951) modified by Rutter (1967). Calibration curves were made from standard solutions of bovine serum albumin (BSA), in which absorbance was read at 750 nm in a Beckman DU 650 spectrophotometer. Each data point represented the mean of triplicate analyses.

5.2.4 The impact of starvation on physiological rates and GDH activity in *L. lingvura*

A new experimental approach was designed to address the effect of starvation on the biochemistry and the physiology of NH_4^+ excretion in *L. lingvura*. After acclimating the mysids in the culture system for two days, mature well-fed males were transferred to individual containers. This procedure prevented cannibalism during the experimental period. In the base of each container was a 1 mm mesh net, which allowed fresh filtered seawater to enter and mysid fecal pellets to exit. During 4 days, successive incubations were carried out in triplicate, using three control bottles in each experiment. NH_4^+ excretion, GDH activity and protein were assayed as previously described, although apparent Michaelis constants (K_m) for glutamate were also calculated on each time by classic Lineaweaver-Burk transformation plots. Furthermore, in order to obtain the relationship between the oxygen consumed and the ammonium excreted ($R_{O_2}/R_{NH_4^+}$), O_2 consumption rates were estimated in the same incubation experiments by the continuous measurements of dissolved O_2 concentrations through a 6-channel Strathkelvin 928 Oxygen System® respirometer. Mysid respiration rates were calculated from O_2 time courses as the difference between the slopes in experimental and control chambers.

5.3 Results

5.3.1 GDH analysis and kinetics

GDH activities were linear over an order of magnitude of biomass (0.014 - 0.084 mg protein) for both spectrophotometry and spectrofluorometry (Fig. 5.2). According to the Student *t*-test applied in SPSS statistics v 19 software (Inc., Chicago, USA), the results showed a high coherence between the mean values of the activities analyzed by the two techniques ($p > 0.05$). This fact facilitates the comparison of our data with other data found in the literature.

Furthermore, in experiments at the low end of the spectrophotometric range we found that with spectrofluorometry we could read dilutions down to another order of magnitude. In fact, we could detect GDH activity at levels of 3.5 µg of protein. The low standard deviations of the samples quantify the superiority of fluorometry over spectrophotometry in this range.

The dependence of the GDH reaction on the substrates in a well-fed adult *L. lingvura* is characterized in Fig. 5.3. Both glutamate and NAD^+ follow

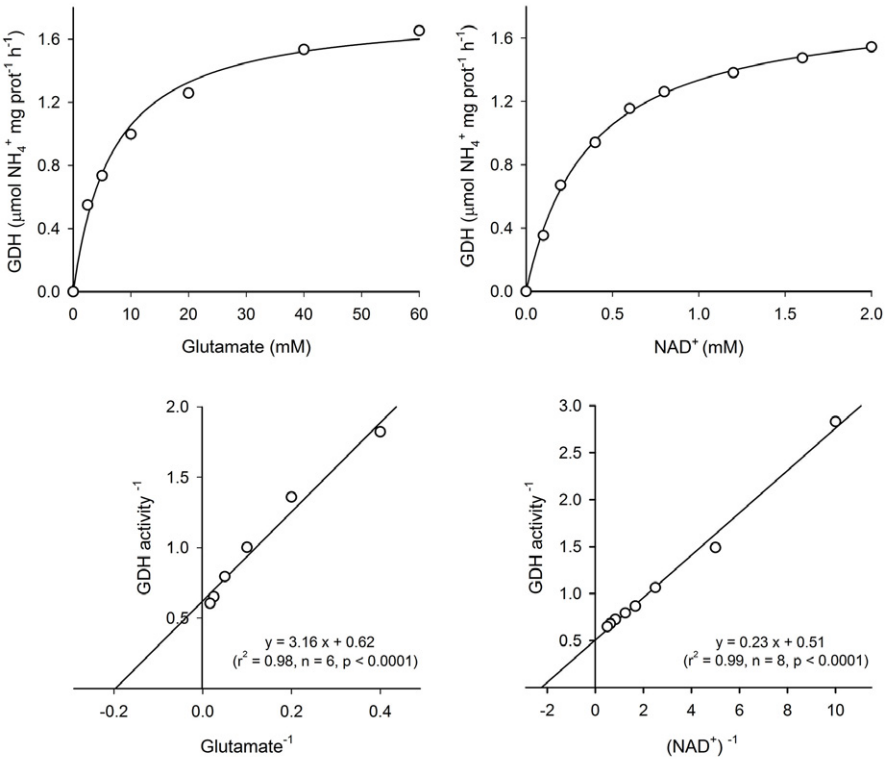

Figure 5.3: Monosubstrate enzyme kinetics of GDH exhibited in a well-fed mysid for each substrate of the reaction, glutamate (left) and NAD^+ (right). When glutamate was varied, the concentration of NAD^+ was 1.2 mM, whereas when NAD^+ was varied, a concentration of 50 mM glutamate was used. Top: Michaelis-Menten curves (primary plots). Bottom: Kinetic parameters extracted from the double-reciprocal transformations of Lineweaver-Burk (Lineweaver and Burk, 1934). Each y-axis intersect is equal to $1 / V_{max}$, and the regression slopes are defined by K_m/V_{max}. The data represent the mean of triplicate analyses.

the classic Michaelian hyperbole, where the V_{max} was 1.60 μmol NH_4^+ h^{-1} mg protein^{-1} and K_{Glu} was 5.61 mM for glutamate, while for NAD^+ the V_{max} and K_{NAD} were 1.97 μmol NH_4^+ h^{-1} mg protein^{-1} and 0.44 mM, respectively.

5.3.2 The influence of age on NH_4^+ excretion and GDH activity in *L. lingvura*

The increases with age of NH_4^+ excretion and GDH activity during the life cycle of *L. lingvura* (Fig. 5.4) are consistent with allometric principles. The physiological rate (r^2 = 0.83), the enzyme activity (r^2 = 0.85), as well as the protein content (r^2 = 0.94) showed an exponential trend with age. Statistical analysis based on the non-parametric Spearman's test exhibited a strong correlation of 0.84 ($p < 0.0001$) between the physiology ($R_{NH_4^+}$) and the biochemistry (GDH) when both were compared per mysid (Fig. 5.5). However, this relationship was obscured by protein normalization, so that the coefficient of determination became less significant (r^2 = 0.72, $p < 0.005$ –see *Chapter* 4–). The slope of the regression of the log-transformed data for GDH showed that its activities scale to a global exponent of 0.93 with protein data (Fig. 5.6), which was indeed considerably greater than the scaling exponent measured for the relationship of NH_4^+ excretion with protein (0.55). The resultant logarithmic relationship of the GDH to $R_{NH_4^+}$ ratio with protein took the form of,

$$\log (GDH/R_{NH_4^+}) = 1.60 \log protein + 0.64 \tag{5.1}$$

Accordingly, the GDH/$R_{NH_4^+}$ ratio tended to increase slightly as mysids grew (Fig. 5.7), with an overall value of 16.05 (see Fig. 5.5).

5.3.3 The influence of starvation on physiological rates and GDH activity

In contrast to the decrease in the specific NH_4^+ excretion after 10 h of starvation, the specific GDH activities did not change as the mysids became starved (Fig. 5.8). The GDH activity held a constant value around 1.47 (± 0.54) μmol NH_4^+ mg protein^{-1} h^{-1} throughout the entire experiment, so that the GDH/$R_{NH_4^+}$ ratio, as one would expect, increased. From an initial value of 11.2, it increased almost 10-fold to 102.4 (Table 5.1). The apparent K_{Glu} seemed to increase during the first 26 h of starvation and then decreased following two days, with

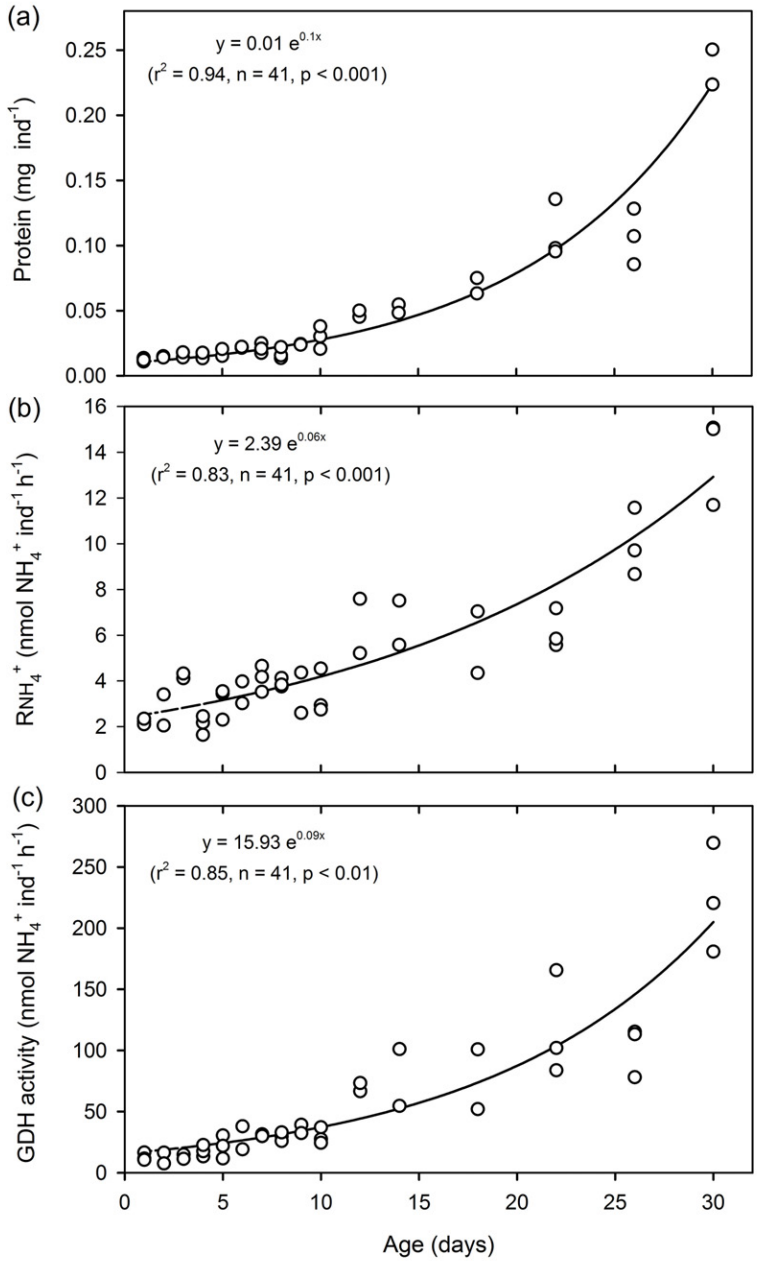

Figure 5.4: (a) Protein mass, (b) NH_4^+ excretion rates and (c) GDH activities per mysid over the month of experimentation.

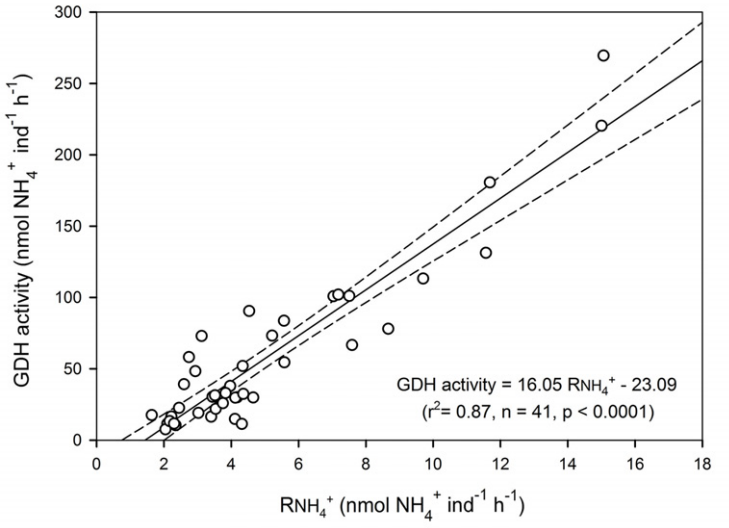

Figure 5.5: Linear regression between GDH activity and physiological NH_4^+ excretion per mysid. Dashed lines stand for the 95 % *CI*s.

a slight increase when the mysids were fed again. On the basis of the enzyme kinetics the effective concentration of glutamate was calculated. These theoretical calculations showed a sharp decrease of glutamate with starvation, from a high of 1.09 mM to a low of 0.03 mM. In regard to the effect of starvation on the O_2 consumption rate, the maximum respiration coincided with the highest value registered for NH_4^+ excretion at the level of 10 h after feeding. Then, there was a decrease of more than 6-fold in 1.5 days. Except for the last measurement, the $R_{O_2}/R_{NH_4^+}$ ratio remained fairly constant in the range of protein-based metabolism.

5.4 Discussion

5.4.1 GDH analysis and kinetics

Most of the oceanographic research on GDH has been focused on the larger sizes of zooplankton despite the recognition that microzooplankton are the major regenerators of NH_4^+ in marine systems (Bode et al., 2004; Bronk and Steinberg, 2008). The main problem with studying GDH in microzooplankton lies in concentrating them in the field sufficiently to obtain a detectable signal in

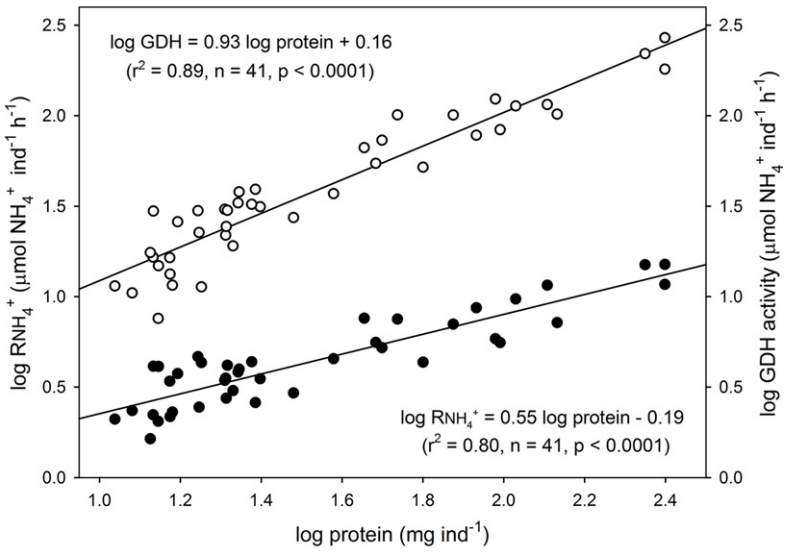

Figure 5.6: Log-transformed NH_4^+ excretion rates (filled circles) and GDH activities (open circles) versus log-transformed protein mass.

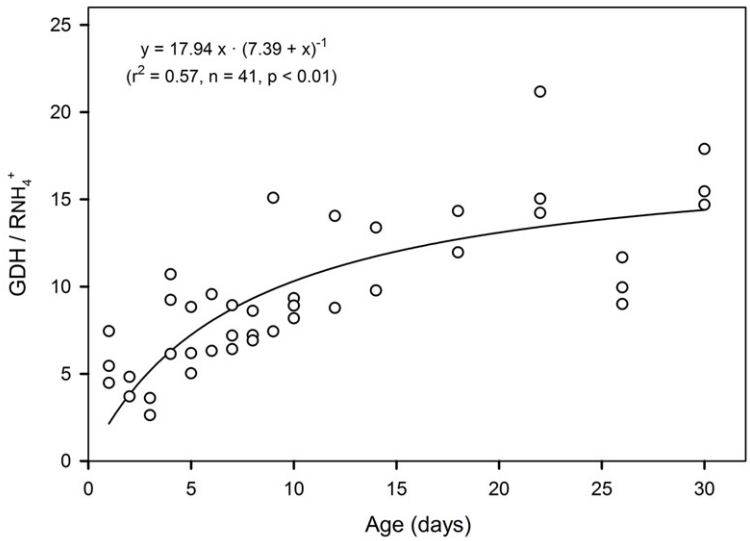

Figure 5.7: GDH/$R_{NH_4^+}$ ratios as a function of age in *L. linvura*.

the spectrophotometer. As a consequence of this difficulty, King et al. (1987) could not evaluate accurately the potential NH_4^+ regeneration in the fraction of zooplankton below 153 μm. In this work we have approached the problem by applying the advantages of spectrofluorometry (Segel, 1993) which, by measuring NADH fluorescence, increases the sensitivity of the assay at least 6-fold. In general, techniques based on fluorescence have a detection limit of about two orders of magnitude lower than those based on absorbance (Bisswanger, 2011). This would be an advantage when studying NH_4^+ excretion processes in the deep ocean (e.g., in *Chapter* 3). At low levels of activity, spectrophotometry has difficulty in discriminating between the true GDH signal and background artifacts. This explains the high variability in the spectrophotometric determinations when the enzyme concentrations in the analysis are too low ($\leq$ 0.043 mg protein). On the other hand, high enzyme concentrations ($>$ 0.084 mg protein) quench fluorescence and leads to underestimation of the true signal. This problem, however, can be solved by a simple dilution of the homogenate. Consequently, when available, fluorometry should be superior to spectrophotometry and here we make the transition to this more sensitive methodology.

The half-saturation Michaelis constant (K_m) for an enzyme is the most important biochemical property of the enzyme that one can measure (Friedmann, 1981). It defines the chemical affinity that the enzyme has for its substrate, the potential control by the substrate over the enzyme reaction, and the approximate concentration of the substrate in the cell (its *in vivo* concentration). Our K_{Glu} estimation on well-fed *L. lingvura* (5.61 mM) fall in the range of K_{Glu} from other well fed marine zooplankters, i.e., from 2.6 mM (Bidigare and King, 1981) to 11.8 mM (Park, 1986a). The dependence of GDH on NAD^+ has been much less addressed. Batrel and Regnault (1985) have data that indicate a K_{NAD} of about 1.3 mM, but their measurements were irregular and scantily described. Our K_{NAD} (0.44 mM) is lower and in comparing it with the K_{Glu} of 5.61 mM, confirms our finding that the affinity of GDH for NAD^+ is higher than it is for glutamate. Furthermore, it suggests that the role of NAD^+ in GDH control is more important than previously thought. Considering the K_m as a proxy of intracellular substrate concentration, the pool of glutamate and NAD^+ in a well-fed *L. lingvura* should be around 5.61 and 0.44 mM, respectively. However, theoretical calculations of the effective glutamate suggest

that intracellular concentration could be 5-fold lower (Table 5.1). Hence the importance of measuring the actual substrates concentrations to understand its role in the *in vivo* enzymatic activity.

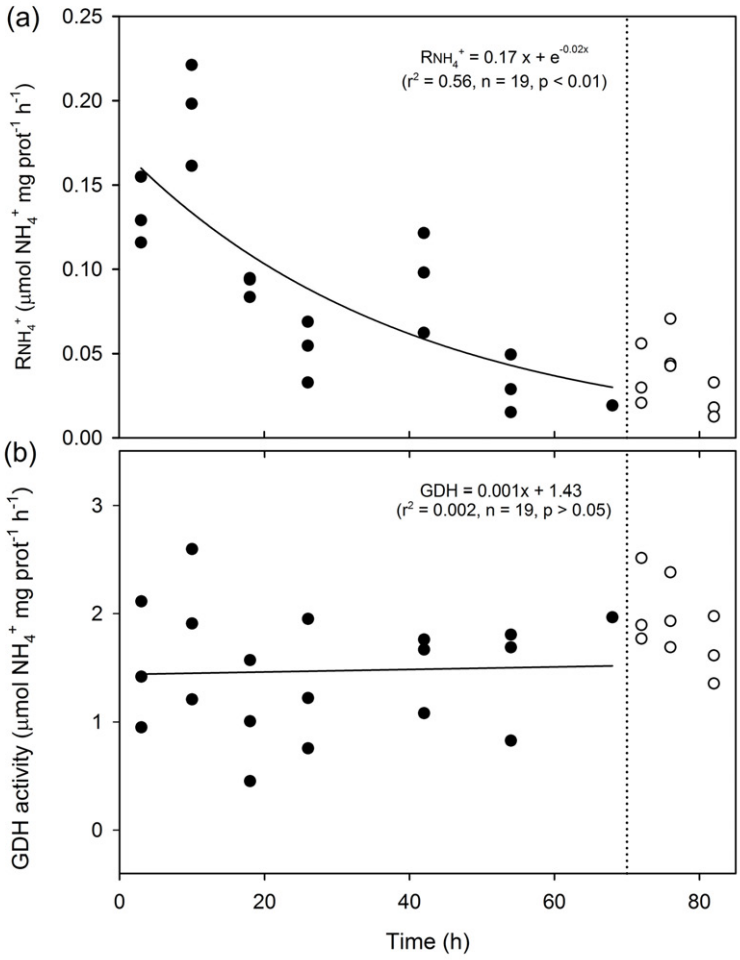

Figure 5.8: Impact of food deprivation on: (a) NH_4^+ excretion rates and (b) GDH activities of *L. lingvura*. The vertical broken line at 70 h represents the time in which one pulse of food was supplied to the mysids again. Thus, filled circles represents the starved mysids, while open circles refers to the experimental organisms which were fed again. However, only the starvation experimental data were considered in calculating the curves. The slope in panel *b* is no statistically different from zero ($p > 0.05$).

5.4.2 The influence of age on NH_4^+ excretion and GDH activity in *L. lingvura*

The amount of NH_4^+ excreted by a well-fed adult *L. lingvura* over time (13.9 ± 1.93 nmol NH_4^+ ind^{-1} h^{-1} –see Fig. 5.4*b*–) is in the lower limit of the range for adult mysids given by Bronk and Steinberg (2008). This could be expected as other mysid species are about 3-times, or more, the size of the *L. lingvura* experimented here. Furthermore, the values of GDH activity measured during mysid growth could account for the total NH_4^+ excretion registered at the same time. The high correlation between both parameters suggests an important role for GDH in the nitrogen metabolism, as was argued previously (Bidigare and King, 1981; Park et al., 1986). However, the apparent NH_4^+ excretion at zero GDH activity suggests the participation of other ezymes which also generate NH_4^+, such as glutaminase and AMP-deaminase. In addition, it is necessary to consider that the V_{max} obtained here represents a potential NH_4^+ excretion capacity of more than one order of magnitude greater than the directly measured NH_4^+ excretion rate. Since the substrate concentration required for the theoretical V_{max} tends to infinity, the actual enzyme velocity (apparent V_{max}) measured, in function of the amount of substrate added (50 mM), was around the 90 % of the true V_{max} (Bisswanger, 2008), so the difference between the potential and the *in vivo* rates becomes even bigger. In any case, the slope of the GDH activity to $R_{NH_4^+}$ of 16.05 (Fig. 5.5) falls between 24.3, the compar-

Table 5.1: Effect of starvation on the Michaelis constant for glutamate, and on the GDH/$R_{NH_4^+}$ and $R_{O_2}/R_{NH_4^+}$ ratios. Effective concentration of glutamate is also given: theoretical estimates are based on the typical monosubstrate Michaelis-Menten equation according to Park et al. (1986). The calculation is as follows: Effective [Glu] = K_{Glu} / [(GDH/$R_{NH_4^+}$) / (K_{Glu} / 50 + 1) − 1].

Starvation (h)	Apparent K_{Glu} (mM)	GDH/$R_{NH_4^+}$	Effective [Glu] (mM)	O_2 consumption (µmol O_2 mg $protein^{-1}$ h^{-1})	$R_{O_2}/R_{NH_4^+}$
4	4.69 ± 0.69	11.23 ± 4.46	0.42	0.61 ± 0.09	4.57 ± 1.90
10	12.10 ± 5.90	9.74 ± 2.98	1.09	1.29 ± 0.32	6.66 ± 1.65
18	8.55 ± 4.04	11.14 ± 5.93	0.71	0.50 ± 0.15	5.51 ± 2.47
26	19.44 ± 10.80	30.87 ± 25.28	0.46	0.60 ± 0.11	11.51 ± 1.73
42	4.67 ± 0.79	16.28 ± 1.55	0.28	0.20 ± 0.18	2.13 ± 0.29
54	5.04 ± 0.27	64.72 ± 51.3	0.07	0.22 ± 0.22	7.07 ± 3.25
68	2.84	102.41	0.03	0.24	12.90
72	4.89 ± 3.45	67.89 ± 29.50	0.07	0.55 ± 0.05	15.49 ± 8.60
76	5.95 ± 2.48	39.10 ± 5.09	0.14	0.74 ± 0.43	14.12 ± 2.96
82	6.25 ± 2.51	89.10 ± 34.58	0.06	0.59 ± 0.36	47.20 ± 15.50

able value from Park et al. (1986), and 3.8, the value from Hernández-León and Torres (1997). However, the slope of the GDH activity to $R_{NH_4^+}$ from Bidigare and King (1981) was almost 3-times higher (43.8). At this stage we do not pretend to think that this relationship is universal and can be applied to all zooplankton (see *Chapter* 4). Its variability is still a focus of investigation.

So, why does the GDH activity exceed the NH_4^+ excretion rate by factors ranging over an order of magnitude? If we assume that GDH activity sets the upper limit for the physiological rate of NH_4^+ excretion and that the K_m is a proxy for the intracellular (*in vivo*) concentrations of glutamate and NAD^+ (Cleland, 1963), then other factors are limiting GDH activity to reduce it to the *in vivo* NH_4^+ excretion rate. In addition to substrate-based regulation, enzyme activity can be modulated by molecules serving as activators or repressors as ADP and GTP serve in the GDH reaction. Consequently, to understand the GDH/$R_{NH_4^+}$ ratio better, more research is needed involving the role of GTP and ADP as a regulatory molecules under different biological conditions.

The strong correlation between GDH activity and biomass (Spearman's Rho = 0.91, $p < 0.001$) suggests that GDH is a constitutive enzyme and that GDH activity could serve as an index of zooplankton biomass in a mixed plankton sample. The potential constitutive nature of GDH would predict that its variability in face of environmental fluctuations should be more moderate than the variability of activity in enzymes that are known to be induced or repressed by environmental changes. Assimilatory nitrate reductase, found in marine phytoplankton, is an example of such a sensitive enzyme. In the case of GDH, if it is a permanent component of cells, then accordingly, it will vary with carbon and nitrogen, i. e., biomass. However, as part of a cell's biomass, it would decompose with the cell death, and as a result, GDH would be a good index of living zooplankton biomass. This fact was previously noted with other mitochondrial enzymes, such as ETS (Martínez et al., 2010).

It is well known that metabolic processes, including excretion, scale with body size in an allometric form defined by the equation $M = a\,W^b$, where M is the metabolic process, W is body weight and, a and b are constants. In that equality, b constitutes the scalar component which determines the relationship between metabolic rate and body mass. It is traditionally assumed that b is 0.75 when body mass is expressed as wet mass (Brown et al., 2007; Kleiber, 1961). However, in invertebrates, as in the case of the organism used here, body composition is highly variable with age (Mayzaud, 1986) so that the exponent must

be reconsidered in terms of protein mass, which constitutes a relatively constant proportion of weight during growth. In this research we show how NH_4^+ excretion is affected by age with an exponent b of 0.55 (r^2 = 0.8). This means that the smaller mysids have higher metabolic rates per unit of protein than do the larger sizes. This b-value is slightly lower than the nitrogen-based b-values reported by Ikeda and Skjoldal (1989), which ranged from 0.65 in many species of antarctic zooplankton to 0.8 in zooplankters from Barents Sea. This dissimilarity can be explained partially by the different specie of zooplankton studied, but also by the more active metabolism in young *L. lingvura*. In contrast, GDH activity is linearly related to protein in the sample (b = 0.93, r^2 = 0.89), which means that its specific activity is invariant over different body sizes. This finding is in agreement with the behavior of GDH (b = 0.98) described by Berges et al. (1990) on different sizes of *Artemia franciscana*, but somewhat at odds with results by Mayzaud (1986) on the copepod *Acartia clausi* (b = 0.8). However, the latter presents a weaker correlation as a consequence of the use of a narrower range of sizes. Consequently, our resultant GDH/$R_{NH_4^+}$ ratio shows a small trend to increase as mysids become adults, especially in the initial development stages. This fact suggests that the effect of size acts unevenly on physiological rate and enzymatic activity, since otherwise the slope would be close to zero. Nevertheless, the mean ratio obtained in this work is in the range of the other calculations in the literature (see Table 4.3 in *Chapter* 4).

5.4.3 **The influence of starvation on physiological rates and GDH activity**

A common characteristic in the physiology of zooplankton is the rapid fall of the metabolic rates after depletion of the food source. Since Mayzaud (1976) described a dramatic decrease in nitrogen release after 12 h of starvation, the same trend has been reported in subsequent works (e.g., Ikeda and Skjoldal, 1980). In this study, NH_4^+ excretion diminishes almost 3-fold in the first 20 h to a basal metabolism. Later, after 70 h of starvation, when a new pulse of food was offered to the mysids, the NH_4^+ excretion increased slightly, although they could not recover the initial values as their physiology was probably injured at this point.

With regard to the GDH activity and its apparent K_m, few studies have attempted to evaluate their variability under different trophic conditions. The

first study was made by Park (1986a) on two species of copepods, but on a larger time-scale and less resolution. Here, GDH seemed to be constant with external changes in food availability. This might be explained by a reduction in substrate catabolism during the tricarboxylic acid (TCA) cycle leading to decreased formation of GTP, the main inhibitor of GDH. A more pronounced increase in GDH activity per mg of protein under food deprivation was found by Park (1986a), who suggested a conversion of GTP into ATP due to the depletion of the high energy forms. However, the range of our results exceeds the variation he measured. The constancy of our GDH data explains the occurrence of the highest value of the ratio GDH/$R_{NH_4^+}$ at the end of the starvation time. The variability in K_{Glu} (Table 5.1) could imply internal adjustments of amino acid catabolism as food becomes limiting, although these differences were not significant due to the high standard deviations. A healthy physiological state results in a low apparent K_{Glu} (4.69 mM) as a result of rapid protein consumption during growth. However, once the ingested food has been metabolized and no other fuel is available, mysids begin to use their own reservoirs as sources of energy and GDH might reduce its affinity for glutamate during the first 24 h in order to prevent its depletion. Then, the basal metabolism seems to fall to its minimum level and the weak GTP generation via TCA restores a high apparent V_{max}. However, the *in vivo* activity is likely much lower due to the absence of substrates at this time, as demonstrated by the effective concentration of glutamate (Table 5.1). This trend of intracellular glutamate with food deprivation fits with the patterns shown in *Chapter* 4, which reinforces the importance of substrate activation in the regulation of the GDH reaction. Furthermore, the changes in excretion rate with starvation are dependent on the body reserves that the mysids metabolize for their energy expenditures. The atomic $R_{O_2}/R_{NH_4^+}$ ratio is used as an indicator of the fuel required for energy. It shows that the substrates oxidized are nearly constant, which is consistent with Kiørboe's et al. (1985) finding in copepods. Values under 13 indicate a reliance on protein (Mayzaud and Conover, 1988), which largely occurs during the experimental period.

5.5 Conclusions

1. The use of fluorometry promises to improve the sensibility of the GDH assay at least 6-fold. This improvement should reduce the amount of biomass required for the assay.

2. GDH activity in *L. lingvura* can account the total physiological NH_4^+ excretion. The disparity between the potential and direct measurements suggests a regulation of GDH by a regulatory mechanism stronger than a substrate control.

3. GDH activity varies with biomass, so that it may serve as an index of zooplankton biomass in mixed plankton samples.

4. Body mass affects the NH_4^+ excretion and GDH activity unevenly. This causes an increases in the GDH/$R_{NH_4^+}$ ratio with biomass.

5. Starvation causes NH_4^+ excretion and GDH activity to diverge more than does body size.

Acknowledgements. We would like to thank to N. Osma and the anonymous reviewers for contributing valuables suggestions which notably improved the manuscript. This research is part of the EXZOME project (CTM 2008-01616/MAR), which is supported by the Spanish Science and Education Ministry. I. Fernández-Urruzola received finantial support from the Formation and Perfection of the Researcher Personal Program from the Basque Government. T. Packard was supported by contract EXMAR SE-10/17 (Proyecto Estructurante en Ciencias Marinas).

The important thing in science is not so much to obtain new facts as to discover new ways of thinking about them.

William Lawrence Bragg

CHAPTER

6

CAPÍTULO

Building a model of ammonium excretion in two species of marine zooplankton based on glutamate dehydrogenase kinetics

I. Fernández-Urruzola, N. Osma, M. Gómez, S. Montesdeoca-Esponda, T.T. Packard,
Submitted to Marine Ecology Progress Series.

Submission ID: MEPS-201510059. ***Minor revisions*****.**

ABSTRACT: NH_4^+ production in two species of marine zooplankton has been predicted from the glutamate dehydrogenase (GDH) activity using general bisubstrate enzyme kinetics during a period of starvation. In addition to starvation, we studied the effect of food quality on both the NH_4^+ excretion rates ($R_{NH_4^+}$) and the biochemical composition of zooplankton. The mathematical function used here relies on the Michaelis-Menten principles, and argues that the synthesis of NH_4^+ is controled mainly by the maximum velocity of the GDH, the intracellular pool of substrates and the kinetic constants. This simple model described reasonably well the shifts in the $R_{NH_4^+}$ that occurred within the time course of starvation in both groups of zooplankton. The calculated $R_{NH_4^+}$, however, underestimated the actual $R_{NH_4^+}$. Furthermore, we used single substrate kinetics to address the magnitude of either the allosteric inhibition or activation by purine nucleotides. We found that allosterism is more important in healthy physiological conditions. Overall, the use of the first-principles kinetics seems to provide better estimates of $R_{NH_4^+}$ than applying a general GDH/$R_{NH_4^+}$ ratio on the potential measurements of GDH.

Keywords: Glutamate dehydrogenase; NH_4^+ excretion; Kinetic model; *Brachionus plicatilis*; *Leptomysis lingvura*.

6.1 Introduction

Most of the transformations of nitrogen that occur in the marine environment are controlled by a few enzymes. Among these, glutamate dehydrogenase (GDH) is of critical importance. It has been found in nearly every living organism, and plays a major role in nitrogen metabolism. In the oxidative deamination reaction, $NAD(P)^+$-specific GDH (EC 1.4.1.3) feeds into the tricarboxilic acid (TCA) cycle, by converting L-glutamate to α-ketoglutarate with the concominant reduction of $NAD(P)^+$ to NAD(P)H, and by serving as the main pathway for NH_4^+ excretion in marine heterotrophs (Bidigare and King, 1981). In view of its metabolic significance, this enzyme has been routinely used in the oceanographic research for the appraisal of NH_4^+ regeneration in the marine ecosystems (e.g., Fernández-Urruzola et al., 2014, –*Chapter* 2, this thesis–). Such an enzymatic technique not only benefits from a high-data aquisition rate, but also circumvents all the inherent constraints of the classical methods (i.e., incubations). However, it requires a substrate surplus to guarantee the specificity of the reaction and the reproducibility of the measurement (Maldonado et al., 2012). These saturating levels of substrates are unlikely *in vivo*, so the actual NH_4^+ excretion rates ($R_{NH_4^+}$) have to be inferred from the potential measurements by applying an empirically determined factor that relates both rates. Unfortunately, their relationship is not universal, but may vary substantially depending on the taxa, size and trophic condition, among other biological factors (*Chapters* 4 and 5, this thesis). This results in large deviations, i.e., inaccurate estimations of $R_{NH_4^+}$, when using a single GDH/$R_{NH_4^+}$ value to study heterogenous populations of zooplankton at sea. Exploring the biochemical mechanisms of NH_4^+ production through the GDH reaction should provide knowledge on the intracellular processes that control it and thereby, improve the predictions of $R_{NH_4^+}$ from the GDH activities. Yet, few attempts have been made to relate metabolic rates such as $R_{NH_4^+}$ to the fundamental chemical principles. Despite being reasonable to conceive, biochemical models based on enzyme kinetics have been rarely used in biological oceanography studies. This was first noted by Packard et al. (1996b), who investigated the respiratory ETS enzymatic control in a marine bacterium, and subsequently demonstrated that an enzyme kinetic model would provide better predictive capability of respiratory

O_2 consumption rates than those models based on allometric equations relating respiration to body size (Aguiar-González et al., 2012). Nevertheless, these studies were mainly heuristic modeling exercises that calculated the substrate concentrations from changes in the carbon sources and the bacterial biomass, rather than perform direct measurements of the intracellular levels of pyridine nucleotides. The kinetic constants, in turn, were taken from other organisms and optimized for their model through successive iterations. It was not until Roy and Packard (2001) that a kinetic model was built in a marine organism by incorporating newly measured kinetic constants and experimentally determined intracellular levels of isocitrate and $NADP^+$. These authors applied the same biochemical principles to the enzyme isocitrate dehydogenase in order to predict the rate of CO_2 production in the bacterium *Pseudomonas nautica*. But this approach could also be extended to many other metabolic processes such as N_2 fixation, ATP production or, as in the case here, NH_4^+ excretion (Packard et al., 2004). All are of major importance in biogeochemical cycles, so this type of model would constitute a suitable alternative for calculating those physiological rates, e.g. $R_{NH_4^+}$, when direct measurements are unfeasible.

A first-principles modeling approach could be designed to describe the mechanics of the GDH reaction in terms of how changes in the metabolite concentrations affect the local NH_4^+ production rate. The rationale behind the kinetic models is that each metabolic process is controlled by the maximum velocity (V_{max}), the substrate availability, and the equilibrium constants. Based on Michaelis-Menten as the fundamental equation, they assume the steady-state condition of the enzyme-substrate (ES) complex, i.e., $d[ES]/dt = 0$, which should be valid as long as the substrate concentration exceeds the enzyme concentration (Bisswanger, 2008). This simple approach, however, is often complicated by the role of inhibitors and activators. In fact, the GDH reaction is allosterically regulated by enzyme modulators such as the purine nucleotides GTP and ADP (Frieden and Colman, 1967). Furthermore, various authors reported substrate inhibition with either glutamate or NAD^+ (Barton and Fisher, 1971; Engel and Dalziel, 1970), but at concentrations that are unlikely in living cells. Aside from allosteric effects, GDH has been proposed to follow a random sequential bi-bi mechanism in the glutamate deamination reaction (Rife and Cleland, 1980). Since substrate availability is the most obvious mechanism in enzyme regulation, here we assume these simple kinetics as the most appropriate to calculate the actual velocity of NH_4^+ production ($V_{NH_4^+}$).

The laboratory experiments here demonstrate the shifts in $R_{NH_4^+}$, GDH activities, as well as in the intracellular substrate (glutamate and NAD^+) and effector (GTP and ADP) levels during a starvation time course, in two species of marine zooplankton (*Brachionus plicatilis* and *Leptomysis lingvura*). Using this demonstrated shift over the starvation time course, we test the ability of the proposed kinetic model to predict changes in the $R_{NH_4^+}$ in response to environmental forcings. Although previous works focused on marine bacterium in order to reduce problems of organelle organization and behavior, the same theoretical concept should work for metazoans (Packard and Gómez, 2008). In this sense, we chose zooplankters of different structural complexity to study how it affects the accuracy of the model. Furthermore, the nitrogen source may also cause a change in the $R_{NH_4^+}$ (Saba et al., 2009), so we address its influence on the excretory machinery by growing both organisms on two diets of different nutritional quality.

6.2 Material and methods

6.2.1 Cultures of marine organisms

Two species of marine zooplankton, the rotifer *Brachionus plicatilis* and the mysid *Leptomysis lingvura*, were used to test the ability of a GDH-kinetic model in the prediction of NH_4^+ excretion rates ($R_{NH_4^+}$). Both organisms, as well as some of their prey (i.e., the algae *Nannochloropsis* sp. and the crustacea *Artemia* sp.), were cultured under laboratory controlled conditions. *B. plicatilis* were grown in 2 plastic tanks containing 20 L of diluted seawater ($\sim$ 23 PSU) at 25 °C, that was previously filtered through GF/F filters. These tanks were gently aerated to keep saturating oxygen conditions, and were maintained in the dark. Solid removal by siphoning and water exchange were performed daily to prevent dissolved NH_4^+ concentrations above 0.1 mg L^{-1}. Rotifers were fed with two diets that differed substantially in the fatty acid composition (Lubzens et al., 1995): one tank was provided with the live microalgae *Nannochloropsis* sp. (ESD = 2 - 3 μm), rich in polyunsaturated fatty acids, at a concentration of 1.2×10^5 cells $rotifer^{-1}$ d^{-1}; the other, was provided with a lower lipidic diet consisting of 0.8 μg dry yeast $rotifer^{-1}$ d^{-1}. Food was supplied continuously through peristaltic pumps for each diet. In such conditions, both treatments achieved relatively high densities of about 200 rotifers mL^{-1}. Thus, it was necessary to grow a *Nannochloropsis* sp. strain as well,

Table 6.1: Culturing conditions for both *B. plicatilis* and *L. lingvura*. Food levels were maintained for one week prior experimentation, and at t_0. The same food levels were provided again after starvation experiments (i.e., after 28 h and 60 h starvation for *B. plicatilis* and *L. lingvura*, respectively).

Culturing conditions	*Brachionus plicatilis*	*Leptomysis lingvura*
Temperature (°C)	25	18
Salinity (PSU)	23	35
Day-night cycle (h)	16:08	14:10
Diet *A*: Lipid-rich	*Nannochloropsis* sp.	Enriched *Artemia* sp.
	1.2×10^5 cells rotifer^{-1} d^{-1}	100 *Artemia* mysid^{-1} d^{-1}
Diet *B*: Lipid-poor	Dry yeast	Yeast-grown *B. plicatilis*
	0.8 µg dry yeast rotifer^{-1} d^{-1}	400 rotifers mysid^{-1} d^{-1}

for food. It was cultured in 8-L plastic carboys filled with autoclaved 0.2 µm filtered seawater, enriched with f/2 medium (Guillard, 1975). Batch cultures of *Nannochloropsis* sp. were kept bubbled in a culture chamber at a constant temperature of 20 °C, and a light intensity of 54.1 µmol photons m^{-2} s^{-1} on a 16:08 h light:dark cycle.

Another experimental organism that was used in the study, was the mysid, *L. lingvura*. These zooplankters were collected at sea and immediately transferred to the culture system installed in the laboratory. The installation consisted of 12 glass aquariums (40 L each) suspended in a circulating water bath. Such a big seawater volume (~ 480 L total), together with both mechanical and biological filtrations, allowed to maintain the levels of NH_4^+, NO_2^- and NO_3^- below 0.1, 0.02 and 0.2 mg L^{-1}, respectively, as recommended by Lussier et al. (1988). All organisms were kept at 18.2 ± 0.1 °C, and on a 14:10 h light:dark cycle. Mysids were fed twice a day with two diets that, again, were characterized by their different nutritional quality: 48 h nauplii of *Artemia* sp., lipid-enriched with Easy-DHA Selco® (INVE, Belgium), were provided at a concentration of 100 *Artemia* mysid^{-1} d^{-1}; the second diet, poor in lipids, consisted of 400 rotifers mysid^{-1} d^{-1} from the aforementioned yeast-grown culture. According to Domingues et al. (2000), those food concentrations would satisfy the mysid's demands. All the culturing conditions are summarized in Table 6.1.

6.2.2 Experimental procedure

Both *B. plicatilis* and *L. lingvura* were acclimated to each feeding treatment for one week before experimentation. Afterwards, the organisms were assayed, after feeding *ad libitum* on each diet, in order to measure the NH_4^+ excretion rates ($R_{NH_4^+}$) and the associated biochemistry during well-fed conditions (t_0). $R_{NH_4^+}$ was measured using water-bottle incubations; once finished each experiment, the zooplankters were frozen in liquid N (−196 °C) and stored at −80 °C for subsequent analyses of the GDH activities, the kinetic constants (K_m, K_{ia}, K_i and K_a) and the concentrations of those metabolites involved in the catabolism of glutamate (glutamate, nicotinamide adenine dinucleotide, adenosine-5'-diphosphate, and guanosine-5'-diphosphate). For statistical strength, we performed several replicates at t_0. Then, rotifers were harvested and deposited in new tanks containing 0.2 μm filtered seawater. Mysids were likewise moved into new aquariums filled with 0.2 μm filtered seawater. No food was provided to these tanks, so that rotifers and mysids starved for 28 h and 60 h, respectively. Accordingly, there were shifts in the morphology of these organisms with starvation (see *Appendix* section, Fig. A.2); in addition, egg production decreased dramatically in both species. Over the entire period, we performed continuous seawater exchanges to avoid high bacterial concentrations, which could contribute the rotifer's nutrition. These periods of starvation were set in accordance to Kirk (1997), who found a mean starvation survival of about 2 days for various species of rotifers. Similarly, Fernández-Urruzola et al. (2011) observed an increased mortality in starved mysids after 68 h. Throughout all this time, organisms were assayed for $R_{NH_4^+}$, on time-intervals from 2 h to 12 h. Afterwards, pulses of food were given to the zooplankters in order to test if any recovery in both the physiological and biochemical rates occurred.

6.2.3 Water-bottle incubations

Organisms were washed twice in filtered seawater before experimentation. To ensure homogeneity in the rotifer samples, we conducted a size-selective harvest by using a 100 μm mesh size. On the other hand, adult mysids were selected for experimentation. Organisms were carefully added to 60 mL gas-tight glass bottles by siphoning. Densities were similar in each bottle and experimental session. All the experiments were conducted in triplicate and included at least two control flasks without organisms. Furthermore, dissolved oxygen was measured in each bottle with continuously installed oxygen electrodes

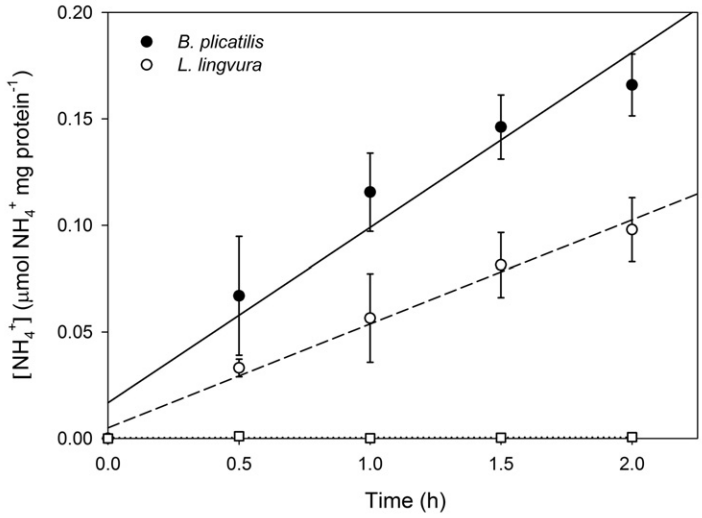

Figure 6.1: Increase in the NH_4^+ concentration with incubation time. Square symbols and dotted line represent the blanks. Error bars stand for the confidence intervals (*CI*s) at 95 %.

(Strathkelvin 928 Oxygen System® respirometer). This allowed exploration of changes in the respiration (R_{O_2}) to $R_{NH_4^+}$ relationship. Incubations were maintained in the dark to avoid any autotrophic activity, and lasted 1 - 1.5 h at culturing temperature. Such short incubation-times ensured linear $R_{NH_4^+}$ over the experimentation (Fig. 6.1). Then, 10 mL of seawater were siphoned off from each bottle for NH_4^+ determinations according to the Holmes et al. (1999) method. Organisms were frozen in liquid nitrogen and stored at −80 °C for subsequent enzymatic analyses.

6.2.4 **Measurements of GDH activities**

Samples were thawed, and sonicated in Tris medium (0.1 mM, pH = 8.6). Aliquots of the homogenate were immediately frozen at −80 °C for the eventual quantification of the protein content, and the intracelular levels of glutamate (Glu), nicotinamide adenine dinucleotide (NAD^+), adenosine-5'-diphosphate (ADP), and guanosine-5'-diphosphate (GTP). The remainder was centrifuged for 8 min at 4000 rpm at 0 °C, and the resultant supernatant fluid was assayed for GDH activity. The whole process was performed at 0 - 4 °C, and did not

exceed 30 min in order to preclude any loss of activity. The GDH assay was run according to Bidigare and King (1981), using fluorometry as introduced by Fernández-Urruzola et al. (2011). We added saturating levels of substrates (50 mM Glu and 1.2 mM NAD^+), as well as 2 mM of ADP to avoid any possible inhibition caused by GTP molecules. The increasing fluorescence signal of NADH was monitored for 4 min. The regression line of NADH production with time (the slope) was used to calculate the GDH activity using a standard curve generated with known concentrations of pure GDH (EC 1.4.1.3).

6.2.5 **Determination of kinetic constants**

Some samples were chosen to evaluate the kinetic constants of the GDH. As postulated by Rife and Cleland (1980), we assumed the steady-state random sequential bi-bi mechanism, which is valid as long as the product is negligible (Bisswanger, 2008). The correspondent Michaelis-Menten equation reads in the form

$$V_{NH_4^+} = \frac{V_{max}\,[Glu]\,[NAD^+]}{K_{ia}\,K_{NAD} + K_{NAD}\,[Glu] + K_{Glu}\,[NAD^+] + [Glu]\,[NAD^+]} \quad (6.1)$$

where $V_{NH_4^+}$ is the actual rate of NH_4^+ production (the *in vivo*), V_{max} is the apparent maximum enzyme reaction rate, K_{ia} is the dissociation constant associated with the first binding substrate (i.e., Glu), and K_{Glu} and K_{NAD} are the Michaelis half-saturation constants for Glu and NAD^+, respectively.

Kinetic parameters were measured with five different concentrations of Glu (0.4, 2, 10, 40 and 60 mM) and NAD^+ (0.05, 0.2, 0.6, 1.2 and 2 mM), leading to a five-by-five data matrix. These substrate concentrations were set according to Bisswanger (2011), who suggests a range starting 1 order of magnitude below and ending 1 order of magnitude above each K_m. The approximate K_m values were already known from preliminary investigations (Fernández-Urruzola et al., 2011, –*Chapter* 5, this thesis–). Furthermore, the measurement of all the combinations in the matrix (25) allowed a compromise with the stability of the enzyme, since each homogenate was assayed for less than an hour in a spectrofluorometer equipped with a 4-cell holder. Changes in the kinetic constants with starvation were tested by analyzing several replicates at t_0, a few hours after feeding and at the end of the experimental period.

The hyperbolic curves that resulted from varying the Glu concentrations at different constant amounts of NAD^+, and vice versa, became linear on apply-

ing the double-reciprocal transformation (Lineweaver and Burk, 1934). Accordingly, primary plots were constructed for each substrate by plotting their inverse concentrations (x-axis, $1\,/\,[\mathrm{Glu}]$ and $1\,/\,[\mathrm{NAD^+}]$) against the inverse of the velocity (y-axis, $1\,/\,v$ –see Fig. 6.2*a*–). All the lines met at a common intercept left of the ordinate, which confirmed the proposed sequential reaction mechanism of the GDH. Both the resultant slopes and y-intercepts from these primary plots of either substrate (e.g., $1\,/\,[\mathrm{NAD^+}]$), were plotted in a secondary plot against the inverse of the other substrate (in this case, $1\,/\,[\mathrm{Glu}]$). The regressions of both slopes and intercepts also resulted in straight lines that cut the abscissa at $-1\,/\,K_{\mathrm{ia}}$ and at $-1\,/\,K_{\mathrm{Glu}}$, respectively (Bisswanger, 2008). The same parameters were deducted for the cosubstrate ($\mathrm{NAD^+}$) by simply changing the order of the substrates plotted in the primary and secondary plots.

Furthermore, the allosteric effect of some purine nucleotides on the GDH activity was studied. GTP and ADP are known to be an inhibitor and activator of the enzyme reaction, respectively (Frieden and Colman, 1967). Their role in modulating the GDH activity is demonstrated in Fig. 6.3. There is a specific binding site for these molecules, which means that they do not compete with the substrates for the binding to the active site. The enzyme-substrate (ES) complex is not linearly inhibited by GTP, i.e., infinite GTP concentrations reduce, but do not completely exclude, the enzyme reaction activity (see Fig. 6.3). The same occurs with the activation by ADP. Accordingly, there is an hyperbolic mixed inhibition, where both the V_{max} and K_{Glu} (considering Glu, as the first binding substrate) are affected by the effector concentrations. These changes in V_{max} and K_{Glu} with the effector molecules will be described by the factors α and β, respectively. In the simplest case study of the monosubstrate reactions, the general Henri-Michaelis-Menten form of the velocity for this type of inhibition, should read as follows (Segel, 1993):

$$V_{\mathrm{NH_4^+}} = \frac{V_{\mathrm{max}}\,[\mathrm{Glu}]}{K_{\mathrm{Glu}}\,(1 + \frac{[\mathrm{GTP}]}{K_{\mathrm{i_{slope}}}}) + [\mathrm{Glu}]\,(1 + \frac{[\mathrm{GTP}]}{K_{\mathrm{i_{int.}}}})} \tag{6.2}$$

where $K_{\mathrm{i_{slope}}}$ refers to the apparent K_{i} value that accounts for the change in the slope of the reciprocal plot,

$$K_{\mathrm{i_{slope}}} = \frac{\beta_{\mathrm{i}}\,[GTP] + \alpha_{\mathrm{i}}\,K_{\mathrm{i}}}{(\alpha_{\mathrm{i}} - \beta_{\mathrm{i}})} \tag{6.3}$$

and $K_{i_{int.}}$ refers to the apparent K_i value calculated from the $1/v$-axis intercept:

$$K_{i_{int.}} = \frac{\beta_i\,[GTP] + \alpha_i\,K_i}{(1 - \beta_i)} \tag{6.4}$$

The same concept should be applied for the ADP activation study:

$$V_{NH_4^+} = \frac{V_{max}\,[Glu]}{K_{Glu}\,\frac{(1+\frac{[ADP]}{K_a})}{(1+\frac{\beta\,[ADP]}{\alpha\,K_a})} + [Glu]\,\frac{(1+\frac{[ADP]}{\alpha\,K_a})}{(1+\frac{\beta\,[ADP]}{\alpha\,K_a})}} \tag{6.5}$$

To derive all these inhibition constants, we followed a similar procedure to the one described above for the bisubstrate kinetics. We plotted the GDH activities at different concentrations (0.2, 1, 5, 20, 40 and 60 mM) of the first binding substrate (i.e., Glu), each measured at different constant amounts of GTP (0, 5, 10, 50 and 100 µM) or ADP (0, 0.02, 0.2, 1 and 2 mM). The hyperbolic curves were then linearized through a reciprocal transformation (Fig. 6.2*b* and *c*). The inverse concentrations of Glu (x-axis, $1/[Glu]$) were plotted in a primary plot against the inverse of the velocity (y-axis, $1/v$). Plotting the resultant slopes and intercepts against the concentrations of the effector, would still result in hyperbolas; therefore, it was necessary to apply a differential method to achieve linearization. The inverse of either $\Delta\,intercepts$ or $\Delta\,slopes$ were represented in a secondary plot against the inverse of the effector concentration (x-axis). Δ stands for the difference between the value at a given concentration of inhibitor and the value at zero inhibitor concentration (and vice versa in the activation case study). The kinetic parameter β, either for inhibition (β_i) or activation (β_a), was calculated from the ordinate intercept in the $1/\Delta\,intercept$ replot as follows,

$$\beta_i = \frac{Intercept}{V_{max} + Intercept} \qquad \beta_a = \frac{Intercept}{Intercept - V_{max}} \tag{6.6}$$

and α, either for inhibition (α_i) or activation (α_a), was determined from the ordinate intercept in the $1/\Delta\,slope$ replot:

$$\alpha_i = \frac{\beta_i\,V_{max}}{K_{Glu}\,Intercept} + \beta_i \qquad \alpha_a = \beta_a - \frac{\beta_a\,V_{max}}{K_{Glu}\,Intercept} \tag{6.7}$$

V_{max} and K_{Glu} were obtained from the ordinate and abscissa intercepts of the control line (i.e., at zero effector concentration) from the primary plot.

Knowing α and β, one can calculate K_i and K_a for both $\Delta\,slope$ and $\Delta\,intercept$ replots through Eq. 6.8:

$$K_\mathrm{i} = \frac{\beta_\mathrm{i}\ slope}{\alpha_\mathrm{i}\ Intercept} \qquad\qquad K_\mathrm{a} = \frac{\beta_\mathrm{a}\ slope}{\alpha_\mathrm{a}\ Intercept} \tag{6.8}$$

6.2.6 Intracellular levels of metabolites

(i) Glutamate. Levels of intracellular glutamate were measured using the method described by Hans-Otto and Michal (1974). It uses the GDH reaction to deaminate all the intracellular free glutamate; the resultant NADH is then oxidized in a second reaction, catalyzed by the diaphorase, where it donates the electrons to the tetrazolium chloride dye, INT (2-p-iodophenyl-3-p-nitrophenyl), to form formazan. The absorbance of this latter molecule was spectrophotometrically measured at 492 nm, and stoichiometrically related to the free glutamate concentration ([Glu]) through Eq. 6.9:

$$[\mathrm{Glu}]\ (\mathrm{mg\ mL^{-1}}) = \frac{V \times MW_\mathrm{Glu}}{\varepsilon \times l \times v \times 1000} \times \Delta\,Glu \tag{6.9}$$

where V is the total volume of the reaction mixture, MW_Glu is the molecular weight of glutamate, ε is the extinction coefficient of INT, l is the cuvette light-path, and v is the subsampled homogenate volume. $\Delta\,Glu$ stands for the difference between the absorbance before adding the GDH to the reaction mixture and the absorbance at the reaction end-point, both corrected by a control measure with MilliQ water instead of subsample homogenate.

(ii) Pyridine nucleotide: NAD^+. It was determined by using the enzymatic cycling system described in Wagner and Scott (1994), with small modifications. Samples were centrifuged as explained above. The supernatant was then assayed on a single-extraction basis that distinguishes between oxidized and reduced forms by means of heat (30 min at 60 °C), which destroys the former forms without affecting the reduced ones. Accordingly, the difference between the total pool of this pyridine nucleotide (NAD_t) and its reduced form would result in the intracellular levels of NAD^+.

A volume of either the heated or unheated extracts (100 µL) were added to 800 µL of ice-cold freshly prepared NAD cycling buffer (100 mM Tris-HCl buffer with 1 % Bovine serum albumin, pH = 8.0), and incubated in the dark

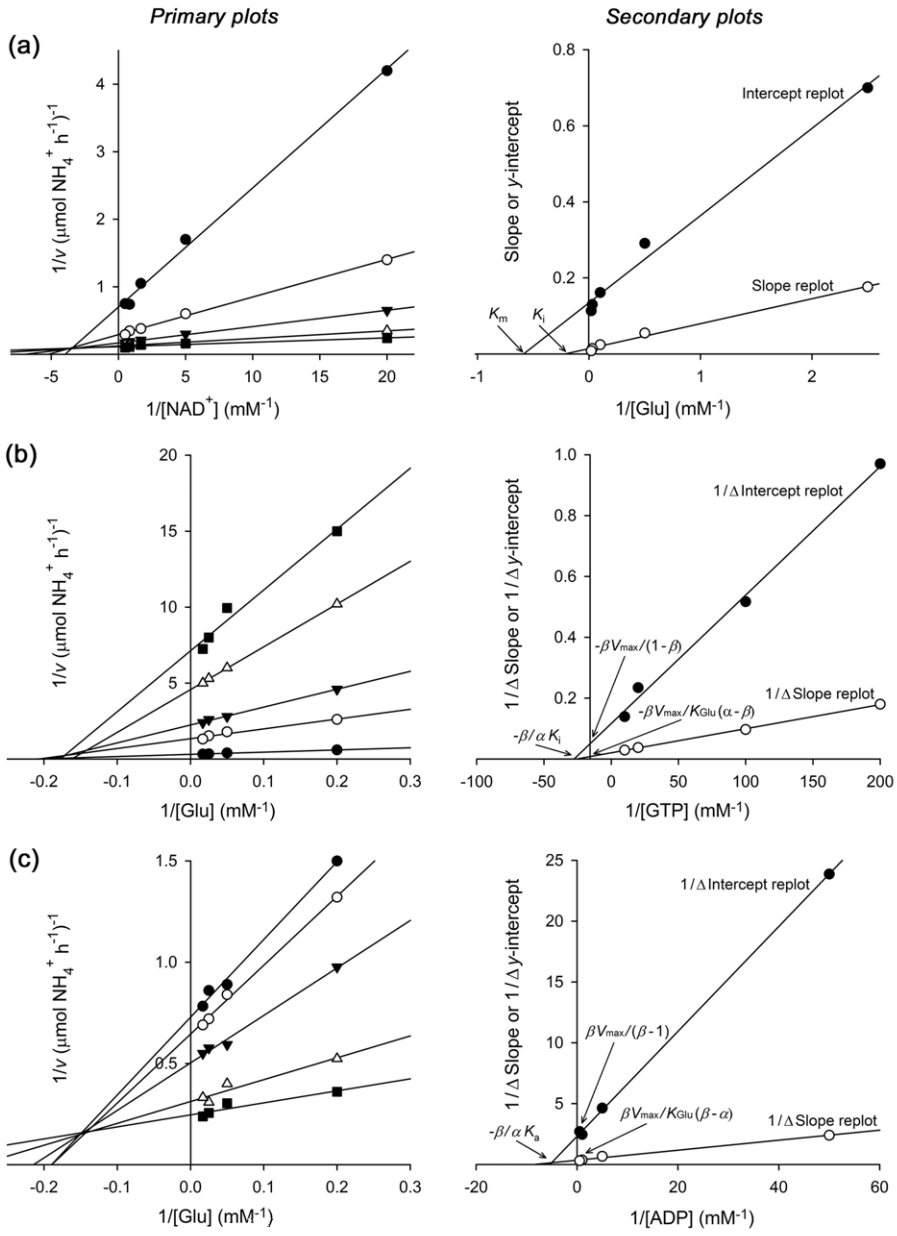

Figure 6.2: Double-reciprocal representations (primary plots) of the Michaelis-Menten equations for (a) a bi-bi random mechanism, (b) an hyperbolic mixed-type inhibition, and (c) a non-essential activation. Kinetic constants were determined from the correspondent secondary plots. All the calculations are described in the *Methods* section.

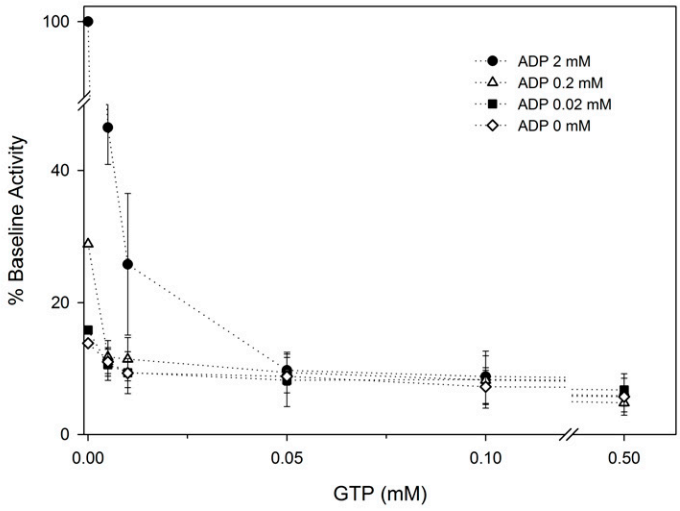

Figure 6.3: GTP inhibition of the GDH activity in the direction of glutamate deamination, at different levels of ADP. The experiment was performed on mysids. Each data point represent the mean of triplicate analyses.

at 37 °C for 5 min. The enzyme cycling system uses 0.2 mg mL^{-1} of the enzyme alcohol deshydrogenase (ADH), and a non-enzymatic reaction to cycle NAD^+ between its oxidized and reduced form in the presence of ethanol (100 μL) and 1 mM phenazine ethosulfate (PES). This PES reduces the 0.5 mM thiazolyl blue (MTT) into its formazan in another non-enzymatic reaction. Before spectrophotometrically measuring the MTT-formazan production, a quick centrifugation (16000 g, 30 s) was performed to remove any insoluble material. Afterwards, the change in absorbance at 570 nm was monitored over 3 min at 37 °C in a thermostated multi-cell holder attached to a refrigerated recirculator.

(iii) Phosphate nucleotides: GTP and ADP. For the determination of the intracellular concentrations of ADP and GTP we employed a Varian Prostar chromatographic system (Varian Inc., Spain). It consisted of a pump, an autosampler, a column valve module with an internal oven and a diode array detector working at 254 nm. The two analytes were separated on an PRP-1 column (5 μm, 2.1 × 150 mm –Hamilton, USA–), applying a column temperature of 50 °C. Mobile phase A was 100 mM monopotassium phosphate (adjusted pH to 7 with potassium hydroxide), 1 mM tetrabutylammmonium

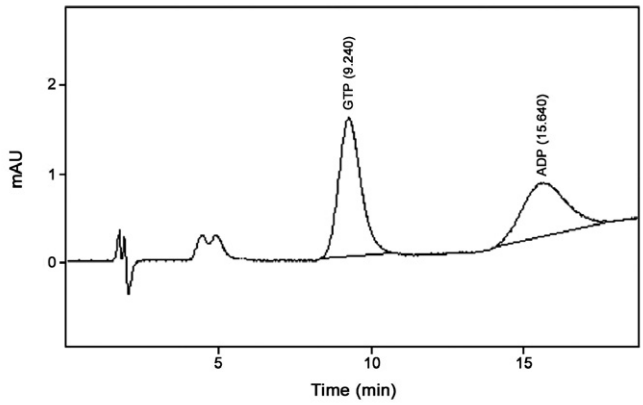

Figure 6.4: Chromatogram for the phosphate nucleotides GTP and ADP from the mysids, using UHPLC coupled to a diode array detector at 254 nm.

phosphate and 2.5 % methanol. Mobile phase B was eluent A + 20 % methanol. Elution was performed with a gradient that initially consisted of 1 % of mobile phase B. It was maintained up to 3 min and then, raised to 15 % in 10 minutes, to 55 % in 15 min, to 95 % in 16 min, and to 99 % in 20 min (see Fig. 6.4). At 25 min the gradient returned to 1 % of mobile phase B and stayed for 5 minutes in order to equilibrate the column for the next injection. The flow rate was set to 0.3 mL min^{-1}, and the injection volume was 10 μL.

Stock solutions of each compound (1.42 mM) were prepared by dissolving appropriate amounts of commercial products in the mobile phase, and stored in glass-stoppered bottles at 4 °C. Concentration curves were constructed in the range 0.01 - 50 μM. In all cases, the correlation coefficients were equal or greater than 0.992. The limits of quantification (*LOQ*s) were calculated as the concentration at which a signal-to-noise ratio was ≥ 10. They were 0.0005 μM for GTP and 0.002 μM for ADP. To evaluate the precision, expressed as relative standard deviation (*% RSD*), six replicate samples at two concentration levels (0.1 and 10 μM) were analyzed. The repeatability values obtained were, in both cases, < 9 %.

6.2.7 **Biomass and biovolume determinations**

Protein content of each sample was determined as a measure of biomass by the method of Lowry et al. (1951) modified by Rutter (1967). Bovine serum

albumin (BSA) was used as a standard. Each data point represented the mean of triplicate analyses.

In order to apply the kinetic equations, the intracellular metabolites were given in terms of biovolume (i.e., molar units). Rotifer biovolume was calculated from protein content by a multiplying-factor of 0.11 μg protein rotifer^{-1} (± 0.04, n = 30), and assuming a rotifer biovolume of 1.36 × 10^6 μm^3 after Boraas and Bennett (1988). Mysids biovolume was calculated using the equation N (mg) = 0.0546 + 0.0137 V (mm^3) given in Alcaraz et al. (2003), and a protein to N conversion factor of 0.521 (Postel et al., 2000).

6.3 Results

6.3.1 Effect of diet on the NH_4^+ excretory metabolism

The response of $R_{NH_4^+}$, GDH activities and intracellular levels of Glu, NAD^+, GTP and ADP to different food qualities was summarized in Table 6.2. In general, the differences caused by the diet were more pronounced in *B. plicatilis* than in *L. lingvura*. Thus, $R_{NH_4^+}$ in *B. plicatilis* rose from 0.13 to 0.20 μmol NH_4^+ mg protein^{-1} h^{-1} when feeding on a more proteinaceous diet (i.e., yeast). This was not the case in *L. lingvura*, with $R_{NH_4^+}$ ranging between 0.08 - 0.09 μmol NH_4^+ mg protein^{-1} h^{-1}. Accordingly, the $R_{NH_4^+}$ per mg protein of rotifers doubled that measured for mysids when exposed to this dietary shift. As shown in Fig. 6.1, these rates were nearly constant over the experimental period (1 - 1.5 h). Longer incubation times (> 1.5 h), however, induced a depression of the $R_{NH_4^+}$, especially in *B. plicatilis*. On the other hand, the higher the lipid content in the diet, the higher the $R_{O_2}/R_{NH_4^+}$ ratios were. This was more noticeable in *B. plicatilis*, so that those rotifers grown on the lipid-rich microalgae *Nannochloropsis* sp. had a maximum $R_{O_2}/R_{NH_4^+}$ ratio of 15.4. The same occurred with the mysids fed with the diet *A* ($R_{O_2}/R_{NH_4^+}$ = 7.66), even though the difference with the correspondent value from those mysids fed with the diet *B* were not significant ($p > 0.05$). Similarly to the $R_{NH_4^+}$, the protein-specific GDH activities were higher for *B. plicatilis*. These potential enzymatic rates followed the same trends observed in $R_{NH_4^+}$. They peaked in the yeast-grown rotifers (2.21 μmol NH_4^+ mg protein^{-1} h^{-1}). However, the differences in the GDH activities between the two treatments of *L. lingvura* were not so marked. All these patterns in the $R_{NH_4^+}$ and in the enzymatic rates, led to various GDH/$R_{NH_4^+}$ ratios depending on both the organism and the diet. They ranged from 11.05 to 14.69

Table 6.2: Comparison of the $R_{NH_4^+}$, GDH activities, ratios $R_{O_2}/R_{NH_4^+}$ and GDH/$R_{NH_4^+}$, as well as of the intracellular levels of Glu and other metabolites (NAD^+, GTP and ADP) in rotifers (*B. plicatilis*) and mysids (*L. lingvura*) acclimated to two different types of diet (see Table 6.1). Data represent the mean values ± *SD*, with the number of replicates in parenthesis. Student *t*-test was applied to study statistical differences for each parameter.

	Diet *A*		Diet *B*		*p*
Brachionus plicatilis	(lipid-rich)		(lipid-poor)		
$R_{NH_4^+}$ (µmol NH_4^+ mg protein^{-1} h^{-1})	0.13 ± 0.04	(16)	0.20 ± 0.06	(16)	**
$R_{O_2}/R_{NH_4^+}$ (molar basis) †	15.38 ± 5.72	(16)	8.75 ± 2.76	(16)	**
GDH Activity (µmol NH_4^+ mg protein^{-1} h^{-1})	1.91 ± 0.35	(16)	2.21 ± 0.13	(16)	***
GDH/$R_{NH_4^+}$	14.69 ± 5.25	(16)	11.05 ± 3.37	(16)	****
Glutamate (mM)	6.49 ± 1.58	(16)	7.27 ± 1.34	(16)	n.s
NAD^+ (µM)	1.73 ± 0.34	(2)	3.36 ± 1.57	(2)	n.s
GTP (mM)	0.38 ± 0.07	(16)	0.27 ± 0.05	(16)	**
ADP (µM)	93.19 ± 33.41	(5)	89.59 ± 32.00	(5)	n.s
Leptomysis lingvura					
$R_{NH_4^+}$ (µmol NH_4^+ mg protein^{-1} h^{-1})	0.09 ± 0.01	(8)	0.08 ± 0.01	(8)	n.s
$R_{O_2}/R_{NH_4^+}$ (molar basis) †	7.66 ± 2.48	(8)	6.50 ± 2.90	(8)	n.s
GDH Activity (µmol NH_4^+ mg protein^{-1} h^{-1})	1.56 ± 0.10	(8)	1.34 ± 0.11	(8)	****
GDH/$R_{NH_4^+}$	19.00 ± 3.94	(8)	17.25 ± 2.85	(8)	n.s
Glutamate (mM)	2.94 ± 0.45	(8)	2.52 ± 0.52	(8)	n.s
NAD^+ (µM)	3.89 ± 1.33	(8)	4.50 ± 0.40	(8)	n.s
GTP (mM)	0.16 ± 0.04	(8)	0.15 ± 0.06	(8)	n.s
ADP (µM)	16.85 ± 5.71	(8)	17.70 ± 2.02	(8)	n.s

* Significant at a level $p < 0.0001$, ** $p < 0.001$, *** $p < 0.01$, and **** $p < 0.05$. n.s. stands for not significant ($p > 0.05$).

† Respiration data have been taken from Osma et al. (in prep.).

in the rotifer case study, and from 17.25 to 19.00 in the mysid one. Overall, these ratios were slightly higher in those treatments consisting of the lipid-rich diet.

Regarding the intracellular levels of the metabolites, there were hardly any significant differences between treatments (Table 6.2). Differences were more evident, however, when organisms were compared. Except for NAD^+, *B. plicatilis* had from 2 to 3-fold more Glu and GTP than *L. lingvura*. More specifically, the intracellular glutamate trends in the two zooplankters coincided with those described for their $R_{NH_4^+}$. The differences in the metabolite concentrations become larger in the case of the ADP, which was ~ 6 times higher in

B. plicatilis.

6.3.2 General kinetics of GDH during starvation

Fig. 6.5 shows the time courses of all the variables (i.e., $R_{NH_4^+}$, GDH activity and the aforementioned metabolite concentrations) considered in testing the general kinetic models of GDH. Despite those differences described above, the two food-treatments in both rotifers and mysids followed similar patterns with starvation. In general, the maximum values of both $R_{NH_4^+}$ and GDH activities were found at t_0, i.e., during well-fed conditions. This also describes the situation with Glu, NAD^+, GTP and ADP. Afterwards, during the next 12 h, the $R_{NH_4^+}$ as well as the metabolite concentrations decreased sharply by half. The GDH activities, however, declined more gradually during the experiment. Furthermore, the decrease in the enzymatic rates were more appreciable in the lipid-poor treatments as compared to the lipid-rich ones. In fact, the latter seemed to maintain relatively constant GDH activities over the experimental period. Except for the GDH activities, all other variables responded to the re-feeding (see vertical dotted lines in Fig. 6.5) by recuperating and even surpassing their initial values at t_0. This is especially clear in the case of the $R_{NH_4^+}$ and the substrates Glu and NAD^+.

The kinetic constants during both well-fed and starved conditions for each zooplankter were calculated following the procedures explained in the *Methods* section, and illustrated in Fig. 6.2. Their values are presented in Table 6.3. Overall, the K_m were lower in rotifers as compared to the mysids, especially in the case of K_{Glu}, which was about an order of magnitude smaller (0.12 - 0.49 mM). This means that the affinity of the GDH for the glutamate is higher in rotifers. The K_{NAD}, however, was similar in the two species (ranging from 0.009 to 0.025 mM). Accordingly, the K_{NAD} was from 1 to 2 orders of magnitude smaller than K_{Glu} depending on the organism, but so were the intracellular levels of NAD^+ compared to those of Glu (Fig. 6.5). On the other hand, the K_{Glu} values increased slightly with starvation. Contrary to the K_m, the K_{ia} of both Glu and NAD^+ were higher in rotifers than in mysids. In this case, the higher the K_{ia}, the weaker would be the binding between the enzyme and the substrate. This also occurred when organisms starved, as the K_{ia} values increased significantly during food deprivation. Thus, both K_{ia} and K_m showed a similar pattern when varying the food availability, indicating a reduced reaction rate during starvation. Conversely, the inhibition (K_i) and activation (K_a) constants for GTP and ADP, respectively, seemed to remain relatively constant

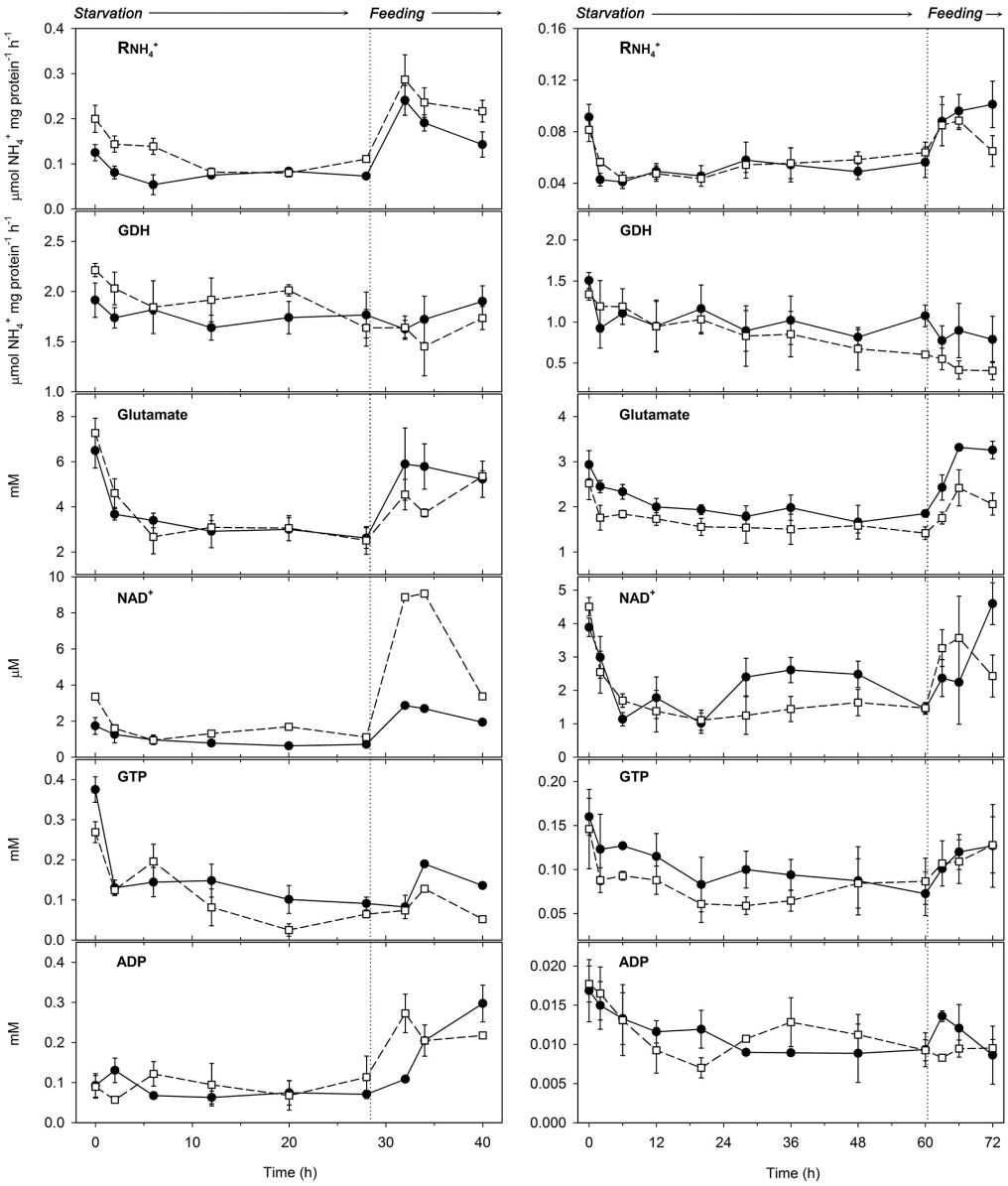

Figure 6.5: Time profiles of $R_{NH_4^+}$ and GDH (both standardized by protein content), as well as of some intracellular metabolites concentration (Glu, NAD^+, GTP and ADP) for both *B. plicatilis* (left panels) and *L. lingvura* (right panels) during starvation. Each panel includes organisms that were grown on the lipid-rich diet (circles, and solid lines) and on the lipid-poor diet (square symbols, and dashed lines). Vertical dotted lines indicate the time at which organisms were fed again. Error bars stand for the 95 % confidence intervals.

through the different feeding conditions. The K_i varied from 5.8 to 6.0×10^{-4} mM in *B. plicatilis*, and from 1.7 to 2.0×10^{-3} mM in *L. lingvura*. The K_a, in turn, ranged between 3.6 - 4.1 mM in *B. plicatilis*, and between 0.7 - 5.8 mM in *L. lingvura*. Despite the wide range in the latter case, the high deviation could explain most of the variability. Other factors to consider when studying either inhibition or activation of the enzymatic rates are α and β. The earlier factor (α) determine how the K_m of the substrate changes when the effector is bound to the enzyme; instead, β is the factor by which V_{max} changes when the effector occupies the enzyme. In the inhibition case study, α was between 1 and ∞ in both rotifers (2.05 - 4.13) and mysids (2.50 - 5.04), and peaked during starvation. The factor β, however, was situated between 0 and 1. It was significantly lower in rotifers (0.03 - 0.04) than in mysids (0.12 - 0.16). The opposite occurred with the factors α and β for the activation. As expected, α was several times lower than β.

All these kinetic constants for the bisubstrate reaction, as well as for the allosteric inhibition and activation, were applied to Eq. 6.1, Eq. 6.2 and Eq. 6.5, respectively. The modeled $V_{NH_4^+}$, considering a bi-bi random mechanism (Eq. 6.1), was plotted together with the *in vivo* $R_{NH_4^+}$ in Fig. 6.6*a*. Although the modeled values underestimated the actual ones, the trends for both treatments and organisms were accurately predicted. Accordingly, the relationship between the modeled $V_{NH_4^+}$ and the measured $R_{NH_4^+}$ yielded to a much better correlation ($r^2 = 0.79$) than that obtained when using fixed GDH/$R_{NH_4^+}$ ratios to estimate the actual $R_{NH_4^+}$ from GDH activities (Fig. 6.7). Furthermore, the percentages of either allosteric activation or inhibition are presented in Fig. 6.6*b*. Each effect resulted from the difference between the $V_{NH_4^+}$ calculated at 0 mM of any effector and the $V_{NH_4^+}$ at the actual effector concentration at any point throughout the time-course. The main effects were found during well fed conditions, either at t_0 or during re-feeding. Nevertheless, the magnitude of both the inhibition and, more particularly, the activation was significantly greater in *B. plicatilis* due to a higher intracellular GTP and ADP concentrations (Fig. 6.5).

6.4 Discussion

6.4.1 Effect of diet on the NH_4^+ excretory metabolism

NH_4^+ production by zooplankton is recognized as a crucial process for nitrogen regeneration in the marine environment (Bronk and Steinberg, 2008). But des-

Table 6.3: Kinetic constants for glutamate dehydrogenase in both well-fed and starved rotifers (*B. plicatilis*) and mysids (*L. lingvura*). The values represent the average ± *SD* of *n* replicates. The last column (Eq.) stands for the equation used to fit the data.

Brachionus plicatilis	*n*	Variable Substrate	Cosubstrate	V_{max} (μmol NH_4^+ mg protein^{-1} h^{-1})	K_m (mM)	K_i^* (mM)	α	β	Eq.
Well-fed	3	Glu	NAD^+ (0.05 - 2 mM)	1.61 ± 0.43	0.12 ± 0.01	14.75 ± 1.70	-	-	1
		NAD^+	Glu (0.2 - 60 mM)		0.016 ± 0.007	0.85 ± 0.21	-	-	1
	3	GTP	Glu (0.2 - 60 mM) †	2.01 ± 0.36	0.37 ± 0.25 ‡	$5.8\times10^{-4} \pm 3.0\times10^{-4}$	2.05 ± 1.19	0.03 ± 0.01	2
	3	ADP	Glu (0.2 - 60 mM) †§	0.078 ± 0.001	2.35 ± 1.20 ‡	4.10 ± 2.88	0.41 ± 0.19	29.98 ± 4.27	5
Starved	3	Glu	NAD^+ (0.05 - 2 mM)	1.39 ± 0.58	0.49 ± 0.14	26.53 ± 1.64	-	-	1
		NAD^+	Glu (0.2 - 60 mM)		0.009 ± 0.003	0.67 ± 0.22	-	-	1
	4	GTP	Glu (0.2 - 60 mM) †	1.51 ± 0.62	1.07 ± 0.54 ‡	$6.0\times10^{-4} \pm 1.1\times10^{-4}$	4.13 ± 2.20	0.04 ± 0.02	2
	3	ADP	Glu (0.2 - 60 mM) †§	0.084 ± 0.002	6.59 ± 3.92 ‡	3.55 ± 1.13	0.23 ± 0.01	11.69 ± 4.31	5
Leptomysis lingvura									
Well-fed	3	Glu	NAD^+ (0.05 - 2 mM)	1.77 ± 0.61	2.14 ± 0.23	7.72 ± 3.49	-	-	1
		NAD^+	Glu (0.2 - 60 mM)		0.018 ± 0.006	0.44 ± 0.22	-	-	1
	3	GTP	Glu (0.2 - 60 mM) †	1.29 ± 0.20	1.39 ± 0.88 ‡	$2.0\times10^{-3} \pm 0.6\times10^{-3}$	2.50 ± 0.52	0.12 ± 0.02	2
	3	ADP	Glu (0.2 - 60 mM) †§	0.34 ± 0.04	6.16 ± 1.85 ‡	0.70 ± 0.25	0.24 ± 0.01	3.16 ± 0.22	5
Starved	5	Glu	NAD^+ (0.05 - 2 mM)	1.02 ± 0.50	2.88 ± 0.32	14.52 ± 3.36	-	-	1
		NAD^+	Glu (0.2 - 60 mM)		0.025 ± 0.005	0.73 ± 0.18	-	-	1
	4	GTP	Glu (0.2 - 60 mM) †	0.98 ± 0.49	2.06 ± 0.11 ‡	$1.7\times10^{-3} \pm 0.9\times10^{-3}$	5.04 ± 2.92	0.16 ± 0.06	2
	6	ADP	Glu (0.2 - 60 mM) †§	0.34 ± 0.07	6.91 ± 2.23 ‡	5.76 ± 3.43	0.31 ± 0.24	4.63 ± 2.11	5

* K_i stands for the ES dissociation constant (K_{ia}) when either Glu or NAD^+ are the variable substrates, the inhibition constant (K_i) when GTP is the variable substrate, and the activation constant (K_a) when ADP is the variable substrate.

† All analyses were done at saturating levels of NAD^+ (1.2 mM).

§ These analyses consider V_{max} and K_{Glu} at 0 mM of ADP (i.e., without activation).

‡ It corresponds to the apparent K_{Glu}.

pite its ecological significance, the biochemical mechanisms that govern the synthesis of NH_4^+ in marine heterotrophs have been poorly elucidated. Although the actual enzyme reaction rates can be difficult to determine from *in vitro* kinetic measurements due to cellular compartimentalization, metabolic channeling and competing reactions (Berges and Mulholland, 2008), their study may provide useful information about the regulatory patterns and biochemical adaptability in face of environmental changes.

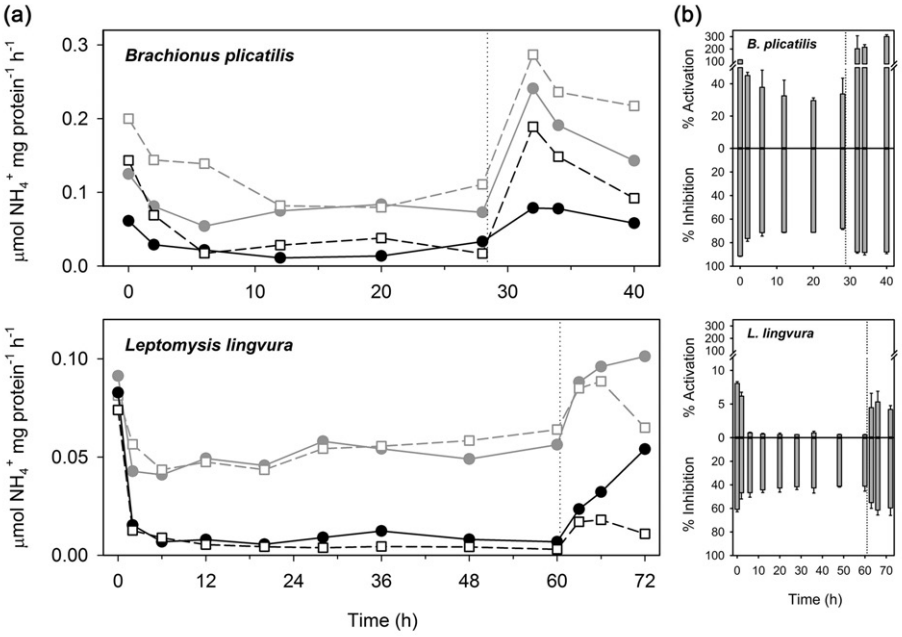

Figure 6.6: (a) Modeled $R_{NH_4^+}$ ($V_{NH_4^+}$) after applying Eq. 6.1 at each sampling time from the starvation experiments. The measured $R_{NH_4^+}$ is also presented for comparison (grey lines and symbols). Circles and solid lines stand for the lipid-rich treatments, whereas squares and dashed lines stand for the lipid-poor treatments. Vertical dotted lines indicate the time at which organisms were fed again. (b) Percentages of both inhibition and activation due to GTP and ADP molecules, calculated by applying the kinetic constants given in Table 3, on Eq. 6.2 and Eq. 6.5, respectively. Both inhibition and activation were estimated as the difference between the $V_{NH_4^+}$ at zero effector (and at the actual concentration of Glu), which is represented by the horizontal line at 0 %, and the $V_{NH_4^+}$ at the actual concentration of effector (and at the actual concentration of Glu) at each sampling time. Note that the scales (in %) for inhibition and activation are different.

One factor that determines the amount of NH_4^+ being excreted by zooplankton is the food ingested for assimilation (Miller and Roman, 2008). In the rotifers case study, we show that the food quality may have an effect on the $R_{NH_4^+}$ (Table 6.2) as high as the food availability (Fig. 6.5). This concurs with previous studies on a marine copepod that excreted more NH_4^+ while being fed on a carnivorous diet than on a herbivorous one (Saba et al., 2009). In this sense, prey, other than phytoplankton cells, would be metabolically beneficial as nitrogen is assimilated more efficiently (Tang and Dam, 1999). Despite the fact that *Nannochloropsis* sp. has a higher nutritional value due to a higher polyunsaturated fatty acid content, as compared to the dry yeast (Tamaru et al., 1993), the latter contains more protein and little structural carbon, which increases the assimilation efficiency. Since nitrogen comes exclusively from nitrogenous compounds, rotifers grown on yeast were expected to excrete more NH_4^+. Such differences were not found in mysids, most likely because both heterotrophic diets were similar to each other at the protein level. GDH activities resembled the $R_{NH_4^+}$ values, so the differences in the GDH/$R_{NH_4^+}$ ratios were barely signi-

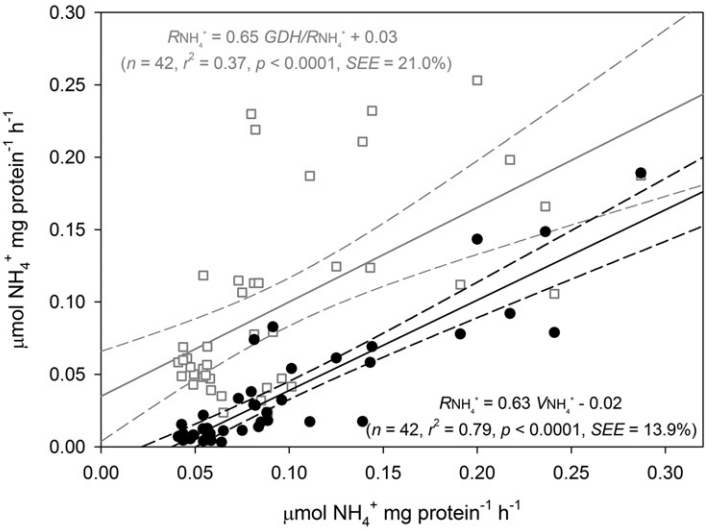

Figure 6.7: Relationship between $V_{NH_4^+}$ (*y*-axis) and the $R_{NH_4^+}$ (*x*-axis) measured during the starvation experiments (black circles). The relationship between the $R_{NH_4^+}$ calculated from the GDH activities shown in Fig. 6.5 after applying the GDH/$R_{NH_4^+}$ factors given in Table 2 (*y*-axis), and the measured $R_{NH_4^+}$ (*x*-axis), is also presented (squares, in grey). Dashed lines stand for the 95 % *CI*s.

ficant between treatments (Table 6.2). These differences were most noticeable between taxonomic groups, so that the ratio peaked in the mysids because of a lower mass-specific $R_{NH_4^+}$. Indeed, the trend for excretion rates to increase with decreasing body size is well known (Steinberg and Saba, 2008), as well as its increase with increasing temperature. The distinct food qualities were also reflected in the $R_{O_2}/R_{NH_4^+}$ ratio, which is an index of metabolism (Mayzaud and Conover, 1988). Thus, both lipid-rich diets resulted in higher $R_{O_2}/R_{NH_4^+}$ values, especially in *B. plicatilis*, whose $R_{O_2}/R_{NH_4^+}$ ratio for the lipid-rich treatment (15.4) almost doubled the one for the lipid-poor treatment (8.8). According to the theoretical computations given in Mayzaud and Conover (1988), the diet based on the microalgae *Nannochloropsis* sp. would induce more lipidic catabolism in the rotifers, whereas all other diets, even that based on enriched *Artemia*, would promote pure protein catabolism in the zooplankters. All these metabolic shifts with the type of food hardly affected the internal pool of metabolites. They were maintained relatively constant during well-fed conditions (Table 6.2).

6.4.2 General kinetics of GDH during starvation

Both rotifers and mysids experienced physiological and biochemical adjustments under varying food conditions. As reported in previous studies on species of marine zooplankton, metabolic rates are highly dependent on food availability, decreasing sharply to a basal metabolism after ~6 - 8 h of starvation (Kiørboe et al., 1985; Mayzaud, 1976). Similar changes in the biochemical composition (in terms of carbon and nitrogen) were also observed by the latter author. Irrespective of the diet used to grow the zooplankters, here the $R_{NH_4^+}$ decreased about 2 - 3 fold within a few hours after food-deprivation, and rapidly restored (or even surpassed) their original well-fed values when organisms were re-fed (Fig. 6.5). Accordingly, the physiological response to the feeding regime was nearly immediate. GDH activities, however, followed a different pattern. In general, enzyme reaction rates are expected to vary more slowly and with a certain delay as compared to the physiological rates (Bamstedt, 1980). This was already confirmed in starved *Leptomysis lingvura* for both GDH and ETS activities during a similar time course of starvation (Fernández-Urruzola et al., 2011; Herrera et al., 2011b). This is reasonable in the short-term, because it is energetically most efficient to maintain constant levels of enzymes in order to exploit the resources when sudden changes in

the food abundance occur. Nevertheless, maintenance of the GDH activities will also depend on the energy expenditure and the biochemical reserves that are available. In fact, those organisms grown on lipid-rich diets maintained their GDH relatively constant as compared to those organisms grown on a lipid-poor diet. Assuming similar energy requirements between treatments, the difference in their enzyme levels may be explained by the substrate that was being oxidized for energy production. Although lipid reserves are preferably used for basal metabolism during starvation (Bamstedt and Holt, 1978), when exhausted, the hydrolysis of proteins would commence. This may result in a higher protein breakdown and a metabolic oxidation of amino acids such as glutamate in the lipid-poor treatments (Fig. 6.5). Furthermore, this biochemical pathway could be more relevant in *B. plicatilis*, as rotifers often have lower lipid stores than crustacean zooplankton. Nevertheless, most of the metabolites varied in parallel with the $R_{NH_4^+}$ in both organisms, peaking during well-fed conditions. Similar trends according to fluctuations in the food environment have been described for the internal pool of glutamate (Aragão et al., 2004) and NAD^+ (Osma et al., in prep.) in small marine heterotrophs. GTP, in turn, is closely related to the energy charge and as such, a reduced tricarboxylic acid (TCA) cycle activity would result in low levels of GTP during starvation. Since GTP is directly involved in cellular biosynthesis (Karl, 1978), its decrease under food-deprivation conditions reinforces the assumption of free amino acids being metabolized for energy production.

Because of the simplicity of the single-substrate Michaelis-Menten equation, most of the biochemical research in marine organisms have used it to calculate the half-saturation Michaelis constant (K_m) for every substrate of the GDH (Bidigare and King, 1981; Fernández-Urruzola et al., 2011; Park, 1986a; Park et al., 1986). However, a more extensive examination of the GDH kinetics needs to derive some other related constants such as the dissociation constant (K_{ia}), which requires bisubstrate enzyme kinetic studies. Due to their complexity (see Fig. 6.2), there is a lack of such determinations in the marine literature, as they have only been estimated on GDH from bovine liver (e.g., Barton and Fisher, 1971). Here the K_{Glu} calculated from bisubstrate analyses ranged from a low of 0.12 mM in rotifers to a high of 2.88 mM in mysids (Table 6.3). These values are slightly lower than those estimated in marine zooplankton from a monosubstrate approach (ranging from 2.6 to 14.4 mM). The same occurs with the K_{NAD}, which varied in a range (0.009 - 0.025 mM),

much lower than the value of K_{NAD} (0.44 mM) reported in Fernández-Urruzola et al. (2011). A significantly lower K_{NAD} as compared to the K_{Glu}, suggests that GDH has a higher affinity for NAD^+ than it has for Glu and therefore, this pyridine nucleotide may be critical in regulating the enzyme reaction rate. Nevertheless, it has been shown that dicarboxylic substrates such as glutamate enhance the affinity of NAD^+ by synergism to form ternary complexes (Rife and Cleland, 1980). On the other hand, our calculations showed differences in the K_m between organisms as well as between feeding regime, even though they were larger in the former case. This is not surprising, as several structures of GDH have been described across the different phyla (Benachenhou-Lahfa et al., 1993), and a number of inducible isozymes that correlate with the nutritional condition can be present in a single species (Srivastava and Singh, 1987). Regardless of such changes in the kinetic constants, the K_{ia} were, in all the cases, higher than the K_m (either for Glu or NAD^+). Visually, this can be inferred from Fig. 6.2*a*, as the intersection point between the straight lines in the primary plot occurs above the abcissa. A higher K_{ia} results in a $K_m/K_{ia} < 1$, which means that the binding of one substrate to the active site increases the affinity for the other (Leskovac, 2003), however, these kinetics are complicated by allosteric modulation. The reaction rate of the GDH can be either inhibited or stimulated by several molecules, among which the most important are the purine nucleotides (Frieden and Colman, 1967). While GTP molecules are potent inhibitors of the glutamate deamination by increasing the binding affinity of the product, the ADP molecules act in an opposite manner facilitating the NH_4^+ release. Their effects on both the K_{Glu} (considering the glutamate as the first binding substrate) and the V_{max} are determined by the factors α and β, respectively. Here, in the inhibition case study with GTP, α varied between 1 and ∞, and β varied between 0 and 1, which argues for a hyperbolic mixed-type inhibition (Segel, 1993). This means that both enzyme (E) and enzyme-inhibitor (EI) complexes bind to the substrate (S), but with different affinities. Although at a different rate, both ES and ESI form product and therefore, an infinite concentration of inhibitor would not reduce the reaction velocity to zero. A similar concept, but applied in the opposite direction, should by applied for the activation with ADP. In absence of an activator, the K_{Glu} increases significantly (see Table 6.3), in other words, the enzyme reduces its affinity for the substrate. In fact, when adding ADP to the standard assay in order to avoid any inhibition effect, what we really calculate is the α-K_m, i.e., the apparent

K_m, and the β-V_{max}.

The benefits of using an enzyme kinetic model have already been shown for several key processes that are involved in respiratory metabolism (Aguiar-González et al., 2012; Packard et al., 1996b; Roy and Packard, 2001). Here we use a similar theoretical concept to predict the velocity of NH_4^+ production in zooplankton, by applying the apparent V_{max}, the kinetic constants and the intracellular levels of Glu and NAD^+ in a first-principles based equation (Eq. 6.1). This approach yields a mechanistic understanding of NH_4^+ excretion. The predicted $V_{NH_4^+}$ along the starvation time course resembled reasonably well the $R_{NH_4^+}$ patterns measured in both the rotifers and mysids (Fig. 6.6*a*). However, it is noticeable that the $V_{NH_4^+}$ underestimated the actual $R_{NH_4^+}$, especially in the mysids case study. This may partially be due to conservative estimates of the intracellular levels of metabolites on a molar basis, as the general equation used for calculating the mysid biovolume was obtained from zooplankters smaller than 5 mm (Alcaraz et al., 2003). Larger zooplankton would likely result in a lower volume per unit biomass. Furthermore, in eukaryotic cells, GDH is known to be mainly located in the mitochondria (Frigerio et al., 2008), so a more precise determination of the mitochondrial matrix pool of substrates would make both $V_{NH_4^+}$ and $R_{NH_4^+}$ more alike. In fact, GDH has been found to use the glutamate available in the close proximity of the reactive site, which comes from the deamidation by glutaminase of transported glutamine (Schoolwerth and LaNoue, 1980). Nevertheless, none of these methodological constraints affect the patterns of $V_{NH_4^+}$, but they could affect its magnitude. Still, this could be solved through calibration. The modeled $V_{NH_4^+}$ was clearly more successful in predicting the shape of the $R_{NH_4^+}$ than the typical estimations from the GDH activities (Fig. 6.7), even though 4 empirically determined GDH/$R_{NH_4^+}$ ratios for each organism and food treatment (Table 6.2) were applied to approximate the actual $R_{NH_4^+}$ from the GDH measurements. Nevertheless, we can see from comparing this modeling effort with our attempts to calculate an oceanic $R_{NH_4^+}$ from open-ocean GDH measurements and a general GDH/$R_{NH_4^+}$ factor (*Chapter* 4) that the enzyme kinetic model is a step in the right direction. Understanding how the effectors interact with each other and modulate the $V_{NH_4^+}$ in a bisubstrate kinetics is still a challenge. In the most simple case of monosubstrate kinetics (Eqs. 6.2 and 6.5), we have demonstrated that the allosteric regulation, either for activation or inhibition, is more important during well-fed conditions (Fig. 6.6*b*). This

concurs with findings of Park et al. (1986), who suggested a greater inhibitory effect by GTP under high chlorophyll-a situations. In spite of these challenges, we conclude that the use of the model's algorithm based on Michaelis-Menten substrate kinetics (Eq. 6.1) promises to provide better estimates of $R_{NH_4^+}$ in a changing environment.

6.5 Conclusions

This work does not pretend to be an extensive enzyme-kinetics binding study, but a relatively simple modeling exercise using the principles of enzymology to calculate the most basic kinetic constants in the control mechanisms of GDH. A more complex model involving other factors of an enzyme reaction could have been constructed (Wells et al., 1977). However, we have applied Ockham's razor (Ariew, 1976) and used a simple model based on substrate activation. Had we done otherwise, the complexity would have been too costly or even impossible to accomplish experimentally. Our experiments argue that, even in complex organisms such as the zooplankton, simple kinetics can predict patterns in the physiological rates ($R_{NH_4^+}$ in our case study) under varying food conditions. Further research on metabolite fluctuations at the mitochondrial level would likely improve the kinetic model's calculations of the steady-state actual velocity of NH_4^+ production.

Acknowledgements. We wish to thank C. M. Hernández and D. López from the aquaculture research group (ULPGC) for providing us with strains of *Brachionus plicatilis* and *Nannochloropsis oculata*, as well as with helpful advices to set up the cultures. We are also grateful to J. J. Santana-Rodríguez for kindly lending us the equipment required to perform UHPLC analyses. Funding was provided, in part, by the BIOMBA project (CTM2012-32729/MAR) and by the Innova Canarias 2020 program (Fundación Universitaria de Las Palmas), granted to M. G. and I. F.-U., respectively. I. F.-U. and N. O. were supported by postgraduate grants from the Formation and Perfection of the Researcher Personal Program from the Basque Government. T.T. P. was largely supported by TIAA-CREF and Social Security (USA).

Now this is not the end. It is not even the beginning of the end. But it is, perhaps, the end of the beginning.

Winston Churchill

CHAPTER

7

CAPÍTULO

Synthesis and Future research

7.1 General discussion

One of the major contributions of this thesis is the elucidation of the role of the mesozooplankton NH_4^+ excretion in the biogeochemical cycles of an important upwelling ecosystem (*Chapters* 2 - 3), as well as the introduction of new insights into the study of zooplankton NH_4^+ excretion from enzymatic measurements (*Chapters* 4 - 6). Below are discussed the most important results of this research work.

(i) The role of the zooplankton NH_4^+ excretion in the biogeochemical cycles from the northern Benguela upwelling system. The field work for this thesis was designed, in part, to address the implications of zooplankton NH_4^+ excretion in an upwelling ecosystem's nitrogen cycling (*Chapters* 2 and 3). Although a minor role is expected for regenerated nutrients in areas with large inputs of new nitrogen, there is no obvious pattern about the importance of zooplankton in fueling the phytoplankton growth throughout different ecosystems (Bronk and Steinberg, 2008). This makes necessary continuous monitoring of this metabolic process in the world oceans. The results here contribute to fill the gap of knowledge about the mesozooplankton NH_4^+ excretion in waters between 20 - 40° S (Hernández-León et al., 2008), and more particularly in the northern Benguela upwelling (21° S).

The use of enzymatic techniques such as the electron transport system

(ETS) and the glutamate dehydrogenase (GDH) allowed to study zooplankton metabolism at a rate that otherwise would have been unachievable. This is essential in oceanography, which requires many measurements made over large time and space scales, especially when characterizing the metabolic dynamics in unstable ecosystems such as the Benguela upwelling (see the complex interplay of water masses in Fig. 1.2). Enzymatic assays, however, are measurements that reflect the maximum rate ($V_{\max}$) at which the reaction may occur, not the actual one, so they have to be converted into *in situ* rates through an empirically determined ratio or through calculations involving enzyme kinetics. Unfortunately, many factors may affect the relationship between enzymatic $V_{\max}$ and *in vivo* rates, as discussed from *Chapter* 4 to *Chapter* 6. Still, the errors caused by these ratios are not greater than those of other methods used in standard ecological procedures for plankton metabolic processes, particularly if they are previously calibrated for the surveyed system (e.g., Packard, 1985; Hernández-León et al., 1999; Bode et al., 2013).

Chapter 2 illustrates the dynamics of zooplankton biomass and potential metabolism in face of the different oceanographic situations recorded in the northern Benguela, while *Chapter* 3 uses GDH measurements throughout the water column to model downward nitrogen fluxes in this upwelling ecosystem. Other aspects involved in zooplankton ecology such as the elemental composition and stable isotopes helped to understand the basis of trophic interactions (*Chapter* 2), which ultimately affect the zooplankton metabolism. In absolute terms, the mesozooplankton respiration and NH_4^+ excretion assessed in the Namibian cell exceeded the correspondent metabolic rates in other eastern boundary upwelling systems (Packard et al., 1974; Hernández-León et al., 2002; Isla and Anadón, 2004; Pérez-Aragón et al., 2011). However, the mesozooplankton metabolism had little impact on the phytoplankton community, as these heterotrophic organisms only respired and regenerated between 1 - 11 % of the daily primary production (see Table 2.3). These percentages were comparable with the mesozooplankton regeneration in the upwelling off NW Spain (Bode et al., 2004; Isla et al., 2004a), where it was suggested a major remineralization pathway through microheterotrophs, especially during the high-productivity situations. Accordingly, most of the organic matter produced in these Namibian waters should be recycled through the microbial loop, which concurs with findings of Probyn (1987) for the southern Benguela. Similarly, the zooplankton carbon demand required a low percentage of the primary

productivity (~ 14%), as is expected in eutrophic ecosystems (Calbet, 2001). Considering this percentage jointly with estimates for microzooplankton and bacterial carbon requirements of about 57 % of the net primary production (Bergen et al., 2015; Chapman et al., 1994), it could be assumed a surplus of organic matter left over to be exported to the bottom, or advected to the open ocean. Accordingly, the downward flux of particulate matter in the mid-water environment was of paramount importance in this ecosystem, stimulating the heterotrophic metabolism as the particles sank to the seabed. Therefore, using the advantages of the GDH assay, that allow to perform many measurements throughout the water column, we modeled particulate nitrogen fluxes (F_N) from zooplankton NH_4^+ excretion rates ($R_{NH_4^+}$). This novel approach served to construct an ocean synoptic section of nitrogen flux along a cross-shelf transect off the Namibian coast (see *Chapter* 3), which would not be feasible by the stationary trap approach given its narrow spatial coverage. In this sense, the comparison between the modeled F_N and the nitrogen collected in the sediment traps best illustrated the general picture of the downward nitrogen export in the Benguela waters, and shed light on those processes that affect the imbalance in the apparent particle budget (Burd et al., 2010). The production history of the waters determined both the nature and size of sinking particles, which resulted critical in explaining the differences between the sedimented particulate nitrogen and the nitrogen required for metabolism in the water column (Fig. 3.5). Thus, the discrepancies between both methodologies were low in a high-productivity scenario dominated by diatoms, becoming larger when coccolitophores and small flagellates were more important in the phytoplankton community. In fact, big recalcitrant cells result in high sinking-velocities that allow the particles to reach the seafloor close to the point at which they left the surface, while small cells with slow sinking velocities are more prone to attenuation and lateral displacement (Alonso-González et al., 2010; Iversen and Ploug, 2010; McDonnell et al., 2015). In general, most of the particulate nitrogen was transformed into dissolved nitrogen (NH_4^+, among other nitrogen species) by the nano/microzooplankton. This confirmed the major role of microheterotrophs in the nutrient recycling of this ecosystem, as suggested in *Chapter* 2. Furthermore, new metrics such as the nutrient retention efficiency (NRE, *sensu* Packard and Gómez, 2013) can be derived from the modeling approach, and demonstrated the inability of the coastal waters to regenerate most of the organic matter available in the epipelagic zone (Fig. 3.6*b* and *c*).

Although upwelled deep waters are rich in nutrients, they contain little zooplankton, so the NH_4^+ excretion processes were limited in this area (see Fig. 2.9, *Chapter* 2). The efficiency in regenerating nutrients was ultimately determined by the curvature, i.e., the *b*-value, of the power function fitted to the vertical $R_{NH_4^+}$. The importance of this parameter in determining the nutrient distribution throughout the ocean water columns was already noted by Marsay et al. (2015). Finally, as part of the biological pump, we assessed the role of migrant mesozooplankton in actively transporting nitrogen into the mesopelagic zone in a station from the transitional area. The migratory F_N was found to be an important component of the nitrogen fluxes as compared to the gravitational flux. Thus, the active F_N represented between the 59 - 361 % of the sinking nitrogen, which was about three- to fivefold the percentages found in oligotrophic gyres from Bermuda (Dam et al., 1995; Steinberg et al., 2002) and Hawai (Al-Mutairi and Landry, 2001).

All this made the Benguela upwelling ecosystem an interesting scenario in the vertical nutrient exchange. Investigating those factors that may introduce uncertainties in the appraisal of $R_{NH_4^+}$ from the GDH measurements would reduce errors in the estimations of this metabolic process and consequently, in assessing the biogeochemical implications of zooplankton $R_{NH_4^+}$. Shedding light on this issue was the main goal of *Chapters* 4, 5 and 6.

(ii) The relationship between NH_4^+ excretion and GDH activities in zooplankton. Understanding the sources of variability between the physiological rates of NH_4^+ production and the enzymatic measurements will help to achieve a more reliable determination of the zooplankton role in nitrogen cycling when direct measurements are unfeasible (e.g., in field work such as those presented in *Chapters* 2 and 3). In these cases, it would be desirable to measure the actual rate of activity in the sample, the *in vivo* rate, but the technology is just not available now. Fostered by these arguments, here we have explored some factors affecting the GDH/$R_{NH_4^+}$ ratio (*Chapters* 4 - 6) and propose a new biochemical approach to face the study of NH_4^+ metabolism in zooplankton by using the principles of enzymology (*Chapter* 6).

Both $R_{NH_4^+}$ and GDH activities in zooplankton are known to vary with environmental conditions (Ikeda et al., 2000). Among others, temperature is potentially an important modulator of oceanic rate processes, so there has been extensive research (e.g., Packard et al., 1975; Alcaraz et al., 2013) of how it

regulate the metabolism in a way described by the Arrhenius equation:

$$k = A\, e^{\frac{-E_a}{RT}} \tag{7.1}$$

where k is the rate constant of the metabolic process on the absolute temperature (T) in kelvin, A is the pre-exponential factor, E_a is the Arrhenius activation energy, and R is the gas constant (1.987 cal K^{-1} mol^{-1}). A large percentage of variation in $R_{NH_4^+}$ is generally related to habitat temperature (Ikeda, 1985), as it is indeed observed in *Chapter* 4 when comparing $R_{NH_4^+}$ between marine ecosystems of different latitudes (Fig. 4.3). Like most chemical reactions, the velocity of the GDH-catalyzed reaction also increases with temperature, most probably through the modification of the kinetic and thermodynamic properties of the enzyme. Nevertheless, enzymes follows the same Arrenhius relationship with temperature as do the metabolic rates. The Q_{10} found by Park et al. (1986) for macrozooplankton GDH (1.78) was thus comparable to the Q_{10} reported by Ikeda (2014) for $R_{NH_4^+}$ of epipelagic marine zooplankton (1.84 - 2.18). This results in similar activation energies (E_a), which ultimately determine the temperature dependence of a rate process. Accordingly, the effect of temperature on the GDH to $R_{NH_4^+}$ ratio seems to be of minor importance, if not negligible as in the case of the the respiration to ETS ratio (King and Packard, 1975). Still, such an effect could be easily eliminated by maintaining the field temperatures in the experimental procedures.

But other biological factors aside from the temperature dependency may constrain the behavior of metabolic processes. The question arises whether both the physiological and enzymatic rates respond equally to these forcings. If this were not the case, the relationship between the actual and the potential rates would vary, and the appraisal of NH_4^+ production from GDH measurements would become less accurate. Similar to the Arrhenius expression (Eq. 7.1) in the temperature case study, the biomass is related to the metabolic processes through the power form of Kleiber's law (1961):

$$M = a\, W^b \tag{7.2}$$

where M is the metabolic process, W is body weight, and a and b are constants. Berges et al. (1993) first hypothesized that there would not be a potential effect of biomass in the inherent variability of the relationship between GDH and $R_{NH_4^+}$, whenever both rates followed the same allometric principles. If so,

both $R_{NH_4^+}$ and GDH activities should scale to the same exponent, i.e., share the same *b*-value, and therefore the slope of the GDH/$R_{NH_4^+}$ relationship with protein would be close to zero. To date, there was no equation that related the biomass to the GDH/$R_{NH_4^+}$ ratio in marine organisms. In *Chapter* 4 we addresed this issue (Fig. 4.2), and found a noticeable mass (in terms of protein) dependence of this ratio in natural mixed zooplankton samples. The Kleiber's logarithmic function took the form of,

$$\log\left(GDH/R_{NH_4^+}\right) = 0.53 \log protein + 1.13 \tag{7.3}$$

This mass effect was corroborated in *Chapter* 5 on a cohort of the marine mysid, *Leptomysis lingvura*. In this latter case, the GDH/$R_{NH_4^+}$ ratio in growing mysids showed even stronger mass dependency (see Fig. 7.1). These results highlight the need to fractionate natural zooplankton samples in order to reduce the mass effect when using GDH activities to approximate $R_{NH_4^+}$ in populations with different size structures. An specific GDH/$R_{NH_4^+}$ ratio should be thus applied to each size category. Even though this procedure could be recommended for every metabolic process that uses enzyme activities as biochemical proxies, other ratios may not present such variability with biomass. For instance, the relationship that respiration maintains with the electron transport system (ETS) has been noted to have little dependence on size (Christensen et al., 1980).

While noting the importance of biomass in the relationship between the actual and the potential rates, the starvation and re-feeding experiments that were accomplished in *Chapters* 5 and 6 proved that the principal factor determining the variability between both rates was the nutritional condition of zooplankton. The GDH/$R_{NH_4^+}$ ratio was indeed found to vary about an order of magnitude during food deprivation (*Chapter* 5). Similar conclusions were reported by Park (1986a) on copepods exposed to long-term starvation. Accordingly, the feeding condition could explain most of the fluctuations observed in *Chapter* 4 when comparing ratios between ecosystems with different productivities. There are basically two ways in which the enzyme activity may be controlled in a changing food environment. On the one hand, the enzyme concentration may vary according to the food avalilability; on the other, it may be regulated by intracellular metabolites. It is reasonable to presume that the earlier mechanism becomes more important in the long-term, as there would be no reason to maintain an excess of enzyme. But, in the short-term, as is the case of the experiments presented in this thesis, it would be energetically more

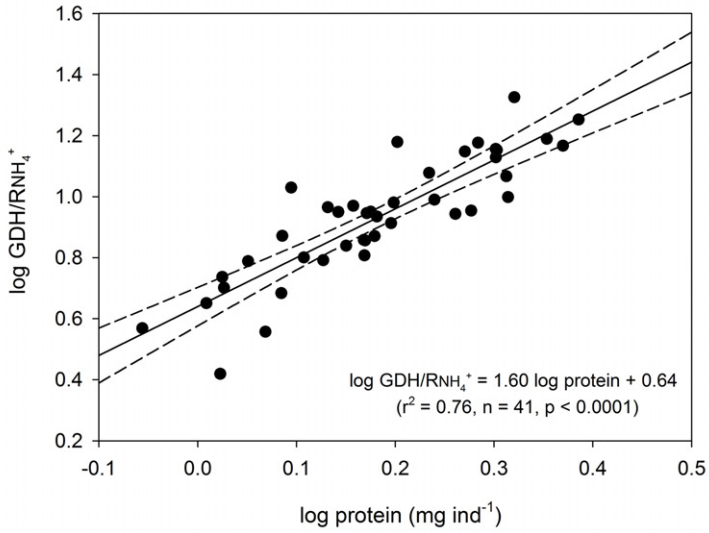

Figure 7.1: Logarithmic relationship between the GDH/$R_{NH_4^+}$ ratio and protein in growing mysids (see *Chapter* 5). Dashed lines stand for the 95 % *CI*s.

efficient to preserve constant levels of enzyme in order to exploit the resources when sudden changes in the food abundance occur. In this latter case, a regulation via intracellular metabolites would result in nearly instantaneous fine-tuned adjustment of enzyme activity. Such a biochemical mechanism would explain the rapid fall of the $R_{NH_4^+}$ with starvation, while the potential activities of GDH (i.e., the V_{max}) remained fairly constant (see Figs. 5.8 and 6.5). If the intracellular pool of substrates shifts the GDH activity into the *in vivo* rate, then the substrate levels should follow the same trend than the $R_{NH_4^+}$ in response to environmental forcings. As shown in natural samples of zooplankton (*Chapter* 4), and in experimental organisms (*Chapters* 5 and 6), glutamate correlated well with $R_{NH_4^+}$ patterns. Although correlation does not necessarily imply causality, these results fit in the general scheme of substrates controlling the GDH-catalyzed reaction rate. On this basis, a bisubstrate kinetic model as the one presented in *Chapter* 6 seems to resolve this uncoupling problem between the $R_{NH_4^+}$ and GDH activities in a changing food environment.

Other potential sources of variability in the GDH/$R_{NH_4^+}$ ratio have to be further investigated. In *Chapter* 6 we introduce the impact that the food quality may cause in that relationship. The amount of NH_4^+ being excreted by zooplankton depends on the food ingested for assimilation (Miller and Roman,

2008), so one could expect higher $R_{NH_4^+}$ when feeding on a proteinic diet. Table 6.2 shows that GDH activities behaved similarly to $R_{NH_4^+}$ with regard to the diet on acclimated organisms, so its implications on the GDH/$R_{NH_4^+}$ variability was not relevant. Still, this should be addressed in the short-term, because, as discussed above, the enzymes often respond with a certain delay to sudden environmental changes. Accordingly, this effect could be more important in ecosystems where there are rapid shifts in the type of prey eaten by zooplankton, as was the case in the Benguela upwelling (*Chapter* 2). In addition, taxonomy has been found essential in understanding the relationship between the physiology and the biochemistry, so that both are closer to each other in non-gelatinous zooplankton than in gelatinous zooplankters (King and Packard, 1975). Different taxonomic composition in the natural samples could thus explain some of the variability that was found in the NH_4^+ excretory metabolism in *Chapters* 2, 3 and 4. All in all, it seems hard to accept a single equation for predicting $R_{NH_4^+}$ from GDH activity in all the circumstances, when the error may rise up to 43 % (see Eq. 4.3). Instead, for the moment, the calculation of a particular GDH/$R_{NH_4^+}$ ratio for each ecosystem and size fraction is recommended.

(iii) Using the kinetics of GDH to predict $R_{NH_4^+}$. Assuming the substrate availability as the critical factor in controlling the velocity of NH_4^+ production, we developed a bisubstrate kinetic model to predict the actual $R_{NH_4^+}$ in two species of zooplankton (*Chapter* 6). This successful attempt introduces new insights in the study of NH_4^+ excretion from *in vitro* enzymology, increasing the reliability of the calculated $R_{NH_4^+}$ under variable trophic conditions. Its application would be of potential interest for field studies of zooplankton metabolism in heterogeneous ecosystems such as that shown in *Chapter* 2, where a single GDH/$R_{NH_4^+}$ may induce a higher error as already discussed. Even though the kinetic principles have been previously applied to other enzymes from the respiratory metabolism, this thesis incorporates them, for the first time, into the study of zooplankton NH_4^+ excretion. In fact, there is no previous attempt to relate direct measurements of intracellular glutamate or NAD^+ to the actual GDH reaction rate in marine organisms. The main objections to the enzyme kinetic studies consist of the cellular compartimentalization, metabolic channeling and competing reactions (Berges and Mulholland, 2008). But while they may interfere with the appraisal of *in vivo* $R_{NH_4^+}$ in terms of magnitude, a

kinetic modeling approach has been demonstrated to provide better estimates of the $R_{NH_4^+}$ patterns than do a model based on a constant GDH/$R_{NH_4^+}$ and the potential NH_4^+ excretion (i.e., GDH activity, see Fig. 6.7). Of course, further research of GDH kinetics at the mitochondrial level would improve the model ability in the $R_{NH_4^+}$ assessment. Moreover, other control mechanisms aside from the substrate activation regulate the reaction rate (Bidigare and King, 1981) and therefore, they need careful consideration. This research presents the first attempt to evaluate the allosteric effect in zooplankton GDH, and it shows that allosterism gains importance in well-fed conditions (Fig. 6.6*b*). This concurs with findings of Park et al. (1986), who suggested a greater inhibitory effect by high-energy molecules such as GTP and ATP under high chlorophyll-a situations. Similar trends in the biomass-specific GDH activities with productivity was found by Hernández-León et al. (2001), as well as in the field data from *Chapters* 2 and 4. According to the kinetic constants presented in Table 6.3, the allosteric regulation, either in its inhibition or activation form, follows a hyperbolic mixed-type mechanism. This means that even when the concentration of an inhibitor is infinite the enzyme reaction activity is not reduced to zero (see Fig. 6.3). The opposite is also true, very high levels of the activator may not stimulate the reaction indefinitely. Although it would be desirable to build a general kinetic model of $R_{NH_4^+}$ that includes regulation mechanisms other than substrate activation, it would have been experimentally too costly. Still, this study establishes a baseline for future research of more complex GDH kinetics in zooplankton.

7.2 Conclusions

The questions raised in *Chapter* 1 have been answered throughout the various sections in this thesis. In general, the main conclusions that arise from the results of this research are:

1. Irrespective of the oceanographic conditions, the control that zooplankton respiration and NH_4^+ excretion exerted over primary productivity in the Benguela upwelling was limited. This was true, even though both rates exceeded the values found in other upwelling ecosystems.

    (a) The ecosystem heterogeneity caused spatio-temporal fluctuations in the biomass and metabolism of zooplankton, even though their maximum values were mostly found over the shelf-break.

(b) The ageing pattern of the upwelled waters promoted changes in the taxonomic composition of the mesozooplankton community, as well as in the carbon and nitrogen sources utilised by these organisms.

(c) Considering the respiratory carbon demand of mesozooplankton jointly with the carbon requirements of bacteria and microzooplankton, these organisms barely consumed the 71 % of the phytoplankton biomass. This means that there was a surplus of net productivity left to be exported either through lateral advection or vertically by sinking into the deep ocean. Accordingly, the Benguela waters act as an autotrophic system during the season of maximum upwelling.

(d) The reduced contribution of mesozooplankton NH_4^+ excretion to the nutrient requirements of phytoplankton (0.5 - 11.5 %) implies that most of the nutrient cycling in this ecosystem occurs through the microbial food web.

2. Unlike other methodologies used in the biogeochemistry, a model based on the integral of $R_{NH_4^+}$ depth profiles allows to construct synoptic sections of vertical nitrogen fluxes, as well as to infer the capacity of the ecosystem to retain its nutrients, and to analyze the active transport of nitrogen driven by vertical migrators.

(a) A combination of nitrogen flux calculations and sediment trap data best illustrates the general picture of the downward nitrogen flux in a highly dynamic marine ecosystem. Both the particle size and production history are critical factors in explaining the imbalance between the sinking particulate nitrogen and the metabolic requirements in the water column.

(b) Depending on the productivity regime, the active nitrogen flux driven by mesozooplankton ranged between 59 - 361 % of the gravitational flux. These organisms actively transported about 5 % of the net primary production, so the active flux was an important component of the biological pump in the Benguela upwelling ecosystem.

3. The use of fluorometry significantly increases the sensibility of the classical GDH assay. This improvement allows the biomass, required for the assay, to be reduced. This is a great advantage when working on samples from the deep ocean.

4. There is important temporal and spatial variability in the relationship between the $R_{NH_4^+}$ and the GDH activities. Thus, a single universal equation cannot describe this relation under all the oceanographic situations. This implies the need for calibration of the GDH/$R_{NH_4^+}$ ratio for each zooplankton community.

   (a) Both variables maintain different allometric relationships with biomass, which produces variability in the GDH/$R_{NH_4^+}$ ratio when comparing different size groups of zooplankton.

   (b) The trophic changes in the ecosystem, and especially those that occur during starvation, induce large differences in the relationship between the $R_{NH_4^+}$ and the GDH activities. While the $R_{NH_4^+}$ immediately responds to shifts in food availability, the enzymatic rates are less responsive to environmental changes. The intracellular pool of substrates explain, to some extent, the difference between the potential NH_4^+ production (V_{max}) and the actual rate, which implies a strong substrate regulation of the GDH.

   (c) Both the food quality and taxonomic composition of the sample also affect the GDH/$R_{NH_4^+}$ ratio.

5. The use of a bisubstrate kinetic model, which assumes the substrate availability as the critical factor in controlling the velocity of NH_4^+ production, predicts the $R_{NH_4^+}$ patterns during a starvation time course better than applying a fixed GDH/$R_{NH_4^+}$ value to the enzymatic measurements.

   (a) The modeled values, however, underestimated the actual rates. A better approximation would require the determination of the substrate concentrations at the mitochondrial level.

   (b) In addition to the substrate activation, the GDH activity is modulated by effector molecules such as the purine nucleotides. The allosteric effect of these molecules is more important in well-fed conditions and should be considered in future models of $R_{NH_4^+}$.

7.3 Future research

This thesis studies the role of the zooplankton in an important eastern boundary upwelling system (i.e., the Benguela upwelling), proposes a novel approach to calculate nitrogen fluxes from zooplankton $R_{NH_4^+}$, and introduces new insights into the regulatory mechanisms of GDH. However, the conclusions that emerge from this study give rise to a number of questions that have to be still resolved in a near future.

1. There is common concern in the oceanographic community about our inability to detect biogeochemical rate processes in oceanic regions, such as oligotrophic waters and the deep-sea, where these signals are weak. This concern is the basis of continual interest in developing more sensitive analytical techniques to measure these processes. Although here we improve the sensitivity of the original GDH assay by applying fluorescence principles, the incorporation of new molecules with a higher emission power, such as resazurin, would allow GDH activity to be analyzed even in those samples taken from the deep oligotrophic oceans.

2. A major part of this thesis focuses on understanding the variability in the relationship GDH/$R_{NH_4^+}$. The impact that some biological factors, such as biomass and starvation, exert on this relationship is addressed in *Chapters* 4 - 6. But they also introduce the importance of taxonomy to explain the GDH/$R_{NH_4^+}$ ratio. Accordingly, future extensive research on the GDH/$R_{NH_4^+}$ variability between taxa would allow this ratio to be corrected according to the taxonomic composition of the sample. This will help the $R_{NH_4^+}$ to be assessed more accurately from measurements of GDH activities.

3. The *Chapter* 6 presents the utility of applying a general enzyme-kinetic model based on first-principles of enzymology to assess the actual $R_{NH_4^+}$. However, our study considers separately both the substrate activation of the GDH reaction, and its modulation by molecular effectors. Developing a model that includes more of these regulation mechanisms would improve the prediction of the actual velocity of NH_4^+ production. On the other hand, future works on this topic should measure the intracellular metabolite concentrations on a mitochondria level.

4. In a global change scenario, the question arises of how the marine acidi-

fication will affect the biogeochemical role of zooplankton. To date, few studies have addressed the consequences of the decrease in the pH in the world ocean for the mesozooplankton community (Niehoff et al., 2013). The gap of knowledge is greater when considering the impact that ocean acidification exerts on the capacity of zooplankton to regenerate nutrients. Likewise, it would be important to elucidate how such a chemical process would affect the relationship between the metabolism and the biochemistry of marine zooplankton.

5. Another effect associated with global change is the increase of gelatinous zooplankton such as jellyfish (Richardson et al., 2009). Under favourable conditions, some gelatinous organisms may dominate the zooplankton community as shown in the *Chapters* 2 and 3, in the case of salps. The rapid growth of gelatinous zooplankton exert a considerable impact on the marine biogeochemistry (e.g., the active transport of nitrogen). However, little is known about the NH_4^+ excretion metabolism of these organisms as well as all the other types of jellyfish. In face of a future warming scenario in which gelatinous organisms dominate the world oceans, there is a clear need to study their role in nutrient cycling and its biochemical control.

Resumen en español

I Introducción general

I.1 Antecedentes y fundamento del estudio

El zooplancton ejerce una importante función en los ciclos biogeoquímicos de todos los océanos del planeta. Es un componente fundamental de la bomba biológica ya que, por un lado, consume materia orgánica para satisfacer su demanda energética, y por otro, libera nutrientes procedentes de los procesos catabólicos que generan dicha energía. Dependiendo del rango de tamaño, estos organismos heterótrofos se clasifican en nanozooplancton (2 - 20 μm), microzooplancton (20 - 200 μm), mesozooplancton (0.2 - 2 mm) y macrozooplancton (> 2 mm). En esta tesis se estudia la actividad metabólica en todas las fracciones de tamaño, si bien parte de la investigación se centra en el mesozooplancton, que constituye un eslabón clave de la cadena trófica al regular el flujo de materia y energía que llega desde los productores primarios hasta los grandes predadores (Moloney, 1992).

Aparte de la presión que ejerce mediante la predación, con la que controla el crecimiento del fitoplancton y la transferencia de materia orgánica al océano profundo, el zooplancton regenera nutrientes que son utilizados por los productores primarios en la fijación de carbono inorgánico disuelto (ver Fig. 1.1). Dentro de los compuestos elementales necesarios para el crecimiento del fitoplancton, el nitrógeno es uno de los nutrientes más limitantes en los océanos. Su disponibilidad depende de los procesos de remineralización que tienen lugar en la capa eufótica, así como de la introducción de nutrientes externos al sistema a partir de eventos de afloramiento de aguas profundas, fijación de nitrógeno atmosférico y escorrentía. De entre todas las especies nitrogenadas, el amonio (NH_4^+) es el principal compuesto que liberan los heterótrofos en la

columna de agua (Ikeda y Skjoldal, 1989; Regnault, 1987) y constituye la forma más reducida y, por tanto, la más eficiente en términos de asimilación. A escala global, la regeneración de NH_4^+ satisface el 80 % de los requerimientos fitoplanctónicos (Harrison, 1992), lo que refleja la importancia que supone esta fuente de nitrógeno en los flujos de nutrientes de los ecosistemas marinos. En general, se considera que el microzooplancton, y más concretamente los flagelados y pequeños ciliados, son los principales regeneradores de NH_4^+ en las aguas epipelágicas (Bronk y Steinberg, 2008; Probyn, 1987), si bien el mesozooplancton también contribuye significativamente al reciclaje de nutrientes (Steinberg y Saba, 2008). De hecho, el mesozooplancton aporta un promedio del 12 - 33 % del NH_4^+ requerido por los autótrofos (Hernández-León et al., 2008). No existe, sin embargo, un patrón espacial que defina el papel de la excreción de NH_4^+ del zooplancton en la regeneración de la producción primaria. Cabe esperar que este proceso metabólico satisfaga un mayor porcentaje de los requerimientos fitoplanctónicos en aguas donde otros aportes nitrogenados (principalmente en las formas de NO_3^- y N_2 fijado) son bajas, como por ejemplo, en el océano abierto y en los mares oligotróficos, y que su contribución disminuya en sistemas costeros y de afloramiento. Así, se ha comprobado que el mesozooplancton es capaz de regenerar hasta un 90 % de la producción primaria en giros oligotróficos (Isla et al., 2004b), mientras que en ecosistemas de afloramiento tan solo aporta el 4 % del nitrógeno requerido por la comunidad de fitoplancton (Bode et al., 2004; Isla et al., 2004a). Esta tendencia general fue confirmada por Hernández-León et al. (2008) en un estudio latitudinal de la contribución potencial de la excreción de NH_4^+ del mesozooplancton a la producción primaria. A partir de datos tomados de la literatura, se estimó que este proceso metabólico reviste una mayor importancia en las aguas tropicales, donde regeneraría alrededor del 47 % del fitoplancton, y cuya aportación al conjunto de nitrógeno disuelto se reduciría conforme aumenta la latitud, alcanzando así un valor mínimo de regeneración en las zonas polares ($\sim 6\,\%$). Pero, comparando estudios individuales de excreción de NH_4^+ en comunidades mixtas de mesozooplancton, se comprueba que estas tendencias no son tan obvias. Por ejemplo, estudios realizados en distintos sistemas de afloramiento han atribuido a estos organismos unos porcentajes de regeneración de la producción primaria que oscilan desde el 4 % (Bode et al., 2004; Isla et al., 2004a) hasta el 44 % (Smith and Whitledge, 1977).

A pesar de que la excreción de NH_4^+ en el zooplancton ha sido estudiada

en una amplia variedad de ecosistemas marinos (ver la compilación de datos –Tabla 8.4– en Bronk y Steinberg, 2008), son pocos los datos del metabolismo del zooplancton disponibles en aguas comprendidas entre 20 - 40° S (Hernández-León et al., 2008). Concretamente, el papel que juega la comunidad de mesozooplancton en el reciclaje de nutrientes en el sistema del afloramiento de Benguela es completamente desconocido. Esta tesis considera este vacío en el conocimiento, y trata de subsanarlo aportando datos novedosos que esclarecen el papel del mesozooplancton en los ciclos biogeoquímicos del norte de Benguela (21° S). Este afloramiento costero es uno de los ecosistemas más productivos de todo el planeta (Nelson and Hutchings, 1983). La divergencia que provoca la fuerza del viento permite el ascenso de aguas profundas, cargadas de nutrientes, a la superficie. De acuerdo con Boyd et al. (1987), los procesos físicos intensifican estos pulsos del afloramiento durante el invierno y la primavera austral. La disponibilidad de nutrientes y luz genera un ambiente propicio para sostener una alta productividad biológica: primero, favorece el crecimiento de fitoplancton en áreas cercanas a la costa (Mitchell-Innes y Walker, 1991), lo que provoca el rápido descenso de la carga de nutrientes conforme la masa de agua envejece en su camino hacia mar abierto. A lo largo de este proceso, se generan eventos de sucesión planctónica (Vinogradov et al., 1972), donde los pequeños flagelados y cocolitofóridos dejan paso a la floración de diatomeas que, a su vez, estimulan el crecimiento del mesozooplancton. Sin embargo, los remolinos y filamentos que proceden del núcleo del afloramiento modifican estos patrones de sucesión específica. En un escenario donde confluyen un conjunto de masas de agua de distinto origen y características hidrográficas (Fig. 1.2), y cuya complejidad física se ve incrementada por los procesos de mesoescala, las dinámicas de las poblaciones planctónicas se ven alteradas en cuestión de días. Esta inestabilidad oceanográfica afecta, por tanto, al metabolismo del zooplancton, cuyo papel en la biogeoquímica del ecosistema puede variar a corto plazo tanto espacial como temporalmente.

Asimismo, los ecosistemas de afloramiento como el de Benguela representan un importante escenario en el intercambio vertical de nutrientes (Longhurst and Harrison, 1989). En las aguas superficiales, el fitoplancton convierte el dióxido de carbono y los nutrientes disueltos en materia orgánica, la cual puede ser regenerada o, en el caso de ecosistemas productivos, transportada al océano profundo. De forma global, alrededor del 5 - 25 % de la producción primaria alcanza la zona mesopelágica, y tan solo el 3 % llega a la batipelági-

ca (De La Rocha and Passow, 2007). Es de esperar que estos porcentajes sean más altos en sistemas de afloramiento que en aguas más oligotróficas (Martin et al., 1987; Buesseler, 1998). Parte de las partículas que se hunden sufre una serie de transformaciones químicas en la columna de agua debidas a procesos biológicos que convierten los elementos orgánicos (principalmente carbono, nitrógeno y fósforo) en sus formas inorgánicas. En general, las bacterias son responsables de remineralizar el 15 % de la materia orgánica que está sedimentado (Ducklow, 2000), mientras que el microzooplancon transforma entre el 30 - 70 % (Calbet and Landry, 2004) y el mesozooplancton, alrededor del 20 - 35 % (Hernández-León and Ikeda, 2005). Junto al hundimiento gravitacional de las partículas, la mezcla de materia orgánica disuelta entre isopicnas y el transporte activo debido al zooplancton migrador (Fig. 1.1) conforman lo que se conoce como la bomba biológica (Volk and Hoffert, 1985). En conjunto, todos estos procesos determinan la actividad metabólica en el océano profundo (Arístegui et al., 2009), así como la capacidad del ecosistema para retener los nutrientes (Packard et al., 1988; Ridgwell et al., 2011).

La relación que mantienen la producción primaria, el flujo vertical de partículas y la regeneración de nutrientes se ha estudiado tradicionalmente mediante las trampas de sedimento. En un sistema en equilibrio, el flujo gravitacional debería ser suficiente como para satisfacer la demanda metabólica en la columna de agua. Basándose en este principio, Packard y Christensen (2004) emplearon medidas de la cadena transportadora de electrones, responsable de los procesos de respiración, para estimar flujos de carbono desde la capa de mezcla hasta el lecho oceánico. En esta tesis se aplica un concepto similar con el fin de calcular el flujo vertical de nitrógeno particulado en aguas de Benguela a partir de procesos de regeneración de NH_4^+ en la columna de agua. Este modelo asume que el zooplancton y los pequeños microheterótrofos consumen, entre otros elementos no conservativos, el nitrógeno particulado que está sedimentando para satisfacer sus requerimientos metabólicos. Como resultado, los organismos liberan nitrógeno inorgánico disuelto (NH_4^+), así como compuestos orgánicos disueltos (urea y aminoácidos) y particulados (deposiciones fecales). A pesar de que la fracción orgánica puede representar una parte importante de la excreción (Steinberg et al., 2002), el cálculo de los flujos de nitrógeno considera exclusivamente el NH_4^+ porque constituye entre el 60 - 100 % del nitrógeno liberado por el zooplancton (Regnault, 1987). Paradojicamente, varios estudios indican un desequilibrio de hasta 2 - 3 órdenes de magnitud entre la materia

particulada que está disponible y las necesidades heterotróficas (Baltar et al., 2009; Steinberg et al., 2008). Los motivos para que se produzca este desacople radican, principalmente, en la baja eficiencia de las trampas de sedimento en la recolección de partículas (Gardner, 2000) o en el uso de factores de conversión que sobreestimarían el metabolismo de la comunidad heterotrófica. El origen de esta discrepancia sigue siendo objeto de discusión en el seno de la comunidad científica (Burd et al., 2010). En este contexto, esta tesis aporta una nueva herramienta para estudiar los flujos de nitrógeno en la columna de agua, y compara estas estimas con el nitrogeno particulado capturado mediante trampas de sedimento en las aguas de Namibia.

Los estudios oceanográficos como los que se plantean en los dos primeros capítulos de esta investigación requieren una rápida adquisición de datos para monitorizar, con una alta resolución espacial, el impacto que supone el metabolismo del zooplancton en los ciclos biogeoquímicos (tanto en el eje horizontal como en el vertical). El estudio detallado de las actividades metabólicas adquiere especial relevancia cuando se trata de ecosistemas que albergan una amplia variabilidad mesoescalar. Lamentablemente, las medidas directas de metabolismo, tales como las clásicas incubaciones en botella, son tediosas y requieren invertir una gran cantidad de tiempo, por lo que la cobertura espacial que ofrecen es limitada. Además, estas técnicas se ven complicadas por artefactos metodológicos tales como el estrés debido a la manipulación, las altas densidades de organismos y los episodios de inanición, que en su conjunto pueden generar resultados alejados de las tasas metabólicas que tienen lugar en el medio natural (Bidigare, 1983). Con el objetivo de solventar todos estos problemas metodológicos, Bidigare y King (1981) introdujeron, en el ámbito de la oceanografía, el ensayo enzimático de la glutamato deshidrogenasa (GDH) como un índice de la excreción de NH_4^+ en el zooplancton. Esta enzima está presente prácticamente en todos los organismos vivos, y constituye un referente para muchas de las reacciones bioquímicas que tienen lugar en la matriz mitocondrial de las células eucariotas. La enzima GDH (EC 1.4.1.3) es una proteína hexamérica con una masa de 320 000 daltons, y cuya estructura apenas a sufrido cambios a lo largo de la evolución. Las 6 subunidades se reorganizan en 3 pares de cadenas poliméricas, cada una de las cuales contiene dos dominios de unión, que sufren cambios conformacionales a lo largo del ciclo catalítico (Peterson and Smith, 1999). Esta arquitectura provee sitios de unión específicos para cada sustrato de la reacción (glutamato y $NAD(P)^+$), así co-

mo para las diversas moléculas efectoras que regulan la actividad enzimática. Aunque la reacción que cataliza la GDH es reversible, la baja afinidad que presenta por el NH_4^+ sugiere que su función en heterótrofos es fundamentalmente la desaminación del glutamato (Fig. 1.3). Esta ruta bioquímica genera, además de NH_4^+, α-ketoglutarato que alimenta el ciclo de los ácidos tricarboxílicos, produciendo donadores de electrones (NADH y $FADH_2$) involucrados en la síntesis de energía (ATP). La actividad catalítica de la GDH está regulada alostéricamente, entre otras, por las moléculas adenosín-5-difosfato (ADP) y guanosín-5-trifosfato (GTP), ambas relacionadas con el estado energético de los organismos (Frieden y Colman, 1967). Esto sugiere que la enzima GDH regula indirectamente la producción de energía y los procesos de biosíntesis, es decir, el crecimiento. A pesar de que varias transaminasas pueden producir NH_4^+ como consecuencia de las reacciones que catalizan, la enzima GDH es la principal responsable de la síntesis de NH_4^+ en los organismos marinos. De hecho, se ha comprobado que su actividad es suficiente para explicar todo el NH_4^+ que es excretado en varias especies de zooplancton (Batrel y Regnault, 1985; Bidigare y King, 1981). Por este motivo, el análisis de la actividad GDH ha sido ampliamente utilizado en oceanografía para inferir las tasas de excreción de NH_4^+ en comunidades mixtas de zooplancton (Bidigare et al., 1982; Hernández-León y Torres, 1997; Hernández-León et al., 2001; Park et al., 1986, entre otros). Por un lado, los ensayos enzimáticos no están afectados por los problemas metodológicos intrínsecos de las incubaciones, y por otro, permiten una rápida toma de muestras. Además, una vez capturadas, las muestras se pueden almacenar para su posterior análisis en el laboratorio. Sin embargo, estas técnicas requieren la adición de sustratos a saturación para asegurar la especificidad y la reproducibilidad de la reacción (Segel, 1993), lo que da como resultado una medida de la velocidad máxima a la que se puede excretar NH_4^+, en lugar de la tasa real de producción. Esta última será probablemente menor ya que la concentración intracelular de sustratos difícilmente se encuentra a saturación en condiciones *in vivo*. Por este motivo, es necesario calibrar las medidas de actividad GDH a partir de un factor empírico que relacione estas medidas potenciales con las tasas reales de excreción de NH_4^+ ($R_{NH_4^+}$). A pesar de que varios estudios han demostrado una relación significativa entre ambas tasas (Bidigare y King, 1981; Park et al., 1986), ésta podría verse afectada por distintos factores. Por ejemplo, Berges et al. (1993) señala la necesidad de considerar la relación alométrica que mantienen tanto la activi-

dad GDH como la excreción de NH_4^+ con la biomasa. Ambas variables deben presentar un coeficiente escalar similar porque, de lo contrario, se daría lugar a interpretaciones erróneas en poblaciones de zooplancton que presenten una estructura de tallas muy variada. Hasta la fecha, no hay un estudio que aborde esta problemática, de modo que esta tesis presenta las primeras ecuaciones que explican la influencia que ejerce la biomasa en el factor GDH/$R_{NH_4^+}$. Por otro lado, Bamstedt (1980) demostró que la actividad de ciertas enzimas responden de una manera más atenuada que la tasas metabólicas a los cambios que se producen en el ambiente. Si este fuera el caso de la GDH, su relación con la $R_{NH_4^+}$ variaría conforme cambian las codiciones tróficas del ecosistema. Por este motivo, probablemente, Hernández-León y Torres (1997) encontraron una fluctuación tan grande en la relación GDH/$R_{NH_4^+}$ en muestras de zooplancton mixto de aguas de Canarias, durante un periodo en el que la denominada floración de finales de invierno provocó cambios en la situación trófica de la comunidad planctónica. Estos autores sugirieron que la disponibilidad de sustratos intracelulares constituiría el factor más determinante para explicar la variabilidad entre la actividad GDH y la excreción de NH_4^+. A lo largo de esta tesis se estudia la relación que mantienen ambas tasas en comunidades naturales de zooplanton procedentes de distintos ecosistemas marinos, así como en cultivos de laboratorio sometidos a distintas condiciones de alimentación, y se discute la idoneidad de utilizar un factor único para estimar las tasas de excreción de NH_4^+ a partir de las medidas enzimáticas de la GDH. Asimismo, se estudian, por primera vez, las cinéticas bisustrato de la enzima GDH en organismos marinos, así como la concentración intracelular de los sustratos involucrados en la reacción: glutamato y NAD^+. Asumiendo la disponibilidad de sustratos como el factor crítico en la regulación de la velocidad a la que tiene lugar la reacción catalizada por la GDH, se construye un modelo cinético basado en los principios fundamentales de la enzimología con el objetivo de predecir la tasa real de excreción de NH_4^+. Este modelo asume que la actividad de la GDH controla la producción de NH_4^+, que los sustratos intracelulares regulan la actividad enzimática, y que la reacción sigue una cinética Michaeliana. El mismo concepto se ha aplicado previamente en otras rutas bioquímicas del metabolismo respiratorio, y se ha demostrado su capacidad para predecir con éxito las tasas de consumo de oxígeno (Aguiar-González et al., 2012; Packard et al., 1996b) y de producción de CO_2 (Roy and Packard, 2001) en varias especies de bacterias marinas. Los resultados pioneros que se presentan en esta tesis refuerzan

la utilidad de los modelos cinéticos en el estudio de la excreción de NH_4^+ en el zooplancton, ya que parecen solucionar muchos de los problemas que entraña el uso de un factor constante (GDH/$R_{NH_4^+}$) para estimar las tasas de excreción de NH_4^+ a partir de la actividad GDH. Asimismo, esta tesis constituye el primer intento de dilucidar, a partir de medidas cinéticas, los mecanismos de control alostérico ligados a las moléculas ADP y GTP en el zooplancton. En general, esta investigación introduce una nueva forma de estudiar la excreción en el zooplancton, y supone una línea base sobre la que construir modelos más complejos que incluyan nuevos mecanismos de regulación además de la activación por los sustratos. En la oceanografía, donde la mayor parte de las observaciones se basan en medidas indirectas, la investigación experimental en el laboratorio es fundamental. Profundizar en el conocimiento de los mecanismos bioquímicos que regulan la velocidad de la reacción de la GDH, permitirá mejorar las estimas de la excreción de NH_4^+ en el zooplancton y, por tanto, extraer conclusiones más robustas acerca de su papel en los ciclos biogeoquímicos.

I.2 **Objetivos y esquema general de la tesis**

En el marco del conocimiento actual sobre el metabolismo del zooplancton y su implicación en los flujos de nutrientes de los ecosistemas marinos, esta investigación aporta resultados novedosos que revelan el papel de la comunidad de mesozooplancton en un importante sistema de afloramiento y que definen los mecanismos bioquímicos de control de la excreción de NH_4^+ en el zooplancton.

Así, el objetivo general de esta tesis consiste en determinar el impacto que ejerce el metabolismo del zooplancton, principalmente la excreción de NH_4^+, en los ciclos biogeoquímicos del ecosistema de Benguela, así como en estudiar los factores que causan variabilidad en la relación existente entre la tasa *in vivo* de excreción de NH_4^+ ($R_{NH_4^+}$) y la actividad potencial de la enzima responsable de este proceso (glutamato deshidrogenasa –GDH–). Estos estudios de carácter más fisiológico utilizan tanto muestras capturadas en ecosistemas marinos con regímenes de productividad diferentes, como organismos de cultivo sometidos a distintas condiciones de alimentación. En este sentido, se pretende comprobar si un modelo cinético, que asume la disponibilidad de sustratos como el factor clave en la regulación de la velocidad de la reacción catalizada por la GDH, mejoraría la predicción de las $R_{NH_4^+}$ en situaciones de variabilidad trófica.

Comprender los mecanismos de control de la actividad de la GDH permitiría determinar de una manera más precisa las $R_{NH_4^+}$ del zooplancton y, con ello, obtener conclusiones más certeras en investigaciones oceanográficas como las que se muestran en los dos primeros capítulos de esta tesis. En este contexto general, se proponen unos objetivos específicos que tratan de resolver una serie de cuestiones:

1. *¿Cuál es el papel del metabolismo del mesozooplancton en un sistema productivo como el afloramiento de Benguela, y cómo influyen las estructuras mesoescalares en su distribución?*

   Estas preguntas encuentran una respuesta en el *Capítulo* 2, donde se presentan los resultados de una campaña oceanográfica llevada a cabo en las aguas de Benguela durante la época activa del afloramiento, en el año 2011. Utilizando un enfoque Euleriano, se analizan las dinámicas de la biomasa y del metabolismo del mesozooplancton a lo largo de un transecto perpendicular a la costa de Namibia. La hipótesis de partida asume la sucesión de las poblaciones de zooplancton conforme la masa de agua aflorada se aleja de la costa, y un impacto menor del metabolismo del mesozooplancton en la productividad primaria en comparación con sistemas más oligotróficos.

2. *¿Cómo determina la excreción de NH_4^+ del zooplancton los flujos verticales de nitrógeno en este sistema de afloramiento? ¿Son comparables los flujos calculados a partir de este proceso metabólico con los valores obtenidos mediante trampas de sedimento? ¿Qué importancia representa en Benguela el flujo activo de nitrógeno debido al mesozooplancton migrador?*

   Una vez conocido el papel que ejerce el metabolismo del mesozooplancton sobre la productividad primaria del sistema de Benguela, se determina la implicación de las $R_{NH_4^+}$ del zooplancton en los flujos verticales de nitrógeno. Los interrogantes propuestos se solucionan en el *Capítulo* 3 al aplicar un modelo potencial a los perfiles de $R_{NH_4^+}$ para calcular el flujo gravitacional de nitrógeno en este sistema de afloramiento. Los valores modelados se comparan con la sedimentación de nitrógeno particulado medida mediante trampas de sedimento en dos estaciones del transecto. En base a trabajos previos de la literatura, cabe esperar un

desacople entre el nitrógeno sedimentado y los requerimientos metabólicos en la columna de agua. Asimismo, los flujos de nitrógeno modelados se utilizan para estudiar el flujo activo debido al mesozooplancton. Atendiendo a la elevada biomasa de estos organismos en los sistemas de afloramiento, este componente de la bomba biológica podría revestir una gran importancia.

3. *¿Existe una ecuación universal que explique la relación que mantiene la $R_{NH_4^+}$ con la actividad de la GDH en cualquier circunstancia? ¿Qué factores influyen en dicha relación, y de qué forma lo hacen?*

   Las $R_{NH_4^+}$ que se determinan en los dos primeros capítulos se obtuvieron necesariamente a partir de medidas de la enzima GDH, que dan como resultado tasas potenciales que se relacionan con las tasas reales mediante un factor empírico. En el *Capítulo* 4 se estudia la relación que mantienen a lo largo de varios sistemas oceánicos las $R_{NH_4^+}$ analizadas mediante incubaciones en botella y las actividades de la GDH en diversas tallas de zooplancton, y se comparan con valores de GDH/$R_{NH_4^+}$ publicados previamente en la literatura. Se discute la idoneidad de utilizar un factor único para inferir las $R_{NH_4^+}$ a partir de las medidas potenciales (es decir, las actividades de la GDH). Si los cambios que se producen en ciertas variables biológicas tales como la biomasa y la alimentación tuvieran el mismo efecto en ambas tasas, la relación entre ellas se mantendría constante. La magnitud de tales efectos se determina más detalladamente en un cultivo monoespecífico del misidáceo marino *Leptomysis lingvura* (*Capítulo* 5).

4. *¿Es capaz un modelo cinético aplicado a la enzima GDH de predecir los patrones de $R_{NH_4^+}$ en el zooplancton? ¿Cuándo es más importante la modulación alostérica de esta enzima?*

   Estas cuestiones de índole puramente bioquímica se abordan en el *Capítulo* 6. Tal y como sugieren los resultados obtenidos en los capítulos previos, la disponibilidad de sustratos podría constituir el mecanismo básico de regulación de la actividad de la GDH. Asumiendo esta premisa, se utiliza un modelo bisustrato basado en las ecuaciones de Michaelis-Menten para predecir las $R_{NH_4^+}$ medidas en dos especies de zooplancton a lo largo de un periodo de inanición. La inhibición y activación alostéricas debidas a los purín nucleótidos se estudiaron de forma

separada utilizando modelos cinéticos que consideraban un único sustrato. Es de esperar que el alosterismo adquiera importancia en situaciones en las que los organismos presenten una mayor carga energética.

II Material y métodos generales

II.1 Medidas oceanográficas

Los muestreos llevados a cabo en el sistema de afloramiento de Benguela, Atlántico Norte, Océano Índico y aguas de Canarias, se realizaron a bordo de tres barcos oceanográficos: RV María S. Merian, BIO Hespérides y BIO Atlantic Explorer. En todos los casos se registraron las variables fisico-químicas de salinidad, temperatura, fluorescencia y oxígeno disuelto mediante el uso de un sensor de conductividad-temperatura-salinidad (CTD) Seabird 911+, que llevaba acoplado un fluorómetro WETlab FLRT-1754. El equipo estaba instalado en una roseta oceanográfica que llevaba incorporadas 6 - 24 botellas Niskin de 4 - 10 L según la campaña oceanográfica.

Las medidas fluorométricas en el rango de emisión de la clorofila-a, se utilizaron como un índice de biomasa de fitoplancton. En todos los casos, dichas medidas se calibraron con determinaciones directas de clorofila. Con este propósito, se filtraban 500 mL de agua de mar a través de filtros GF/F, que posteriormente eran congelados a $-20\,^{\circ}$C. La concentración de clorofila se determinó mediante técnicas espectrofotométricas (Parsons et al., 1984), o aplicando sus propiedades de fluorescencia tal y como describen Yentsch y Menzel (1963).

Por otro lado, en el *Capítulo* 3 se presentan datos de nitrógeno particulado depositado en trampas de sedimento. Estas trampas estaban equipadas con 21 contenedores de vidrio, programados para muestrear cada 24 h. Los viales de muestreo contenían una solución salmuera al 70 ‰, así como una solución preservadora compuesta por formaldehido al 2 %. Una vez recuperadas las trampas de sedimento, se filtró una alícuota de las muestras a través de filtros GF/F esterilizados previamente mediante combustión, y congelados a $-20\,^{\circ}$C. En el laboratorio, las muestras se analizaron mediante un autoanalizador de elementos Carlo Erba/Fisons 1108.

El flujo gravitacional de nitrógeno particulado se comparó con los flujos estimados a partir de medidas de la actividad de la GDH en el zooplancton. Estas estimaciones asumen que el zooplancton juega un papel fundamental

transformando el nitrógeno orgánico particulado (PON) en NH_4^+ a través de procesos de excreción. Considerando las tasas de excreción de NH_4^+ ($R_{NH_4^+}$) a distintas profundidades de la columna de agua se generaron perfiles de $R_{NH_4^+}$ heterotrófica al ajustar una función potencial a las medidas discretas. La función resultante es la que sigue:

$$R_{NH_4^+} = (R_{NH_4^+})_m \, (z/z_m)^b \tag{II.1}$$

siendo $(R_{NH_4^+})_m$ la hipotética tasa de excreción de NH_4^+ en la superficie, z la profundidad y b el factor que determina la curvatura de la función. Así, la $R_{NH_4^+}$ a una profundidad debería igualar la diferencia entre el PON que entra en esa profundidad, y el que queda disponible por debajo de dicha profundidad. Asumiendo un flujo vertical unidimensional y un efecto de la advección lateral poco relevante, el flujo vertical de PON que se requeriría para sustentar todo el NH_4^+ excretado en la columna de agua podría calcularse integrando el perfil de $R_{NH_4^+}$ desde la superficie hasta el fondo oceánico. Basándose en este concepto, se podría calcular el flujo vertical de nitrógeno (F_N) a una profundidad dada (z_f) aplicando la Eq. II.2:

$$F_{N_{f-s}} = \{(R_{NH_4^+})_m / [(b+1)\, z_m^b]\} \, (z_s^{b+1} - z_f^{b+1}) \tag{II.2}$$

Estos cálculos del F_N se utilizaron, además, con el fin de inferir la capacidad que tiene una capa de agua para retener nutrientes, tal y como se describe en la Eq. II.3:

$$NRE_{z_1-z_2} = (\int_{z_2}^{z_1} R_{NH_4^+} \, dz) / F_{N_{Z_1}} \tag{II.3}$$

Asimismo, se calculó el F_N activo que viene determinado por las migraciones verticales del mesozooplancton. De acuerdo con Postel et al. (2007), se asume que la mayor parte del zooplancton migrador reside en los 150 m superficiales durante la noche. El F_N activo resultaría de sustraer el valor del F_N estimado a 150 m de profundidad durante el día, del correspondiente valor calculado durante la noche. Este F_N activo se comparó con el cálculo clásico de flujo activo descrito por Dam et al. (1995), que se basa en la diferencia de biomasas entre el día y la noche (Eq. II.4):

$$N_B = BM_z \times \text{spc-}(R_{NH_4^+}) \times 12\,(h) \tag{II.4}$$

donde N_B es la tasa de consumo de nitrógeno por el mesozooplancton (mmol

N m^{-2} d^{-1}), BM_z es la biomasa del mesozooplancton (g N m^{-2}) y spc-($R_{NH_4^+}$) es la tasa de excreción de amonio por unidad de biomasa (mmol NH_4^+ g N^{-1} h^{-1}).

II.2 **Muestreo de zooplancton**

Las muestras de nano/microzooplancton (0.7 - 100 μm) utilizadas para el cálculo de flujos verticales de nitrógeno en el sistema de Benguela (*Capítulo* 3), se tomaron en 8 - 9 profundidades discretas de la columna de agua mediante botellas Niskin (10 L) montadas en una roseta oceanográfica. Una vez prefiltrados a través de una malla de 100 μm, 5 - 6 L de agua de mar correspondientes a cada profundidad se filtraron a temperatura ambiente mediante filtros GF/F. Estos filtros se congelaron a −80 °C para el posterior análisis de la actividad de la GDH.

La toma de muestras de mesozooplancton para los estudios enzimáticos y análisis de biomasa que se llevaron a cabo en aguas del afloramiento de Benguela (*Capítulos* 2 y 3), consistió en lances verticales de una red Multinet (Hydrobios GmbH, Kiel, Alemania). El marco de la red, cuya superficie de apertura ascendía a 0.25 m^2, llevaba acopladas redes con luz de malla de 100 μm y 500 μm, dispuestas de forma alternativa. Cada red terminaba en un colector plástico provisto de una pequeña abertura cubierta por una malla de 100 μm, cuya función consistía en evacuar el agua para evitar el reflujo dentro de la propia red. Dos flujómetros instalados en las caras externa e interna de la red medían el volumen de agua filtrada en cada lance, mientras que un sensor de presión indicaba la profundidad en la que se encontraba la red en tiempo real. Este sistema permitía recolectar muestras estratificadas de zooplancton en un mismo lance vertical. Se consideraron tres capas de profundidad: 200 - 75 m, 75 - 25 m y 25 - 0 m. Gracias a la disposición de las mallas, la red tomaba dos muestras distintas por cada profundidad: la malla con un tamaño de poro de 100 μm se utilizaba para la fracción de zooplancton menor a 500 μm, mientras que la malla de 500 μm retenía el zooplancton más grande. Esta estrategia posibilitó un muestreo cuantitativo de organismos con un tamaño comprendido entre 0.1 - 10 mm. Una vez en superficie, la parte exterior de la red se lavaba con agua de mar con el fin de asegurar que todo el zooplancton quedase atrapado en el colector. En el laboratorio, las muestras fueron divididas en varias submuestras mediante la técnica de separación en jarra (Van Guelpen et al., 1982). Las submuestras resultantes fueron fraccionadas en 4 clases de tamaño

(100 - 200 μm, 200 - 500 μm, 500 - 1000 μm, y > 1000 μm) y a continuación, apropiadamente almacenadas según cual fuera su propósito. Las muestras destinadas a análisis enzimáticos, se congelaron inmediatamente a −80 °C. La fracción que iba a ser utilizada en estudios isotópicos y análisis de biomasa, se almacenó a −20 °C. El resto de la muestra se introdujo en botellas de plástico rellenas de formaldehido al 4 %, para su posterior estudio taxonómico.

El mesozooplancton empleado en estudios fisiológicos (*Capítulos* 2, 3 y 4) se capturó, en cambio, mediante lances verticales de una red UNESCO WP-2 (60 cm de diámetro), cuya malla presentaba un tamaño de poro de 100 μm o 200 μm, dependiendo de la campaña oceanográfica. En este caso, el izado de la red se realizó a una velocidad inferior a 0.3 m s^{-1}, tal y como se recomienda para estudios de metabolismo que requieren organismos sanos (Sameoto et al., 2000). Por otro lado, el microzooplancton (50 - 100 μm) incubado en botellas para la determinación de las tasas de excreción de NH_4^+ (*Capítulo* 4), se capturó mediante lances oblícuos de una red de plancton Hansen-Egg (20 cm de diámetro), con una luz de malla de 50 μm.

II.3 **Cultivo de organismos marinos**

Los experimentos realizados en los *Capítulos* 5 y 6 utilizaron organismos cultivados en el laboratorio. A diferencia de los estudios oceanográficos, el cultivo de organismos permite controlar las condiciones fisico-químicas del medio, modular factores externos como la alimentación, y trabajar con muestras de zooplancton monoespecíficas. Todo ello en su conjunto posibilitó el desarrollo de estudios metabólicos más específicos. Esta tesis contiene experimentos realizados en cultivos de dos especies de zooplancton marino: el rotífero *Brachionus plicatilis* (*Capítulo* 4) y el misidáceo *Leptomysis lingvura* (*Capítulos* 4 y 5).

(i) *Brachionus plicatilis.* Rotíferos de la especie *B. plicatilis* se cultivaron en contenedores plásticos de 20 L cada uno, rellenos con agua de mar filtrada a través de filtros GF/F, diluida (~ 23 PSU) y mantenida a 25 °C en condiciones de oscuridad. Los tanques fueron aireados suavemente con el fin de mantener concentraciones de oxígeno a saturación. El material sólido que se acumuló de forma progresiva en el fondo de los tanques era sifonado diariamente, y una parte del agua era reemplazada. Este procedimiento evitó concentraciones de NH_4^+ disuelto superiores a 0.1 mg L^{-1}. Los rotíferos fueron alimentados con

dos dietas distintas que diferían sustancialmente en su composición lipídica (Lubzens et al., 1995): los rotíferos de un tanque fueron alimentados con la especie de microalga viva *Nannochloropsis* sp., rica en ácidos grasos poliinsaturados, en una concentración de 1.2×10^5 por rotífero y día; los rotíferos del otro tanque, fueron provistos de una dieta menos lipídica, compuesta por 0.8 g de levadura seca. Ambos alimentos se añadieron a los tanques de forma progresiva mediante bombas peristálticas. Con este procedimiento se alcanzaron densidades relativamente altas de hasta 200 rotíferos mL^{-1}. El uso de *Nannochloropsis* sp. como alimento de los rotíferos requirió, por tanto, cultivos paralelos de esta microalga de 2 - 3 μm de diámetro, tal y como se detalla más adelante.

(ii) *Leptomysis lingvura.* Otro cultivo de zooplancton utilizado en esta tesis fue el del misidáceo marino *L. lingvura*. Los organismos se recolectaron en el medio natural, mediante un equipo de buceo y una red de mano. Los misidáceos salvajes se capturaron en aguas de la costa de Gran Canaria (19.5 °C), cerca de fondos arenosos situados entre 8 - 12 m de profundidad, y se trasladaron inmediatamente a los sistemas de cultivo instalados en la universidad. Dicha instalación está formada por 12 acuarios de cristal (40 L cada uno) conectados a un sistema de recirculación. El sistema se mantuvo bajo un ciclo luz:oscuridad de 14:10 h, y a una temperatura próxima a la registrada *in situ*. El enorme volumen de agua implicado, junto con los sistemas de filtración biológica y mecánica que llevaba acoplados la instalación, hicieron posible mantener los niveles de NH_4^+, NO_2^- y NO_3^- por debajo de 0.1, 0.02 y 0.2 mg L^{-1}, respectivamente, tal y como recomienda Lussier et al. (1988). Los misidáceos fueron alimentados con nauplios de 48 h de *Artemia* sp. enriquecidos con Easy-DHA Selco® (INVE, Bélgica), en una concentración de 100 artemias por misidáceo y día. En el *Capítulo* 5, se ofreció una dieta alternativa compuesta por 400 rotíferos por misidáceo y día, que sería suficiente para satisfacer la demanda de los misidáceos (Domingues et al., 2000). En ambos casos, el alimento se suministró en dos tomas diarias.

(iii) *Nannochloropsis* sp. Una cepa de *Nannochloropsis* sp. se cultivó en botellas plásticas de 8 L que contenían agua de mar, sometida a un proceso de esterilización en un autoclave y filtrada por 0.2 μm, enriquecida con medio f/2 (Guillard, 1975). Las botellas de crecimiento se mantuvieron aireadas en

una cámara de cultivo a una temperatura constante de 20 °C, y una intensidad lumínica de 54.1 μmol fotones m^{-2} s^{-1} en un ciclo día:noche de 16:08 h.

II.4 **Composición taxonómica de la comunidad de zooplancton**

El *Capítulo* 2 muestra el estudio taxonómico de la comunidad de zooplancton residente en las aguas de Benguela. Las muestras analizadas pertenecieron a estaciones oceanográficas situadas a 12, 20, 110, 200 y 230 km de la costa, caracterizadas por distintas condiciones físico-químicas. En todos los casos, las muestras fueron tomadas durante la noche.

El análisis de la composición taxonómica se realizó mediante un estereomicroscopio (Leica, MZ 8), cuyo aumento oscilaba entre 16 y 80 ×. Las tallas más pequeñas se analizaron con un microscopio invertido (Labovert FS, Leitz) de 50 ×. En ambos casos se utilizaron cámaras Bogorov para el recuento de organismos. Por lo general, fue necesario trabajar con una alícuota de cada muestra debido a la alta concentración de zooplancton. La clasificación taxonómica se realizó a nivel de género, en base a la literatura disponible para el zooplancton de las regiónes de Angola-Sudáfrica (Gibbons, 1997), Atlántico Sur (Boltovskoy, 1999), Hemisferio norte (ICES, 2001) y Mediterráneo (Trégouboff y Rose, 1978; Riedl, 1983).

II.5 **Análisis de biomasa y medidas de isótopos estables**

El análisis de proteínas fue la medida de biomasa más utilizada en los trabajos de investigación que se presentan en esta tesis. El contenido proteico de cada muestra se determinó en base al método de Lowry et al. (1951), modificado por Rutter (1967). En todos los casos se utilizó albúmina bovina (BSA) como estándar.

Además, en el *Capítulo* 2 se determinaron otras medidas de biomasa tales como el peso seco y las composiciones elementales de carbono y nitrógeno. Asimismo, se realizaron análisis de los isótopos estables de estos elementos. Las muestras congeladas se secaron a 60 °C y a continuación, homogeneizadas mediante un proceso mecánico de trituración y pesadas en cápsulas. Las medidas se realizaron por combustión a 1020 °C (CE Instruments Flash EA 1112) en el espectrómetro de masas Finigan Delta S. La medidas de carbono orgánico particulado (POC) y nitrógeno orgánico particulado (PON) se calibraron diariamente con un estándar de acetanilida. Los isótopos estables de carbono y nitrógeno analizados en cada muestra se corrigieron con los valores

obtenidos a partir de estándares con composiciones isotópicas de carbono y nitrógeno conocidas mediante el balance de masas (Agencia Internacional de Energía Atómica IAEA: IAEA-N1, IAEA-N2, IAEA-N3, NBS 22, IAEA-C3 y IAEA-CH-6). Los valores se consideraron en relación al valor de referencia del N_2 atmosférico (^{15}N) y VPDB (^{13}C-Vienna Peedee belemnite). La precisión analítica de ambas relaciones isotópicas fue de 0.2 ‰. Los contenidos elementales de carbono y nitrógeno se calcularon como porcentajes del peso seco total. La relación C/N se calculó a partir de sus valores molares. En general, las muestras no se acidificaron antes de la combustión y, por tanto, no se eliminó el carbono inorgánico de las mismas. Por este motivo, se seleccionaron 45 muestras que sirvieron para estimar el posible efecto de la ausencia de acidificación. La diferencia entre ambos tratamientos no fue significativa ($p > 0.05$), ascendiendo a un máximo de 7.5 %.

En el *Capítulo* 6 se determinó, adicionalmente, el biovolumen de rotíferos y misidáceos a partir de medidas de biomasa. El contenido proteico de los rotíferos se transformó en biovolumen multiplicando por un factor de 0.11 μg proteína rotífero^{-1} ($\pm$ 0.04, n = 30), y asumiendo un biovolumen por rotífero adulto igual a 1.36×10^6 μm^3 según Boraas y Bennett (1988). El biovolumen de misidáceos se estimó a partir de la ecuación N (mg) = 0.0546 + 0.0137 V (mm^3) dada por Alcaraz et al. (2003), considerando un factor proteína : N de 0.521 (Postel et al., 2000).

II.6 **Medidas fisiológicas mediante incubaciones en botella**

En la amplia mayoría de los capítulos se realizaron incubaciones en botella para cuantificar tasas fisiológicas, principalmente de excreción de NH_4^+, en el zooplancton. Después de un periodo de aclimatación, los organismos eran introducidos cuidadosamente en botellas de cristal de 60 mL que contenían agua de mar filtrada por 0.2 μm. De acuerdo con Ikeda et al. (2000), las botellas con un volumen comprendido entre 30 - 160 mL ejercen un pequeño efecto en las tasas fisiológicas del zooplancton. Un volúmen de botella de 60 mL permitiría, por tanto, alcanzar un equilibrio entre el efecto botella y el tiempo de incubación, que en el caso de ser demasiado largo podría inducir estados de inanición. Con el fin de determinar la concentración de NH_4^+ disuelto (μM) en el punto inicial, se tomaban 3 réplicas (10 mL cada una) del agua del mar filtrada utilizada para rellenar las botellas. Los organismos se incubaron durante 60 - 90 min, dependiendo de la densidad de la población experimental.

Durante este periodo, las botellas se mantuvieron reguladas a la temperatura *in situ* y en condiciones de oscuridad para prevenir cualquier tipo de actividad autotrófica. Finalizadas las incubaciones, se tomaba una muestra de agua (10 mL) de cada botella mediante la técnica de sifonado. El NH_4^+ disuelto en estas muestras de agua era analizado espectofluorométricamente mediante el protocolo descrito en Holmes et al. (1999), que aprovecha la fluorescencia del o-ftaldialdehido (OPA) al reaccionar con el NH_4^+. En las campañas oceanográficas donde no había disponibilidad de espectrofluorómetro, se utilizó el método del fenol-hipoclorito que se basa en la absorbancia del indofenol (Solorzano, 1969). En ambos casos las concentraciones se extraían mediante la aplicación de una curva estándar hecha con cloruro de NH_4^+ (0.04 - 10.24 μM). La concentración final de NH_4^+ disuelto resultaba de sustraer la concentración medida en las muestras control (incubadas sin organismos en el interior), de la determinada en las propias botellas experimentales.

En muchas de estas incubaciones se realizaron de forma paralela medidas de respiración con el objetivo de estudiar la relación $R_{O_2}/R_{NH_4^+}$. Las tasa de consumo de oxígeno se determinó en las mismas botellas a partir de medidas de la concentración de oxígeno disuelto que eran registradas de manera contínua mediante de un sistema de electrodos de 6 canales (Strathkelvin 928 Oxygen System®).

II.7 **Ensayos enzimáticos y constantes cinéticas**

(i) Análisis de la enzima glutamato deshidrogenasa (GDH). Uno de los fundamentos de esta tesis doctoral radica en el análisis bioquímico de ciertas rutas metabólicas presentes en el zooplancton marino. Concretamente, se centra en la ruta metabólica controlada por la enzima GDH (EC 1.4.1.3), que determina la excreción de NH_4^+ en organismos heterotróficos. El ensayo enzimático de la GDH fue introducido en el campo de la oceanografía por Bidigare y King en 1981. En esta tesis utilizamos este ensayo enzimático, aunque introducimos una ligera modificación que la hace más sensibles mediante el uso de la fluorometría. En general, los análisis se realizaron en organismos que estaban almacenados a −80 °C. Las muestras eran descongeladas y sonicadas durante 50 s a 70 % de amplitud (VXC 130 Sonics), en 2 mL de tampón Tris (pH = 8.6). A continuación, el homogeneizado era centrifugado durante 8 min a 4000 rpm. El líquido sobrenadante que resultaba de la centrifugación, era utilizado para el análisis de la actividad de la GDH. Durante todo el procedimiento la muestra

se mantenía en frío con el fin de evitar una pérdida de actividad enzimática. La mezcla de reacción constaba de 200 μL del extracto centrifugado, 300 μL de NAD^+ (1.2 mM) y 250 μL de ADP (2 mM). La solución resultante era incubada durante unos pocos minutos hasta que no se registraban fluctuaciones en la fluorescencia del NADH. Entonces, se desencadenaba la reacción mediante la incorporación de 500 μL de glutamato (50 mM). El incremento de la fluorescencia debida a la producción de NADH se monitorizaba durante 4 minutos en un espectrofluorómetro Horiba Jobin Ybon Fluoromax® 4. La temperatura de la reacción se mantenía a la misma temperatura que la registrada *in situ*, o por el contrario, las actividades se corregían mediante la ecuación de Arrhenius utilizando una energía de activación igual a 10 Kcal mol^{-1} (calculada a partir del valor Q_{10} publicado por Park et al., 1986, para la GDH). Las unidades arbitrarias de fluorescencia se convirtieron a actividades de la GDH (μmol NH_4^+ h^{-1}) mediante una curva de calibrado que utilizaba GDH pura (1.4.1.3) de hígado bovino. Esta curva se determinaba en cada tanda experimental, en un rango que oscilaba entre $0.07 - 2.9 \times 10^{-4}$ unidades enzimáticas (U) de GDH por mL, donde 1 U equivale a la cantidad de enzima que transforma 1 μmol NAD^+ min^{-1}. La posible reducción no enzimática del NAD^+ en las muestras se corrigió mediante la sustracción de las pendientes correspondientes a las muestras control (sin sustratos añadidos) que se analizaban conjuntamente.

(ii) Análisis del sistema de transporte de electrones (ETS). Otra técnica enzimática empleada en el *Capítulo* 2 es la que determina la actividad del sistema de transporte de electrones (ETS). El ensayo enzimático del ETS se realizó de acuerdo al protocolo de Owens y King (1975), con las modificaciones introducidas por Packard et al. (1996b). Se basa en la incorporación a saturación de los sustratos NADH (1.7 mM) y NADPH (0.25 mM), que donan los electrones que serán transportados a lo largo de este complejo enzimático. Además, se añade 2-p-iodofenil-3-p-nitrofenil (INT), que reemplaza al oxígeno como aceptor de electrones, dando como resultado la forma reducida INT-formazán. El incremento de la absorbancia de esta última molécula se monitorizó de manera constante a 490 nm durante 6 min, en cubetas de 1 cm de grosor. Al igual que ocurría con los análisis de la actividad de la GDH, las cinéticas se midieron a la misma temperatura que la registrada *in situ*; en caso contrario, eran corregidas mediante la ecuación de Arrhenius. La regresión de la absorción frente al tiempo se utilizó para estimar la actividad del ETS y la tasa potencial

de respiración conforme se describe en Packard y Williams (1981). Hay que tener en cuenta que el oxígeno acepta 4 electrones, mientras que el INT sólo acepta 2. Así, la reducción del INT debe relacionarse estequiométricamente con la actividad del ETS mediante un factor de 2, y con la respiración potencial, mediante un factor de 0.5.

(iii) Análisis cinéticos. Las constantes cinéticas de la GDH se analizaron en los *Capítulos* 5 y 6. Aunque en el *Capítulo* 5 se presentan resultados preliminares de la $V_{\max}$ y las constantes de Michaelis (K_{m}), es en el *Capítulo* 6 donde se realiza un estudio pormenorizado de los mecanismos cinéticos que gobiernan la GDH ante diversas condiciones ambientales. Tal y como postularon Rife y Cleland (1980), se asumió un mecanismo secuencial aleatorio en una reacción bisustrato estacionaria, que es válido siempre que la concentración del producto sea despreciable con respecto a la concentración del sustrato (Bisswanger, 2008). La ecuación de Michaelis-Menten que describe este mecanismo cinético es el siguiente:

$$V_{\mathrm{NH_4^+}} = \frac{V_{\max}\,[\mathrm{Glu}]\,[\mathrm{NAD^+}]}{K_{\mathrm{ia}}\,K_{\mathrm{NAD}} + K_{\mathrm{NAD}}\,[\mathrm{Glu}] + K_{\mathrm{Glu}}\,[\mathrm{NAD^+}] + [\mathrm{Glu}]\,[\mathrm{NAD^+}]} \qquad \text{(II.5)}$$

donde $v_{\mathrm{NH_4^+}}$ es la tasa real de producción de $\mathrm{NH_4^+}$, V_{max} es la velocidad máxima aparente de la reacción enzimática, K_{ia} es la constante de disociación asociada al sustrato principal (es decir, el glutamato), y K_{Glu} y K_{NAD} son las constantes de Michaelis para el glutamato y el $\mathrm{NAD^+}$, respectivamente.

Los parámetros cinéticos se midieron combinando 5 concentraciones de Glu (0.4, 2, 10, 40 y 60 mM) con 5 concentraciones de $\mathrm{NAD^+}$ (0.05, 0.2, 0.6, 1.2 y 2 mM). El rango de estas concentraciones incluye valores que se encuentran 1 orden por encima y por debajo del valor aproximado de K_{m}, tal y como recomienda Bisswanger (2011). Además, esta matriz de concentraciones de 5×5 mantenía un compromiso con la estabilidad de la enzima, ya que el tiempo necesario para analizar cada homogeneizado en un espectrofluorómetro de 4 cubetas no superaba 1 h. Las curvas hiperbólicas que resultaron de analizar distintas concentraciones de glutamato frente a varias concentraciones fijas de $\mathrm{NAD^+}$, y viceversa, se hicieron lineales mediante una transformación doble recíproca (Lineweaver y Burk, 1934). Así, se realizaron gráficos primarios para cada sustrato mediante la representación de sus concentraciones inversas (en abscisas, $1/[\mathrm{Glu}]$ y $1/[\mathrm{NAD^+}]$) frente al inverso de la velocidad (en

ordenadas, $1/v$ –ver Fig. 6.2*a*–). Las líneas resultantes se cruzaron entre sí a la izquierda del eje de ordenadas, lo que confirmó el mecanismo de GDH propuesto anteriormente. Las pendientes y los interceptos en el eje de las ordenadas que se obtuvieron en las gráficas primarias para un sustrato dado (por ejemplo, $1/[NAD^+]$) fueron representadas en un segundo diagrama frente al inverso del otro sustrato (en este caso, $1/[Glu]$). Las regresiones tanto de las pendientes como de los interceptos dieron lugar a líneas rectas que cortaban en el eje de las abscisas en $-1/K_{ia}$ y en $-1/K_{Glu}$, respectivamente (Bisswanger, 2008).

Asimismo, se estudió el efecto alostérico que ejercen algunos nucleótidos purínicos en las actividades de la GDH. Concretamente, el GTP y el ADP actúan como inhibidor y activador de la reacción enzimática, respectivamente (Frieden y Colman, 1967). La estructura de la enzima GDH incluye un dominio de unión específico para los nucleótidos purínicos, lo que significa que no compite con los sustratos por unirse al sitio activo. El complejo enzima-sustrato (ES) no se ve inhibido de manera lineal por el GTP, de forma que concentraciones infinitas de GTP reducen la actividad de la GDH, pero no la inhiben por completo. Lo mismo ocurre con la activación del ADP. Este comportamiento indica una inhibición mixta hiperbólica, donde la V_{max} y K_{Glu} (considerando el glutamato como el sustrato principal) se ven modificados por la concentración de efector. Estos cambios en la V_{max} y K_{Glu} vienen determinados por los factores α y β, respectivamente. De acuerdo con Segel (1993), la ecuación general de Henri-Michaelis-Menten para este tipo de inhibición, considerando el caso más sencillo de una reacción monosustrato, es la que se detalla a continuación:

$$V_{NH_4^+} = \frac{V_{max}\,[Glu]}{K_{Glu}\,(1 + \frac{[GTP]}{K_{i_{pend.}}}) + [Glu]\,(1 + \frac{[GTP]}{K_{i_{int.}}})} \tag{II.6}$$

donde $K_{i_{slope}}$ se refiere al valor aparente de K_i que proviene de los cambios en las pendientes del diagrama secundario,

$$K_{i_{pend.}} = \frac{\beta_i\,[GTP] + \alpha_i\,K_i}{(\alpha_i - \beta_i)} \tag{II.7}$$

y $K_{i_{int.}}$ se refiere al valor aparente de K_i calculado del intercepto en las ordena-

das ($1 / v$) del diagrama secundario:

$$K_{i_{int.}} = \frac{\beta_i\,[GTP] \;+\; \alpha_i\,K_i}{(1 \;-\; \beta_i)} \qquad \text{(II.8)}$$

El mismo concepto debe aplicarse para el estudio de la activación por el ADP:

$$V_{NH_4^+} = \frac{V_{max}\,[Glu]}{K_{Glu}\,\frac{(1+\frac{[ADP]}{K_a})}{(1+\frac{\beta\,[ADP]}{\alpha\,K_a})} \;+\; [Glu]\,\frac{(1+\frac{[ADP]}{\alpha\,K_a})}{(1+\frac{\beta\,[ADP]}{\alpha\,K_a})}} \qquad (1.12)$$

Para deducir estas constantes de inhibición, se utilizó un procedimiento similar al descrito previamente para las cinéticas bisustrato. Se midió la actividad de la GDH a 6 concentraciones (0.2, 1, 5, 20, 40, 60 mM) del sustrato principal (Glu), cada una de ellas expuesta a distintas concentraciones de GTP (0, 5, 10, 50 y 100 μM) o ADP (0, 0.02, 0.2, 1 y 2 mM). Las curvas hiperbólicas resultantes se hicieron lineales mediante la transformación doble recíproca. Las concentraciones inversas del Glu (eje de abscisas, $1 / [Glu]$) se representaron en un diagrama primario frente al inverso de la velocidad (eje de ordenadas, $1 / v$). Al representar las pendientes y los interceptos resultantes frente a la concentración de efector, se obtuvieron nuevas hipérbolas; por tanto, fue necesario aplicar de nuevo un método diferencial para hacer lineales las curvas obtenidas (Fig. 6.2*b* y *c*). Los inversos tanto de Δ *interceptos* como de Δ *pendientes* fueron representados en un diagrama secundario frente al inverso de la concentración del efector (eje de abscisas). Δ indica la diferencia entre los valores obtenidos para una concentración de efector dada y los valores obtenidos en ausencia de efector. El parámetro cinético β, ya sea para la inhibición (β_i) o para la activación (β_a), se calculó del intercepto en el eje de ordenadas del gráfico secundario $1 / \Delta$ *interceptos*, a partir de la siguiente igualdad:

$$\beta_i = \frac{Intercepto}{V_{max} \;+\; Intercepto} \qquad \beta_a = \frac{Intercepto}{Intercepto \;-\; V_{max}} \qquad \text{(II.10)}$$

y el parámetro α, ya sea para la inhibición (α_i) o para la activación (α_a), se determinó del intercepto en el eje de ordenadas del gráfico secundario $1 / \Delta$ *pendientes*

$$\alpha_i = \frac{\beta_i\,V_{max}}{K_{Glu}\;Intercepto} \;+\; \beta_i \qquad \alpha_a = \beta_a \;-\; \frac{\beta_a\,V_{max}}{K_{Glu}\;Intercepto} \qquad \text{(II.11)}$$

V_{max} y K_{Glu} se obtuvieron de los interceptos en los ejes de ordenadas y abscisas, respectivamente, en la línea control del diagrama primario (es decir,

en ausencia de efector). Conociendo α y β se pueden deducir las K_i y K_a correspondientes a las representaciones $\Delta\,interceptos$ y $\Delta\,pendientes$, mediante la ecuación

$$K_\mathrm{i} = \frac{\beta_\mathrm{i}\, Pendiente}{\alpha_\mathrm{i}\, Intercepto} \qquad K_\mathrm{a} = \frac{\beta_\mathrm{a}\, Pendiente}{\alpha_\mathrm{a}\, Intercepto} \tag{II.12}$$

II.8 Niveles intracelulares de metabolitos

En los *Capítulos* 5 y 6 se determinaron ciertos metabolitos involucrados en la reacción de la enzima glutamato deshidrogenasa (GDH):

(i) Glutamato. La concentración del glutamato libre en el interior celular se analizó de acuerdo con el protocolo de Hans-Otto y Michal (1974), que utiliza diaforasa, sales de tetrazolio y GDH purificada (EC 1.4.1.3) para desaminar el glutamato disponible en la muestra. El NADH resultante dona sus electrones al INT, generando formazán. La absorbancia de esta última molécula es medida espectrofotométricamente, y relacionada con la concentración de glutamato ([Glu]) mediante la siguiente ecuación:

$$[\mathrm{Glu}]\ (\mathrm{mg\ mL^{-1}}) = \frac{V \times MW_\mathrm{Glu}}{\varepsilon \times l \times v \times 1000} \times \Delta\, Glu \tag{II.13}$$

donde V es el volumen total de la reacción, MW_Glu es el peso molecular del glutamato, ε es el coeficiente de extinción del INT, l es el ancho de la cubeta, y v es el volúmen de homogeneizado añadido a la reacción. $\Delta\, Glu$ representa la diferencia entre la absorbancia medida antes de añadir un volumen de GDH a la mezcla de reacción, y la absorbancia registrada una vez finalizada la reacción. Ambas absorbancias se corrigieron utilizando como blanco las medidas realizadas sobre una muestra control, que contenía agua Milli-Q en lugar de una alícuota de homogeneizado.

(ii) Piridín nucleótido: $\mathbf{NAD^+}$. Los niveles intracelulares de NAD^+ se determinaron mediante una serie de reacciones enzimáticas acopladas entre sí, tal y como detallan Wagner y Scott (1994). Las formas oxidadas (NAD^+) y las formas reducidas (NADH) se diferenciaron mediante la aplicación de calor, de manera que sesiones de 30 min a 60 °C destruirían las formas oxidadas sin afectar las reducidas. Así, la diferencia entre el contenido total de piridín nubleótidos (NAD_t) y sus formas reducidas resultaría en los niveles intracelulares

de NAD^+. Un volumen del extracto (100 μL), sometido o no al proceso de calentamiento, se añadió a 800 μL de tampón de reacción (100 mM Tris-HCl con 1 % de albúmina, pH = 8.0). El tampón de reacción se preparaba fresco para cada tanda experimental y se mantenía en frío durante todo el proceso. Este sistema tampón utilizaba 0.2 mg mL^{-1} de la enzima alcohol deshidrogenasa (ADH) y una reacción no enzimática que acoplaba la producción de las formas oxidadas y reducidas en presencia de etanol (100 μL) y 1 mM de etosulfato de fenazina (PES). Este PES reducía 0.5 mM de azul de tiazolil (MTT) a su formazán en otra reacción no enzimática. La producción de MTT-formazán se monitorizó espectrofotométricamente a una longitud de onda de 570 nm, durante 3 min a una temperatura constante de 37 °C.

(iii) Nucleótidos fosfato: ADP y GTP. La determinación de ambos metabolitos se realizó en un sistema cromatográfico Varian Prostar (Varian Inc., España), que constaba de una bomba, un autoanalizador y un módulo de columna de válvulas con un horno interno y un detector de fotodiodos en serie que trabajaba a 254 nm. Los metabolitos ADP y GTP se separaron en una columna PRP-1 (5 μm, 2.1 × 150 mm –Hamilton, USA–) a una temperatura de 50 °C. La fase móvil *A* estaba compuesta por 100 mM de fosfato monopotasio (pH = 7, ajustado con hidróxido de potasio), 1 mM de fosfato de tetrabutilamonio y 2.5 % de metanol. La fase móvil *B* la constituyeron el eluyente A y 20 % de metanol. La elución se llevó a cabo con un gradiente que consistía en 1 % de la fase móvil *B*, mantenida a dicha concentración durante 3 min, y aumentada gradualmente hasta el 15 % durante los 10 min siguientes, hasta el 55 % en 15 min, hasta el 95 % en 16 min y hasta el 99 % en 20 min. A los 25 min el gradiente retornó al 1 % de la fase móvil *B* y se mantuvo durante 5 min para equilibrar la columna de cara a la siguiente inyección. El flujo se estableció en 0.3 mL min^{-1}, y el volumen de inyección fue de 10 μL.

Las soluciones madre de cada compuesto (en ambos casos, 1.42 mM) se prepararon disolviendo la cantidad apropiada del producto comercial en la fase móvil, y almacenaron en botellas de cristal a 4 °C. La concentración de los componentes se determinó mediante curvas de calibrado que oscilaban entre 0.01 y 50 μM. Los coeficientes de correlación fueron, en todos los casos, iguales o superiores a 0.992. Los límites de cuantificación (*LOQ*s) se calcularon como la concentración en la que la relación entre la señal y el ruido debido al propio aparato era igual o mayor a 10, siendo 0.0005 μM para el GTP y 0.002

μM para el ADP. Con el fin de evaluar la precisión, expresada como la desviación estándar relativa (*% RSD*), se analizaron 6 réplicas de las muestras a dos niveles de concentración distintos (0.1 y 10 μM). Los valores de repetibilidad fueron menores a 9 % en ambos casos.

III Principales resultados y discusión

III.1 Distribución de la biomasa y las actividades metabólicas potenciales del zooplancton en el norte del sistema de afloramiento de Benguela

El *Capítulo* 2 caracteriza la forma en que los procesos físicos afectan la biomasa del zooplancton en las aguas del norte de Benguela, así como el impacto que la respiración y la excreción de NH_4^+ de estos organismos ejercen sobre la productividad primaria. Además, se analiza la composición elemental del zooplancton y sus isótopos estables con el fin de inferir cambios en la cadena trófica de este ecosistema pelágico. El plan de muestreo utilizó un enfoque Euleriano, de manera que se muestreó un transecto perpendicular a costa en cuatro ocasiones consecutivas. Este hecho permitió monitorizar la estructura y funcionamiento de una comunidad planctónica que era afectada por la irrupción de remolinos y filamentos. Estas estructuras físicas modificaron el típico patrón de maduración de las aguas, según el cual, éstas envejecen conforme se alejan de la costa. Del mismo modo, las estructuras mesoescalares afectarían a los procesos de sucesión de las poblaciones planctónicas. En este escenario, la investigación ilustra las dinámicas de la biomasa y el metabolismo potencial de la comunidad zooplanctónica, conforme se sucedían distintas situaciones oceanográficas en el norte de Benguela.

(i) Biomasa del zooplancton y estructura de la comunidad. Las condiciones hidrográficas encontradas a lo largo de la campaña se han descrito detalladamente en Mohrholz et al. (2014). Así, se encontraron distintas masas de agua ocupando el área de estudio, correspondiéndose, según sus características físico-químicas, con masas de Agua Central Suratlántica (SACW) y Agua Central del Atlántico Sudeste (ESACW). Por otro lado, un filamento rico en nutrientes procedente del centro del afloramiento se extendió a lo largo del transecto durante la primera mitad de la campaña. Una disposición similar de masas de agua ya fue descrita previamente en la misma región por Boyd et al.

(1987). Así, la productividad primaria se vió estrechamente relacionada con la presencia de aguas frías cargadas de nutrientes, de manera que el pico máximo de clorofila se encontró a comienzos de septiembre coincidiendo con la irrupción del filamento. En general, el transecto se dividió en distintas zonas con respecto a la costa, en función de las características hidrográficas dominantes en cada una de ellas (ver Fig. 2.1): las estaciones costeras (NAM001 - NAM004) estaban dominadas por la divergencia generada por el transporte de Ekman, que favorecía el afloramiento de agua profunda cerca de la costa, rica en nutrientes pero con poco plancton asociado; la zona de transición (NAM005 - NAM011), situada sobre el borde entre la plataforma continental y el talud, estaba influenciada tanto por el filamento maduro procedente de la costa, como por un afloramiento debido al efecto del viento (cuya velocidad máxima vertical ascendió a 0.35 m d^{-1}); las estaciones oceánicas (NAM014 - NAM027), caracterizadas por la presencia mayoritaria de aguas más cálidas y envejecidas. La selección de estos límites espaciales se vió reforzada por un análisis de agrupamiento que consideraba las propiedades físicas y químicas de cada estación (ver *Apéndice*, Fig. A.1).

Los biomasa del zooplancton varió temporal y espacialmente a lo largo del transecto en estrecha relación con los patrones mesoescalares (Fig. 2.2). Así, aguas maduras ricas en nutrientes ocuparon gran parte de la zona de estudio a finales de agosto, favoreciendo el crecimiento del fitoplancton (Hansen et al., 2014) y posteriormente, del zooplancton, tal y como predice el modelo de Vinogradov et al. (1972). Los picos de zooplancton se encontraron en esta época, coincidiendo con la máxima productividad primaria, incluso en estaciones oceánicas como la NAM017 (Hansen et al., 2014). Este escenario fue debido a la fuerte influencia del filamento que se extendía desde la costa. Después, el filamento se dispersó hacia el noroeste, y como consecuencia, descendió la concentración de fitoplancton y zooplancton en el área de estudio. En general, la biomasa del zooplancton alcanzó su valor máximo a 90 km de costa, en la estación NAM009 (Fig. 2.4). El valor promedio registrado en la capa superficial de la columna de agua en esta estación fue de 81 mg DM m^{-3}. Como era de esperar, este pico se encontró ligeramente desplazado lejos de costa con respecto al máximo de clorofila. La concentración de zooplancton disminuyó en aguas oceánicas hasta un mínimo de 3 mg DM m^{-3}. Cabe destacar la presencia de un inesperado pico de zooplancton que se encontró a 380 km de costa, compuesto principalmente por zooplancton de gran

tamaño (> 1000 μm). La extraordinaria concentración de zooplancton en esta región (70 mg DM m^{-3}) podría explicarse por la intrusión de aguas SACW (ver Fig. 6*e* en Mohrholz et al., 2014). Estas aguas maduras transportarían una población zooplanctónica que, debido a procesos de sucesión específica, estaba dominada por zooplancton predador en un ambiente de baja productividad primaria (*sensu* Vinogradov y Shushkina, 1978). En general, la magnitud de la biomasa zooplanctónica que se cuantificó durante el invierno austral (agosto - septiembre, 2011), es comparable con que se registró en el estudio realizado en 1979 a lo largo del mismo transecto (campaña SWA, Fig. 2.4 –ver Postel, 1995, para más información–). En cambio, los valores promedio de biomasa zooplanctónica que se encontraron en la plataforma continental durante periodos de quiescencia fueron significativamente menores (Verheye y Hutchings, 1988; Olivar y Barangé, 1990). Estas últimas investigaciones se llevaron a cabo durante el otoño austral, cuando el afloramiento es más débil, resultando en una concentración de zooplancton cercana a 26 mg DM m^{-3}. Este valor se encuentra en el rango medido en otros sistemas de afloramiento menos productivos (Hernández-León et al., 2002; Bode et al., 2005).

La estrecha relación espacial que existió entre el zooplancton y las diatomeas (Fig. 2.11) sugiere un control desde la base de la cadena trófica, tal y como se espera en sistemas tan productivos (Cury y Shannon, 2004). La predominancia de cadenas de diatomeas en la región de transición pudo suponer, sin embargo, una limitación para el microzooplancton (100 - 200 μm), cuya dieta consiste principalmente en células individuales y pequeños microheterótrofos (Irigoien, 2005). Así, la contribución del pequeño zooplancton a la biomasa total fue menor en la zona de transición. Desafortunadamente, la baja resolución taxonómica de la que dispone este estudio limita la discusión acerca de cómo los factores físicos y biológicos determinaron la composición de la comunidad zooplanctónica. En general, los copépodos ciclopoides dominaron la fracción de tamaño más pequeña (100 - 500 μm) a lo largo de todo el transecto (ver Fig. 2.5*a*). En las estaciones costeras, la abundancia relativa de larvas meroplanctónicas (ofiuroideos) fue también alta (~ 30 %). Éstas decrecieron conforme aumentaba la distancia a costa, mientras tomaban importancia otros grupos tales como los copépodos calanoides, los copépodos harpacticoides y los tintínidos. La variabilidad taxonómica fue mayor en la fracción superior a 500 μm (Fig 2.5*b*). Los taliáceos predominaron en el borde de la plataforma continental, mientras que los copépodos calanoides fueron más importantes

en las regiones costera y oceánica. La prevalencia numérica de los copépodos coincide con las observaciones de Timonin (1997) y Loick et al. (2005), si bien estos autores, a diferencia de lo descrito en este estudio, encontraron las mayores abundancias de los copépodos en zonas más oceánicas debido a la advección generada por el transporte de Ekman. De hecho, este efecto junto con las células costeras generadas por el afloramiento, podrían explicar la presencia de zooplancton típico de aguas neríticas como los quetognatos (Gibbons et al., 1992), los tintínidos (Dolan et al., 2012) y los harpacticoides bentónicos que se observaron en estaciones oceánicas. Por tanto, factores tales como la competición biológica estarían controlando la población de copépodos. En condiciones de una gran disponibilidad de alimento, las salpas aprovechan sus altas tasas de filtración y rápido crecimiento (Ikeda, 1977), de manera que podrían haber excluido fácilmente altas densidades de otros grupos de zooplancton en la parte externa de la plataforma continental.

(ii) Composición elemental y análisis de isótopos estables en el zooplancton. En cuanto a la composición elemental, la relación entre el carbono orgánico y el peso seco (DM) del zooplancton varió entre 0.11 y 0.33, mientras que la proteína y el DM se relacionaron por un factor de 0.18 ± 0.05. Por otro lado, el contenido de nitrógeno orgánico consituyó el 36 % de la proteína (ver Tabla 2.1). Estas relaciones son comparables con las publicadas por Bode et al. (1998) para el afloramiento del noroeste de España. Por el contrario, el contenido de carbono orgánico con respecto al peso seco fue relativamente bajo si se compara con los valores encontrados en las zonas polares (23.5 - 61.0 % en Ikeda y Skjoldal, 1989). Esto sugiere una menor presencia de lípidos en el zooplancton de Benguela, típico de ecosistemas que presentan una continua disponibilidad de alimento, donde las reservas metabólicas principales son las proteínas (Postel et al., 2000). La relación atómica C/N osciló entre 4.2 y 6.4 (Fig. 2.7), cuyos valores fueron significativamente mayores en la zona de transición (ANOVA de una vía, $F_{2,210} = 11.16$, $p < 0.0001$; post hoc HSD de Tukey, $p < 0.0001$). Este incremento podría explicarse por un cambio en la dieta que, unido a menores tasas específicas de actividades de la GDH, resultaría en tasas de excreción de NH_4^+ más bajas. De forma general, las tallas más pequeñas (100 - 500 μm) presentaron relaciones superiores a 5.2, mientras que su valor fue inferior en los organismos más grandes. En cualquier caso, el rango de los valores C/N coincidió con los valores encontrados en distintos grupos de me-

sozooplancton del norte de Benguela (Schukat et al., 2014), y en los crustáceos marinos en general (Bode et al., 1998).

El estudio de los isótopos estables facilita una mayor compresión de los procesos ecológicos que tienen lugar en la columna de agua. Los valores de δ^{13}C del zooplancton (que oscilaron entre −21.3 y −18.9 ‰) revelaron una variabilidad en la fuente de carbono a lo largo del transecto. Los valores más negativos de δ^{13}C se encontraron en las estaciones costeras (test Kruskal-Wallis, $p < 0.005$), probablemente como consecuencia de una mayor predación sobre organismos pobres en lípidos tales como los dinoflagelados (Saupe et al., 1989). Una alimentación compuesta principalmente por diatomeas, que están enriquecidas en ^{13}C en comparación con los pequeños flagelados (Fry y Wainright, 1991), pudo dar lugar a valores más altos de δ^{13}C en las aguas de transición. En el caso del δ^{15}N asociado al zooplancton, se observó un pronunciado descenso de 11.0 a 4.8 ‰ en los primeros 100 km (test Kruskal-Wallis, $p < 0.0001$). Este patrón se repitió en todas las tallas de zooplancton, lo que sugiere que el origen de la variabilidad espacial en las señales de δ^{15}N radicaría en la fuente de nitrógeno que estaba siendo utilizada por el fitoplancton, y no en los procesos de sucesión específica. Así, conforme el nitrato aflorado cerca de la costa (enriquecido en ^{15}N por procesos de remineralización bacteriana en aguas profundas) era utilizado en superficie por los productores primarios, éstos se irían enriqueciendo en ^{15}N (O'Reilly et al., 2002; Bode and Álvarez-Ossorio, 2004). Lejos de costa, otras especies nitrogenadas empobrecidas en ^{15}N, como el N_2 fijado por los diazotrofos o el NH_4^+ excretado por heterótrofos, sustentarían la productividad primaria. En estas aguas oceánicas, por tanto, se propagarían unas señales más bajas de δ^{15}N al resto de componentes de la cadena trófica. Por otro lado, la variabilidad en las señales de δ^{15}N también podría explicarse por diferencias en el número de niveles tróficos intermedios que conectan la transferencia de materia a lo largo de la cadena alimentaria. Lamentablemente, sería necesario disponer de los valores de referencia de δ^{15}N del fitoplancton para poder confirmarlo.

(iii) Metabolismo del zooplancton. A la hora de comprender el balance de carbono en un ecosistema, es esencial conocer si los heterótrofos consumen toda la productividad primaria o si, por el contrario, hay un exceso de carbono fijado que es exportado a las profundidades (Ducklow y Doney, 2013). Esto depende del nivel de productividad primaria que está limitado, entre otros

factores, por la disponibilidad de nitrógeno. En este escenario, el zooplancton ejerce un impacto directo sobre los ciclos de carbono y nitrógeno. Su papel será más o menos importante según cual sea el ecosistema, el periodo del año y la composición taxonómica de la comunidad. En este estudio, las mayores actividades metabólicas del zooplancton se registraron a finales de agosto (es decir, durante los transectos 1 y 2), coincidiendo con el patrón descrito para la biomasa. Durante este periodo, las actividades del ETS y de la GDH fueron casi 2 veces superiores a las encontradas a mediados de septiembre (transecto 4). Asimismo, se encontraron importantes diferencias con respecto a la distancia a costa. Ambas tasas presentaron sus valores máximos durante los dos primeros transectos, entre las estaciones NAM007 y NAM011 (Fig. 2.9). Durante el mes de septiembre, conforme el filamento se dispersaba, los picos metabólicos se acercaron a la costa. En general, la contribución de la talla más pequeña del zooplancton fue mayor en las aguas costeras (ANOVA de una vía, $F_{1,51} = 26.42$, $p < 0.0001$), mientras que las tasas metabólicas en las aguas de transición estuvieron dominadas principalmente por el zooplancton de mayor tamaño. Los valores promedio de respiración y excreción de NH_4^+ para toda la comunidad de mesozooplancton fueron de 112.4 μmol O_2 m^{-3} d^{-1} y 10.3 μmol NH_4^+ m^{-3} d^{-1}, superando las tasas de respiración y excreción de NH_4^+ encontradas en aguas de plataforma de otros sistemas de afloramiento (Packard et al., 1974; Hernández-León et al., 2002; Isla y Anadón, 2004; Pérez-Aragón et al., 2011). A pesar de las altas tasas metabólicas registradas en este estudio, si se comparan con la productividad primaria, los valores relativos para ambos procesos fueron similares a los medidos en el afloramiento del Atlántico Noroeste (Packard, 1979) y de Benguela (Chapman et al., 1994).

El carbono consumido por los procesos de respiración del mesozooplancton (cuyas tasas variaron de 0.73 a 16.90 mmol C m^{-2} d^{-1} en los 75 m superficiales) osciló entre 1.1 - 10.6 % del carbono que estaba siendo fijado por los productores primarios (Tabla 2.3). El rango de estos porcentajes fue más amplio en las aguas de transición. En promedio, la demanda respiratoria de carbono para todo el transecto fue igual a 7.1 ± 4.7 mmol C m^{-2} d^{-1}. De acuerdo con Ikeda y Motoda (1978), la tasa de ingestión se calcula aplicando a la respiración un factor de 2.5. Esto significa que el mesozooplancton retira entre 6.0 y 29.5 mmol C m^{-2} d^{-1} en los 75 m superficiales de la columna de agua, es decir, ∼ 14 % de la producción diaria si se asume una mayoritaria herviboría y una eficiencia de asimilación del 70 % (Kiørboe et al., 1985). Aunque

Hernández-León e Ikeda (2005) estimaron una demanda de carbono por parte del mesozooplancton que oscila entre 34 y 63 % de la productividad primaria global, el porcentaje decae considerablemente cuando se trata de ecosistemas eutróficos (Calbet, 2001). Considerando estudios paralelos con bacterias, cuyo consumo fue cercano al 29 % de lo que se producía (Bergen et al., 2015), y las estimas de Chapman et al. (1994) en el norte de Benguela, que sugieren una pérdida de carbono debido al microzooplancton del 28 %, parece razonable asumir que este sistema es autotrófico durante la época de máximo afloramiento. Es decir, hay un exceso de productividad primaria que es transportada por el filamento, o bien exportada por debajo de 75 m. De forma similar, la contribución de la excreción de NH_4^+ (media global = 0.97 mmol NH_4^+ m^{-2} d^{-1}) no superó el 5 % de los requerimientos del fitoplancton (Tabla 2.3). Este porcentaje se mantuvo relativamente constate independientemente de la productividad del sistema, si bien el zooplancton contribuyó ligeramente más a las demandas del fitoplancton en aguas oceánicas. Estos resultados revelan un papel secundario del zooplancton en la regeneración de NH_4^+ en el sistema de Benguela. Conclusiones similares se han descrito para el zooplancton residente en otros sistemas de afloramiento (Bode et al., 2004; Isla et al., 2004a). Así, el NH_4^+ disuelto mostró una baja correlación con la distribución del mesozooplancton (Fig. 2.11), si bien es necesario tener precaución con la interpretación de estos resultados, ya que el NH_4^+ que está disponible es rápidamente incorporado por el fitoplancton. De hecho, el nitrógeno (Benavides et al., 2014) y el fósforo (Nausch y Nausch, 2014) remineralizados fueron necesarios para sustentar una parte importante del fitoplancton. Esto podría deberse a un importante reciclaje de nutrientes a través de los pequeños microheterótrofos, tal y como Probyn (1987) encontró en el sur de Benguela.

Desde un punto de vista fisiológico, los índices metabólicos no siguieron el mismo patrón de la clorofila-a. Mientras que la productividad primaria decreció en las aguas más envejecidas, probablemente debido a la presión del pastaje y al agotamiento de los nutrientes, los valores de ETS por unidad de proteína fueron relativamente invariables incluso en las aguas oceánicas (Tabla 2.2). El ligero descenso encontrado en la zona de transición se explica por la presencia de grandes densidades de salpas (Fig. 2.5*b*), cuyo metabolismo específico es menor si se compara con otros grupos de zooplancton. Por otro lado, unos ciclos de vida más largos hacen que el zooplancton se encuentre más expuesto que el fitoplancton a procesos de advección y transporte activo

hacia zonas más alejadas de costa. Durante este proceso, la dieta del zooplancton tiende a la omnivoría (Hernández-León et al., 2002), lo que sustentaría un metabolismo activo incluso en la región oceánica. De hecho, el aumento de la carnivoría pudo explicar una reducción de la biomasa y un metabolismo más proteico, tal y como denotan unos valores $R_{O_2}/R_{NH_4^+}$ más bajos. Por el contrario, las actividades específicas de la GDH se redujeron en las aguas productivas de la zona de transición. Este hecho concuerda con los resultados descritos por Hernández-León et al. (2001) en aguas de Canarias. Estos autores observaron correlaciones negativas de las actividades de la GDH con respecto al contenido estomacal y las concentraciones de clorofila-a. De hecho, las actividades de la GDH no sólo dependen de la disponibilidad intracelular de sustratos, sino también de la carga energética de los organismos. Conforme aumentan los niveles de guanosín-5'-trifosfato (GTP) en respuesta a un estado metabólico saludable, la GDH sería inhibida, y en lugar de utilizarse en procesos de desaminación, el glutamato se destinaría para el crecimiento y la biosíntesis de proteínas (Bidigare y King, 1981). Independientemente de estos ajustes bioquímicos, ambos índices enzimáticos mostraron una buena correlación con el contenido proteico (en ambos casos $p < 0.0001$, Fig. 2.10), lo que refleja su naturaleza constitutiva como un componente permanente de las células vivas. Los exponentes escalares (b) de las enzimas ETS y GDH fueron igual a 1.04 y 0.88, respectivamente, mostrando una relación casi isométrica con la biomasa. Sin embargo, cambios en la disponibilidad de alimento provocarían una divergencia entre ambos exponentes. Esto repercutiría en las relaciones R_{O_2}/ETS y GDH/$R_{NH_4^+}$ (Berges et al., 1993; Fernández-Urruzola et al., 2011), aunque su influencia no sería lo suficientemente importante como para impedir el uso de estas enzimas como índices ecológicos.

III.2 **Modelaje del flujo vertical de nitrógeno particulado a partir de la regeneración de amonio en el norte de Benguela**

En el *Capítulo* 3 se calcula el flujo de nitrógeno (F_N) a partir de perfiles verticales de excreción de NH_4^+ ($R_{NH_4^+}$) del nano/micro- y mesozooplancton, y se comparan estos flujos modelados con los flujos gravitacionales medidos con trampas de sedimento en dos estaciones del norte de Benguela. El modelo que se propone para calcular el F_N vertical, permite determinar la variabilidad espacial de estos flujos a una tasa relativamente alta en comparación con otros métodos utilizados para estimar otras variables biogeoquímicas, y permite cal-

cular ciertos parámetros relacionados con el reciclaje de nutrientes. Así, cambios en la atenuación del flujo, es decir, en la curvatura del perfil, afectan a la capacidad del ecosistema para retener sus nutrientes (Packard et al., 2015) y como consecuencia, a la producción regenerada. Además, se estudia la importancia del flujo activo con respecto al flujo gravitacional de nitrógeno orgánico particulado (PON).

(i) Cálculo del F_N vertical a partir de medidas de $R_{NH_4^+}$. Un modelo de una sola dimensión, como el que aquí se propone, lleva asociadas una serie de asunciones y limitaciones. Sin embargo, ninguna invalida por sí misma todo el concepto. A pesar de que la advección lateral es relativamente importante en los sistemas de afloramiento (Alonso-González et al., 2009), las dinámicas verticales dominan sobre las horizontales, dado que cada una opera a una escala diferente (desde unos cientos de metros hasta varios km, respectivamente). Además, la velocidad del agua advectada durante la campaña oceanográfica fue de ~ 0.06 m s^{-1}, mientras que la velocidad de corrientes en la banda inercial osciló entre 0.02 - 0.06 m s^{-1} (Mohrholz et al., 2014). Estas velocidades generan una pequeña dispersión de las partículas, lo que les permite alcanzar el lecho marino cerca del lugar que ocupaban en la superficie. En esta situación, Jaeger et al. (1996) demostraron la validez de un modelo unidimensional, capaz de predecir la acumulación de partículas en el Mar de Ross. Por otro lado, las estimas del F_N deben considerarse como medidas conservadoras, ya que no todo el PON es necesariamente transformado en DIN mediante el metabolismo del zooplancton. En cualquier caso, el NH_4^+ es el principal producto nitrogenado que resulta de la excreción del microzooplancton (Caron y Goldman, 1990) y del mesozooplancton (Bidigare, 1983; Ikeda et al., 2000), y a menudo supone más del 70 % del nitrógeno inorgánico liberado al medio. La proporción de nitrógeno orgánico disuelto (DON) que se libera con respecto al NH_4^+ depende de la calidad y la cantidad del alimento consumido (Miller y Roman, 2008), así como de los taxones involucrados (Steinberg y Saba, 2008). Pero, en general, la excreción de DON que no es considerada por el modelo supondría un impacto inferior al 32 % (Steinberg et al., 2002). En cualquier caso, este mismo porcentaje debería aplicarse a la gran mayoría de estudios oceanográficos que a menudo obvian la contribución de la fracción de DON al flujo total (e.g., Dam et al., 1995; Longhurst y Harrison, 1988, 1989).

Los datos hidrológicos registrados durante la campaña, revelaron un patrón

irregular en la distribución de las masas de agua, en lugar del típico escenario en el que un flujo continuo de agua recién aflorada se dirige hacia el océano abierto. La interacción de las estructuras mesoscalares indujeron cambios abruptos en la biomasa de fitoplancton (Hansen et al., 2014) y del zooplancton (Fernández-Urruzola et al., 2014), evitando un patrón homogeneo de sucesión conforme las aguas envejecían. Los máximos de clorofila-a se registraron durante los dos primeros transectos; a mediados de septiembre, sus valores disminuyeron casi tres veces (Fig. 3.2*a*). Sin embargo, este descenso en la concentración de clorofila-a, no se tradujo en un descenso en la abundancia de las células fitoplanctónicas (Hansen et al., 2014), lo que sugiere una transición desde células más grandes (diatomeas) hasta células más pequeñas (nanoflagelados y cocolitofóridos). El momento del muestreo fue, por tanto, más determinante para explicar las condiciones oceanográficas en una estación dada, que la propia distancia a costa. Por otro lado, las dinámicas de los factores físicos y de la productividad primaria se reflejaron en la variabilidad de la zona eufótica (E_z), que fue más profunda durante el transecto 4, debido a una menor concentración de plancton en unas aguas más envejecidas. En todos los casos, la E_z constituyó el límite superior para el cálculo de los flujos verticales de nitrógeno. Los cambios en las dinámicas físicas y biológicas a lo largo de la capa de mezcla determinaron, por tanto, el patrón de transferencia vertical de las partículas.

La $R_{NH_4^+}$ en el nano/micro- y mesozooplancton fue máxima en los 50 m superficiales (Fig. 3.3). Debido a la similitud en las condiciones oceanográficas, los perfiles de $R_{NH_4^+}$ para el nano/microzooplancton fueron semejantes entre las estaciones NAM006 y NAM011d. En cambio, la $R_{NH_4^+}$ disminuyó desde 53.2 μmol NH_4^+ m^{-3} d^{-1} hasta 29.6 μmol NH_4^+ m^{-3} d^{-1} en la capa superficial de la estación NAM011r. Sorprendentemente, el comportamiento del mesozooplancton fue el inverso: el valor de $R_{NH_4^+}$ aumentó desde 26.7 NH_4^+ m^{-3} d^{-1} hasta un máximo de 49.3 NH_4^+ m^{-3} d^{-1} en la estación NAM011r, coincidiendo con un descenso en la concentración de clorofila-a (Fig 3.2*b*). Es necesario considerar que el aumento de $R_{NH_4^+}$ en la NAM011r se debió principalmente al NH_4^+ excretado por el zooplancton de mayor tamaño (> 1000 μm, Fig. 3.3). Este patrón encaja dentro del esquema general de la sucesión planctónica (Vinogradov et al., 1972), donde la comunidad se encontraría dominada por el zooplancton de mayor tamaño, salpas en este caso, en un estadío de sucesión tardío. El mismo comportamiento se ha descrito en otros sistemas de aflora-

miento, en los que la contribución del mesozooplancton a la regeneración total de NH_4^+ era más relevante en las situaciones de baja productividad (Bode et al., 2004). En cualquier caso, el nano/microzooplancton regeneró más NH_4^+ en la columna de agua que el mesozooplancton, cuyo papel en la regeneración de amonio en las aguas de Benguela pareció ser limitado (Fernández-Urruzola et al., 2014). Estos resultados coinciden con la mayoría de estimas realizadas a lo largo de distintos sistemas oceánicos, que otorgan al nano/microzooplancton un papel fundamental en la regeneracion de NH_4^+ (Bronk y Steinberg, 2008). En esta misma línea, Probyn (1987) concluyó que tanto los protozoos como los nanoflagelados eran cruciales en el reciclaje de nutrientes en aguas del sur de Benguela.

En todos los casos, los perfiles verticales de $R_{NH_4^+}$ se ajustaron a una función potencial. Estas funciones no sólo coincidieron con las utilizadas en estudios similares, sino que explicaron de forma significativa los valores medidos en la columna de agua. En la ecuación propuesta, el exponente *b* determina el descenso de $R_{NH_4^+}$ conforme aumenta la profundidad. Los valores *b* más negativos se encontraron en los perfiles del mesozooplancton, lo que significa que la $R_{NH_4^+}$ asociada a estos organismos decrecía de forma más notable en la superficie. La precisión de los modelos fue verificada mediante la comparación de los valores de $R_{NH_4^+}$ predichos, con los valores de $R_{NH_4^+}$ medidos en la misma profundidad (Tabla 3.1). Por lo general, ambos valores se correlacionaron de manera significativa. Los flujos de nitrógeno (F_N) fueron entonces calculados integrando estos modelos de $R_{NH_4^+}$ desde cualquier profundidad por debajo de la E_z hasta el fondo oceánico (Fig. 3.4). De nuevo, se ajustó una función a los valores obtenidos, siendo el modelo logarítmico el que mejor explicaba el perfil. Los F_N siguieron un patrón similar en las estaciones NAM011d y NAM011r, a pesar de que la E_z era mucho más profunda en esta última estación. Así, el PON requerido por debajo de la E_z varió entre 6.59 mmol N m^{-2} d^{-1} en la estación NAM011d y 5.47 mmol N m^{-2} d^{-1}, 10 días más tarde, en la NAM011r. De manera similar, 5.46 mmol N m^{-2} d^{-1} fueron regenerados en la columna de agua de la estación NAM006. Estos valores representan el PON necesario para sustentar los procesos de excreción de NH_4^+ por debajo de 150 m y 320 m en las estaciones NAM006 y NAM011, respectivamente. Los valores modelados fueron comparados con el flujo gravitacional medido con trampas de sedimento (Fig. 3.5). Debido a que los perfiles verticales constituyen medidas puntuales en el tiempo, la comparación con las tasas de sedimentación

se realizó en base al régimen de productividad. Así, una alta productividad estaría determinada por la floración de diatomeas, cuyo tamaño y capacidad para formar cadenas darían lugar a una rápida sedimentación. En este escenario, se registraron tasas de sedimentación alrededor de 1.01 mmol N m^{-2} d^{-1} en la NAM006, y de 0.90 mmol N m^{-2} d^{-1} en la NAM011d. Estos valores no distaron significativamente de los estimados mediante los perfiles de $R_{NH_4^+}$ (*t*-Student, $p > 0.05$). En cambio, la estación NAM011r estaba dominada por cocolitofóridos, más pequeños que las diatomeas, que dieron lugar a una tasa de sedimentación menor. En este caso, la diferencia con el F_N aumentó hasta 5 veces. La discrepancia entre el flujo calculado a partir de modelos ecológicos y el flujo cuantificado mediante trampas de sedimento ha sido, precisamente, objeto de una gran controversia en el seno de la comunidad científica (Burd et al., 2010; Steinberg et al., 2008). Su origen radica en la base conceptual de cada método. Así, el F_N modelado provee una imagen instantánea de las interacciones biológicas que se están produciendo en la columna de agua. Las trampas de sedimento, en cambio, integran las partículas que están sedimentando durante un tiempo determinado, pero no ofrecen información de los procesos que afectan a la transformación de PON conforme sedimenta. Ambos enfoques se complementan entre sí, ya que las debilidades en uno son los puntos fuertes del otro. Por otro lado, debe considerarse que el PON que se modela a partir de medidas puntuales de $R_{NH_4^+}$ se depositan en las trampas de sedimento a distintas velocidades según cual sea el tamaño y la composición de las partículas (Alonso-González et al., 2010) y, por tanto, puede estar desacoplado con las medidas realizadas por las trampas. Por este motivo, la comparación entre los dos enfoques debe realizarse de acuerdo con el régimen de productividad y el carácter de las propias partículas. Así, agregados y partículas recalcitrantes de gran tamaño tendrían velocidades de sedimentación relativamente rápidas, que les permitiría alcanzar el lecho marino cerca de su origen en la superficie. Por el contrario, las células pequeñas más lábiles son propensas a la atenuación o a la advección (Alonso-González et al., 2010; Iversen y Ploug, 2010; McDonnell et al., 2015). Durante la campaña, las grandes diatomeas dominaron la comunidad planctónicas en el momento en que se muestrearon las estaciones NAM006 y NAM011d. Este hecho, combinado con una mayor concentración de material biogénico y litogénico, supondrían un efecto de lastre durante el periodo de mayor productividad (Osma et al., 2014). En este escenario, el F_N modelado y el registrado por las trampas de sedimento fueron similares. Con-

forme las aguas envejecían, la producividad se relajó, y la relación entre diatomeas y dinoflagelados disminuyó (Hansen et al., 2014). Una menor biomasa fitoplanctónica y una reducida carga litogénica, resultaron en una reducida formación de agregados, tal y como demuestran las observaciones microscópicas (Fig. 7*c* en Osma et al., 2014). Además, los productos fecales originados de una dieta basada en nanoflagelados, son más lábiles que los originados en una dieta basada en el consumo de diatomeas (Ploug et al., 2008). Todo en conjunto, reflejó un régimen de baja productividad durante el muestreo de la estación NAM011r, que podría explicar el desajuste en entre el F_N calculado y el nitrógeno depositado en las trampas. De hecho, estas partículas de baja sedimentación favorecen el metabolismo en la columna de agua (McDonnell et al., 2015), y al mismo tiempo, tienden a ser subestimadas por las trampas de sedimento (Trull et al., 2008). En cualquier caso, el PON sedimentado durante el periodo de baja productividad (0.15 mmol N m^{-2} d^{-1}) fue mayor que el medido por Giraudeau et al. (2000) frente a la costa de Walvis Bay, en una fase quiescente del afloramiento (0.06 ± 0.01 mmol N m^{-2} d^{-1}).

Los perfiles verticales de $R_{NH_4^+}$ se utilizaron, además, para representar una sección sinóptica de F_N perpendicular a la costa de Namibia (Fig. 3.6*a*). Esto no hubiera sido posible mediante el enfoque estacionario de las trampas de sedimento, cuya cobertura espacial es más reducida (tanto en el eje vertical como en el horizontal). Con el fin de considerar el mayor número de estaciones posible, los cálculos de F_N no tuvieron en cuenta el excedente de nitrógeno que se depositaba en el lecho marino, sino solo el nitrógeno necesario para sustentar los procesos de excreción de NH_4^+ del mesoozooplancton en la columna de agua. En cambio, las Fig. 3.6*b* y *c* sí consideran el excedente de nitrógeno que sedimenta en el lecho oceánico en aquellas estaciones cuyos perfiles de NH_4^+ presentan un exponente b más negativo que -1. Este hecho permite integrar la función hasta infinito, requisito imprescindible para este tipo de cálculos. La sección de F_N que representaba la primera parte de la campaña oceanográfica (28 - 02 sep.) mostró los valores máximos en la base de la E_z de las estaciones más oceánicas (~ 1.7 mmol m^{-2} d^{-1}). Después, estos picos se acercaron a costa, alcanzando valores cercanos a 2.1 mmol m^{-2} d^{-1} en la estación NAM006. En cualquier caso, la mayor parte del reciclaje del PON siempre ocurrió en la zona epipelágica. El uso que el mesozooplancton hizo del PON en las distintas capas de la columna de agua, se comparó en las Fig. 3.6*b* y *c*. El concepto de la eficiencia en la retención de nutrientes (NRE), introducido por Packard y

Gómez (2013), representa la relación entre la regeneración de nutrientes que tiene lugar en una capa dada y la cantidad de nutrientes que se han introducido en dicha capa. Este parámetro podría considerarse, en términos prácticos, como el inverso de la denominada eficiencia de transferencia (T_{eff}) propuesta por Buesseler et al. (2007). Esto significa que la NRE está inversamente relacionado con el F_{N}, de manera que una alto valor procedente de la relación entre la $R_{\text{NH}_4^+}$ y el F_{N}, resultaría en una alta NRE. Así, las medidas de NRE demostraron que las capas profundas fueron las más eficientes a la hora de regenerar el PON disponible (hasta el 36.7 % en las aguas batipelágicas de la estación NAM017). Por otro lado, la Fig. 3.6*b* representa el nitrógeno disponible por debajo de la E_z que estaba siendo retenido en cada capa mediante la transformación de PON en nitrógeno inorgánico disuelto (DIN). Las estimas de NRE indicaron que la mayor parte del PON era consumido en la zona epipelágica, y que la sedimentación en el lecho oceánico era más importante en las estaciones costeras. Esta deposición de partículas sería considerablemente menor si los cálculos incluyeran las tasas de remineralización asociadas al nano/microzooplancton. En general, el NRE está controlado por la forma que adquiere la $R_{\text{NH}_4^+}$ con respecto a la profundidad (Packard et al., 2015); si gráficamente se representa mediante una función potencial, como ocurre en este caso, la atenuación del flujo se define por el exponente *b*. Cuanto mayor sea el valor de *b* (en términos absolutos), mayor será la curvatura de la función y, por tanto, mayor sera el flujo atenuado en las capas superficiales. Por este motivo, el estudio de este parámetro reviste una especial relevancia a la hora de determinar la distribución de nutrientes en las columnas de agua de los distintos sistemas oceánicos (Marsay et al., 2015).

(ii) F_{N} activo debido al mesozooplancton migrador. Las ecuaciones de F_{N} propuestas en este trabajo también se utilizaron para determinar el flujo activo debido al zooplancton migrador. Este transporte activo constituye un importante componente del flujo de PON (Longhurst y Harrison, 1988), y frecuentemente se presenta en relación al flujo gravitacional para facilitar la comparación entre regiones. El flujo activo se ha estimado tradicionalmente a partir de la diferencia que existe entre la biomasa de zooplancton medida en la capa eufótica durante el día y la biomasa medida en la misma capa durante la noche (asumiendo que los migradores residen en la capa eufótica por la noche durante 12 h), a la que se multiplica la $R_{\text{NH}_4^+}$ específica (Dam et al., 1995). Aunque

conceptualmente es correcto, este procedimiento solo permite calcular el flujo activo en profundidades discretas, como por ejemplo, la correspondiente a la zona eufótica. En cambio, las ecuaciones que se aplican a lo largo de este estudio, integran los perfiles verticales de $R_{NH_4^+}$ diurnos y nocturnos para modelar el flujo activo en toda la columna de agua desde la base de la capa eufótica (Fig. 3.7). Las diferencias entre los valores diurnos y nocturnos del F_N se estudiaron en la estación NAM011, desde el 07 al 17 de septiembre (Tabla 3.2). Los muestreos correspondientes a la primera noche (7 sep.) y día (09 sep.) se correspondieron con un régimen de alta productividad (33.3 - 36.8 mmol N m^{-2} d^{-1}), dominado por diatomeas, y caracterizado por E_z más someras y picos de Chl-a superiores a 5 mg m^{-3}. Posteriormente, la productividad de las aguas cambió, dando como resultado unas condiciones más oligotróficas con valores de Chl-a inferiores a 2.5 mg m^{-3} durante los dos siguientes muestreos. Independientemente de la productividad, el momento del día pareció ser fundamental a la hora de explicar la distribución vertical del mesozooplancton en la estación NAM011. Así, la biomasa promedio de mesozooplancton fue ~ 3.5 veces superior durante la noche (0.93 g N m^{-2}) que durante el día (0.26 g N m^{-2}). La tasa específica de $R_{NH_4^+}$ osciló entre 0.08 - 0.31 mmol NH_4^+ g N^{-1} h^{-1} dependiendo de la estructura de la comunidad: a mayor presencia de zooplancton gelatinoso tales como salpas, menor sería la $R_{NH_4^+}$ específica. Los perfiles de $R_{NH_4^+}$ modelados mostraron, por tanto, los mayores valores durante la noche (32.3 - 35.1 μmol NH_4^+ m^{-3} d^{-1}, en la capa más superficial de la columna de agua –ver Tabla 3.2–). Estos valores máximos decrecieron durante las horas diurnas hasta 27.9 μmol NH_4^+ m^{-3} d^{-1}, y a menos de la mitad apenas 4 días después (14.2 μmol NH_4^+ m^{-3} d^{-1}). Como era de esperar, el F_N entre la base de la E_z y los 150 m de profundidad decreció mucho más abruptamente durante la noche que durante el día. El mesozooplancton necesitó así 1.58 mmol N m^{-2} d^{-1} para satisfacer sus demandas metabólicas durante la noche, mientras que solo fueron necesarios 0.57 mmol N m^{-2} d^{-1} durante el día. Esto significa que 1.01 mmol N m^{-2} d^{-1} fueron transportados activamente por el zooplancton migrador por debajo de 150 m (profundidad que presumiblemente contiene gran parte del zooplancton migrador durante la noche). Este flujo activo modelado (F_{N_M}) concordó significativamente (*t*-Student, $p > 0.05$) con los clásicos cálculos de flujo activo basados en las diferencias de biomasa entre el día y la noche (F_{N_B} = 0.91 mmol N m^{-2} d^{-1}). En la Fig. 3.6 se representan los F_N promedio durante el día y durante la noche. La diferencia entre ambos

fue significativa (*t*-Student, $p < 0.001$), siendo más aparente en la zona epipelágica. Es decir, el mesozooplancton consumía PON en la superficie durante la noche, y lo transportaba activamente a zonas más profundas durante el día. Así, el 4.7 % de la producción primaria neta (NPP) fue activamente transportado por debajo de 150 m (ver *e*-ratio, en la Tabla 3.2). La comparación del F_{N_M} (1.01 mmol N m^{-2} d^{-1}) con el flujo graviational a 150 m, demostró que el flujo activo de nitrógeno inorgánico supuso una parte importante del flujo gravitacional. Durante un régimen de alta productividad, cuando el flujo gravitacional de PON se estimó en 1.72 mmol N m^{-2} d^{-1}, el F_{N_M} supuso un 59 % del flujo gravitacional. Sin embargo, cuando partículas de menor tamaño dominaron la productividad primaria, el F_{N_M} potencial debido a los migradores verticales fue 3.6 veces superior (es decir, un 361 %) al flujo gravitacional (= 0.28 mmol N m^{-2} d^{-1}). Estos porcentajes se duplicaron al compararse con los valores obtenidos por las trampas de sedimento a 320 m. Los valores obtenidos en este trabajo engloban el porcentaje resultante de la relación entre el flujo respiratorio y el flujo gravitacional de POC (79 %) estimado por Schukat et al. (2013a) para los decápodos pelágicos en el Frente de Angola-Benguela. Por el contrario, la relación entre el flujo activo de NH_4^+ y el flujo gravitacional de PON descritos para las aguas oligotróficas de Bermuda (Dam et al., 1995; Steinberg et al., 2002) y Hawai (Al-Mutairi y Landry, 2001) fueron entre 3 y 5 veces menores a las relaciones encontradas en este estudio. Esta discrepancia no resulta sorprendente, ya que la biomasa de zooplancton migrador que medimos en el norte de Benguela fue varios órdenes de magnitud superior a la encontrada por estos autores en los giros oligotróficos. Por otro lado, es necesario considerar que las salpas dominaron la fracción migradora en la estación NAM011. Estos organismos oportunistas tienen la capacidad de crecer rápidamente si se encuentran en las condiciones apropiadas, y se caracterizan por ser unos migradores activos capaces de producir deshechos fecales enriquecidos en nitrógeno (Andersen, 1998), lo que les confiere un importante papel en el transporte de nitrógeno a las profundidades del océano (Wiebe et al., 1979). De hecho, $\sim$5 % de la productividad primaria neta fue transportada activamente por el mesozooplancton por debajo de 150 m.

Por último, hay que tener en cuenta que en el estudio del flujo activo se asume que los organismos se alimentan exclusivamente durante la noche. Sin embargo, durante el día, una parte del zooplancton migrador como salpas (Phillips et al., 2008) y quetognatos (Stuart y Verheye, 1991) pueden alimentarse

bien de la materia orgánica particulada que está sedimentándose, o bien de otros organismos zooplanctónicos, de manera que habría un transporte activo inverso (es decir, hacia capas más superficiales) que no estaría siendo considerado. En cualquier caso, la inclusión del macrozooplancton y del micronecton en nuestros cálculos incrementarían nuestras estimas del flujo activo, ya que conforman un importante componente en el transporte de partículas (Hidaka et al., 2001; Schukat et al., 2013a).

III.3 Variabilidad espacio-temporal en la relación entre la actividad de la GDH y la excreción de amonio en el zooplancton epipelágico marino

En el *Capítulo* 4 se estudió la variabilidad en la relación entre la actividad de la GDH y la excreción de amonio en zooplancton procedente de distintos ecosistemas marinos. El objetivo consistió en determinar si es o no apropiado utilizar un único factor para calcular las $R_{NH_4^+}$ fisiológicas a partir de medidas potenciales de la enzima GDH. Proveer de una ecuación universal para cada proceso ecológico ha sido durante mucho tiempo un reto para las ciencias marinas (por ejemplo, Arístegui y Montero, 1995; Ikeda et al., 2001), pero hay tantos factores involucrados en modular las tasas biológicas que difícilmente una única función matemática puede explicar una variable ante cualquier circunstancia. En cualquier caso, entender las fuentes de variabilidad en el metabolismo planctónico ayudará a predecir los flujos de nutrientes en los océanos. Lamentablemente, es poco el conocimiento que hay en la variabilidad de la relación GDH/$R_{NH_4^+}$ que resulta de la gran heterogeneidad espacial y temporal de los sistemas marinos.

(i) $R_{NH_4^+}$ en el zooplancton a lo largo de distintos sistemas oceánicos. El periodo de muestreo y las propiedades oceanográficas de los ecosistemas donde se capturaron las muestras utilizadas en este estudio se recopilan en la Tabla 4.1. Los valores de la temperatura superficial (SST) oscilaron desde los 14.6 °C en el sistema de Benguela (BU), hasta los 25.1 °C registrados en el Atlántico Norte (NA). El patrón mostrado por la clorofila-a siguió la tendencia opuesta, cuyos valores máximos se encontraron en el BU (3.18 mg m^{-3}) y los mínimos, en el NA (0.08 mg m^{-3}). Todo en su conjunto reflejó las características propias de un sistema de afloramiento y de aguas oligotróficas, respectivamente. Por otro lado, también se encontraron diferencias estacionales, aunque en menor

medida, en las características hidrográficas en una misma estación en aguas de las islas Canarias. Así, durante el periodo de floración de finales de invierno (CI-LWB) las aguas fueron más frías y contenían más fitoplancton que durante la época de estratificación (CI-ST).

La Fig. 4.2 presenta la relación entre el contenido proteico en las muestras con respecto a las $R_{NH_4^+}$ y las actividades enzimáticas medidas en los distintos sistemas marinos estudiados, sin considerar el efecto de la temperatura. Ambas variables se correlacionaron significativamente con la biomasa ($p < 0.0001$), aunque la varianza explicada por la proteína fue mayor para las actividades de la GDH (62 %) que para las $R_{NH_4^+}$ (29 %). Por otro lado, ambas pendientes fueron significativamente distintas entre sí (ANCOVA, $F_{1,243} = 16.39$, $p < 0.01$), lo que generaría variabilidad en la relación GDH/$R_{NH_4^+}$ con respecto a la biomasa. Tal y como señalaron Berges et al. (1993), no habría un efecto de la biomasa en la relación GDH/$R_{NH_4^+}$ si ambas variables siguieran los mismos principios alométricos, es decir, compartieran el mismo exponente escalar (b). En este trabajo, la pendiente que relaciona la $R_{NH_4^+}$ con la biomasa fue de 0.87, lo que implica que muestras con biomasas de zooplancton más pequeñas excretan más NH_4^+ por unidad de biomasa que muestras con biomasas más grandes. En cualquier caso, este exponente se incluye dentro del rango típico (0.7 - 0.9) para el zooplancton marino (Bidigare, 1983). Aparte del efecto de la biomasa, este exponente puede venir determinado por un efecto botella sobre las tasas fisiológicas, según el cual, mayores densidades de zooplancton resultarían en $R_{NH_4^+}$ más bajas (Bidigare, 1983). Por el contrario, las actividades de la GDH mostraron la tendencia contraria, ya que la pendiente que describe su relación con la biomasa superó el valor de 1.0 ($b = 1.38$). Esta diferencia en los exponentes b de ambas tasas generarían, por tanto, variabilidad en la relación GDH/$R_{NH_4^+}$ si se consideran muestras de distinta biomasa. Por otro lado, aunque las muestras se fraccionaron en varias tallas, se debe tener en cuenta que cada muestra de zooplancton se consideró como un todo, y por tanto, su relación con la biomasa podría estar sesgada debido a la composición taxonómica y al espectro de tamaño de aquellos organismos que conformaban la muestra. Aun así, el exponente b para la GDH superó al exponente b de la $R_{NH_4^+}$ en una magnitud similar a la descrita por Fernández-Urruzola et al. (2011) en ejemplares del misidáceo marino *Leptomysis lingvura* con distinto contenido proteico (ver *Capítulo* 5 para más información). Por todo ello, el fraccionamiento del zooplancton en distintas clases de tamaño es recomendable para

reducir el efecto de la biomasa cuando se comparan poblaciones con distintas estructuras de tamaño. Asimismo, el uso de una relación GDH/$R_{NH_4^+}$ para cada talla reduciría el error asociado. Por otro lado, hay que considerar que la dispersión que presentaron las $R_{NH_4^+}$ con respecto a la biomasa fue mayor que la mostrada por las tasas enzimáticas. Este hecho puede deberse a los errores metodológicos intrínsecos a las propias incubaciones en botella, que pueden dar como resultado unas $R_{NH_4^+}$ experimentales que disten de las tasas reales de una manera poco predecible. Además, las diferencias tróficas entre los distintos ecosistemas oceánicos pudieron afectar más a las tasas fisiológicas que a las enzimáticas, ya que estas últimas presentan una respuesta más atenuada a los cambios ambientales (Bamstedt, 1980).

Tanto la $R_{NH_4^+}$ como las actividades de la GDH fueron estandarizadas por unidad de proteína para comparar las distintas áreas y fracciones de talla (Fig. 4.3). Como cabía esperar de los resultados previos, las $R_{NH_4^+}$ específicas demostraron cierta alometría, ya que fueron, en general, mayores en las fracciones de talla más pequeñas (Tabla 4.2). Este comportamiento concuerda con las $R_{NH_4^+}$ específicas presentadas por Steinberg y Saba (2008) para un amplio rango de tamaño del zooplancton marino. Si se considera el área de estudio, las diferencias más significativas en las $R_{NH_4^+}$ se encontraron en las regiones CI-ST y BU, las cuales mostraron los valores más bajos por unidad de biomasa. Esta variabilidad se puede atribuir a las fracciones de tamaño más pequeñas, ya que el zooplancton de mayor tamaño (> 1000 μm) fue relativamente invariable a lo largo de los distintos sistemas marinos (test ANOVA, $F_{2,28} = 1.55$, $p = 0.231$). Las $R_{NH_4^+}$ específicas promedio variaron desde un mínimo de 0.09 μmol NH_4^+ mg proteína^{-1} h^{-1} en la región BU hasta un máximo de 0.38 μmol NH_4^+ mg proteína^{-1} h^{-1} en la CI-LBW. Estos valores se incluyen dentro del rango predicho por las ecuaciones de Ikeda (1985) (0.13 - 0.27 μmol NH_4^+ mg proteína^{-1} h^{-1}), y estuvieron próximos al límite inferior de los valores publicados en Hernández-León et al. (2008) para las aguas de latitudes tropicales y templadas (0.43 - 0.67 μmol NH_4^+ mg proteína^{-1} h^{-1}, considerando un factor de conversión N/proteína de 0.52 –Postel et al., 2000–). No obstante, estas tasas no son estáticas, sino que fluctúan estacionalmente de acuerdo con las diferentes escenarios de alimentación y temperatura. De hecho, las tasas metabólicas se ven fuertemente influenciadas por la temperatura ambiental, y como tal, la $R_{NH_4^+}$ alcanzó su mínimo en las frías aguas de la región BU, a pesar de ser el ecosistema más productivo de todo el estudio (ver Tabla 4.1). Aplicando un

factor Q_{10} de 3.60 (Hernández-León et al., 2008) y estandarizando con respecto a la temperatura más alta registrada en el estudio (25.1 °C), las $R_{NH_4^+}$ específicas en la región BU serían tan altas como en la NA (0.35 μmol NH_4^+ mg proteína^{-1} h^{-1}). La misma dependencia de la temperatura debe aplicarse a las actividades de la GDH (Packard et al., 1975; Park et al., 1986). En cualquier caso, las actividades específicas de la GDH fueron, en todos los casos, mayores que sus correspondientes $R_{NH_4^+}$ (Fig. 4.3*b*). Esto no es sorprendente tendiendo en cuenta que se trata de medidas potenciales. Las actividades de la GDH mostraron, sin embargo, un patrón distinto al descrito para las $R_{NH_4^+}$ fisiológicas, siendo mayores en la talla de zooplancton más grande (Tabla 4.2). En general, la variabilidad de la actividad de la GDH entre regiones no fue tan marcada, aunque paradójicamente, la estación CI-LWB presentó las actividades de la GDH más bajas. El amplio rango mostrado por las actividades de la GDH en la región BU fue particularmente interesante. Los sistemas de afloramiento son ecosistemas complejos que dan lugar a una gran variedad de estados metabólicos en comunidades heterogéneas de plancton que resultan de la interacción de las masas de agua con distintas productividades (ver Fernández-Urruzola et al., 2014, –*Capítulo* 2 en esta tesis–, y el rango de clorofila-a en la Tabla 4.1). Estas aguas contenían poblaciones en crecimiento exponencial dominadas por procesos anabólicos, así como por poblaciones maduras caracterizadas por un mayor catabolismo. Todo esto pudo conducir a distintos niveles de GTP intracelular en las diferentes poblaciones, lo que produciría una inhibición desigual en las actividades de la GDH. Además, varios estudios han demostrado la gran variabilidad que existe en el metabolismo específico por unidad de biomasa cuando se comparan múltiples taxones (Steinberg y Saba, 2008). Por tanto, el balance entre el zooplancton gelatinoso y el crustáceo en las muestras estudiadas podría explicar ciertas diferencias en las $R_{NH_4^+}$ específicas entre los distintos sistemas oceánicos. Por ejemplo, si se estandarizan por el peso seco, las $R_{NH_4^+}$ son alrededor de un orden de magnitud más pequeñas, aunque la diferencia no es tan amplia si se usa el carbono como medida de referencia (Schneider, 1990). Esto significa que la unidad de biomasa utilizada para la estandarización también determina las diferencias entre las $R_{NH_4^+}$. Así, cualquier tasa metabólica debe compararse siempre en la misma unidad de biomasa, lo que también se extiende a la comparación entre variables adimensionales tales como los exponentes escalares (*b*) arriba mencionados, y las propias relaciones GDH/$R_{NH_4^+}$. Las tasas enzimáticas son frecuentemente estandarizadas por

unidad de proteína, ya que el análisis de ésta puede realizarse en el mismo homogeneizado. De este modo, las relaciones GDH/$R_{NH_4^+}$ que se presentan en este trabajo para las distintas tallas de zooplancton fueron comparados con las relaciones publicadas en la literatura en términos de proteína (Tabla 4.3). No obstante, como la estandarización por biomasa asume que la variación de las tasas metabólicas con respecto a la propia biomasa no supone ningún efecto (Bidigare, 1983), todas nuestras tasas fueron representadas en la Fig. 4.4 sin estandarizar por la biomasa.

La relación entre las actividades de la GDH y las $R_{NH_4^+}$ en cada área y fracción de tamaño, en términos de μmol NH_4^+ mg proteína^{-1} h^{-1}, se presentan en la Tabla 4.3. Ambas variables se relacionaron entre sí de una manera lineal, de modo que no fue necesario transformar los datos. Además, cada conjunto de datos presentó una distribución normal (test de Kruskall-Wallis, $p > 0.05$) y una varianza homogénea (test de Levene, $p > 0.05$). Esto permitió obtener regresiones significativas y comparar las pendientes, que definen la relación entre las actividades de la GDH y las $R_{NH_4^+}$, entre sí y con el resto de datos publicados en la literatura. Las pendientes de las regresiones fueron similares entre las regiones NA, IO (Océano Índico) y CI-LWB, oscilando entre 1.7 (NA) y 2.3 (IO) para el total de la comunidad. Por otro lado, la relación medida en la región CI-LWB fue similar a la relación publicada por Hernández-León y Torres (1997) para la misma región y época del año. En cambio, la relación entre ambas tasas ascendió ∼ 6 veces durante la época de estratificación. El zooplancton de otros ecosistemas marinos presentó relaciones GDH/$R_{NH_4^+}$ más altas, alcanzando un valor máximo de 43.8 en la especie de misidáceo marino, *Praunus flexuosus* (Bidigare y King, 1981). En general, todas las regresiones fueron significativas (en su mayoría a nivel de $p < 0.01$). La correlación entre ambas tasas (r^2) fue, en general, más alta en los experimentos monoespecíficos que en aquellos que utilizaron poblaciones mixtas de zooplancton. Solo Park et al. (1986) obtuvo una mejor correlación en muestras naturales de zooplancton. Por otro lado, estudios previos sugieren que los modelos de regresión entre las tasas enzimáticas y fisiológicas generan un error menor que el resultante de promediar las relaciones individuales (Arístegui y Montero, 1995; Packard y Williams, 1981). El error estándar promedio de los análisis de regresión para cada grupo de datos fue del ± 17.6 % (Tabla 4.3), mientras que el coeficiente de variación ($CV = 100 \times SD \div \bar{x}$) para el valor medio de las relaciones GDH/$R_{NH_4^+}$ ascendió al 60.4 %. Esta comparación evidencia las bondades de utilizar los

análisis de regresión a la hora de determinar un factor empírico que relacione las actividades potenciales (GDH) y las fisiológicas ($R_{NH_4^+}$). En cualquier caso, el error de la regresión entre ambas tasas (en µmol NH_4^+ muestra^{-1} h^{-1}) incrementó hasta ± 42.6 % cuando se analizaron todos los datos en conjunto (Eq. III.1). En esta ocasión, los datos fueron transformados logarítmicamente para reducir las heterodasticidad de los residuos. La ecuación general fue:

$$\begin{gathered} \log GDH = 0.64\ \log R_{NH_4^+} + 0.36 \\ (r^2 = 0.37,\ n = 235,\ p < 0.0001,\ SEE = \pm 42.6\,\%) \end{gathered} \tag{III.1}$$

Los datos correspondientes a las 5 campañas oceanográficas se distribuyeron de manera uniforme a lo largo de la línea de regresión, pero en su conjunto, generaron una mayor dispersión que la observada individualmente para cada grupo de datos. Tal y como se ha discutido previamente, múltiples factores inherentes a las propias comunidades de zooplancton, como la biomasa, el crecimiento, la alimentación y la composición taxonómica, determinan cómo se relacionan la fisiología y la bioquímica. Así, el zooplancton no gelatinoso, presenta tasas fisiológicas más cercanas a las tasas potenciales (es decir, actividades de la GDH) que el zooplancton gelatinoso (King y Packard, 1975); lo mismo se espera para el zooplancton más pequeño y bien alimentado (Fernández-Urruzola et al., 2011, –*Capítulo* 5 en esta tesis–). A parte de los factores biológicos, se asume que los errores metodológicos derivados de la manipulación (estrés, daño y sobrepoblación) y de los propios procedimientos analíticos, actúan de la misma manera en todas las medidas, pero es probable que esta premisa no siempre se cumpla. Todo ello implica que un único factor difícilmente podría considerar todas estas fuentes de variabilidad, por lo que su capacidad para predecir las $R_{NH_4^+}$ a partir de las medidas de actividad de la GDH en varios ecosistemas y comunidades planctónicas es limitada. En cualquier caso, la regresión que consideró el conjunto de datos analizados fue significativa ($p < 0.0001$), y su error asociado (± 42.6 %) se mantuvo en el mismo orden que los errores producidos por otras técnicas estándar utilizadas en el análisis de procesos ecológicos vinculados al metabolismo del plancton (King y Packard, 1975; Richardson, 1991).

No obstante, la precisión de la ecuación parece mejorar si se consideran ciertas variables ambientales, como la temperatura *in situ* (T) y la clorofila-a

(*Chl-a*), en una regresión multivariante:

$$\log GDH = -2.25 + 0.72 \log R_{NH_4^+} + 0.12\, T + 0.42\, Chl\text{-}a$$
$$(r^2 = 0.59,\ n = 235,\ p < 0.0001,\ SEE = \pm 34.5\,\%) \qquad \text{(III.2)}$$

Esta nueva ecuación mejoró la predicción de las actividades de la GDH hasta un 59 %. Asimismo, el error asociado a la Eq. III.2 decreció un 8.1 % con respecto al modelo de regresión simple. En el caso de organismos menos complejos como los procariotas y los nanoflagelados, una ecuación general podría dar lugar a unas estimas de $R_{NH_4^+}$ más precisas, tal y como demostraron Arístegui y Montero (1995) para el metabolismo respiratorio.

(ii) Variabilidad temporal de la $R_{NH_4^+}$ en el mesozooplancton. Por otro lado, se estudió la variabilidad temporal de la relación GDH/$R_{NH_4^+}$, así como de otros factores bioquímicos relacionados con el metabolismo excretor del zooplancton, en una misma estación de la costa de Gran Canaria. Durante la floración de finales de invierno (CI-LWB), que habitualmente ocurre entre finales de enero y abril en aguas de Canarias, la erosión de la termoclina permite la entrada de nutrientes en la capa eufótica y, por consiguiente, el aumento de la productividad primaria (De León y Braun 1973). Esto se refleja en los valores de clorofila-a más altos durante la época CI-LWB en comparación con el periodo de estratificación (CI-ST, ver Tabla 4.1). La Fig. 4.5 muestra las $R_{NH_4^+}$ promediadas, las actividades de la GDH, las concentraciones intracelulares de glutamato y las relaciones $R_{O_2}/R_{NH_4^+}$ durante los dos periodos de muestreo. Si bien las actividades de la GDH incrementaron ligeramente desde 1.21 μmol NH_4^+ mg proteína^{-1} h^{-1} durante el periodo de mezcla (CI-LWB) hasta 1.58 μmol NH_4^+ mg proteína^{-1} h^{-1} durante el periodo de estratificación (CI-ST), otras variables decrecieron notablemente. Así, las $R_{NH_4^+}$ disminuyeron su valor a la mitad de abril a octubre (0.39 y 0.18 μmol NH_4^+ mg proteína^{-1} h^{-1}, respectivamente), mientras que el glutamato intracelular presentó concentraciones 4 veces más pequeñas durante el último periodo (Fig. 4.5). Hernández-León y Torres (1997) monitorizaron de noviembre a mayo la $R_{NH_4^+}$ de la comunidad de mesozooplancton en aguas situadas frente a la costa de Gran Canaria, y también encontraron una gran variabilidad en las tasas conforme fluctuaban las condiciones tróficas. De forma similar a nuestros resultados, sus actividades de la GDH no siguieron el mismo patrón descrito para las $R_{NH_4^+}$, lo que generó fluctuaciones en las relaciones GDH/$R_{NH_4^+}$ durante el periodo de estu-

dio. De hecho, muchos estudios han observado que los valores máximos de las actividades de la GDH no coinciden con los máximos de clorofila-a, sino que se encuentran ligeramente atenuados (Fernández-Urruzola et al., 2014; Hernández-León et al., 2001; Park et al., 1986). Una posible explicación bioquímica fue dada por Park et al. (1986), quien sugirió el efecto de una mayor inhibición provocada por la alta concentración de GTP generado mediante el ciclo de los ácidos tricarboxílicos en aquellos organismos que están creciendo activamente en condiciones tróficas favorables. En esta situación, la actividad de la GDH podría estar subestimada por el ensayo enzimático estándar, ya que requeriría mayores niveles de ADP para contrarrestar el efecto del GTP. Esto podría explicar relaciones GDH/$R_{NH_4^+}$ más bajas durante condiciones de buena alimentación, así como las diferencias en los valores de los interceptos en el eje de las ordenadas que se presentan en la Tabla 4.3. Una tendencia similar en las relaciones GDH/$R_{NH_4^+}$ se encontró en experimentos de laboratorio que exponían los organismos a condiciones de inanición (Fernández-Urruzola et al., 2011; Park, 1986a). A parte de la regulación alostérica, la actividad de la GDH está controlada por la concentración interna de glutamato. Tal y como ocurre en todas las enzimas, la disponibilidad del sustrato de la reacción determina la tasa a la que la enzima puede funcionar (Bisswanger, 2008). Sin embargo, apenas se han realizado medidas directas de ambas variables con el fin de relacionarlas en el contexto de las ciencias marinas. Park et al. (1986) calculó la concentración efectiva de glutamato a partir de los parámetros cinéticos en el macrozooplancton, y demostró un incremento de la concentración total de glutamato en aquellos periodos caracterizados por una mayor disponibilidad de alimento. Un resultado similar para el metabolismo respiratorio ha sido descrito por Osma et al. (en revisión), quien observó un descenso de la concentración intracelular de piridín nucleótidos en el organismo *Oxyrrhis marina* sometido a condiciones de inanición. En este trabajo, la concentración intracelular de glutamato decreció drásticamente de abril a octubre, lo que sostiene la hipótesis que plantea la importancia de los sustratos intracelulares como mecanismo de regulación de la $R_{NH_4^+}$ (Hernández-León y Torres, 1997). Así, una mayor disponibilidad de glutamato pordría favorecer un incremento en la $R_{NH_4^+}$ por unidad de biomasa durante la floración de final de invierno. La correlación positiva que se determinó entre las $R_{NH_4^+}$ y el glutamato intracelular estandarizado por la actividad de la GDH (Fig. 4.6), refuerza la utilidad de los modelos cinéticos para el estudio del metabolismo del zooplancton (Packard y Gómez,

2008). La medida de parámetros bioquímicos como la constante de Michaelis (K_m) junto con las concentraciones intracelulares de los sustratos y efectores involucrados en la reacción, abrirían nuevas perspectivas a la hora de estimar los valores reales de $R_{NH_4^+}$ a partir de las medidas potenciales que suponen las actividades de la GDH. Además, se estudió la relación entre las tasas de respiración (R_{O_2}) y las $R_{NH_4^+}$, ya que actúa como un indicador del alimento que está siendo metabolizado (Mayzaud y Conover, 1988). Aunque fue ligeramente mayor durante la época CI-ST, los bajos valores que presentó la relación $R_{O_2}/R_{NH_4^+}$ (en todos los casos, por debajo de 13 –ver Fig. 4.5–) reflejaron un metabolismo basado en el catabolismo proteico durante los dos periodos de estudio. Esto no es sorprendente ya que los pequeños microheterótrofos, pobres en ácidos grasos, constituyen el 35 - 80 % de la dieta del mesozooplancton en estas aguas (Hernández-León et al., 2004). De este modo, más que un cambio en la propia dieta, un cambio en la densidad de las presas parece ser el responsable de la variabilidad medida en el metabolismo excretor del zooplancton.

III.4 **Actividad de la GDH y excreción de amonio en el misidáceo marino, *Leptomysis lingvura*: efectos de la edad y la inanición**

En este capítulo se estudió el efecto de la edad y de la inanición en la relación que mantienen la actividad GDH y la excreción de NH_4^+ en el misidáceo marino *Leptomysis lingvura*. Los misidáceos juegan un papel importante en los ecosistemas marinos costeros, ya que presentan un pastaje selectivo sobre otras especies y son claves en el reciclaje de nutrientes a través de su metabolismo. Se escogió esta especie de misidáceo debido a su amplia distribución en las aguas someras de las Islas Canarias. De esta forma, el principal objetivo de esta investigación fue comprender, desde el punto de vista bioquímico, el metabolismo de nitrógeno en *L. lingvura* durante su crecimiento, así como en diferentes condiciones fisiológicas. Además, este trabajo introduce la espectrofluorometría con el fin de aumentar la sensibilidad del ensayo clásico de la GDH en el zooplancton, lo que permitirá disminuir la biomasa necesaria para un correcto análisis.

(i) Análisis de la GDH y constantes cinéticas. La mayor parte de las investigaciones oceanográficas sobre la GDH se han centrado en el zooplancton de mayor tamaño a pesar de que se sabe que el microzooplancton es el principal regenerador de NH_4^+ en los sistemas marinos (Bode et al., 2004; Bronk y Stein-

berg, 2008). El mayor problema al estudiar la GDH en el microzooplancton es concentrar los organismos lo suficiente como para obtener una lectura fiable en el espectrofotómetro. Así, King et al. (1987) no pudieron cuantificar con precisión la regeneración de NH_4^+ en el zooplancton de tamaño inferior a 153 μm. En este trabajo, se ha solucionado este problema mediante la aplicación de las ventajas que confiere la espectrofluorimetría (Segel, 1993). Los resultados mostraron un linealidad de la actividad de la GDH en un rango de biomasa superior a un órden de magnitud (0.014 - 0.084 mg proteína) tanto en el análisis espectrofotométrico como en el espectrofluorimétrico (Fig. 5.2). De acuerdo a la *t*-Student (v 19 SPSS, Inc., Chicago, USA), los resultados mostraron una alta coherencia entre los valores promedios de actividad determinados mediante las dos técnicas ($p > 0.05$), lo que facilitó la comparación de nuestros resultados con otros valores encontrados en la literatura. El uso de la espectrofluorimetría permitió detectar señal en muestras que se habían diluido incluso en un orden de magnitud. De esta forma, la medida de la fluorescencia del NADH incremento la sensibilidad del ensayo en, al menos, 6 veces. A bajos niveles de actividad, la espectrofotometría no fue capaz de discriminar entre la verdadera señal de GDH y el ruido de fondo. Esto explicó las altas desviaciones estándar en las medidas espectrofotométricas cuando la concentración de enzima en el homogenizado era muy baja (≤ 0.043 mg proteína). Por otro lado, se observó que unas concentraciones de enzima altas (> 0.084 mg proteína) provocaron una atenuación en la fluorescencia, ocasionando una subestima de la señal real. En cualquier caso, este problema puede resolverse fácilmente diluyendo el homogenizado.

La constante de semi-saturación de Michaelis (K_m) es la característica bioquímica más importante de una enzima (Friedmann, 1981). Define la afinidad química que tiene la enzima pos sus sustratos, el control potencial que ejercen los sustratos en la velocidad de la reacción, así como la concentración aproximada de sustratos en las células (es decir, su concentración *in vivo*). La Fig. 5.3 muestra la dependencia que la reacción de la GDH mantiene con los sustratos en un adulto de *L. lingvura* bien alimentado. Tanto el glutamato como el NAD^+ describieron la clásica hipérbola Michaeliana. En el caso del glutamato, la V_{max} fue 1.60 μmol NH_4^+ h^{-1} mg proteína^{-1} y la K_{Glu} fue 5.61 mM, mientras que para el NAD^+ la V_{max} y la K_{NAD} fueron de 1.97 μmol NH_4^+ h^{-1} mg proteína^{-1} y 0.44 mM, respectivamente. Los valores de K_{Glu} se encontraron dentro del rango descrito en otras especies de zooplancton marino, que

oscilaban entre 2.6 mM (Bidigare y King, 1981) y 11.8 mM (Park, 1986a). La dependencia de la GDH con respecto al NAD^+ ha sido mucho menos estudiada. Batrel y Regnault (1985) mostraron valores de K_{NAD} que fueron superiores a los encontrados en nuestro trabajo, alrededor de 1.3 mM, pero sus medidas fueron más irregulares y pobremente descritas. La comparación de la K_{NAD} (0.44 mM) y la K_{Glu} (5.61 mM) confirmó que la afinidad de la GDH por el NAD^+ es mayor que la que tiene por el glutamato, lo que sugiere que el papel del NAD^+ en el control de la GDH podría ser más importante de lo que se esperaba.

(ii) La influencia de la edad en la excreción y la actividad GDH en *L. lingvura*. El aumento de la excreción de NH_4^+ y de la actividad GDH a lo largo del ciclo de vida de *L. lingvura* (Fig. 5.4) fue consistente con los principios alométricos. Así, las tasas fisiológicas de excreción de NH_4^+, las actividades enzimáticas de la GDH y el contenido proteico presentaron un aumento exponencial con la edad. Los valores de excreción de NH_4^+ en un individuo adulto de *L. lingvura* (13.9 ± 1.93 nmol NH_4^+ ind^{-1} h^{-1} –ver Fig. 5.4*b*–) se encuentran en el límite inferior del rango dado por Bronk y Steinberg (2008) para misidáceos adultos, lo que era de esperar si se tiene en cuenta que otras especies de misidáceos pueden alcanzar un tamaño mucho mayor que el de los *L. lingvura* analizados aquí.

El análisis estadístico basado en el test no paramétrico de Spearman mostró una fuerte correlación de 0.84 ($p < 0.0001$) entre la tasa fisiológica ($R_{NH_4^+}$) y la tasa enzimática (GDH) cuando se compararon por individuo (Fig. 5.5). Sin embargo, esta relación quedó enmascarada al normalizar las tasas por proteína, de manera que la correlación entre ambas fue menos significativa ($r = 0.72$, $p < 0.005$ –ver *Capítulo* 4–). La alta correlación que mantienen ambas tasas confirma el importante papel que desempeña la enzima GDH en el metabolismo del nitrógeno, tal como han expuesto previamente otros autores (Bidigare and King, 1981; Park et al., 1986). Sin embargo, la excreción de NH_4^+ aparente registrada cuando la actividad GDH era igual a cero, sugiere la participación de otras enzimas que también producen NH_4^+, tales como la glutaminasa y la AMP-deaminasa. Por otro lado, es necesario considerar que la V_{max} aparente obtenida a partir de los análisis de la GDH representa la capacidad potencial de excreción de NH_4^+. Teniendo en cuenta que la concentración de sustratos para alcanzar la V_{max} teórica tiende a infinito, la velocidad medida a una concentra-

ción de glutamato igual a 50 mM se encontraría alrededor del 90 % de la $V_{\max}$ teórica (Bisswanger, 2008), de modo que la diferencia entre la tasa potencial y la tasa *in vivo* sería aún mayor. En cualquier caso, la relación GDH/$R_{NH_4^+}$ de 16.05 obtenida en este trabajo (Fig. 5.5), se sitúa entre el valor de 24.3 obtenido por Park et al. (1986) y el valor de 3.8 medido por Hernández-León y Torres (1997). Sin embargo, la pendiente que relaciona la actividad GDH y la $R_{NH_4^+}$ publicada por Bidigare and King (1981) fue significativamente mayor (43.8). En este punto, no se puede pensar que esta relación es universal y puede aplicarse a todo el zooplancton. Su variabilidad es todavía objeto de investigación.

Entonces, ¿por qué la actividad GDH excede la tasa de excreción de NH_4^+ en un factor que puede alcanzar un orden de magnitud? Si se asume que la actividad GDH determina el límite superior de la tasa fisiológica de excreción de NH_4^+ y que la K_m es un índice de la concentración intracelular *in vivo* de glutamato y NAD^+ (Cleland, 1963), otros factores deben estar limitando la velocidad de la reacción GDH hasta la tasa *in vivo*. Junto con la regulación debida a los sustratos, otras moléculas actúan como activadores e inhibidores de la reacción. Este es el caso del ADP y GTP, respectivamente. Por lo tanto, una investigación exhaustiva del papel que ejercen estas moléculas en la regulación de la actividad GDH permitiría comprender mejor la variabilidad de la relación GDH/$R_{NH_4^+}$.

La fuerte correlación existente entre la actividad GDH y la biomasa (test de Spearman, r = 0.91, $p < 0.001$) sugiere que la GDH es una enzima constitutiva, por lo que serviría como un índice de la biomasa de zooplancton en una muestra de plancton mixta. La naturaleza constitutiva de la GDH implicaría que la variabilidad de la concentración de la GDH de cara a las fluctuaciones ambientales sería menor que la sufrida por otras enzimas que son inducidas o reprimidas por los cambios externos. La nitrato reductasa encontrada en el fitoplancton es el ejemplo de una enzima más sensible a los factores ambientales. En el caso de la GDH, al ser un componente permanente de las células, debe variar con los cambios en el carbono y nitrógeno, es decir, con la biomasa. Un comportamiento similar se ha encontrado en otros complejos enzimáticos mitocondriales como es el caso del sistema de transporte de electrones (Martínez et al., 2010).

Se sabe que los procesos metabólicos, incluyendo la excreción, mantienen una relación alométrica con la biomasa definida por la ecuación $M = a\,W^b$,

donde *M* es el proceso metabólico, *W* es la biomasa, y *a* y b son constantes. En esta igualdad, *b* constituye el componente escalar que determina la relación entre la tasa metabólica y la biomasa. Generalmente, se asume que el valor de *b* es 0.75 cuando la biomasa se encuentra expresada en términos de peso húmedo (Brown et al., 2007; Kleiber, 1961). Sin embargo, en invertebrados, como es el caso de los organismos que se usan en este trabajo, la composición elemental varía conforme los organismos crecen (Mayzaud, 1986), de modo que se aconseja reconsiderar el componente escalar (*b*) en términos de proteína, cuya proporción es relativamente constante a lo largo de todo el crecimiento. En esta investigación se muestra cómo la $R_{NH_4^+}$ es afectada por la biomasa con un exponente *b* de 0.55 ($r^2 = 0.8$). Esto significa que los misidáceos más pequeños presentan unas tasas metabólicas más altas por unidad de proteína que los individuos adultos. Este valor de *b* es ligeramente inferior a los valores publicados por Ikeda y Skjoldal, (1989), que oscilaron entre 0.65 y 0.8 en varias especies de zooplancton. Esta diferencia puede deberse a la propia especie de zooplancton estudiada, así como a un metabolismo más activo en los misidáceos más pequeños. Por el contrario, la actividad GDH mantiene una relación más lineal con la biomasa ($b = 0.93$), lo que significa que su actividad específica es prácticamente invariable a lo largo de las distintas tallas. Este comportamiento de la enzima GDH concuerda con la tendencia alométrica descrita por Berges et al. (1990) en distintas tallas de *Artemia franciscana*. Sin embargo, Mayzaud (1986) encontró un comportamiento más alométrico de la GDH, con un exponente *b* igual a 0.8 en el copépodo *Acartia clausi*. La relación en este último trabajo entre ambas variables es más débil, probablemente debido al estrecho rango de tallas utilizado en el estudio. Así, la relación GDH/$R_{NH_4^+}$ resultante de nuestro trabajo muestra una ligera tendencia a aumentar conforme los misidáceos se convertían en adultos (Fig. 5.7), principalmente en las primeras fases de desarrollo. Este comportamiento sugiere que el efecto de la talla actúa de manera diferente en la tasas fisiológica y la enzimática, ya que de lo contrario, la pendiente entre la relación GDH/$R_{NH_4^+}$ y la biomasa sería igual a cero. Ambas variables se relacionaron mediante la Eq. III.3:

$$\log (GDH/R_{NH_4^+}) = 1.60 \log proteína + 0.64 \qquad \text{(III.3)}$$

(ii) La influencia de la inanición en la excreción y la actividad GDH en *L. lingvura*. Una característica común en la fisiología del zooplancton es el descenso rápido de sus tasas metabólicas cuando se produce un agotamiento de su

fuente de alimento. Mayzaud (1976) ya describió el descenso en la excreción de nitrógeno después de 12 h de inanición, lo que se ha corroborado en otros trabajos posteriores (por ejemplo, Ikeda y Skjoldal, 1980). En este estudio, la excreción de NH_4^+ disminuyó casi 3 veces en las primeras 20 h hasta un metabolismo basal. Posteriormente cuando se suministró de nuevo alimento a los misidáceos tras 70 h en inanición, la excreción de NH_4^+ aumentó ligeramente, aunque no alcanzó los niveles iniciales debido, probablemente, a que su fisiología estaba dañada en este punto. A diferencia del descenso presentado en la $R_{NH_4^+}$ específica, la actividad específica de GDH prácticamente no cambió a medida que los misidáceos entraron en inanición (Fig. 5.8). La actividad GDH mantuvo un valor constante de entorno a 1.47 (± 0.54) μmol NH_4^+ mg proteína^{-1} h^{-1} durante todo el experimento. Esta constancia en la actividad GDH explicó que la relación GDH/$R_{NH_4^+}$ aumentara con la inanición. Así, de un valor inicial de 11.2 aumentó casi diez veces a un valor de 102.4 (ver Tabla 5.1). La K_m aparente aumentó en las primeras 26 h de inanición, descendió en los siguientes dos días y, posteriormente, volvió a aumentar ligeramente cuando se les suministró alimento de nuevo. En base a la cinética enzimática, se determinó asimismo la concentración efectiva de glutamato. Estos cálculos teóricos mostraron un fuerte descenso de glutamato durante la inanición, de un máximo de 1.09 mM hasta un mínimo de 0.03 mM. En la bibliografía, existen muy pocos estudios que hayan tratado de evaluar la variabilidad de la actividad GDH y de su K_m aparente a lo largo de diferentes condiciones tróficas. El primer estudio fue el realizado por Park (1986a) en dos especies de copépodos, pero en una escala temporal más larga y con una menor resolución. En nuestro trabajo, el hecho de que la actividad de la GDH se mantuviera constante frente a cambios en la disponibilidad de alimento pudo ser debido a una disminución en el catabolismo de los sustratos durante el Ciclo de los Ácidos Tricarboxílicos (TCA). Ésto provocaría un descenso en la producción de GTP, siendo éste el mayor inhibidor de la GDH. Por su parte, Park (1986a) mostró un mayor aumento de la actividad GDH específica por proteínas, que atribuyó a una conversión del GTP a ATP debido al agotamiento de los compuestos de mayor energía. Sin embargo, el rango de nuestros resultados excedió la variación mostrada en su estudio. La variabilidad de la K_{Glu} (ver Tabla 5.1) pudo deberse a ajustes internos del catabolismo de aminoácidos a medida que el alimento se volvía limitante, a pesar de que estas diferencias no fueron significativas debido a las altas desviaciones estándar. Los organismos en un estado fisiológico saluda-

ble presentaron una K_{Glu} aparente baja (4.69 mM) como consecuencia de un consumo rápido de proteínas durante el crecimiento. Sin embargo, cuando el alimento ingerido fue metabolizado y al no haber otra fuente disponible, los misidáceos comenzaron a utilizar sus propias reservas como fuente de energía y la GDH pudo disminuir su afinidad por el glutamato durante las primeras 24 h con el fin de prevenir su consumo. Posteriormente, el metabolismo basal pareció disminuir hasta su nivel mínimo y la baja producción de GTP en el TCA hizo que se restableciera una V_{max} aparente alta. Sin embargo, la actividad *in vivo* fue probablemente más baja debido a la ausencia de sustratos en este punto, tal y como demuestra la concentración efectiva de glutamato. Esta tendencia del glutamato intracelular durante la privación de alimento concuerda con el patrón encontrado en el *Capítulo* 4, lo que confirma la importancia de la activación por sustratos en la regulación de la GDH.

Los cambios en la tasa de excreción durante la inanición dependen de las reservas que los misidáceos metabolicen para obtener energía. La relación atómica $R_{O_2}/R_{NH_4^+}$ se utiliza como un indicador de los compuestos que se utilizan para obtener energía. Durante la inanición, la tasa de consumo de O_2 presentó un valor máximo que coincidió con los máximos registrados de excreción de NH_4^+, 10 h después de la última toma de alimento. Después, estas tasas disminuyeron en 1.5 días hasta valores 6 veces inferiores. Excepto en la última medida, la relación $R_{O_2}/R_{NH_4^+}$ se mantuvo prácticamente constante durante todo el experimento, coincidiendo con la tendencia registrada por Kiørboe et al. (1985) en copépodos. Los valores por debajo de 13, como los encontrados en este estudio, indican una mayor dependencia del metabolismo de las proteínas (Mayzaud y Conover, 1988).

III.5 **Construyendo un modelo cinético para la enzima glutamato deshidrogenasa en dos especies de zooplancton marino**

A pesar de la importancia ecológica que tiene la regeneración de NH_4^+ en los ecosistemas marinos, aún no se han dilucidado en profundidad los mecanismos bioquímicos que gobiernan la síntesis de NH_4^+ en el zooplancton. Aunque la velocidad de la reacción enzimática es difícil de determinar a partir de medidas cinéticas *in vitro*, debido a la compartimentalización celular y la competitividad por los sustratos entre distintas rutas metabólicas (Berges y Mulholland, 2008), su estudio arrojaría luz acerca de los patrones de regulación de la enzima GDH y su adaptación frente a los cambios ambientales. En el *Capítulo* 6

se determinó la variación de las $R_{NH_4^+}$, las actividades de la GDH, así como de los niveles intracelulares de los sustratos (glutamato y NAD^+) y los efectores (GTP y ADP) que se produjeron durante un periodo de inanición en dos especies de zooplancton marino (*Brachionus plicatilis* y *Leptomysis lingvura*). Los valores medidos se aplicaron a un modelo cinético basado en los principios fundamentales de Michaelis-Menten con el fin de predecir los cambios registrados en las $R_{NH_4^+}$ conforme variaban las condiciones de alimentación.

(i) Efecto de la calidad del alimento en el metabolismo excretor de NH_4^+. Un factor que determina la cantidad de NH_4^+ excretado por el zooplancton es la composición nutricional del alimento que ingieren estos organismos (Miller y Roman, 2008). En la Tabla 6.2 se presentan los valores de las $R_{NH_4^+}$, las actividades de la GDH y las concentraciones intracelulares de Glu, NAD^+, GTP y ADP asociados a las distintas dietas. En general, las diferencias causadas por el tipo de alimento fueron más acusadas en *B. plicatilis* que en *L. lingvura*. Así, las $R_{NH_4^+}$ en los rotíferos aumentaron de 0.13 a 0.20 μmol NH_4^+ mg proteína^{-1} h^{-1} cuando los organismos eran alimentados con una dieta más proteica (levadura). Esta tendiencia coincide con estudios previos que reportan mayores $R_{NH_4^+}$ en copépodos alimentados con una dieta carnívora en comparación con aquellos alimentados con algas (Saba et al., 2009). En este sentido, presas de un origen distinto al fitoplancton serían asimiladas más fácilmente (Tang y Dam, 1999). Aunque la microalga *Nannochloropsis* sp. tiene un mayor valor nutricional debido a un alto contenido de ácidos grasos poliinsaturados en comparación con la levadura (Tamaru et al., 1993), ésta contiene una mayor cantidad de proteínas y menos carbono estructural, lo que aumentaría su eficiencia de asimilación. Como el nitrógeno proviene exclusivamente de los compuestos nitrogenados, cabe esperar que los rotíferos alimentados con levadura presenten mayores $R_{NH_4^+}$. Tales diferencias no se encontraron en los misidáceos, cuyos valores oscilaron entre 0.08 - 0.09 μmol NH_4^+ mg proteína^{-1} h^{-1}, probablemente porque ambas dietas heterotróficas contenían un nivel similar de proteína. La Fig. 6.1 demuestra que estas tasas fueron relativamente constantes a lo largo del periodo experimental (1 - 1.5 h). Incubaciones más largas (es decir, superiores a 1.5 h) provocaron una disminución en las $R_{NH_4^+}$, especialmente en el caso de *B. plicatilis*. En general, las actividades GDH se comportaron de una manera similar a las $R_{NH_4^+}$ en los organismos aclimatados a cada dieta, de modo que las diferencias en la relación GDH/$R_{NH_4^+}$ apenas

fueron significativas. En el caso de los rotíferos, la relación GDH/$R_{NH_4^+}$ osciló entre 11.05 - 14.69, mientras que en los misidáceos los valores estuvieron comprendidos entre 17.25 - 19.00. Como cabía esperar, las $R_{NH_4^+}$ por unidad de proteína en los rotíferos doblaron las tasas encontradas en los misidáceos. La tendencia según la cual las $R_{NH_4^+}$ específicas disminuyen conforme aumenta el tamaño del individuo es bien conocida (Steinberg y Saba, 2008), al igual que lo es el incremento de estas tasas con la temperatura. Por otro lado, cuanto mayor era el contenido lipídico en la dieta, mayor era la relación $R_{O_2}/R_{NH_4^+}$. Esto fue más evidente en *B. plicatilis*, de manera que los rotíferos alimentados con la microalga *Nannocloropsis* sp. presentaron un valor máximo de $R_{O_2}/R_{NH_4^+}$ igual a 15.4. De acuerdo con lo cálculos de Mayzaud y Conover (1988) la dieta basada en esta microalga fue la única en inducir un metabolismo lipídico, mientras que el resto de dietas, incluida la de *Artemia* enriquecida en el caso de los misidáceos, promoverían un catabolismo típicamente proteico. En cuanto a los niveles intracelulares de los metabolitos, apenas se observaron diferencias significativas entre los distintos tratamientos (Tabla 6.2). Sin embargo, las diferencias fueron más evidentes si se comparaban las concentraciones medidas en ambos organismos. Excepto en el caso del NAD^+, *B. plicatilis* mostró entre 2 - 3 veces más Glu y GTP que *L. lingvura*. Las mayores diferencias se encontraron en el ADP, cuyas concentraciones en *B. plicatilis* fueron 6 veces superiores a las medidas en *L. lingvura*.

(ii) Medidas cinéticas durante la inanición. La Fig. 6.5 muestra un perfil temporal de las variables mencionadas en el apartado anterior ($R_{NH_4^+}$, actividad de la GDH, Glu, NAD^+, GTP y ADP). A pesar de las diferencias descritas anteriormente, ambos tratamientos siguieron un patrón similar cuando se sometió a los organismos a un periodo de inanición. En general, los valores máximos de las $R_{NH_4^+}$ y las actividades enzimáticas se encontraron al comienzo del experimento (t_0). Lo mismo ocurrió con los niveles intracelulares de Glu, NAD^+, GTP y ADP. Después, tanto la $R_{NH_4^+}$ como las concentraciones de los metabolitos disminuyeron a la mitad en las primeras 12 h de inanición. De hecho, la disponibilidad de alimento determina la actividad metabólica de los organismos, cuyas tasas disminuyen rápidamente a un metabolismo basal después de $\sim$ 6 - 8 h en condiciones de inanición (Kiørboe et al., 1985; Mayzaud, 1976). Una vez se volvió a alimentar a los organismos, las $R_{NH_4^+}$ recuperaron, e incluso superaron, los valores originales medidos en el t_0. La respuesta fisiológica

al régimen de alimentación fue, por tanto, casi inmediata. En cambio, las actividades de la GDH decrecieron de una manera más gradual a lo largo de todo el experimento. Las tasas enzimáticas varían, en general, de una manera más atenuada y con un cierto retraso con respecto a las tasas metabólicas (Bamstedt y Holt, 1980). Este mismo comportamiento se observó para las actividades de la GDH y ETS del misidáceo *L. lingvura* (Fernández-Urruzola et al., 2011; Herrera et al., 2011b). Esto es razonable a corto plazo, ya que es energéticamente más eficiente mantener los niveles constantes de enzima con el fin de explotar los recursos si se producen cambios repentinos en la abundancia de alimento. No obstante, el mantenimiento de las actividades de la GDH también depende del gasto energético y de las reservas bioquímicas disponibles. Así, los organismos alimentados con una dieta rica en lípidos mantuvieron las actividades de la GDH relativamente constantes en comparación con aquellos organismos alimentados con una dieta poco lipídica. Asumiendo unos requerimientos energéticos similares entre ambos tratamientos, la diferencia en sus niveles enzimáticos podría explicarse mediante el sustrato que está siendo metabolizado para producir energía. Durante los periodos de inanición se utilizan preferiblemente las reservas lipídicas como fuente de energía (Bamstedt y Holt, 1978), pero cuando éstas se agotan, comienza la hidrólisis de las proteínas. Esto resulta en una mayor degradación proteica y un aumento de la oxidación metabólica de aminoácidos como el glutamato en aquellos tratamientos basados en dietas pobres en lípidos. Además, esta ruta bioquímica sería más importante en *B. plicatilis*, ya que los rotíferos tienen, por lo general, un menor contenido lipídico que los crustáceos. Las concentraciones intracelulares de los metabolitos variaron de forma paralela a las $R_{NH_4^+}$. Unas tendencias similares para el glutamato (Aragão et al., 2004) y el NAD^+ (Osma et al., in prep.) se han descrito previamente en pequeños heterótrofos sometidos a condiciones variables de alimentación. A su vez, el GTP está directamente relacionado con la carga energética de los organismos, de manera que una actividad reducida del ciclo de los ácidos tricarboxílicos durante el periodo de inanición resultaría en unos bajos niveles de GTP. Como esta molécula está involucrada en la biosíntesis celular (Karl, 1978), una menor concentración en ausencia de alimento reforzaría la hipótesis según la cual los organismos estarían metabolizando aminoácidos libres para la obtención de energía.

Hasta la fecha, todas las investigaciones bioquímicas realizadas en organismos marinos han utilizado, debido a su simplicidad, la ecuación de Michaelis-

Menten monosustrato para calcular las constantes de semi-saturación (K_m) de cada sustrato de la GDH (Bidigare y King, 1981; Fernández-Urruzola et al., 2011; Park, 1986a; Park et al., 1986). Sin embargo, un estudio más exhaustivo de las cinéticas de la GDH debe determinar otras constantes cinéticas relacionadas, tales como la constante de disociación (K_{ia}), lo que requiere estudios de cinéticas enzimáticas bisustrato. Debido a su complejidad (ver Fig. 6.2), este tipo de medidas no existen en la literatura marina. En este trabajo, la K_{Glu} calculada a partir de análisis bisustrato osciló desde un valor mínimo de 0.12 mM en rotíferos, hasta un valor máximo de 2.88 mM en misidáceos (Tabla 6.3). Estos valores son ligeramente inferiores a aquellos estimados a partir de análisis monosustrato en otras especies de zooplancton marino (2.6 - 14.4 mM). Lo mismo ocurrió con respecto a la K_{NAD}, la cual varió en un rango (0.009 - 0.025) mucho menor que el valor previamente medido por Fernández-Urruzola et al. (2011) en *L. lingvura* (0.44 mM). Una K_{NAD} significativamente menor a la K_{Glu} sugiere que la GDH presenta una mayor afinidad por el NAD^+ que por el glutamato, de manera que este piridín nucleótido podría ser crucial a la hora de regular la velocidad de la reacción enzimática. Sin embargo, es necesario considerar que los niveles intracelulares de NAD^+ fueron mucho menores que los niveles de glutamato (Fig. 6.4). La gran afinidad de la GDH por el NAD^+ podría verse favorecida por la propia interacción con el glutamato, ya que los sustratos dicarboxílicos aumentan la afinidad del enzima por el NAD^+ debido a su sinergia para formar complejos ternarios (Rife y Cleland, 1980). Unos valores de K_{ia} más altos que los valores de K_m corroboran este comportamiento de cooperatividad ($K_m/K_{ia} < 1$), ya que la unión de un sustrato al sitio activo incrementaría la afinidad de la enzima por el otro sustrato (Leskovac, 2003). Por otro lado, tanto las K_m como las constantes de disociación (K_{ia}) incrementaron ligeramente sus valores en condiciones de ausencia de alimento. Esto podría explicarse por la presencia de distintas isozimas cuya actividad estaría inducida por la condición trófica (Srivastava y Singh, 1987). Valores más altos de las constantes cinéticas durante la inanición indicarían un descenso en la velocidad de la reacción enzimática durante este periodo. Pero estas cinéticas se ven complicadas por la regulación alostérica. La velocidad de la reacción que cataliza la GDH puede ser inhibida o estimulada por una gran variedad de moléculas, entre las que destacan los purín nucleótidos (Frieden y Coman, 1967). Mientras que las moléculas de GTP son potentes inhibidoras de la deaminación del glutamato al aumentar la afinidad de la enzima por el producto,

las moléculas de ADP actúan de forma contraria al facilitar la producción de NH_4^+. Las constantes de inhibición (K_i) y de activación (K_a) para el GTP y el ADP, respectivamente, se mantuvieron relativamente constantes a lo largo de las distintas condiciones de alimentación. Las K_i oscilaron entre 5.8 y 6.0×10^{-4} mM en *B. plicatilis*, y entre 1.7 y 2.0×10^{-3} en *L. lingvura*. A su vez, las K_a variaron entre 0.7 - 5.8 mM. Otros factores a considerar a la hora de estudiar la regulación alostérica son las variables α y β. El primer factor (α) determina la forma en que cambia la K_{Glu} (considerando el glutamato como el sustrato principal) cuando el efector está unido a la enzima; el factor β, en cambio, describe cómo varía la V_{max} en presencia del efector. En el caso de la inhibición debida al GTP, el factor α osciló entre 1 y ∞, mientras que el factor β osciló entre 0 y 1. Estos valores indicarían una inhibición hiperbólica mixta de la reacción catalizada por la GDH (Segel, 1993). Esto significa que tanto la enzima (E) como el complejo enzima-inhibidor (EI) se unen al sustrato (S), aunque con diferentes afinidades. Así, tanto el complejo ES como el ESI producen NH_4^+, aunque a distintas velocidades. Una concentración infinita de inhibidor, por tanto, no reduciría por completo la velocidad de la reacción. Un concepto similar, aunque en la dirección contraria, se aplicaría a la activación alostérica por el ADP. En ausencia de activador, la K_{Glu} aumentó significativamente (Tabla 6.3), es decir, la enzima redujo su afinidad por el sustrato. De hecho, cuando se añade ADP al ensayo enzimático con el fin de evitar cualquier tipo de inhibición, lo que realmente se calcula es α-K_m, es decir, la K_m aparente, y la β-V_{max}.

Los beneficios de usar un modelo cinético ya se han demostrado en otros procesos involucrados en el metabolismo respiratorio (Aguiar-González et al., 2012; Packard et al., 1996b; Roy y Packard, 2001). En este trabajo utilizamos un concepto teórico similar para predecir la velocidad de producción de NH_4^+ en el zooplancton, aplicando la V_{max} aparente, las constantes cinéticas que se presentan en la Tabla 6.2, y los niveles intracelulares de glutamato y NAD^+ (Fig. 6.5) a una ecuación bisustrato basada en los principios fundamentales de la enzimología (Eq. II.5). Asimismo, las constantes cinéticas relacionadas con la inhibición y activación alostéricas, se aplicaron a las Eqs. II.6 y II.9, respectivamente. Las velocidades calculadas de producción de NH_4^+ ($V_{NH_4^+}$) a lo largo del periodo de inanición se asemejaron razonablemente bien a las $R_{NH_4^+}$ medidas tanto en rotíferos como en misidáceos (Fig. 6.6*a*). Sin embargo, los valores modelados subestimaron las tasas reales de excreción de NH_4^+,

especialmente en el caso de los misidáceos. Esto podría deberse, en parte, a medidas conservadoras de las concentraciones molares de los sustratos, ya que la ecuación general utilizada para calcular el biovolumen de los misidáceos se obtuvo a partir de organismos zooplanctónicos menores a 5 mm (Alcaraz et al., 2003). Zooplancton de mayor tamaño como los misidáceos podría dar lugar a un menor biovolúmen por unidad de biomasa. Además, en las células eucariotas, la enzima GDH se localiza principalmente en la mitocondria (Frigerio et al., 2008), de manera que la cuantificación de los sustratos dentro de estos orgánulos intracelulares haría que las tasas calculadas y las reales se pareciesen más entre sí. De hecho, se ha demostrado que la enzima GDH utiliza el glutamato próximo al sitio activo, que proviene en su mayoría de la deamidación de la glutamina (Schoolwerth y LaNoue, 1980). En cualquier caso, ninguno de estos problemas metodológicos afectó a los patrones de las $V_{NH_4^+}$, sino a su magnitud. Esto podría resolverse mediante una simple calibración. Así, las $V_{NH_4^+}$ modeladas fueron capaces de predecir los patrones de $R_{NH_4^+}$ de una manera más precisa ($r^2 = 0.79$) que las típicas estimaciones realizadas a partir de las actividades potenciales de la GDH (Fig. 6.7), a pesar de que se aplicaron 4 factores empíricos específicos para cada organismo y dieta (ver Tabla 6.2). Comprender cómo los efectores interactúan entre sí y modulan la $V_{NH_4^+}$ en un mecanismo bisustrato es aún un reto por resolver. En el caso más sencillo de las cinéticas monosustrato (Eqs. II.6 y II.9) se demostró que la regulación alostérica, ya fuera la activación o la inhibición, es más importante en condiciones de buena alimentación (Fig. 6.6*b*). Estos resultados coinciden con los hallazgos obtenidos por Park et al. (1986), quien sugirió una mayor inhibición de la GDH por moléculas de GTP en situaciones oceanográficas con altas concentraciones de clorofila-a. A pesar de estas incertidumbres, a la luz de nuestros resultados se puede concluir que un algoritmo basado en las cinéticas de Michaelis-Menten (Eq. II.5) provee de estimas más precisas de las $R_{NH_4^+}$ en ambientes donde la disponibilidad de alimento es variable.

IV Conclusiones generales

A lo largo de los sucesivos apartados de la tesis se ha respondido a las preguntas planteadas en el *Capítulo* 1. En líneas generales, las principales conclusiones que se desprenden de los resultados de esta investigación son:

1. Independientemente de las condiciones oceanográficas, el control que

ejerció la respiración y la excreción de NH_4^+ del mesozooplancton sobre la productividad primaria de las aguas de Benguela fue limitado. Aún así, ambas tasas metabólicas fueron superiores a las encontradas en otros sistemas de afloramiento.

(a) La heterogeneidad del ecosistema provocó importantes fluctuaciones espacio-temporales en la biomasa y el metabolismo del zooplancton, si bien sus valores máximos se registraron siempre en el borde de la plataforma continental.

(b) El patrón de maduración de las aguas determinó cambios en la composición taxonómica de la comunidad mesozooplanctónica, así como en las fuentes de carbono y nitrógeno utilizadas por estos organismos.

(c) Considerando la demanda respiratoria del mesozooplancton junto con los requerimientos de carbono de las bacterias y el microzooplancton, apenas se consumió el ~ 71 % de la biomasa fitoplanctónica. Esto significa que hubo un exceso de producción neta que se exportó bien lateralmente o bien al océano profundo, lo que sugiere que las aguas de Benguela se comportan como un ecosistema autotrófico durante la época activa del afloramiento.

(d) La reducida contribución de la excreción de NH_4^+ a los requerimientos fitoplanctónicos en este sistema de afloramiento (0.5 - 11.3 %) implica que la mayor parte del reciclaje de nutrientes se produjo a través de la red microbiana.

2. A diferencia del resto de metodologías utilizadas en estudios biogeoquímicos, el ajuste de un modelo potencial a las tasas de excreción de NH_4^+ permite realizar estudios sinópticos de los flujos verticales de nitrógeno, así como inferir la capacidad del ecosistema para retener nutrientes y analizar el transporte activo de nitrógeno debido a los migradores verticales.

(a) La combinación de los flujos de nitrógeno modelados y las medidas realizadas mediante trampas de sedimento ilustra de una manera más precisa los patrones de sedimentación del nitrógeno particulado (PON). Tanto el tamaño de las partículas que sedimentan

como el historial productivo de las aguas fueron factores fundamentales a la hora de explicar el desequilibrio entre el PON sedimentado y los requerimientos metabólicos en la columna de agua.

(b) Dependiendo del régimen de productividad, el flujo activo de nitrógeno debido al mesozooplancton constituyó entre 59 - 361 % del flujo gravitacional. Estos organismos fueron responsables de transportar activamente alrededor del 5 % de la productividad primaria neta, de modo que el flujo activo constituye un importante componente de la bomba biológica en el sistema de Benguela.

3. El uso de las propiedades fluorométricas aumenta significativamente la sensibilidad del ensayo clásico de la glutamato deshidrogenasa. Esto permite analizar muestras con poca biomasa, como por ejemplo las que proceden del océano profundo.

4. Existe una importante variabilidad espacial y temporal en la relación que mantiene la tasa de excreción de NH_4^+ con la actividad de la GDH. Por este motivo, no hay una ecuación universal capaz de describir dicha relación en cualquier situación oceanográfica. Esto implica la necesidad de calibrar el factor GDH/$R_{NH_4^+}$ para cada comunidad de zooplancton.

   (a) La distinta relación alométrica que ambas tasas presentan con respecto a la biomasa es un factor que genera variabilidad en la relación GDH/$R_{NH_4^+}$. El efecto de la biomasa debe considerarse, por tanto, a la hora de comparar muestras de zooplancton de distintas tallas.

   (b) Los cambios tróficos en el sistema, y especialmente los periodos de inanición, inducen importantes diferencias entre las $R_{NH_4^+}$ y las actividades de la GDH. Mientras que la tasa metabólica responde inmediatamente a alteraciones en la disponibilidad de alimento, el efecto que se produce en la tasa enzimática es más atenuado. La concentración intracelular de los sustratos explica, hasta cierto punto, la discrepancia entre la velocidad máxima de producción de NH_4^+ y la velocidad real, lo que implica una regulación de la GDH por los sustratos.

   (c) La calidad nutricional del alimento y la composición taxonómica de la muestra son otros factores que alteran la relación GDH/$R_{NH_4^+}$.

5. La aplicación de un modelo cinético bisustrato, que asume la disponibilidad de sustratos como el factor fundamental en la regulación de la síntesis de NH_4^+, predice los patrones de variación de las $R_{NH_4^+}$ encontradas durante un periodo de inanición de una forma más precisa que si se aplicase un valor general de GDH/$R_{NH_4^+}$ a las medidas enzimáticas.

   (a) Los valores estimados por el modelo, sin embargo, subestimaron las tasas reales. Una mejor aproximación requeriría la determinación de la concentración de los sustratos a nivel de mitocondria.

   (b) Además de la activación por los sustratos, la actividad de la GDH está modulada por diversos efectores, entre los que destacan los purín nucleótidos. El efecto alostérico de estas moléculas es más importante en condiciones de buena alimentación.

V Líneas futuras de investigación

Esta tesis analiza el papel del zooplancton en un importante sistema de afloramiento, y presenta nuevos enfoques enzimáticos para estudiar la implicación del zooplancton en los ciclos biogeoquímicos. Sin embargo, de las conclusiones obtenidas en este trabajo surgen una serie de interrogantes que aún deben ser resueltos.

1. Una preocupación recurrente en la comunidad científica dedicada a la oceanografía consiste en desarrollar técnicas analíticas capaces de detectar una señal incluso en las muestras menos accesibles. Si bien en esta tesis se aumenta la sensibilidad del ensayo original de la enzima GDH al aplicar los principios de fluorescencia, su capacidad de detección aún debe mejorarse. Incorporar en el experimento nuevas moléculas que se caractericen por un mayor poder de emisión de fluorescencia, tales como el resazurín, permitiría analizar la actividad de la GDH en muestras tomadas a gran profundidad en mares oligotróficos.

2. Una parte importante de esta tesis trata de comprender las causas de la variabilidad encontrada en la relación GDH/$R_{NH_4^+}$. Los *Capítulos* 4 - 6 abordan el impacto que ciertos factores biológicos como son la biomasa, la inanición y la calidad nutricional ejercen en dicha relación. Pero, además, introducen la importancia que puede tener la composición taxonómica a la hora de explicar la relación entre la tasa fisiológica y la

enzimática. Un estudio pormenorizado de la relación GDH/$R_{NH_4^+}$ en distintos grupos taxonómicos permitiría corregir dicha relación en función de la composición taxonómica de la muestra y por tanto, estimar la $R_{NH_4^+}$ a partir de las actividades de la GDH de una manera más precisa.

3. El *Capítulo* 6 presenta la utilidad de aplicar los principios fundamentales de la bioquímica para estimar la $R_{NH_4^+}$ a partir de un modelo cinético. Sin embargo, el estudio considera por separado la activación de la reacción debido a la disponibilidad de los sustratos, y la modulación alostérica que se produce sobre la propia reacción. Generar un modelo que incluya todos estos mecanismos de control de la actividad de la GDH mejoraría la predicción de la velocidad real de la producción de NH_4^+. Asimismo, estudios futuros deberían cuantificar a nivel de mitocondria la concentración intracelular de los metabolitos involucrados en la reacción.

4. Ante un panorama de cambio global, cabe preguntarse cómo afecta la acidificación marina al papel biogeoquímico del zooplancton. Pocos estudios han investigado, sin embargo, las consecuencias que tienen los cambios en el pH de los océanos sobre la comunidad de mesozooplancton (Niehoff et al., 2013). Este vacío en el conocimiento es aún mayor si se considera el impacto que la acidificación ejerce sobre las tasas fisiológicas y enzimáticas de esta comunidad planctónica. Su estudio es, por tanto, una prioridad para predecir cambios en la capacidad que tienen estos organismos para regenerar NH_4^+. Asimismo, es importante dilucidar si la relación entre las actividades enzimáticas y las tasas metabólicas se ve afectada por los procesos de acidificación.

5. Otro de los efectos del cambio global es el aumento del zooplancton gelatinoso, como por ejemplo, de las medusas (Richardson et al., 2009). En condiciones favorables, los gelatinosos pueden llegar a dominar la comunidad zooplactónica tal y como se muestra en los *Capítulos* 2 y 3 para el caso concreto de las salpas. El crecimiento masivo de estos organismos ejerce un fuerte impacto en la biogeoquímica marina (por ejemplo, en el transporte activo de nitrógeno). Sin embargo, poco se sabe del metabolismo excretor del zooplancton gelatinoso en general, y de las medusas, en particular. En un escenario en el que esta clase de organismos revestirá una gran importancia en todos los océanos del planeta,

estudiar su papel en el reciclaje de nutrientes y la relación que la excreción de NH_4^+ mantiene con el sistema bioquímico, es una necesidad.

References

Aguiar-González, B., Packard, T.T., Berdalet, E., Roy, S., Gómez, M., 2012. Respiration predicted from an enzyme kinetic model and the metabolic theory of ecology in two species of marine bacteria. J. Exp. Mar. Biol. Ecol. 412, 1–12.

Al-Mutairi, H., Landry, M.R., 2001. Active export of carbon and nitrogen at Station ALOHA by diel migrant zooplankton. Deep-Sea Res. II 48, 2083–2103.

Alcaraz, M., Almeda, R., Calbet, A., Saiz, E., Duarte, C.M., Lasternas, S., Agustí, S., Santiago, R., Movilla, J., Alonso, A., 2010. The role of arctic zooplankton in biogeochemical cycles: respiration and excretion of ammonia and phosphate during summer. Polar Biol. 33 (12), 1719–1731.

Alcaraz, M., Almeda, R., Saiz, E., Calbet, A., Duarte, C.M., Agustí, S., Santiago, R., Alonso, A., 2013. Effects of temperature on the metabolic stoichiometry of Arctic zooplankton. Biogeosciences 10 (2), 689–697.

Alcaraz, M., Saiz, E., Calbet, A., Trepat, I., 2003. Estimating zooplankton biomass through image analysis. Mar. Biol. 143 (2), 307–315.

Alonso-González, I.J., Arístegui, J., Lee, C., Sánchez-Vidal, A., Calafat, A., Fabrés, J., Sangrá, P., Masqué, P., Hernández-Guerra, A., Benítez-Barrios, V., 2010. Role of slowly settling particles in the ocean carbon cycle. Geophys. Res. Lett. 37 (13), L13608.

Alonso-González, I.J., Arístegui, J., Vilas, J.C., Hernández-Guerra, A., 2009. Lateral POC transport and consumption in surface and deep waters of the Canary Current region: A box model study. Global Biogeochem. Cy. 23 (2), GB2007.

Andersen, V., 1998. Salp and pyrosomid blooms and their importance in biogeochemical cycles. In: Q. Bone (Ed.), The biology of pelagic tunicates. The biology of pelagic tunicates. Oxford University Press, Oxford, pp. 125–137.

Anderson, T.R., 1992. Modelling the influence of food C:N ratio, and respiration on growth and nitrogen excretion in marine zooplankton and bacteria. J. Plankton Res. 14 (12), 1645–1671.

Aragão, C., Conceição, L.E.C., Dinis, M.T., Fyhn, H.J., 2004. Amino acid pools of rotifers and Artemia under different conditions: Nutritional implications for fish larvae. Aquaculture 234 (1-4), 429–445.

Ariew, R., 1976. Ockham's razor: A historical and philosophical analysis of Ockham's principle of parsimony. Pap. Bibliogr. Soc. Am. 70, 101.

Arístegui, J., Gasol, J.M., Duarte, C.M., Herndl, G.J., 2009. Microbial oceanography of the dark ocean's pelagic realm. Limnol. Oceanogr. 54 (5), 1501–1529.

Arístegui, J., Montero, M.F., 1995. The relationship between community respiration and ETS activity in the ocean. J. Plankton Res. 17 (7), 1563–1571.

Ariza, A., Garijo, J.C., Landeira, J.M., Bordes, F., Hernández-León, S., 2015. Migrant biomass and respiratory carbon flux by zooplankton and micronekton in the subtropical northeast Atlantic Ocean (Canary Islands). Prog. Oceanogr. 134, 1–13.

Atkinson, A., Whitehouse, M.J., 2001. Ammonium regeneration by Antarctic mesozooplankton: an allometric approach. Mar. Biol. 139, 301–311.

Baltar, F., Arístegui, J., Gasol, J.M., Sintes, E., Herndl, G.J., 2009. Evidence of prokaryotic metabolism on suspended particulate organic matter in the dark waters of the subtropical North Atlantic. Limnol. Oceanogr. 54 (1), 182–193.

Bamstedt, U., 1980. ETS activity as an estimator of respiratory rate of zooplankton populations. The significance of variations in environmental factors. J. Exp. Mar. Biol. Ecol. 42 (3), 267–283.

Bamstedt, U., Holt, M.R., 1978. Experimental studies on the deep-water pelagic community of Korsfjorden, Western Norway. Prey-size preference and feeding of *Euchaeta norvegica* (Gopepoda). Sarsia 63 (4), 225–236.

Banse, K., 1977. Determining the carbon-to-chlorophyll ratio of natural phytoplankton. Mar. Biol. 41 (3), 199–212.

Barton, J.S., Fisher, J.R., 1971. Nonlinear kinetics of glutamate dehydrogenase. Studies with substrates - glutamate and nicotinamide-adenine dinucleotide. Biochemistry 10 (4), 577–585.

Batrel, Y., Regnault, M., 1985. Metabolic pathways of Ammoniogenesis in the shrimp Crangon crangon L.: Possible role of glutamate dehydrogenase. Comp. Biomchem. Physiol. 82B (2), 217–222.

Beckmann, A., Hense, I., 2009. A fresh look at the nutrient cycling in the oligotrophic ocean. Biogeochemistry 96, 1–11.

Benachenhou-Lahfa, N., Forterre, P., Labedan, B., 1993. Evolution of glutamate dehydrogenase genes: evidence for two paralogous protein families and unusual branching patterns of the archaebacteria in the universal tree of life. J. Mol. Evol. 36 (4), 335–346.

Benavides, M., Santana-Falcón, Y., Wasmund, N., Arístegui, J., 2014. Microbial uptake and regeneration of inorganic nitrogen off the coastal Namibian upwelling system. J. Mar. Syst. 140 (B), 123–129.

Bergen, B., Herlemann, D.P.R., Jürgens, K., 2015. Zonation of bacterioplankton communities along aging upwelled water in the northern Benguela upwelling. Front. Microbiol. 6, 1–13.

Berges, J.A., Mulholland, M.R., 2008. Enzymes and nitrogen cycling. In: E.J. Carpenter, D.G. Capone (Eds.), Nitrogen in the marine environment. Academic Press, London, pp. 1385–1444.

Berges, J.A., Roff, J.C., Ballantyne, J.S., 1990. Relationship between body size, growth rate and maximal enzyme activities in the brine shrimp, *Artemia franciscana*. Biol. Bull. 179, 287–296.

Berges, J.A., Roff, J.C., Ballantyne, J.S., 1993. Enzymatic indices of respiration and ammonia excretion: relationships to body size and food levels. J. Plankton Res. 15 (2), 239–254.

Bidigare, R.R., 1983. Nitrogen excretion by marine zooplankton. In: E.J. Carpenter, D.G. Capone (Eds.), Nitrogen in the marine environment. Academic Press, Inc., New York, pp. 385–409.

Bidigare, R.R., King, F.D., 1981. The measurement of glutamate dehydrogenase activity in *Praunus flexuosus* and its role in the regulation of ammonium excretion. Comp. Biochem. Physiol. 70 (B), 409–413.

Bidigare, R.R., King, F.D., Biggs, D.C., 1982. Glutamate dehydrogenase (GDH) and respiratory electron-transport-system (ETS) activities in Gulf of México zooplankton. J. Plankton Res. 4 (4), 895–911.

Bisswanger, H., 2008. Enzyme kinetics: Principles and methods. 2nd ed. Wiley-VCH Verlag GmbH & Co., Weinheim, 301 pp.

Bisswanger, H., 2011. Practical enzymology. 2nd ed. Wiley-VCH Verlag GmbH & Co., Weinheim, 360 pp.

Bode, A., Álvarez-Ossorio, M.T., 2004. Taxonomic versus trophic structure of mesozooplankton: a seasonal study of species succession and stable carbon and nitrogen isotopes in a coastal upwelling ecosystem. ICES J. Mar. Sci. 61 (4), 563–571.

Bode, A., Álvarez-Ossorio, M.T., González, N., 1998. Estimations of mesozooplankton biomass in a coastal upwelling area off NW Spain. J. Plankton Res. 20 (5), 1005–1014.

Bode, A., Álvarez-Ossorio, M.T., González, N., Lorenzo, J., Rodríguez, C., Varela, M., Varela, M.M., 2005. Seasonal variability of plankton blooms in the Ria de Ferrol (NW Spain): II. Plankton abundance, composition and biomass. Est. Coast. Shelf Sci. 63 (1-2), 285–300.

Bode, A., Barquero, S., González, N., Álvarez-Ossorio, M.T., Varela, M., 2004. Contribution of heterotrophic plankton to nitrogen regeneration in the upwelling ecosystem of A Coruña (NW Spain). J. Plankton Res. 26 (1), 11–28.

Bode, M., Schukat, A., Hagen, W., Auel, H., 2013. Predicting metabolic rates of calanoid copepods. J. Exp. Mar. Biol. Ecol. 444, 1–7.

Boltovskoy, D., 1999. South Atlantic zooplankton, vol. 1. Backhuys Leiden, 1075 pp.

Boraas, M.E., Bennett, W.N., 1988. Steady-state rotifer growth in a two-stage, computer-controlled turbidostat. J. Plankton Res. 10 (5), 1023–1038.

Boyd, A.J., Salat, J., Masó, M., 1987. The seasonal intrusion of relatively saline water on the shelf off northern and central Namibia. S. Afr. J. Mar. Sci. 5 (1), 107–120.

Boyer, D., Cole, J., Bartoholomae, C., 2000. Southwestern Africa: Northern Benguela current region. Mar. Pollut. Bull. 41 (1-6), 123–140.

Bronk, D.A., Glibert, P.M., Ward, B.B., 1994. Nitrogen uptake, dissolved organic nitrogen release and new production. Science 265, 1843–1846.

Bronk, D.A., Steinberg, D.K., 2008. Nitrogen regeneration. In: E.J. Carpenter, D.G. Capone (Eds.), Nitrogen in the marine environment. Academic Press, London, pp. 385–467.

Brown, J.H., Allen, A.P., Gillooly, J.F., 2007. The metabolic theory of ecology and the role of body size in marine and freshwater ecosystems. In: A. Hildrew, D. Raffaelli, R. Edmonds Brown (Eds.), Body size: the structure and function of aquatic ecosystems. Cambridge University Press, Cambridge, pp. 1 – 15.

Brown, P.C., Painting, S.J., Cochrane, K.L., 1991. Estimates of phytoplankton and bacterial biomass and production in the northern and southern Benguela ecosystems. Afr. J. Mar. Sci. 11 (1), 537–564.

Buchan, A., LeCleir, G.R., Gulvik, C.A., González, J.M., 2014. Master recyclers: Features and functions of bacteria associated with phytoplankton blooms. Nat. Rev. Microbiol. 12, 686–698.

Buesseler, K.O., 1991. Do upper-ocean sediment traps provide an accurate record of particle flux? Nature 353, 420–423.

Buesseler, K.O., 1998. The decoupling of production and particulate export in the sea surface. Global Biogeochem. Cy. 12 (2), 297–310.

Buesseler, K.O., Boyd, P.W., 2009. Shedding light on processes that control particle export and flux attenuation in the twilight zone of the open ocean. Limnol. Oceanogr. 54 (4), 1210–1232.

Buesseler, K.O., Lamborg, C.H., Boyd, P.W., Lam, P.J., Trull, T.W., Bidigare, R.R., Bishop, J.K.B., Casciotti, K.L., Dehairs, F., Elskens, M., Honda, M., Karl, D.M., Siegel, D.A., Silver, M.W., Steinberg, D.K., Valdes, J., Van Mooy, B., Wilson, S., 2007. Revisiting carbon flux through the ocean's twilight zone. Science 316, 567–570.

Burd, A.B., Hansell, D.A., Steinberg, D.K., Anderson, T.R., Arístegui, J., Baltar, F., Beaupré, S.R., Buesseler, K.O., Dehairs, F., Jackson, G.A., Kadko, D.C., Koppelmann, R., Lampitt, R.S., Nagata, T., Reinthaler, T., Robinson, C., Robison, B.H., Tamburini, C., Tanaka, T., 2010. Assessing the apparent imbalance between geochemical and biochemical indicators of meso- and bathypelagic biological activity What: the @$#! is wrong with present calculations of carbon budgets? Deep-Sea Res. II 57 (16), 1557–1571.

Calbet, A., 2001. Mesozooplankton grazing impact on primary production: A global comparative analysis in marine ecosystems. Limnol. Oceanogr. 46 (7), 1824–1830.

Calbet, A., Landry, M.R., 2004. Phytoplankton growth, microzooplankton grazing, and carbon cycling in marine systems. Limnol. Oceanogr. 49 (1), 51–57.

Campbell, R.W., Boutillier, P., Dower, J.F., 2004. Ecophysiology of overwintering in the copepod Neocalanus plumchrus: changes in lipid and protein contents over a seasonal cycle. Mar. Ecol. Prog. Ser. 280, 211–226.

Caron, D.A., Goldman, J.C., 1990. Protozoan nutrient regeneration . In: G.M. Capriulo (Ed.), Ecology of marine protozoa. Oxford University Press, New York, pp. 283–306.

Chapman, P., Mitchell-Innes, B.A., Walker, R., 1994. Microplankton ETS measurements as a means of assessing respiration in the Benguela ecosystem. Afr. J. Mar. Sci. 14, 297–312.

Christensen, J.P., Owens, T.G., Devol, A.H., Packard, T.T., 1980. Respiration and physiological state in marine bacteria. Mar. Biol. 55, 267–276.

Cleland, W.W., 1963. The kinetics of enzyme - catalyzed reactions with two or more substrates or products: I. Nomenclature and rate equations. Biochim. Biophys. Acta 67, 104 – 137.

Cury, P., Shannon, L., 2004. Regime shifts in upwelling ecosystems: Observed changes and possible mechanisms in the northern and southern Benguela. Prog. Oceanogr. 60, 223–243.

Dam, H.G., Roman, M.R., Youngbluth, M.J., 1995. Downward export of respiratory carbon and dissolved inorganic nitrogen by diel-migrant mesozooplankton at the JGOFS Bermuda time-series station. Deep-Sea Res. I 42 (7), 1187–1197.

De La Rocha, C.L., Passow, U., 2007. Factors influencing the sinking of POC and the efficiency of the biological carbon pump. Deep-Sea Res. II: Top. Stud. Oceanogr. 54 (5-7), 639–658.

De León, A.R., Braun, J.G., 1973. Annual cycle of primary production and its relation to nutrients in the Canary Islands waters. Bol. Inst. Esp. Oceanogr. 167, 1–24.

del Giorgio, P.A., 1992. The relationship between ETS (electron transport system) activity and oxygen consumption in lake plankton: A cross-system calibration. J. Plankton Res. 14 (12), 1723–1741.

Dolan, R.J., Montagnes, D.J.S., Agatha, S., Coats, D.W., Stoecker, D.K., 2012. The biology and ecology of tintinnid ciliates: Models for marine plankton. Wiley-Blackwell, Chichester, UK, 296 pp.

Domingues, P.M., Fores, R., Turk, P.E., Lee, P.G., Andrade, J.P., 2000. Mysid culture: lowering costs with alternative diets. Aquac. Res. 31, 719–728.

Domingues, P.M., Turk, P.E., Andrade, J.P., Lee, P.G., 1998. Pilot-scale production of mysid shrimp in a static water system. Aquacult. Int. 6, 387–402.

Ducklow, H., 2000. Bacterial production and biomass in the oceans. In: D.L. Kirchman (Ed.), Microbial ecology of the oceans. Wiley-Liss, New York, pp. 85–120.

Ducklow, H.W., Doney, S.C., 2013. What is the metabolic state of the oligotrophic ocean? A debate. Annu. Rev. Mar. Sci. 5 (1), 525–533.

Dugdale, R.C., Goering, J.J., 1967. Uptake of new and regenerated forms of nitrogen in primary productivity. Limnol. Oceanogr. 12, 196–206.

Engel, P.C., Dalziel, K., 1970. Kinetic studies of glutamate dehydrogenase: The reductive amination of 2-oxoglutarate. Biochem. J. 118, 409–419.

Eppley, R.W., 1978. Nitrate reductase in marine phytoplankton. In: J.A. Hellebust, J.S. Craige (Eds.), Handbook of phycological methods. Physiological and biochemical methods. Cambridge University Press, Cambridge, pp. 217–223.

Eppley, R.W., Peterson, B.J., 1979. Particulate organic matter flux and planktonic new production in the deep ocean. Nature 282, 677–680.

Falkowski, P.G., Barber, R.T., Smetacek, V., 1998. Biogeochemical Controls and Feedbacks on Ocean Primary Production. Science 281, 200–206.

Fernández-Urruzola, I., Osma, N., Packard, T.T., Gómez, M., Postel, L., 2014. Distribution of zooplankton biomass and potential metabolic activities across the northern Benguela upwelling system. J. Mar. Syst. 140 (B), 138–149.

Fernández-Urruzola, I., Packard, T.T., Gómez, M., 2011. GDH activity and ammonium excretion in the marine mysid, *Leptomysis lingvura*: Effects of age and starvation. J. Exp. Mar. Biol. Ecol. 409 (1-2), 21–29.

Frieden, C., Colman, F., 1967. Glutamate dehydrogenase concentration as a determinant in the effect of purine nucleotides on enzymatic activity. J. Biol. Chem. 242, 1705–1715.

Friedmann, H.C., 1981. Enzymes, benchmark papers in biochemistry, vol. I. Hutchinson Ross Publishing Company, Pennsylvania.

Frigerio, F., Casimir, M., Carobbio, S., Maechler, P., 2008. Tissue specificity of mitochondrial glutamate pathways and the control of metabolic homeostasis. Biochim. Biophys. Acta 1777 (7-8), 965–972.

Fry, B., Wainright, S.C., 1991. Diatom sources of ^{13}C-rich carbon in marine food webs. Mar. Ecol. Prog. Ser. 76, 149–157.

Gardner, W.D., 2000. Sediment trap sampling in surface waters. In: The changing ocean carbon cycle: a midterm synthesis of the Joint Global Ocean Flux Study. Cambridge University Press, Cambridge, pp. 240–284.

Gibbons, M.J., 1997. An introduction to the zooplankton of the Benguela current region. Zoology department, University of Western Cape, Cape Town, South Africa, 51 pp.

Gibbons, M.J., Hutchings, L., 1996. Zooplankton diversity and community structure around southern Africa, with special attention to the Benguela upwelling system. S. Afr. J. Sci. 92 (2), 63–77.

Gibbons, M.J., Stuart, V., Verheye, H.M., 1992. Trophic ecology of carnivorous zooplankton in the Benguela. Afr. J. Mar. Sci. 12 (1), 421–437.

Giraudeau, J., Bailey, G.W., Pujol, C., 2000. A high-resolution time-series analyses of particle fluxes in the Northern Benguela coastal upwelling system: carbonate record of changes in biogenic production and particle transfer processes. Deep-Sea Res. II 47 (9-11), 1999–2028.

Glazier, D.S., 2006. The 3/4-Power law is not universal: Evolution of isometric, ontogenetic metabolic scaling in pelagic animals. BioScience 56 (4), 325–332.

Glibert, P.M., 1993. The interdependence of uptake and release of NH_4^+ and organic nitrogen. Mar. Microbiol. Food Webs 7 (1), 53–67.

Glibert, P.M., 1998. Interactions of top-down and bottom-up control in planktonic nitrogen cycling. Hydrobiologia 363, 1–12.

Glibert, P.M., Lipschultz, F., McCarthy, J.J., Altabet, M.A., 1982. Isotope dilution models of uptake and remineralization of ammonium by marine plankton. Limnol. Oceanogr. 27 (4), 639–650.

Guillard, R.R.L., 1975. Culture of phytoplankton for feeding marine invertebrates. In: Culture of marine invertebrate animals. Plenum Publishing Corp., New York, pp. 108–132.

Hans-Otto, B., Michal, G., 1974. L-glutamate: Determination with glutamate dehydrogenase, diaphorase, and Tetrazolium salts. In: H.U. Bergmeyer (Ed.), Methods of enzymatic analysis. Verlag Chemie GmbH, pp. 1708–1713.

Hansen, A., Wasmund, N., Ohde, T., 2014. Phytoplankton succession in aging upwelled waters off Namibia. J. Mar. Syst. 140 (B), 130–137.

Hansen, F.C., Cloete, R.R., Verheye, H.M., 2005. Seasonal and spatial variability of dominant copepods along a transect off Walvis Bay (23°S), Namibia. Afr. J. Mar. Sci. 27 (1), 55–63.

Harrison, W.G., 1992. Regeneration of nutrients. In: P.G. Falkowski, A.D. Woodhead (Eds.), Primary productivity and biogeochemical cycles in the sea. Plenum Press, New York, pp. 385–409.

Harrison, W.G., Platt, T., Lewis, M.R., 1987. f-Ratio and its relationship to ambient nitrate concentration in coastal waters. J. Plankton Res. 9 (1), 235–248.

Hernández-León, S., Almeida, C., Bécognée, P., Yebra, L., Arístegui, J., 2004. Zooplankton biomass and indices of grazing and metabolism during a late winter bloom in subtropical waters. Mar. Biol. 145 (6), 1191–1200.

Hernández-León, S., Almeida, C., Gómez, M., Torres, S., Montero, I., Portillo-Hahnefeld, A., 2001. Zooplankton biomass and indices of feeding and metabolism in island-generated eddies around Gran Canaria. J. Mar. Syst. 30 (1-2), 51–66.

Hernández-León, S., Almeida, C., Portillo-Hahnefeld, A., Gómez, M., Rodríguez, J.M., Arístegui, J., 2002. Zooplankton biomass and indices of feeding and metabolism in relation to an upwelling filament off northwest Africa. J. Mar. Res. 60, 327–346.

Hernández-León, S., Fraga, C., Ikeda, T., 2008. A global estimation of mesozooplankton ammonium excretion in the open ocean. J. Plankton Res. 30 (5), 577–585.

Hernández-León, S., Gómez, M., 1996. Factors affecting the respiration/ETS ratio in marine zooplankton. J. Plankton Res. 18 (2), 239–255.

Hernández-León, S., Ikeda, T., 2005. A global assessment of mesozooplankton respiration in the ocean. J. Plankton Res. 27 (2), 153–158.

Hernández-León, S., Postel, L., Arístegui, J., Gómez, M., Montero, M.F., Torres, S., Almeida, C., Kühner, E., Brenning, U., Hagen, E., 1999. Large-scale and mesoscale distribution of plankton biomass and metabolic activity in the Northeastern Central Atlantic. J. Oceanogr. 55, 471–482.

Hernández-León, S., Torres, S., 1997. The relationship between ammonia excretion and GDH activity in marine zooplankton. J. Plankton Res. 19 (5), 587–601.

Herrera, A., Gómez, M., Molina, L., Otero, F., Packard, T., 2011a. Rearing techniques and nutritional quality of two mysids from Gran Canaria (Spain). Aquac. Res. 42, 677–683.

Herrera, A., Packard, T., Santana, A., Gómez, M., 2011b. Effect of starvation and feeding on respiratory metabolism in *Leptomysis lingvura* (G.O. Sars, 1866). J. Exp. Mar. Biol. Ecol. 409, 154–159.

Hidaka, K., Kawaguchi, K., Murakami, M., Takahashi, M., 2001. Downward transport of organic carbon by diel migratory micronekton in the western equatorial Pacific: its quantitative and qualitative importance. Deep-Sea Res. I 48, 1923–1939.

Holmes, R.M., Aminot, A., Kérouel, R., Hooker, B.A., Peterson, B.J., 1999. A simple and precise method for measuring ammonium in marine and freshwater ecosystems. Can. J. Fish. Aquat. Sci. 56, 1801–1808.

Huenerlage, K., Buchholz, F., 2013. Krill of the northern Benguela current and the Angola-Benguela frontal zone compared: physiolofical performance and short-term starvation in *Euphausia hanseni*. J. Plankton Res. 35 (2), 337–351.

Huggett, J., Verheye, H., Escribano, R., Fairweather, T., 2009. Copepod biomass, size composition and production in the southern Benguela: Spatio-temporal patterns of variation, and comparison with other eastern boundary upwelling systems. Prog. Oceanogr. 83 (1-4), 197–207.

Hutchings, L., Pillar, S.C., Verheye, H.M., 1991. Estimates of standing stock, production and consumption of meso- and macrozooplankton in the Benguela ecosystem. Afr. J. Mar. Sci. 11 (1), 499–512.

Hutchings, L., Van der Lingen, C.D., Shannon, L.J., Crawford, R.J.M., Verheye, H.M.S., Bartholomae, C.H., van der Plas, A.K., Louw, D., Kreiner, A., Ostrowski, M., Fidel, Q., Barlow, R.G., Lamont, T., Coetzee, J., Shillington, F., Veitch, J., Currie, J.C., Monteiro, P.M.S., 2009. The Benguela current: An ecosystem of four components. Prog. Oceanogr. 83 (1-4), 15–32.

ICES, 2001. ICES identification leaflets for plankton, 1939-2001. International Council for the Exploration of the Sea 1-187.

Ikeda, T., 1977. The effect of laboratory conditions on the extrapolation of experimental measurements to the ecology of marine zooplankton. IV. Changes in respiration and excretion rates of boreal zooplankton species maintained under fed and starved conditions. Mar. Biol. 41 (3), 241–252.

Ikeda, T., 1985. Metabolic rates of epipelagic marine zooplankton as a function of body mass and temperature. Mar. Biol. 85, 1–11.

Ikeda, T., 2014. Respiration and ammonia excretion by marine metazooplankton taxa: synthesis toward a global-bathymetric model. Mar. Biol. , 1–14.

Ikeda, T., Fay, E.H., Hutchinson, S.A., Boto, G.M., 1982. Ammonia and inorganic phosphate excretion by zooplankton from inshore waters of the Great Barrier Reef, Queensland. I. Relationship between excretion rates and body size. Mar. Freshwater Res. 33 (1), 55–70.

Ikeda, T., Kanno, Y., Ozaki, K., Shinada, A., 2001. Metabolic rates of epipelagic marine copepods as a function of body mass and temperature. Mar. Biol. 139, 587–596.

Ikeda, T., Motoda, S., 1978. Estimated zooplankton production and their ammonia excretion in the Kuroshio and adjacent seas. Fish. Bull. 76 (2), 357–367.

Ikeda, T., Skjoldal, H.R., 1980. The effect of laboratory conditions on the extrapolation of experimental measurements to the ecology of marine zooplankton VI. Changes in physiological activities and biochemical components of *Acetes sibogae australis* and *Acartia australis* after capture. Mar. Biol. 58 (4), 285 – 293.

Ikeda, T., Skjoldal, H.R., 1989. Metabolism and elemental composition of zooplankton from the Barents Sea during early Arctic summer. Mar. Biol. 100, 173–183.

Ikeda, T., Torres, J.J., Hernández-León, S., Geiger, S.P., 2000. Metabolism. In: R.P. Harris, P.H. Wiebe, J. Lenz, H.R. Skjoldal, M. Huntley (Eds.), ICES Zooplankton methodology manual. Academic Press, San Diego, pp. 455–532.

Irigoien, X., 2005. Phytoplankton blooms: a "loophole" in microzooplankton grazing impact? J. Plankton Res. 27 (4), 313–321.

Isla, J.A., Anadón, R., 2004. Mesozooplankton size-fractionated metabolism and feeding off NW Spain during autumn: effects of a poleward current. ICES J. Mar. Sci. 61 (4), 526–534.

Isla, J.A., Ceballos, S., Anadón, R., 2004a. Mesozooplankton metabolism and feeding in the NW Iberian upwelling. Est. Coast. Shelf Sci. 61 (1), 151–160.

Isla, J.A., Llope, M., Anadón, R., 2004b. Size-fractionated mesozooplankton biomass, metabolism and grazing along a 50°N-30°S transect of the Atlantic Ocean. J. Plankton Res. 26 (11), 1301–1313.

Iversen, M.H., Ploug, H., 2010. Ballast minerals and the sinking carbon flux in the ocean: carbon-specific respiration rates and sinking velocity of marine snow aggregates. Biogeosciences 7 (9), 2613–2624.

Jaeger, J.M., Nittrouer, C.A., DeMaster, D.J., Kelchner, C., Dunbar, R.B., 1996. Lateral transport of settling particles in the Ross Sea and implications for the fate of biogenic material. J. Geophys. Res. 101 (C8), 18,479–18,488.

Karl, D.M., 1978. Occurrence and ecological significance of GTP in the ocean and in microbial cells. Appl. Environ. Microbiol. 36 (2), 349–355.

King, F.D., 1984. Vertical distribution of zooplankton glutamate dehydrogenase in relation to chlorophyll in the vicinity of the Nantucket Shoals. Mar. Biol. 79, 249–256.

King, F.D., Cucci, T.L., Townsend, D.W., 1987. Microzooplankton and macrozooplancton glutamate dehydrogenase as indices of the relative contribution of these fractions to ammonium regeneration in the Gulf of Maine. J. Plankton Res. 9 (2), 277–289.

King, F.D., Packard, T.T., 1975. Respiration and the activity of the respiratory electron transport system in marine zooplankton. Limnol. Oceanogr. 20 (5), 849–854.

Kiørboe, T., Møhlenberg, F., Hamburger, K., 1985. Bioenergetics of the planktonic copepod Acartia tonsa: relation between feeding, egg production and respiration, and composition of specific dynamic action. Mar. Ecol. Prog. Ser. 26, 85–97.

Kirk, K.L., 1997. Life-history responses to variable environments: Starvation and reproduction in planktonic rotifers. Ecology 78 (2), 434–441.

Kleiber, M., 1961. The fire of life: An introduction to animal energetics. John Wiley & Sons Ltd, New York, 478 pp.

Koppelmann, R., Bottger-Schnack, R., Mobius, J., Weikert, H., 2009. Trophic relationships of zooplankton in the eastern Mediterranean based on stable isotope measurements. J. Plankton Res. 31 (6), 669–686.

Langford, R.R., Youssara, F., 2003. Variations of zooplankton metabolism and feeding in the frontal area of the Alboran Sea (western Mediterranean) in winter. Oceanol. Acta 26 (2), 179–189.

Leskovac, V., 2003. Comprehensive enzyme kinetics. Kluwer Academic Publishers, New York, 438 pp.

Lindén, E., Kuosa, H., 2004. Effects of grazing and excretion by pelagic mysids (*Mysis* spp.) on the size structure and biomass of the phytoplankton community. Hydrobiologia 514, 73–78.

Lineweaver, H., Burk, D., 1934. The determinations of enzyme dissociation constants. J. Am. Chem. Soc. 56, 658–666.

Loick, N., Ekau, W., Verheye, H.M., 2005. Water-body preferences of dominant calanoid copepod species in the Angola-Benguela frontal zone. Afr. J. Mar. Sci. 27 (3), 597–608.

Longhurst, A.R., Harrison, W.G., 1988. Vertical nitrogen flux from the oceanic photic zone by diel migrant zooplankton and nekton. Deep-Sea Res. 35 (6), 881–889.

Longhurst, A.R., Harrison, W.G., 1989. The biological pump: Profiles of plankton production and consumption in the upper ocean. Prog. Oceanogr. 22 (1), 47–123.

Lowry, O.H., Rosebrough, N.J., Farr, A.L., Randall, R.J., 1951. Protein measurement with the Folin phenol reagent. J. Biol. Chem. 193, 265–275.

Lubzens, E., Gibson, O., Zmora, O., Sukenik, A., 1995. Potential advantages of frozen algae (*Nannochloropsis* sp.) for rotifer (*Brachionus plicatilis*) culture. Aquaculture 133, 295–309.

Lussier, S.M., Kuhn, A., Chammas, M.J., Sewall, J., 1988. Techniques for the laboratory culture of Mysidopsis species (Crustacea: Mysidacea). Environ. Toxicol. Chem. 7, 969–977.

Maiti, K., Benitez-Nelson, C.R., Buesseler, K.O., 2010. Insights into particle formation and remineralization using the short-lived radionuclide, Thorium-234. Geophys. Res. Lett. 37 (15), L15608.

Maldonado, F., Packard, T.T., Gómez, M., 2012. Understanding tetrazolium reduction and the importance of substrates in measuring respiratory electron transport activity. J. Exp. Mar. Biol. Ecol. 434-435, 110–118.

Margalef, R., 1982. Ecología. Omega, Barcelona, 951 pp.

Marsay, C.M., Sanders, R.J., Henson, S.A., Pabortsava, K., Achterberg, E.P., Lampitt, R.S., 2015. Attenuation of sinking particulate organic carbon flux through the mesopelagic ocean. Proc. Nati. Acad. Sci. U.S.A. 112 (4), 1089–1094.

Martin, J.H., Knauer, G.A., Karl, D.M., Broenkow, W.W., 1987. VERTEX: carbon cycling in the northeast Pacific. Deep-Sea Res. 34 (2), 267–285.

Martínez, I., Gómez, M., Packard, T.T., 2010. Potential respiration is a better respiratory predictor than biomass in young *Artemia salina*. J. Exp. Mar. Biol. Ecol. 390, 78 – 83.

Mayzaud, P., 1976. Respiration and nitrogen excretion of zooplankton. IV. The influence of starvation on the metabolism and the biochemical composition of some species. Mar. Biol. 37, 47–58.

Mayzaud, P., 1986. Enzymatic measurements of metabolic processes concerned with respiration and ammonia excretion. In: E.D.S. Corner, S.C.M. O'Hara (Eds.), The biological chemistry of marine copepods. Clarendon Press, Oxford, pp. 226–259.

Mayzaud, P., Conover, R.J., 1988. 0:N atomic ratio as a tool to describe zooplankton metabolism. Mar. Ecol. Prog. Ser. 45, 289–302.

McDonnell, A.M.P., Boyd, P.W., Buesseler, K.O., 2015. Sinking velocities and microbial respiration rates alter the attenuation of particulate carbon fluxes through the mesopelagic zone. Global Biogeochem. Cy. 29 (2), 175–193.

Miller, C.A., Roman, M.R., 2008. Effects of food nitrogen content and concentration on the forms of nitrogen excreted by the calanoid copepod, *Acartia tonsa*. J. Exp. Mar. Biol. Ecol. 359, 11–17.

Mitchell-Innes, B.A., Walker, D.R., 1991. Short-term variability during an anchor station study in the southern Benguela upwelling system: Phytoplankton production and biomass in relation to specie changes. Prog. Oceanogr. 28 (1), 65–89.

Mohrholz, V., Eggert, A., Junkers, T., Nausch, G., Ohde, T., Schmidt, M., 2014. Cross shelf hydrographic and hydrochemical conditions and their short term variability at the northern Benguela during a normal upwelling season. J. Mar. Syst. 140 (B), 92–110.

Møller, L.F., Riisgrd, H.U., 2007. Respiration in the scyphozoan jellyfish *Aurelia aurita* and two hydromedusae (*Sarsia tubulosa* and *Aequorea vitrina*): effect of size, temperature and growth. Mar. Ecol. Prog. Ser. 330, 149–154.

Moloney, C.L., 1992. Simulation studies of trophic flows and nutrient cycles in Benguela upwelling foodwebs. Afr. J. Mar. Sci. 12 (1), 457–476.

Montoya, J.P., 2008. Nitrogen Stable Isotopes in Marine Environments. In: E.J. Carpenter, D.G. Capone (Eds.), Nitrogen in the marine environment. Academic Press, London, pp. 1277–1302.

Nausch, M., Nausch, G., 2014. Phosphorus speciation and transformation along transects in the Benguela upwelling region. J. Mar. Sys. 140 (B), 111–122.

Nelson, G., Hutchings, L., 1983. The Benguela upwelling area. Prog. Oceanogr. 12 (3), 333–356.

Niehoff, B., Schmithüsen, T., Knüppel, N., Daase, M., Czerny, J., Boxhammer, T., 2013. Mesozooplankton community development at elevated CO_2 concentrations: results from a mesocosm experiment in an Arctic fjord. Biogeosciences 10 (3), 1391–1406.

Olivar, M.P., Barangé, M., 1990. Zooplankton of the northern Benguela region in a quiescent upwelling period. J. Plankton Res. 12 (5), 1023–1044.

Omori, M., Ikeda, T., 1984. Methods in marine zooplankton ecology. John Wiley & Sons, Ltd., New York, 332 pp.

O'Reilly, C.M., Hecky, R.E., Cohen, A.S., Plisnier, P.D., 2002. Interpreting stable isotopes in food webs: Recognizing the role of time averaging at different trophic levels. Limnol. Oceanogr. 47 (1), 306–309.

Osma, N., Fernández-Urruzola, I., Packard, T.T., Postel, L., Gómez, M., Pollehne, F., 2014. Short-term patterns of vertical particle flux in northern Benguela: a comparison between sinking POC and respiratory carbon consumption. J. Mar. Syst. 140 (B), 150–162.

Owens, T., King, F.D., 1975. The measurement of respiratory electron transport system activity in marine zooplankton. Mar. Biol. 30 (1), 27–36.

Packard, T.T., 1979. Respiration and respiratory electron transport activity in plankton from the Northwest African upwelling area. J. Mar. Res. 37 (4), 711–742.

Packard, T.T., 1985. Oxygen consumption in the ocean: Measuring and mapping with enzyme analysis. In: A. Zirino (Ed.), Mapping Strategies in Chemical Oceanography. American Chemical Society, Washington D.C., pp. 177–209.

Packard, T.T., Berdalet, E., Blasco, D., Roy, S.O., St-Amand, L., Lagacé, B., Lee, K., Gagné, J.P., 1996a. CO_2 production predicted from isocitrate dehydrogenase activity and bisubstrate enzyme kinetics in the marine bacterium *Pseudomonas nautica*. Aquat. Microb. Ecol. 11, 11–19.

Packard, T.T., Berdalet, E., Blasco, D., Roy, S.O., St-Amand, L., Lagacé, B., Lee, K., Gagné, J.P., 1996b. Oxygen consumption in the marine bacterium *Pseudomonas nautica* predicted from ETS activity and bisubstrate enzyme kinetics. J. Plankton Res. 18 (10), 1819–1835.

Packard, T.T., Blasco, D., Estrada, M., 2004. Modeling Physiological processes in plankton on enzyme kinetic principles. Sci. Mar. 68 (1), 49–56.

Packard, T.T., Christensen, J.P., 2004. Respiration and vertical carbon flux in the Gulf of Maine water column. J. Mar. Res. 62 (1), 93–115.

Packard, T.T., Denis, M., Rodier, M., Garfield, P., 1988. Deep-ocean metabolic CO_2 production: calculations from ETS activity. Deep-Sea Res. 35 (3), 371–382.

Packard, T.T., Devol, A., King, F.D., 1975. The effect of temperature on the respiratory electron transport system in marine plankton. Deep-Sea Res. 22 (4), 237–249.

Packard, T.T., Gómez, M., 2008. Exploring a first-principles-based model for zooplankton respiration. ICES J. Mar. Sci. 65 (3), 371–378.

Packard, T.T., Gómez, M., 2013. Modeling vertical carbon flux from zooplankton respiration. Prog. Oceanogr. 110 (C), 59–68.

Packard, T.T., Harmon, D., Boucher, D., 1974. Respiratory electron transport activity in plankton from upwelled waters. Tethys 6 (1-2), 213–222.

Packard, T.T., Healy, M.L., Richards, F.A., 1971. Vertical distribution of the activity of the respiratory electron transport system in marine plankton. Limnol. Oceanogr. 16 (1), 60–70.

Packard, T.T., Osma, N., Fernández-Urruzola, I., Codispoti, L.A., Christensen, J.P., Gómez, M., 2015. Peru upwelling plankton respiration: calculations of carbon flux, nutrient retention efficiency, and heterotrophic energy production. Biogeosciences 12, 2641–2654.

Packard, T.T., Williams, P.J.L., 1981. Rates of respiratory oxygen consumption and electron transport in surface seawater from the northwest Atlantic. Oceanol. Acta 4 (3), 351–358.

Park, Y.C., 1986a. Impact of starvation and feeding experiments on ammonium excretion and glutamate dehydrogenase activity of zooplankton. Kor. Biochem. J. 19 (1), 251–256.

Park, Y.C., 1986b. Nitrogen regeneration and glutamate dehydrogenase activity of macrozooplankton in the Southeastern Sea of Korea. J. Oceanol. Soc. Korea 21 (2), 110–117.

Park, Y.C., Carpenter, E.J., Falkowski, P.G., 1986. Ammonium excretion and glutamate dehydrogenase activity of zooplankton in Great South Bay, New York. J. Plankton Res. 8 (3), 489–503.

Parsons, T.R., Maita, Y., Lalli, C.M., 1984. Manual of chemical and biological methods for seawater analysis. Pergamon Press, New York, 173 pp.

Pérez-Aragón, M., Fernández, C., Escribano, R., 2011. Nitrogen excretion by mesozooplankton in a coastal upwelling area: Seasonal trends and implications for biological production. J. Exp. Mar. Biol. Ecol. 406 (1-2), 116–124.

Peterson, P.E., Smith, T.J., 1999. The structure of bovine glutamate dehydrogenase provides insights into the mechanism of allostery. Structure 7 (7), 769–782.

Phillips, B., Kremer, P., Madin, L.P., 2008. Defecation by Salpa thompsoni and its contribution to vertical flux in the Southern Ocean. Mar. Biol. 156 (3), 455–467.

Ploug, H., Iversen, M.H., Koski, M., Buitenhuis, E.T., 2008. Production, oxygen respiration rates, and sinking velocity of copepod fecal pellets: Direct measurements of ballasting by opal and calcite. Limnol. Oceanogr. 53 (2), 469–476.

Postel, L., 1995. Rostock zooplankton studies off West Africa. Helgol. Meeresunters 49, 829–857.

Postel, L., da Silva, A.J., Mohrholz, V., Lass, H.U., 2007. Zooplankton biomass variability off Angola and Namibia investigated by a lowered ADCP and net sampling. J. Mar. Syst. 68 (1-2), 143–166.

Postel, L., Fock, H., Hagen, W., 2000. Biomass and abundance. In: R.P. Harris, P.H. Wiebe, J. Lenz, H.R. Skjoldal, M. Huntley (Eds.), ICES Zooplankton methodology manual. Academic Press, San Diego, pp. 83–192.

Postel, L., Mohrholz, V., Packard, T.T., 2014. Upwelling and successive ecosystem response in the Northern Benguela Region – an in situ experiment. J. Mar. Syst. 140 (B), 73–81.

Probyn, T.A., 1987. Ammonium regeneration by microplankton in an upwelling environment. Mar. Ecol. Prog. Ser. 37, 53–64.

Regnault, M., 1987. Nitrogen excretion in marine and fresh-water crustacea. Biol. Rev. 62, 1–24.

Richardson, A.J., Bakun, A., Hays, G.C., Gibbons, M.J., 2009. The jellyfish joyride: causes, consequences and management responses to a more gelatinous future. Trends Ecol. Evol. 24 (6), 312–322.

Richardson, A.J., Verheye, H.M., 1999. Growth rates of copepods in the southern Benguela upwelling system: The interplay between body size and food. Limnol. Oceanogr. 44 (2), 382–392.

Richardson, K., 1991. Comparison of ^{14}C primary production determinations made by different laboratories. Mar. Ecol. Prog. Ser. 72, 189–201.

Ricker, W.E., 1973. Linear Regressions in Fishery Research. J. Fish. Res. Bd. Can. 30 (3), 409–434.

Ridgwell, A., Rodengen, T.J., Kohfeld, K.E., 2011. Geographical variations in the effectiveness and side effects of deep ocean carbon sequestration. Geophys. Res. Lett. 38 (17), L17610.

Riedl, R., 1983. Flora und fauna des mittelmeeres. Paul Parey, Hamburg und Berlin, 836 pp.

Rife, J.E., Cleland, W.W., 1980. Kinetic mechanism of glutamate dehydrogenase. Biochemistry 19, 2321–2328.

Roy, S.O., Packard, T.T., 2001. CO_2 production rate predicted from isocitrate dehydrogenase activity, intracellular substrate concentrations and kinetic constants in the marine bacterium *Pseudomonas nautica*. Mar. Biol. 138, 1251–1258.

Rutter, W.J., 1967. Protein determination in embryos. In: F.H. Wilt, N.V. Wessels (Eds.), Methods in Developmental Biology. Academic Press, London, pp. 671–684.

Saba, G.K., Steinberg, D.K., Bronk, D.A., 2009. Effects of diet on release of dissolved organic and inorganic nutrients by the copepod *Acartia tonsa*. Mar. Ecol. Prog. Ser. 386, 147–161.

Sameoto, D., Wiebe, P., Runge, J., Postel, L., Dunn, J., Miller, C., Coombs, S., 2000. Collecting zooplankton. In: ICES Zooplankton methodology manual. Academic Press, San Diego, pp. 55–81.

Santero, E., B, A., Canosa, I., Govantes, F., 2012. Glutamate dehydrogenases: Enzymology, physiological role and biotechnological relevance. In: Dehydrogenases. InTech, pp. 289–318.

Saupe, S.M., Schell, D.M., Griffiths, W.B., 1989. Carbon-isotope ratio gradients in western arctic zooplankton. Mar. Biol. 103 (4), 427–432.

Schlüter, L., Havskum, H., 1997. Phytoplankton pigments in relation to carbon content in phytoplankton communities. Mar. Ecol. Prog. Ser. 155, 55–65.

Schneider, G., 1990. A comparison of carbon based ammonia excretion rates between gelatinous and non-gelatinous zooplankton: Implications and consequences. Mar. Biol. 106 (2), 219–225.

Schoolwerth, A.C., LaNoue, K.F., 1980. The role of microcompartmentation in the regulation of glutamate metabolism by rat kidney mitochondria. J. Biol. Chem. 255 (8), 3403–3411.

Schukat, A., Auel, H., Teuber, L., Lahajnar, N., Hagen, W., 2014. Complex trophic interactions of calanoid copepods in the Benguela upwelling system. J. Sea Res. 85, 186–196.

Schukat, A., Bode, M., Auel, H., Carballo, R., Martin, B., Koppelmann, R., Hagen, W., 2013a. Pelagic decapods in the northern Benguela upwelling system: Distribution, ecophysiology and contribution to active carbon flux. Deep-Sea Res. I 75, 146–156.

Schukat, A., Teuber, L., Hagen, W., Wasmund, N., Auel, H., 2013b. Energetics and carbon budgets of dominant calanoid copepods in the northern Benguela upwelling system. J. Exp. Mar. Biol. Ecol. 442, 1–9.

Segel, I.H., 1993. Enzyme kinetics. Behaviour and analysis of rapid equilibrium and steady-state enzyme systems. John Wiley & Sons, Inc., New York, 992 pp.

Shannon, L.V., 2001. Benguela Current. In: J.H. Steele, S.A. Thorpe, K.K. Turekian (Eds.), Encyclopedia of Ocean Sciences. Academic Press, Amsterdam, pp. 255–267.

Shannon, L.V., Nelson, G., 1996. The Benguela: Large scale features and processes and system variability. In: G. Wefer, W.H. Berger, G. Siedler, D.J. Webb (Eds.), The South Atlantic: Present and past circulation. Springer-Verlag, Heidelberg, pp. 163–210.

Shannon, L.V., Pillar, S.C., 1986. The Benguela ecosystem. Part III. Plankton. Oceanogr. Mar. Biol. Ann. Rev. 24, 65–170.

Smetacek, V., Hendrikson, P., 1979. Composition of particulate organic matter in Kiel Bight in relation to phytoplankton succession. Oceanol. Acta 2 (3), 287–298.

Smith, S.L., Whitledge, T.E., 1977. The role of zooplankton in the regeneration of nitrogen in a coastal upwelling system off northwest Africa. Deep-Sea Res. 24 (1), 49–56.

Solorzano, L., 1969. Determination of ammonia in natural waters by the phenolhypochlorite method. Limnol. Oceanogr. 14 (5), 799–801.

Sprugel, D.G., 1983. Correcting for bias in log-transformed allometic equations. Ecology 64 (1), 209–210.

Srivastava, H.S., Singh, R.P., 1987. Role and regulation of L-glutamate dehydrogenase activity in higher plants. Phytochemistry 26 (3), 597–610.

Steinberg, D.K., Goldthwait, S.A., Hansell, D.A., 2002. Zooplankton vertical migration and the active transport of dissolved organic and inorganic nitrogen in the Sargasso Sea. Deep-Sea Res. I 49, 1445–1461.

Steinberg, D.K., Saba, G.K., 2008. Nitrogen consumption and metabolism in marine zooplankton . In: E.J. Carpenter, D.G. Capone (Eds.), Nitrogen in the marine environment. Academic Press, London, pp. 1135–1196.

Steinberg, D.K., Van Mooy, B.A.S., Buesseler, K.O., Boyd, P.W., Kobari, T., Karl, D.M., 2008. Bacterial vs. zooplankton control of sinking particle flux in the ocean's twilight zone. Limnol. Oceanogr. 53 (4), 1327–1338.

Stuart, V., Verheye, H.M., 1991. Diel migration and feeding patterns of the chaetognath, *Sagitta friderici*, off the west coast of South Africa. J. Mar. Res. 49, 193–515.

Sverdrup, H.U., Johnson, M.W., Fleming, R.H., 1942. The oceans: Their physics, chemistry and general biology. Prentice-Hall, Inc., New York, 1087 pp.

Tamaru, C.S., Murashige, R., Lee, C.S., Ako, H., Sato, V., 1993. Rotifers fed various diets of baker's yeast and/or *Nannochloropsis oculata* and their effect on the growth and survival of striped mullet (*Mugil cephalus*) and milkfish (*Chanos chanos*) larvae. Aquaculture 110 (3), 361–372.

Tang, K.W., Dam, H.G., 1999. Limitation of zooplankton production: beyond stoichiometry. Oikos 84 (3), 537–542.

Timonin, A.G., 1997. Diurnal vertical migrations of zooplankton in the upwelling area off the western coast of South Africa. Oceanology 37 (1), 83–88.

Timonin, A.G., Arashkevich, E.G., Drits, A.V., Semenova, T.N., 1992. Zooplankton dynamics in the northern Benguela ecosystem, with special reference to the copepod *Calanoides carinatus*. Afr. J. Mar. Sci. 12 (1), 545–560.

Trégouboff, G., Rose, M., 1978. Manuel de planctonologie méditerranéenne. Centre National de la Recherche Scientifique, Paris, 587 pp.

Trull, T.W., Bray, S.G., Buesseler, K.O., Lamborg, C.H., Manganini, S., Moy, C., Valdes, J., 2008. In situ measurement of mesopelagic particle sinking rates and the control of carbon transfer to the ocean interior during the Vertical Flux in the Global Ocean (VERTIGO) voyages in the North Pacific. Deep-Sea Res. II: Top. Stud. Oceanogr. 55 (14-15), 1684–1695.

Van Guelpen, L., Markle, D.F., Duggan, D.J., 1982. An evaluation of accuracy, precision, and speed of several zooplankton subsampling techniques. J. Conseil 40 (3), 226–236.

Verheye, H.M., Hutchings, L., 1988. Horizontal and vertical distribution of zooplankton biomass in the southern Benguela, May 1983. Afr. J. Mar. Sci. 6 (1), 255–265.

Verheye, H.M., Hutchings, L., Huggett, J.A., Painting, S.J., 1992. Mesozooplankton dynamics in the Benguela ecosystem, with emphasis on the herbivorous copepods. Afr. J. Mar. Sci. 12 (1), 561–584.

Verheye, H.M., Richardson, A.J., Hutchings, L., Marska, G., Gianakouras, D., 1998. Long-term trends in the abundance and community structure of coastal zooplankton in the southern Benguela system, 1951-1996. Afr. J. Mar. Sci. 19 (1), 317–332.

Verheye, H.M., Rogers, C., Maritz, B., Hashoongo, V., Arendse, L.M., Gianakouras, D., Giddey, C.J., Herbert, V., Jones, S., Kemp, A.D., C, R., 2001. Variability of zooplankton in the region of the Angola-Benguela Front during winter 1999. S. Afr. J. Sci. 97, 257–258.

Vinogradov, M.E., Metshunkin, V.V., Shushkina, E.A., 1972. On mathematical simulation of a pelagic ecosystem in tropical waters of the ocean. Mar. Biol. 16 (4), 261–268.

Vinogradov, M.E., Shushkina, E.A., 1978. Some development patterns of plankton communities in the upwelling areas of the Pacific ocean. Mar. Biol. 48, 357–366.

Volk, T., Hoffert, M.I., 1985. Ocean carbon pumps: Analysis of relative strengths and efficiencies in ocean-driven atmospheric CO_2 changes. Geoph. Monog. Series 32, 99–110.

Wagner, T.C., Scott, M.D., 1994. Single extraction method for the spectrophotometric quantification of oxidized and reduced pyridine nucleotides in eritrocytes. Anal. Biochem. 222, 417–426.

Wells, B.D., Parks, L.A., Tam, I., Fisher, J.R., 1977. A kinetic model for glutamate dehydrogenase. J. Theor. Biol. 66, 81–93.

Wiebe, P.H., Madin, L.P., Haury, L.R., Harbison, G.R., Philbin, L.M., 1979. Diel vertical migration by *Salpa aspera* and its potential for large-scale particulate organic matter transport to the deep-sea. Mar. Biol. 53 (3), 249–255.

Yentsch, C.S., Menzel, D.W., 1963. A method for the determination of phytoplankton chlorophyll and phaeophytin by fluorescence. In: Deep Sea Research and Oceanographic Abstracts. Elsevier, pp. 221–231.

Yool, A., Martin, A.P., Fernández, C., Clark, D.R., 2007. The significance of nitrification for oceanic new production. Nature 447 (7147), 999–1002.

Zehr, J.P., Ward, B.B., 2002. Nitrogen cycling in the ocean: new perspectives on processes and paradigms. Appl. Environ. Microbiol. 68 (3), 1015–1024.

APÉNDICE

APPENDIX

Appendix I. Zonal patterns in the Benguela waters on a cluster approach basis

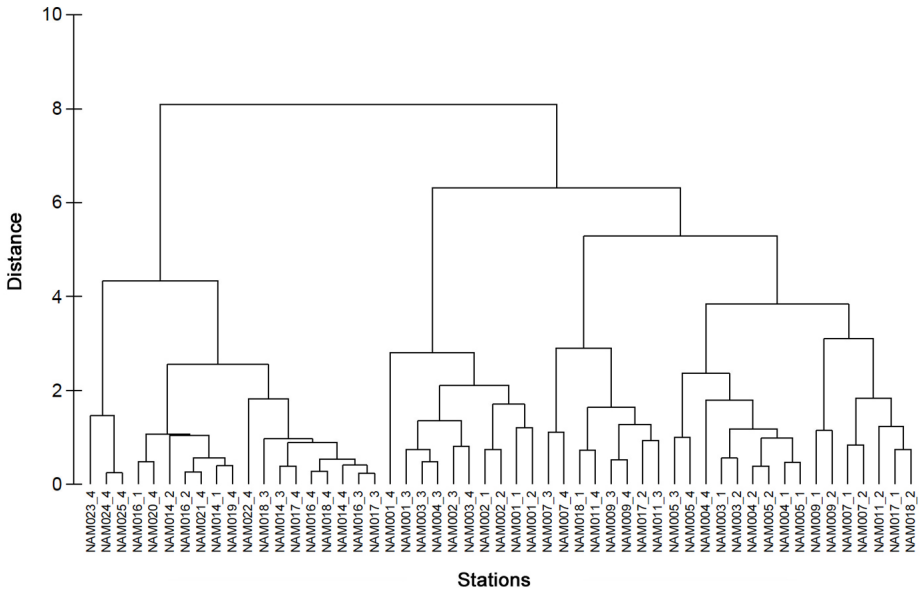

Figure A.1: Euclidean distances between all the stations sampled during the SUCCESSION cruise in the northern Benguela. Stations were clustered according to the near surface normalized data of temperature, salinity, and nutrients (NO_2^-, NO_3^-, PO_4^- and NH_4^+). Analysis was performed by PRIMER software. See Postel et al. (2014) for further details.

Appendix II. Morphological shifts in rotifers and mysids with both starvation and diet

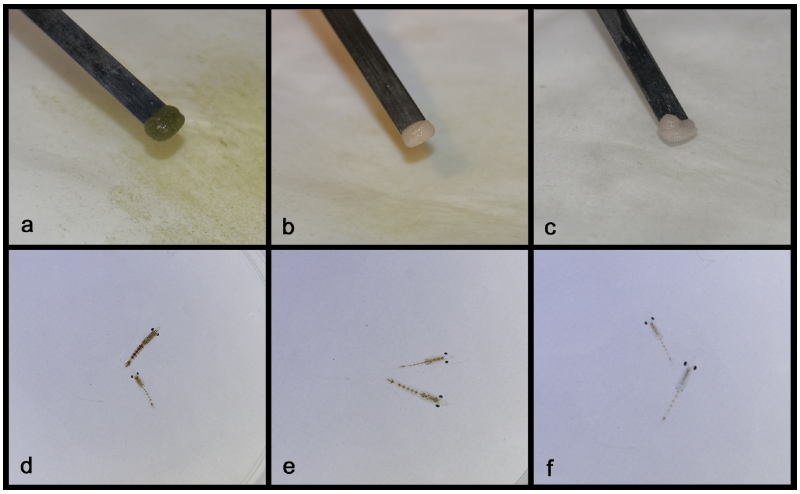

Figure A.2: Morphological shifts in the rotifers *Brachionus plicatilis* (upper panels) and the mysids *Leptomysis lingvura* (bottom panels), under different diets and food levels: (a) *B. plicatilis* fed *ad libitum* with the microalgae *Nannochloropsis* sp.; (b) *B. plicatilis* fed *ad libitum* with dry yeast; (c) *B. plicatilis* fed with the microalgae *Nannochloropsis* sp., after 28 h starvation; (d) *L. lingvura* fed *ad libitum* with *Artemia salina* (orange) and *B. plicatilis* (green-gray), (e) after 12 h starvation, and (f) after 60 h starvation.

Appendix III. Other published articles related with this thesis

AIII.1 Osma, N., **Fernández-Urruzola, I.**, Packard, T.T., Postel, L., Gómez, M., Pollehne, F., 2014. Short-term patterns of vertical particle flux in northern Benguela: a comparison between sinking POC and respiratory carbon consumption. J. Mar. Syst. 140 (B), 150 - 162.

AIII.2 Packard, T.T., Osma, N., **Fernández-Urruzola, I.**, Codispoti, L.A., Christensen, J.P., Gómez, M., 2015. Peru upwelling plankton respiration: calculations of carbon flux, nutrient retention efficiency, and heterotrophic energy production. Biogeosciences 12, 2641 - 2654.

Journal of Marine Systems 140 (2014) 150–162

Contents lists available at ScienceDirect

Journal of Marine Systems

journal homepage: www.elsevier.com/locate/jmarsys

Short-term patterns of vertical particle flux in northern Benguela: a comparison between sinking POC and respiratory carbon consumption

N. Osma [a,*], I. Fernández-Urruzola [a], T.T. Packard [a], L. Postel [b], M. Gómez [a], F. Pollehne [c]

[a] Plankton Ecophysiology Group, Instituto de Oceanografía y Cambio Global, Universidad de Las Palmas de Gran Canaria, 35017 Canary Islands, Spain
[b] Zooplankton Ecology Group, Baltic Sea Research Institute, D-18119 Rostock, Warnemünde, Germany
[c] Bentho-pelagic Coupling Group, Baltic Sea Research Institute, D-18119 Rostock, Warnemünde, Germany

ARTICLE INFO

Article history:
Received 26 August 2013
Received in revised form 22 December 2013
Accepted 20 January 2014
Available online 25 January 2014

Keywords:
Electron transport system (ETS)
Respiratory oxygen consumption
Particulate organic carbon (POC) flux
Sediment traps
Namibian upwelling system

ABSTRACT

Short-term variability of vertical carbon flux (C-flux) was assessed by two approaches at two stations on the Namibian shelf upwelling system (20°S). The first approach was based on modeling water-column respiratory CO_2 production (F_c) by integrating vertical profiles of the respiratory electron transport system. The second approach was based on automated sediment trap sampling daily. In both cases, temporal variability at the same station proved to be greater than the spatial variability between stations. Comparison of the two methods yielded higher C-flux values from the sediment traps in the presence of upwelling filaments (7.85 vs 3.67 mmol C m^{-2} d^{-1}). Contrarily, in the post-filament stage of the upwelling system, the values from the F_c models were higher (1.43 vs 2.57 mmol C m^{-2} d^{-1}). This difference was attributed to compositional changes in sinking particles and their settling velocities. In combination, both approaches served to increase current understanding of the short-term particle fluxes in this northern Benguela upwelling system. The F_c approach was further applied to zooplankton from the same area in order to quantify their importance in attenuating the particulate organic C-flux. This attenuation, as measured by fractional consumption of the primary productivity, ranged from 2% to 20%.

© 2014 Elsevier B.V. All rights reserved.

1. Introduction

Both loss of material from the water column and gain to the sediment are important processes in marine ecology and biogeochemistry, as the transport balance between the water and the sediment controls the biodiversity and the abundance of marine organisms on local and global scales. Upwelling systems, as hotspots of marine productivity, are particularly interesting in this concern, as pelagic and benthic processes are coupled by direct feedback loops, which often affect the speciation of elements (carbon, nitrogen and phosphorus) on a basin-wide level. Both pelagic and benthic biodiversities in upwelling regions reflect these conditions, where organisms adapt to the specific environmental constraints and, at the same time, are actively involved in the production of them. Thus, the balance between sinking particles and the benthic metabolism determines the role of sediments in either accumulating elements or modifying their speciation with a direct effect on surface layer productivity, e.g., when fueling the "new production" (*sensu* Dugdale and Goering, 1967). The vertical flux of particulate organic carbon (POC) is an important driver in this network, as it is considered a key mechanism in sequestering carbon to the ocean's interior. Nutrient-rich upwelled waters in the sunlit layer favor photosynthetic organisms to convert inorganic carbon into organic carbon, which is transferred to the deep ocean by gravitational sinking processes, active transport by animals and water mixing, altogether known as the "biological pump" (Volk and Hoffert, 1985). This downward flux of POC is consumed by the water column organisms to support their metabolic requirements and, eventually, placed onto the seafloor where it is consumed by benthic organisms and buried in the sediments. The magnitude of the vertical carbon export from the surface varies from higher values found at systems with more variable production owing to strong seasonal changes, to lower values at environments with more stable conditions (Berger and Wefer, 1990). Indeed, several authors have estimated that the biologically produced carbon export from the euphotic zone is about 25% in high production areas, such as the coastal upwellings, whereas it drops to 10% in the oligotrophic open-ocean areas (Berger et al., 1989; Buesseler, 1998; Martin et al., 1987; Schlitzer, 2000).

Quantification of vertical carbon fluxes (C-flux) has been the focus of international research programs during the last decades (e.g., Joint Global Ocean Flux Study, JGOFS), in which the rain of POC through the ocean water column was measured by either sediment traps or the $^{234}Th/^{238}U$ method. Elemental fluxes in upwelling and adjacent oligotrophic regions have been compared, for instance, by Pollehne et al. (1993a,b) with drifting traps in short term intervals. However, the number of studies that relate these fluxes to the metabolic activities of the organisms in the water column is sparse in the literature, despite the importance of respiration as the major biological process involved in POC attenuation. Steinberg et al. (2008) compared the bacteria and zooplankton metabolic

* Corresponding author. Tel.: +34 928 45 44 73; fax: +34 928 45 29 22.
E-mail address: nosma@becarios.ulpgc.es (N. Osma).

0924-7963/$ – see front matter © 2014 Elsevier B.V. All rights reserved.
http://dx.doi.org/10.1016/j.jmarsys.2014.01.004

Appendix

requirements to the sinking POC flux by inferring their respiration and carbon demands from growth efficiencies and biomass, respectively. But to our knowledge, no study has determined the carbon flux associated with the respiration profiles of both microplankton and zooplankton and directly compared it with the sinking POC collected by the sediment traps. In this context, Packard and Christensen (2004) proposed a conceptual model to determine the C-flux from vertical profiles of plankton respiration (modeled C-flux, hereafter, F_c), and it has been recently applied to estimate the zooplankton associated F_c in waters of the Canary Islands (Packard and Gómez, 2013). The basis of this approach is the reality that plankton in the ocean water column eat and degrade sinking POC, metabolize this organic matter within their cells, and, via respiration, release it as CO_2 gas into the water column. Considering a cube of seawater, the amount of CO_2 released into the dissolved phase (into the water) equals the difference between the POC entering at the top of the cube and the POC leaving through the bottom of the cube. If each cube is 1 m^3 then the C-flux through the 100 m level of the ocean with a depth of 5000 m is the respiratory CO_2 production rate (R_{CO2}) of every cube of seawater from 100 m to the bottom of the ocean. Mathematically, the integration of the R_{CO2} depth profiles from any depth in the water column to the seafloor indicates the amount of POC required to fuel the respiration of the organisms below that depth. Here, we have determined the respiration from the enzymatic activity of the respiratory electron transfer system (ETS). Since it was originally described by Packard et al. (1971), this methodology has been widely applied in the field of oceanography, as it allows a high data acquisition rate and provides sensitivity enough to quantify community respiration even in the mesopelagic and bathypelagic realms.

The present research work was accomplished at the Terrace Bay shelf off Namibia (20°S), under the influence of the northern Benguela upwelling system. This region is bordered at the north by the warm waters of the southward Angola Current and by the permanent Luderitz (26°S) upwelling cell at the south (Boyer et al., 2000). Although it is mostly perennial, it presents a pronounced seasonal peak during the austral winter and spring and an upwelling relaxation in autumn (Shannon and Nelson, 1996). The domain of the upwelled waters in this region extends further offshore than in the southern Benguela (Bakun and Nelson, 1991), mainly due to differences in the wind regimes and the shelf morphology. Moreover, this part is usually affected by the jets and filaments emerging from the main upwelling cell (Shillington et al., 1992). Therefore, the shelf off Terrace Bay is characterized by important instabilities and a high temporal and spatial variability. Previous works in this area have focused on long term patterns of vertical particle fluxes in order to study seasonality or inter-annual variability (Fisher and Wefer, 1996; Giraudeau et al., 2000; Romero et al., 2002), as well as to describe spatial patchiness in the organic matter deposition on the continental shelf (Monteiro et al., 2005), with the finest temporal scale of weeks. In our case, we decreased the sampling frequency to 24 h, which enabled us to detect the daily variability of the particle export. The high productivity in the surface layer (Carr, 2001; Estrada and Marrasé, 1987), in turn, allowed the sediment traps to catch material enough for the analysis within this sampling time.

Accordingly, we simultaneously performed direct measurements of particle flux by daily means of sediment traps and collected ETS data for the calculation of carbon losses from the water column respiration in a comparative approach. A secondary aim was to apply the F_c determination to zooplankton samples collected along a cross-shelf transect carried out at 20°S during the same cruise, so as to quantify the impact of these organisms on the vertical carbon flux via their respiration and to show the usefulness of this approach when high spatial resolution is needed.

2. Methods

2.1. Location and sampling

Samples were collected during the Succession cruise aboard RV *Maria S. Merian* off Terrace Bay (Namibia), from 24 August to 17 September 2011. Aside from the cross-shelf transect sampling, two stations were specifically studied (Table 1): an inshore station NAM006 (20°15.66′ S, 12°33.18′ E) located on the shelf at 206 m depth and an offshore station NAM011 (20°30.48′ S, 12°7.98′ E) on the shelf break at 395 m depth. Moorings were placed successively for 13 days at NAM006 and 10 days at NAM011. Water column samples for ETS activity were taken when the sediment trap was recovered at the inshore station (NAM006R) and both times when it was deployed and recovered at the offshore station (NAM011D and NAM011R). Seawater samples for microplankton ETS activity and chlorophyll *a* determination were taken at eight to nine discrete depths with 10-L Niskin bottles mounted on a rosette. At each cast, physical properties such as temperature, salinity and dissolved oxygen concentration were determined by the sensors of the CTD unit (SBE 911 +, Seabird Electronics). Zooplankton samples were obtained from net hauls at five to six depth intervals with a 100 μm mesh MultiNet (Hydrobios GmbH, Kiel, Germany).

The station position, sampling procedure and ETS activities of the zooplankton samples collected likewise along the four transects surveyed during this cruise are explained in Fernández-Urruzola et al. (2014). The mean ETS activity values for the four transects were used to determine the F_c at ten selected stations, which were divided into coastal, transition and oceanic areas, according to the distinct differences in geological and oceanographical properties.

2.2. ETS activity and respiration

Seawater samples for microplankton ETS activity were prefiltered through a 100 μm mesh in order to avoid the incidental inclusion of larger zooplankton. Then, 4 to 6 l of this seawater were filtered at room temperature using Whatman GF/F 25 mm glass fiber filters. They were folded to an eighth and blotted to remove excess water, placed in cryovials and frozen in liquid N_2 (−196 °C). Zooplankton samples were split into 100–200 μm, 200–500 μm, 500–1000 μm and larger than 1000 μm size fractions, placed in cryovials and frozen in liquid N_2. After 30 min, all the samples were transferred to an ultrafreezer and stored at −80 °C until analysis.

The ETS activity was measured kinetically by the Owens and King (1975) method, according to the variations described in Maldonado et al. (2012). Additionally, the reagents and reaction volumes were reduced by a factor of 2.5 and the assay time was reduced to 6 min, depending on the linearity of the reaction and the large coefficients of determination (in most cases, $r^2 \geq 0.99$) during the reaction. The INT-formazan production rate was related to ETS activity and to potential respiration rates (Φ) as previously defined in Packard and Williams (1981). Table 2 shows the step-by-step procedure to calculate the respiratory oxygen consumption (R_{CO2}) from the formazan production rates. The chromogenic tetrazolium INT (2-p-iodophenyl-3-p-nitrophenyl monotetrazolium chloride) is preferentially reduced by the respiratory ETS enzymes, replacing O_2 as the electron acceptor. The INT accepts two electrons while the O_2 would accept four. Therefore, the INT-formazan production rate (μmol m^{-3} d^{-1}) is stoichiometrically related by a factor of 2 to ETS activity (μmol$^-$ m^{-3} d^{-1}) and by a factor of 0.5 to Φ (μmol O_2 m^{-3} d^{-1}). All the Φ rates were corrected to in situ temperature using the Arrhenius equation (Packard et al., 1975).

Although, in the majority of the zooplankton samples (82%) there was no detectable contamination by phytoplankton, in a minority of the samples (18%), phytoplankton contamination was noticeable. Principally, it was observed during zooplankton size fractionation process, mostly in the 100–200 μm and 200–500 μm sizes from the surface waters at the mid shelf. On a biomass basis, these contaminated zooplankton samples contained 35 ± 24% phytoplankton, on average. To correct the measured zooplankton ETS activity for this, we measured the chlorophyll and protein in both the phytoplankton and the zooplankton samples. The measured protein/chlorophyll ratio in the phytoplankton samples was 4.6 mg chl *a* per mg protein ($n = 16$, $r^2 = 0.80$, $p < 0.0001$). This ratio was used to estimate the phytoplankton

Table 1
Station location and seawater characteristics at inshore (NAM006) and offshore (NAM011) stations where the vertical fluxes were determined during the Succession cruise in August/September 2011. NAM006R and NAM011R represent the water column sampling when the sediment traps (STs) were recovered, while NAM011D represents the water column sampling when the ST was deployed. Temperature (Temp), salinity (S) and oxygen concentration (O_2) for each sampling are given. The euphotic zone (E_z) was set at 60 m, as the maximum chlorophyl peaks were above this depth at the three stations (Fig. 1). 150 m and 320 m indicate the depths at which the STs were moored at NAM006 and NAM011, respectively.

Sediment traps		NAM006			NAM011					
	Position	20°15.66′ S, 12°33.18′ E			20°30.48′ S, 12°7.98′ E					
	Distance to shore	60 km			110 km					
	Bottom	206 m			395 m					
	STs depth	150 m			320 m					
	Deployment	24 Aug.–6 Sept.			7 Sept.–17 Sept.					
		NAM006R			NAM011D			NAM011R		
Water column		Temp (°C)	S	O_2 (μM)	Temp (°C)	S	O_2 (μM)	Temp (°C)	S	O_2 (μM)
	Surface	14.1	35.23	258	14.7	35.29	272	15.8	35.43	242
	60 m (E_z)	13.5	35.28	92	13.9	35.23	217	15.3	35.41	203
	150 m	12.6	35.20	41	12.9	35.22	62	12.9	35.23	43
	320 m	–	–	–	9.8	34.88	24	9.9	34.90	27

associated-protein in zooplankton samples. After subtracting this algal contribution to the protein content, an ETS/protein ratio of 61.6 μmol O_2 d^{-1} mg^{-1} protein was applied to determine the zooplankton associated-ETS activity. This ratio was obtained from a regression analysis of non-contaminated zooplankton samples taken along the transect survey during this cruise (ETS = 61.6 protein, n = 91, $r^2 = 0.93$).

R_{CO2} (μmol O_2 m^{-3} d^{-1}) for microplankton and zooplankton at the sediment trap stations is presented in Fig. 3. It was calculated from the relationship between the Φ and R_{CO2} in the water column. The R_{O2}/Φ value used for microplankton was 0.26 (Packard and Christensen, 2004) and for zooplankton was 0.48, both ratios are unitless. The latter was determined in parallel incubation experiments conducted onboard, in which the ETS activity and R_{O2} were measured in organisms of different size fractions. Zooplankters were collected by vertical WP-2 net hauls and immediately fractionated into 200–500 μm, 500–1000 μm and >1000 μm size classes. Once acclimated in filtered seawater at in situ temperature (15 ± 1 °C), healthy organisms were transferred into 60 ml cap-glass bottles and incubated for 2 h. This short incubation-time ensured no bias due to starvation episodes. The dissolved O_2 concentrations in the bottles were continuously measured through a 6-channel Strathkelvin 928 Oxygen System respirometer. Each batch of work included at least one control flask without organisms. Afterwards, the zooplankters were removed and frozen at −80 °C so as to analyze the ETS activity as described above. A mean R_{O2}/Φ value of 0.48 (±0.29, n = 19), as mentioned above, was obtained for the mesozooplankton community, which agrees with previous values reported in the literature of 0.5 (Hernández-León and Gómez, 1996).

2.3. Modeled carbon flux (F_c) calculations

The respiratory CO_2 production (R_{CO2}) was determined from R_{O2} and a revised molar Redfield ratio for C/O_2 of 0.71 (Takahashi et al., 1985). The R_{CO2} (μmol C m^{-3} d^{-1}) data were used to determine the respiration depth-profile (z) for microplankton and zooplankton at the three stations. According to a non-linear least-square method used in the Excel software (Brown, 2001), the best fits for each profile were the power function ($R_{CO2} = R_o z^{-b}$) and the logarithmic function ($R_{CO2} = a\ln(z) + c$), without significant differences between them (one-way ANOVA, p = 0.653). Therefore, and in order to follow the approach adopted in previous studies (Buesseler et al., 2007b; Martin et al., 1987; Packard and Christensen, 2004), the power function was applied. Additionally, Packard et al. (1983) pointed out that this model fits the data better in the deeper part of the water column. The term R_o in the equation represents the surface R_{CO2} and the exponent "b" determines the curvature of the profile; more negative values indicate greater decrease of respiration with depth, and vice versa. If a layer in the water column is considered, the difference between the C-flux at the top depth and the C-flux at the bottom depth can be equated to the respiratory CO_2 production within this layer under steady state conditions. Therefore, the definite integral of the R_{CO2} profile from the top of a water column (z_t) down to the seafloor (z_s) indicates the carbon flux into the top of that water column that is respired within this depth interval (Eq. (1)).

$$F_{t-s} = \int_{z_t}^{z_s} R_{CO_2}\,dz = \int_{z_t}^{z_s} R_o z^b\,dz \quad (1)$$

Table 2
Example of the step-by-step calculation of ETS activity and water column respiration (R_{O2}) from INT-formazan production in microplankton from NAM011D. The formazan production rate is stoichiometrically related by a factor of 2 to ETS activity and by a factor of 0.5 to potential respiration (Φ). The Arrhenius equation was applied to determine Φ at in situ temperature in column 5 (Packard et al., 1975). R_{O2} was calculated from Φ in column 5 using a R_{O2}/Φ ratio of 0.26. All these calculations are described in Packard and Christensen (2004).

Depth (m)	Formazan prod. (μmol m^{-3} d^{-1})	ETS activity (μmol$^-$ m^{-3} d^{-1})	Φ(μmol O_2 m^{-3} d^{-1})		R_{O2}(μmol O_2 m^{-3} d^{-1})
			T_{assay}	$T_{in\ situ}$	$T_{in\ situ}$
5	1797	3594	898	832	216
10	1546	3093	773	751	195
50	822	1644	411	378	98
75	1111	2222	555	507	132
100	473	946	237	217	56
180	365	729	182	148	38
280	417	833	208	142	37
330	391	781	195	127	33
380	417	833	208	134	35

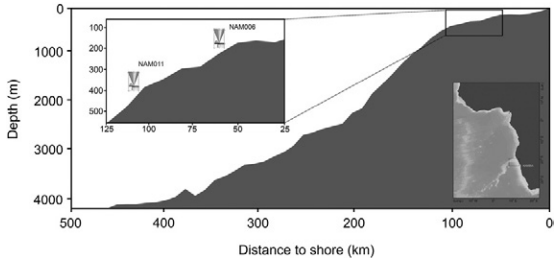

Fig. 1. Cross-shelf section of the study area at 20°S off Terrace Bay (Namibia), showing the sediment trap moorings on the continental shelf at 150 m (NAM006) and close to the shelf-break at 320 m (NAM011). Station positions and sampling time are described in Table 1.

Accordingly, these calculations with the lower limit to the definite integral at z_s, do not consider either the benthic respiration or carbon burial. If the upper boundary of the integral is any depth in the water column (z_f), e.g. the sampling depths, the carbon flux from z_f to the sea-floor (F_{f-s}) is calculated as in Eq. (2).

$$F_{f-s} = [R_o/(b+1)]\left[z_s^{(b+1)} - z_f^{(b+1)}\right] \quad (2)$$

Note that these calculations should only be applied from below the euphotic zone (E_z), due to the high POC production in this upper layer. Thus, if z_f is the bottom of E_z, then the F_{f-s} represents the carbon export from this layer that fuels the deep water-column respiration to the sediment. By resolving the Eq. (2) at several z_f and determining the best fit for these data, the F_c models were determined at each station. The equations of these profiles (see Section 3.3) can be used to predict the carbon flux at any depth below the E_z.

2.4. Sinking particle sampling

Automatic sediment traps of the type Kiel Multitrap K/MT 234 with 0.5 m sample area, 21 collecting glasses and a sampling period of 24 h were moored successively at NAM006 and NAM011, 50 m above ground at 150 m and 320 m respectively (Table 1). The sampling vials contained a salt brine of 70‰ in order to prevent rinsing and 2% formaldehyde for preservation of the collected material. After the recovery of

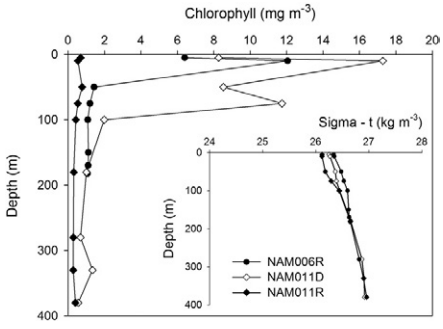

Fig. 2. Depth-profiles of microplankton chlorophyll (mg m^{-3}) from filtered samples and seawater density as sigma-t (inset, kg m^{-3}) at the sediment trap stations, during the three water column samplings.

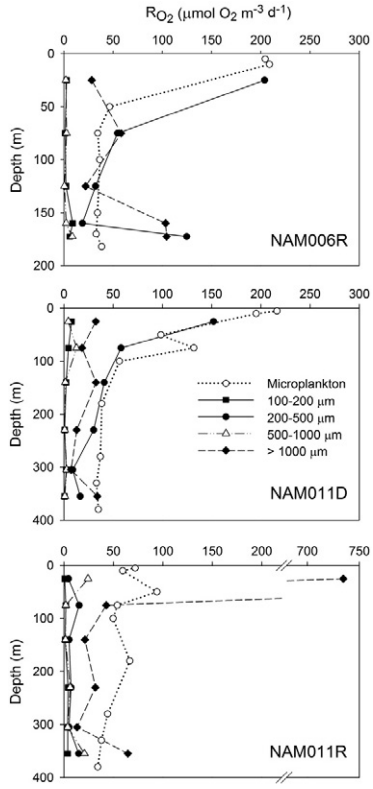

Fig. 3. Respiratory oxygen consumption (R_{O2}) depth profiles of microplankton and zooplankton at the three sampling dates, in µmol O_2 m^{-3} d^{-1} units. Zooplankton samples were divided into four size fractions, from 100 µm to sizes greater than 1000 µm. Note that the *x* axis scale is larger in the NAM011R plot. The legend in the middle panel applies to all three panels.

the traps, the samples were kept cool (4 °C) until further treatment. Once the samples were split, aliquots were filtered on GF/F glass fiber filters for the analysis of particulate carbon, nitrogen and the isotopic composition of both by means of a Carlo Erba/Fisons 1108 elemental analyzer connected to a Finnigan Mat Delta S isotope ratio mass spectrometer. The isotope values are given in the conventional δ-notation which is related to a known isotope standard and expressed as the difference to the Pee Dee Belemnite (PDB)-standard for carbon and to atmospheric nitrogen (Mariotti et al., 1984) for nitrogen, in per mil. The analytical error for organic carbon and nitrogen determinations is less than 5%, for the stable isotope composition less than $\pm$0.2‰. The amount of particulate biogenic silica (bSi) was determined from splits on polycarbonate filters according to procedures described in (von Bodungen et al., 1991) whereas the analysis of total particulate phosphorus (TPP) was carried out after Grasshoff (1976) from splits on GF/F glass fiber filters. Aliquots of the samples were inspected under an inverted microscope and, if possible, organisms were identified up to the species level. Other aliquots of the collected material were filtered through preweighed Millipore Isopore membrane filters (0.45 μm pore size, polycarbonate PC) for SEM–EDX investigations and multi-element analyses, respectively. Scanning electron microscopy (SEM) and energy dispersive X-ray micro-analyses (EDX) were performed on a FEIQuanta 400 microscope connected with an EDAX-Genesis system. About 1 cm^2 of PC filters was glued on Al stubs and covered by pure carbon (vacuum sputtered) to assure electric conductivity. Measurement parameters of the microscope system during analyses were: high vacuum; 15 kV electron beam; working distance: 10 mm; SE and BSE detectors; and variable enlargement. The X-ray microanalyses were done by spot analyses on selected particles taking EDX-spectra (EDAX-Econ 4 detector), identification and quantification of the elements after ZAF-correction. Peak overlapping (e.g. Mn kβ and Fe kα lines at 6.4 to 6.5 keV) was solved by holographic peak deconvolution (HPD). Besides manual single particle analyses, the system provides the opportunity of automated particle analyses. The method is based on image processing, particle recognition and element analyses of the particles on a series of different fields of the sample. On average, 2000 single particles of each sample were analyzed by this method. The resulting data set was processed for mineral (or particle group) identification and quantification (counting). Minerals and particle groups are defined by "border values" of the proven elements and calculated element concentrations (or ratios). Analyses of standard mineral samples were used to verify this method (Leipe et al., 1999).

3. Results

3.1. Sea water characteristics

Temporal variability in the hydrographic properties at the two sampling sites was greater than the spatial effect of the distance from the coast or from the core of the upwelling. These variations are described in Mohrholz et al. (2014), where they show the presence of different water masses in this area and the influence of cold water filaments arising from the south. Accordingly, during the water column sampling, both NAM006R and NAM011D exhibited similar sea water characteristics, but notably different from that of NAM011R (Table 1). Surface water at the first two samplings was low in temperature (14.4 $\pm$ 0.3 °C), low in salinity (35.26 $\pm$ 0.03) and high in O_2 concentration (265 $\pm$ 7 μM). Fig. 2 shows no strong stratification of the water column at these stations and depicts a surface chlorophyll maximum of 12 mg m^{-3} and 17 mg m^{-3} at NAM006R and NAM011D, respectively. NAM011R, in contrast, exhibited higher temperature, with higher salinity and lower O_2 concentration. The water column was more strongly stratified and the chlorophyll concentration in the surface was more than fifteen times lower than that at NAM006R and NAM011D. The chlorophyll reached a maximum value of 0.78 mg m^{-3} at 50 m, which is characteristic for the transition to a deep chlorophyll maximum layer in an oligotrophic situation (Pollehne et al., 1993a).

The three water column samplings were conducted at dawn and, accordingly, on the basis of the observations, we established the euphotic zone (E_z) depth. This we defined as the 1% light level, after considering the values from the nearby stations during the transect survey. They ranged from 23 to 58 m (see Section 3.6). In order to be conservative in our calculations of the carbon flux, we decided to set the E_z depth of these three stations at 60 m which included the chlorophyll maxima in all the cases. Although NAM011D displayed a subsurface chlorophyll peak of 12 mg m^{-3} below this depth (at 75 m), it could be attributed to moribund sinking phytoplanktonic cells and, hence, not highly active. Similar events were observed in other high productive systems such as the Costa Rica Dome (Packard et al., 1977) and the Peruvian upwelling (Packard et al., 1983). For the zooplankton-associated F_c calculations of the transect survey, we used the different E_z depths measured at each station (see Section 3.6).

3.2. Microplankton and zooplankton respiration in the water column

Step-by-step examples of the ETS activity, Φ and R_{O2} calculations from formazan production rates for microplankton at station NAM011D are given in Table 2. As these parameters are related stoichiometrically by constants, changes in the ETS activity will relate linearly to change in Φ and R_{O2}. Fig. 3 shows the R_{O2} depth profiles at the three stations. Microplankton respiration in the water column followed the same profile as that of chlorophyll at the three stations, although the correlation between these two parameters was higher at NAM006R and NAM011D than at NAM011R. This correlation difference suggests a higher proportion of non-photosynthetic organisms at station NAM011R. Maximum R_{O2} values were found at the surface of NAM006R and NA011D, with another subsurface R_{O2} peak in the latter at 75 m. At NAM011R the maximum value was half (93 μmol O_2 m^{-3} d^{-1}) the values found for the other two stations.

From the four size fractions of zooplankton, the contribution of 100–200 μm and 500–1000 μm sizes to the total water column respiration was considerably lower at the three stations. The highest value of the three samplings for the 500–1000 μm organisms was 24 μmol O_2 m^{-3} d^{-1} at NAM011R, while for the 100–200 μm size fraction it was 8 μmol O_2 m^{-3} d^{-1} at NAM011D. On the other hand, the maximum respiration rates at NAM006R and NAM011D were due to the 200–500 μm size fraction and were found at the surface, with an average value of 178 μmol O_2 m^{-3} d^{-1}. However, the respiration value of this size fraction decreased to below 15 μmol O_2 m^{-3} d^{-1} at NAM011R. The respiration, in this case, was dominated by the largest size fraction, with a value of 734 μmol O_2 m^{-3} d^{-1} at the surface. Finally, a slight increase of respiration near the bottom was noticed at all stations, mainly due to the 200–500 μm and >1000 μm size fractions.

3.3. Modeled vertical carbon flux, F_c

Respiratory CO_2 production rates (R_{CO2}) were calculated from the R_{O2} values in Fig. 3 and a molar Redfield ratio for C/O_2 of 0.71 (Takahashi et al., 1985). Since the conversion from R_{O2} to R_{CO2} only involves one constant, the shape of the depth profiles in both cases would be the same. For instance, Fig. 4 shows the R_{CO2} depth profile (μmol CO_2 m^{-3} d^{-1}) for microplankton at NAM006R, with the two best mathematical descriptions of the data, the power and the logarithmic functions. As stated above, there was no statistically significant difference between them in all the samplings (one-way ANOVA, $p = 0.653$). Visually the power function describes the data better, and hence, the power function for R_{CO2} was used in our calculations. The equation parameters of Eq. (1) for microplankton and zooplankton at the three stations are listed in Table 3. R_o refers to the calculated surface R_{CO2} and follows the same pattern as the measured R_{O2}: the highest values for microplankton were found at NAM006R

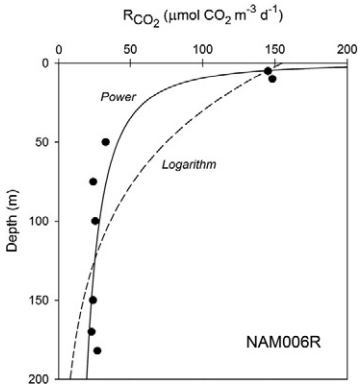

Fig. 4. Respiratory CO_2 production (R_{CO2}) depth profile of microplankton at NAM006R. The two best fits for the data, the power and the logarithmic functions, are given.

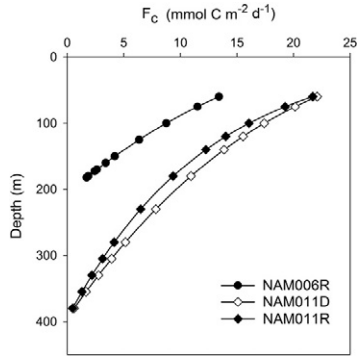

Fig. 5. Carbon flux depth profiles measured on the shelf off Terrace Bay (Namibia). F_c represents the addition of the microplankton and zooplankton contributions to the carbon flux, via their respiration rates. The units are mmol C m^{-2} d^{-1}. Maximum depths were 206 m at station NAM006 and 395 m at station NAM011.

and NAM011D, while the highest value for zooplankton was found at NAM011R. Even the "b-value", which reflects the curvature of the respiration depth profile, was higher (more negative) when the surface respiration values were higher, i.e., at NAM006R and NAM011D for microplankton and at NAM011R for zooplankton. Total R_{CO2} (Table 3) refers to the addition of the modeled R_{CO2} for microplankton and zooplankton at each station. The F_c from the base of the euphotic zone to the seafloor was calculated by the integration of this total R_{CO2}, as described in Eq. (2) (Fig. 5). The function that best fits the carbon flux data was the logarithmic ($r^2 > 0.99$). The equations for the three profiles are as follows: $F_c = -10.47\ln(z) + 56.37$ for NAM006R; $F_c = -12.96\ln(z) + 77.96$ for NAM011D; and $F_c = -11.54\ln(z) + 69.13$ for NAM011R, all in mmol C m^{-2} d^{-1} units. These equations were employed to calculate the respiration based-F_c at 150 and 320 m in order to compare them with the sediment trap-derived C-flux values.

3.4. Particle fluxes and composition

Vertical fluxes, mass and elemental, at both moorings can be separated into periods of high and low sedimentation (Fig. 6). Again, temporal variations in these fluxes from both traps were much greater than spatial effects such as differences in water depth or distance to the coast. Therefore, in an initial analysis, rather than comparing the data from the two sediment trap stations, the data from the two different sedimentation regimes were compared as in Table 4. In this table, arithmetic means of fluxes during high (high-sed) or low (low-sed) sedimentation phases and elemental ratios derived by the division of the total accumulated masses over the respective periods are shown. The upper limit for the low range was set at 2.53 mmol POC m^{-2} d^{-1}. The two data sets are clearly distinct, as the lowest value of the high sedimentation range is more than twice this value.

High sedimentation phases (mean C-flux of 7.85 mmol POC m^{-2} d^{-1}) were characterized by 4–6 times higher mass and elemental fluxes, with a remarkable difference in the particulate biogenic silica (PSi) in which the value was 11 times higher (Table 4). A great abundance of diatoms and a mineralogical composition of the inorganic material with high contributions of both opal and intermixtures of quartz and a microscopic picture of mainly diatoms, either intact or in pieces, were also recorded. Dominant diatom species were *Pseudonitzschia australis* (Fig. 7A) and *Coscinodiscus walesi* (Fig. 7B) with a high proportion of debris (mainly broken diatom shells) in the material. Low sedimentation phases (mean C-flux of 1.52 mmol POC m^{-2} d^{-1}) comprised mass and element fluxes that were distinctly lower for POC, PON, POP and PSi. In these periods, coccolithophorides (Fig. 7C) increased together with carbonaceous minerals ($CaCO^3$) and $CaPO^4$ and intermixtures of feldspar (data not shown).

Elemental ratios differed between the phases (Table 4). Due to high diatom contents the C/Si atomic ratio in the high-sed samples was half the value found in the low-sed situation and the weight percentage of carbon against total dry mass was accordingly lower. The C/N-ratio was lower (7.5 vs. 8.3) in the low sedimentation periods, whereas the C/P-ratio was slightly higher (259 vs. 239). However, as phosphorus is involved, these ratios from particulate material may be misleading. Phosphorus is removed from cells very quickly during their first phase of sinking (Faul et al., 2005; Paytan et al., 2003) as compared to carbon, nitrogen and silica. Under our specific conditions of intercepting sinking cells (and particularly breaking or broken diatoms) close below the mixed layer we must assume, that a certain amount of dissolved material may have leached out of the vacuoles during the collecting time in the cups with a bias towards phosphorus. We, in fact, measured elevated concentrations of orthophosphate in the sampling vials which were

Table 3
Equation parameters for the power function fit for the respiratory CO_2 production, $R_{CO2} = R_o z^b$. Here, R_{CO2} represents the modeled respiration in µmol C m^{-3} d^{-1} at any depth (z) in the water column, R_o (µmol C m^{-3} d^{-1}) is the R_{CO2} at the surface, b is the curvature of the profile and n is the number of samples. The coefficient of determination (r^2) indicates the goodness of the fit between the modeled R_{CO2} and the R_{CO2} calculated from the R_{CO2}. Total R_{CO2} (µmol C m^{-3} d^{-1}) represents the addition of the modeled R_{CO2} for microplankton and zooplankton. The Total R_{CO2} equations are integrated from below the euphotic zone to the ocean bottom in order to calculate the carbon fluxes (see Fig. 3).

Station		R_o	b	r^2	n
NAM006R	Microplankton	433	−0.604	0.91	7
	Zooplankton	883	−0.540	0.79	4
	Total R_{CO2}	1309	−0.558	–	–
NAM011D	Microplankton	401	−0.472	0.89	9
	Zooplankton	2077	−0.801	0.97	5
	Total R_{CO2}	2111	−0.663	–	–
NAM011R	Microplankton	63	−0.140	0.90	7
	Zooplankton	18,737	−1.254	0.97	5
	Total R_{CO2}	8464	−0.939	–	–

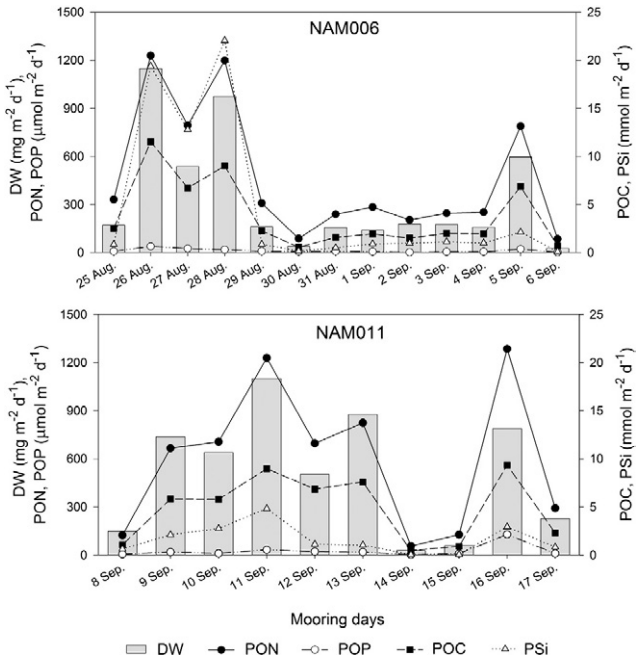

Fig. 6. Vertical mass (bars) and elemental (lines) fluxes at NAM006 and NAM011 derived from sediment traps. Mass flux was measured as dry weight (DW), in mg m^{-2} d^{-1}. Particulate organic carbon (POC) and particulate silica (PSi) are given in mmol (C and SiO_2) m^{-2} d^{-1}, while particulate organic nitrogen (PON) and particulate organic phosphate (POP) are in µmol (N and PO_4) m^{-2} d^{-1}. The sampling time was of 13 days at NAM006 and 10 days at NAM011. The legend at the bottom applies to the two panels.

higher than the respective silica concentrations, if normalized to the particulate phases of these elements. Due to the fixation with formalin, dissolved carbon and nitrogen species could not be reliably estimated in the supernatant water of the collecting cups and so a complete reassessment of whole input, including both particulate and dissolved elemental phases, was not possible. During the early period of cell sinking, these selective leaching processes, largely enhanced by grazing, occur in the water column as well and are, therefore, not easy to discriminate. In our case, they may have affected particularly the C/P ratio of the material, which we expected to be lower for a comparatively fresh diatom bloom.

Clear systematic differences in the isotopic composition between the two phases could not be observed (Table 4). Whereas the $\delta^{13}C$ signature of POC between these two situations was virtually the same (−21.96 vs. −22.04), the difference in $\delta^{15}N$ between high (5.07) and low (5.57) sedimentation phases may be due to a fractionation effect of nitrate between eutrophic and oligotrophic waters (Altabet et al., 1991). Without knowledge of the source composition of nutrients in the surface layer and consecutive trophic changes this can, however, not be substantiated.

3.5. Comparison of respiration based F_c vs. sinking POC

The main challenge of the present study was to compare the POC that is exported from the euphotic zone and reaches the sediment traps with the calculated F_c at the same depths based on plankton respiration in the water column. Fig. 8 shows such a comparison. As stated above, the sampling time of the sediment traps was divided into high and low sedimentation periods, which were attributed to high and

Table 4
Average values of particle composition at NAM006 and NAM011, grouped by the sedimentation level. Tot. flux stands for the mean values of the daily total mass flux measured at the different conditions. Note that the values for the elemental fluxes (Elem. flux.) are in µmol m^{-2} d^{-1}. In order to simplify the reading, the atomic ratios are referred as C/N, C/P and C/Si throughout the text. The carbon content as a percentage of the dry weight (C as %DW) was estimated from the weight ratios in each case. The isotopic composition of C and N ($\delta^{13}C$ and $\delta^{15}N$) are also given.

	Total flux	Elemental flux (µmol m^{-2} d^{-1})				Atomic ratios			C as % DW	$\delta^{15}N$	$\delta^{13}C$
	(mg m^{-2} d^{-1})	POC	PON	pP	PSi	POC/PON	POC/pP	POC/PSi	wt. ratio	per mil	per mil
All low-sed	128.3	1522	202.6	5.87	623	7.51	259	2.4	16.17	5.57	−22.04
All high-sed	790.3	7849	941.6	32.82	7110	8.34	239	1.1	12.30	5.07	−21.96
Ratio high/low sed	6.16	5.16	4.65	5.59	11.40	1.11	0.92	0.45	0.76	0.91	1.00

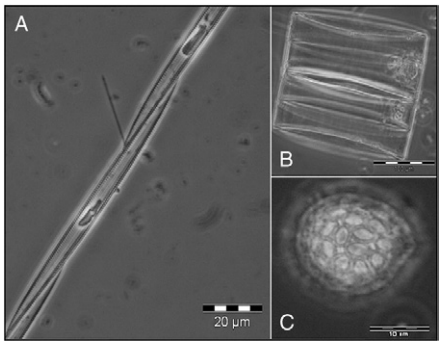

Fig. 7. Dominant species of chain-forming diatoms during the high sedimentation period, *Pseudonitzschia australis* (A) and *Coscinodiscus walesi* (B). Coccolithophorides (C) were more abundant during the low sedimentation rates. Note that they maintained the assemblages of coccoliths covering the cell. All these photographs were taken by means of an inverted microscope.

low primary productivity events in the surface layer (Eppley and Peterson, 1979). Mean values (±SD) of POC during the high-sed periods were of 8.54 (±2.26) at NAM006 and 7.39 (±1.54) at NAM011, while when the particle sedimentation was low, the values decreased to 1.67 (±0.66) at NAM006 and 1.18 (±0.79) at NAM011, all in mmol C m^{-2} d^{-1} units. Regarding the water column samplings, they were also related to periods of high and low production, by using the chlorophyll to estimate the primary productivity as described by Brown et al. (1991). Thus, NAM006R and NAM011D coincided with periods of high production, while NAM011R was associated with lower primary production. At the mooring depths (150 m and 320 m), the modeled F_c yielded values of 3.90, 3.43 and 2.57 mmol C m^{-2} d^{-1} at NAM006R, NAM011D and NAM011R, respectively. Then, these values for NAM006R and NAM011D were compared with the POC values obtained from the sediment traps during the high-sed period, and it turned out that the latter were more than two times higher. However, this difference was only significant for NAM011D (*t - test*, $p<0.05$). The value for NAM011R, in turn, was compared with the POC concentration in the sediment traps when the particle sedimentation was low. In this case, the value from the F_c model was higher, although there was no statistically significant difference (*t - test*, $p = 0.11$).

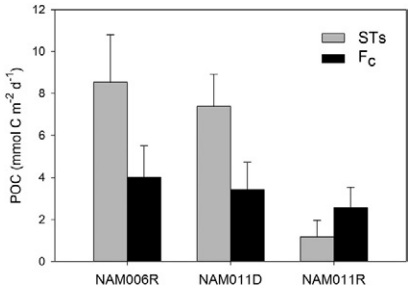

Fig. 8. Comparison of carbon fluxes measured by sediment traps (STs) and by respiration-based models (F_c) at 150 m (NAM006R) and 320 m (NAM011D and NAM011R). Differences are only significant ($p < 0.05$) for NAM011D. Error bars on the ST approach correspond to the standard deviation of the measurements, while on the F_c approach reflect the maximum uncertainty in the carbon flux calculations (38%).

3.6. Application of F_c approach to zooplankton

The zooplankton contribution to the vertical carbon flux was also determined from ETS activities in water column profiles from the cross-shelf transect (20°S) during the Succession cruise. For further information about the zooplankton biomass distribution and metabolic activities along this transect see Fernández-Urruzola et al. (2014). We determined the respiratory CO_2 production as a function of depth and integrated it from the base of the E_z to the seafloor by applying, as before, Eq. (2). Table 5 shows the logarithmic, exponential and power fits to the F_c profiles for ten stations along the transect. The data from the two stations of sediment traps are also included. The best fit at the coastal and transition stations was the logarithmic function. It was significantly different from the power and exponential functions for the transition stations (two-way ANOVA, $p < 0.05$). In the oceanic area, however, the best fit was the exponential equation, although no significant differences were found between it and the logarithmic fit. It is noteworthy that the coefficient of correlation (r^2) for the power function is consistently lower than the r^2 for the other two functions at all the stations (Table 5). The calculated carbon loss associated with zooplankton respiration for the entire water column yielded mean values of 17.32, 39.72, 16.63 mmol C m^{-2} d^{-1} at the coastal, transition and oceanic areas, respectively. These values represent the zooplankton respiratory carbon demands for the entire water column. With these F_c models, one could also estimate some key values (Table 6), such as the zooplankton associated carbon export ratio from the E_z (e-ratio), the carbon transfer efficiency (T_{eff}) and the nutrient retention efficiency (NRE). Here, the e-ratio stands for the percentage of the primary productivity that is consumed by the zooplankton respiration below the E_z. Note that, in these calculations, the microplankton contribution is not taken into account. These values varied distinctly from about 2 to 13% at the three regions, mainly with higher e-ratios found at the oceanic area. The T_{eff} (Buesseler et al., 2007b) is defined as the ratio between the C-flux at 500 m to C-flux at 150 m, multiplied by 100 when it is expressed as a percent. Higher values indicate higher efficiency of the system in transferring the carbon from the surface to deep waters. Contrary to the e-ratio, we estimated a practically constant T_{eff} value of 60% at the stations from the oceanic area, the only ones deep enough for this determination. The NRE, which was recently proposed by Packard and Gómez (2013), refers to the capability of the plankton community to retain the nutrients in the upper layer of the water column ($z \leq 500$ m) and equals $(F_c^{150} - F_c^{500}) / F_c^{150} * 100$. In fact, it reflects the opposite concept of the T_{eff} and the e-ratio. It should correlate directly with

Table 5
Carbon flux depth profiles associated with zooplankton respiration along the transect. The best fits for the data are given, the logarithmic ($F_c = a\ln(z) + F_o$), the exponential ($F_c = F_o\, e^{bz}$) and the potential ($F_c = F_o\, z^b$) functions. F_o is the estimated F_c at the surface, i. e., when $z = 0$ for the logarithmic equation and $z = 1$ for the exponential and potential equations. Units are mmol C m^{-2} d^{-1} for the three functions, z is in meters (m). These equations should only be applied to calculate the F_c at any depth from below the euphotic zone to the seafloor. The data for the sediment trap stations (NAM006 and NAM011) are also included.

Area	Station	Logarithmic equation	r^2	Exponential equation	r^2	Power equation	r^2
Coastal	NAM002	$-2.29\ln(z) + 10.71$	0.999	$10.06e^{-0.036z}$	0.982	$10000z^{-2.233}$	0.956
	NAM003	$-3.02\ln(z) + 14.77$	0.999	$11.72e^{-0.029z}$	0.966	$2000z^{-1.688}$	0.881
	NAM004	$-5.34\ln(z) + 26.49$	0.996	$20.02e^{-0.026z}$	0.962	$5000z^{-1.785}$	0.916
	Average		0.999		0.970		0.918
Transition	NAM006 [a]	$-7.69\ln(z) + 41.41$	0.996	$30.06e^{-0.016z}$	0.967	$10000z^{-1.702}$	0.929
	NAM007	$-4.52\ln(z) + 26.15$	0.992	$15.00e^{-0.010z}$	0.994	$167.31z^{-0.798}$	0.912
	NAM009	$-9.89\ln(z) + 58.66$	0.987	$32.46e^{-0.009z}$	0.972	$1000z^{-1.054}$	0.877
	NAM011 [a]	$-5.46\ln(z) + 32.64$	0.999	$22.95e^{-0.010z}$	0.931	$20000z^{-1.722}$	0.820
	Average		0.994		0.966		0.885
Oceanic	NAM014	$-3.67\ln(z) + 29.52$	0.954	$16.25e^{-0.002z}$	0.999	$63.48z^{-0.355}$	0.896
	NAM017	$-2.38\ln(z) + 19.17$	0.988	$9.88e^{-0.001z}$	0.996	$78.87z^{-0.504}$	0.893
	NAM018	$-1.56\ln(z) + 12.34$	0.999	$6.35e^{-0.001z}$	0.995	$78.29z^{-0.625}$	0.914
	NAM022	$-0.86\ln(z) + 6.79$	0.994	$3.09e^{-0.001z}$	0.969	$41.99z^{-0.602}$	0.969
	NAM026	$-1.40\ln(z) + 15.31$	0.935	$9.52e^{-0.0004z}$	0.999	$23.38z^{-0.212}$	0.880
	Average		0.974		0.992		0.910

[a] From the zooplankton values at the ST stations.

regenerated production and correlate inversely with new production (sensu Dugdale and Goering, 1967). We obtained values for NRE of around 40% (Table 6), except for the station NAM026, where the downward transmission of carbon was higher.

4. Discussion

4.1. Temporal variability in the community structure and sinking particle composition

Sinking particle composition and vertical fluxes have been described here, as well as the planktonic contribution to the heterotrophic POC degradation via respiration. The variability of the hydrological properties during the sampling time impacted both approaches. The sediment trap data from the two successive moorings at different water depths and distances from the coastal core of the upwelling (Fig. 1) displayed similar patterns. Peaks and means of C-flux were in the same range in both the deeper offshore and the shallower onshore traps (Fig. 6). Note that the latter was situated closer to the core of the upwelling. Depth profiles of community respiration, in turn, also reflected this pattern. The shape of R_{O2} profiles at station NAM011D was more akin to NAM006R than it was to NAM011R (Fig. 3). This was because the two samplings at the NAM011 were made ten days apart, whereas NAM011D and NAM006R were sampled within a day of each other. Thus, we observed that temporal variability in this area was stronger than the spatial variability. Although this does not fit into the general scheme of a system that ages strictly with distance from the center of the upwelling, it fits well into the complex spatial pattern of the Benguela upwelling characterized by filaments and eddies as can be seen in satellite images of color and temperature as well as in modeling results (Mohrholz et al., 2014).

On a general level, the pattern of vertical particle export represented an image of the structure and state of the pelagic system in the surface mixed layer. Independent of geographical position and depth, we found two states that differed both in quality and quantity of the material and which alternated on a daily basis. One was the result of particle loss from a eutrophic upwelling filament (Mohrholz et al., 2014). It originated farther south and was characterized by high phytoplankton biomass due to strong diatom growth (Hansen et al., this volume). The other, by contrast, derived its particle load from a mixed layer, which contained elements of both upwelling and oligotrophic Atlantic waters. Here, the oligotrophic state can be described as the late temporal phase of an upwelling system, which after a period of warming, mixing and reduction of free nutrients is transformed from a typical "new" into a "regenerating" production system. Nevertheless, the material collected

Table 6
Application of respiration based-carbon flux model (F_c) to zooplankton samples collected along the transect. Carbon fluxes at the euphotic zone (E_z), 150 m and 500 m were determined from the logarithmic equations in Table 5. Carbon export (e-ratio) and the efficiency of the biological pump in the carbon transfer (T_{eff}) and in the nutrient retention (NRE) from 150 m to 500 m were also determined. Net primary productivity (NPP) in this layer was estimated from chlorophyll and ^{14}C incubation measurements made on board; the calculations followed the procedure given in Brown et al. (1991) for the Benguela system, with the regression model of best fit to the data being $^{14}C = 3.75\ \mathrm{Chl}\ a^{0.653}$ ($n = 24$, $r^2 = 0.60$, $p = 0.001$). It comprises the integrated NPP in the E_z. The e-ratio stands for the percentage of the NPP that is consumed by zooplankton respiration from the base of the E_z to the seafloor. Gaps indicate no determination due to insufficient water column depth.

Zone	Station	Depth (m)	E_z depth (m)	F_c (mmol C m^{-2} d^{-1})			NPP (mmol C m^{-2} d^{-1})	e-Ratio (%)	T_{eff} (%)	NRE (%)
				E_z	150 m	500 m				
Coastal	NAM002	107	39	2.34	–	–	123.0	1.9	–	–
	NAM003	132	26	4.94	–	–	123.7	4.0	–	–
	NAM004	133	38	7.06	–	–	169.7	4.2	–	–
Transition	NAM006 [a]	206	60	9.94	2.90	–	357.7	2.8	–	–
	NAM007	266	23	11.99	3.53	–	215.2	5.6	–	–
	NAM009	308	58	18.52	9.13	–	210.8	8.8	–	–
	NAM011 [a]	395	60	10.32	5.28	–	211.5	4.9	–	–
Oceanic	NAM014	871	52	14.53	11.77	5.55	109.4	13.3	47.1	52.9
	NAM017	2159	46	9.31	8.12	5.13	154.1	6.0	63.2	36.8
	NAM018	2611	40	6.02	5.19	3.25	110.0	5.5	62.6	37.4
	NAM022	3775	50	2.92	2.61	1.76	106.1	2.8	67.3	32.7
	NAM026	4339	50	9.32	8.92	7.68	72.9	12.8	86.0	14.0

[a] From the zooplankton values at the ST stations.

Appendix

in the traps itself did, in no way, reflect a growth limited or senescent biological community. Similar C/P, lower C/N and higher C/Si ratios (Table 4) indicated a shift in the community towards smaller and probably to a higher percentage of heterotrophic cells, which corresponded to our microscopic observations. Mass transfer was, however, quite different between the two basic states and whereas the high-sed values of C, N and P fluxes with means of 7850, 940 and 33 μmol m^{-2} d^{-1} formed the trophic base of the highly productive Benguela upwelling system, the low-sed values of 1500, 200 and 6 μmol m^{-2} d^{-1} of C, N and P respectively, constituted the transition to oligotrophic open ocean conditions. In fact, our POC values for the two sedimentation situations are comparable to fluxes measured in other eastern upwelling systems, such as the California Current (Pilskaln et al., 1996) and Humboldt Current (González et al., 2009). Pilskaln et al. (1996) reported values in Monterey Bay of 0.8–2.5 mmol C m^{-2} d^{-1} during non-upwelling situation and of 4–15 mmol C m^{-2} d^{-1} when the upwelling was active. Values from González et al. (2009), were relatively higher, ranging from 3 to 87 mmol C m^{-2} d^{-1}, likely due to a shallower sample collection. Therefore, the basic difference in our short term measurements is related to the suspension of the traps either beneath a comparatively young upwelling filament or beneath water between these filaments.

An interesting, although at the moment just descriptive, finding is that the mineralogical loads of the two sedimentation regimes revealed not only different biogenic minerals, like carbonates or opal, but also lithogenic minerals, like quartz or feldspars and different clay minerals as well. If this dichotomy is related to changes in particle sizes, forms or stickiness of the organic load or to different input terms of aeolian dust it is not known and still has to be resolved.

Similarly, the respiration profiles also reflected a change in the structure of the communities between the two basic situations. While the water column respiration associated with the filament of mature water was dominated by the microplankton and the 200–500 μm size fraction zooplankton, the highest respiration rates in the more oligotrophic waters were due to >1000 μm size fraction zooplankton, with a significantly lower contribution from the microplankton (Fig. 3). If, as stated above, the oligotrophic state here refers to a later temporal phase of an upwelling system, this pattern agrees with that modeled by Vinogradov et al. (1972). They predicted that the small-sized herbivores would peak right after the maximum of phytoplankton, followed by the maximum of large-sized herbivores and carnivores with a delay of days. Accordingly, the >1000 μm organism in the more oligotrophic waters of the NAM011R were predominantly salps. Maximum values of microplankton respiration during the most productive period (200 μmol O_2 m^{-3} d^{-1}) were around 4-fold lower than others found farther south in the same northern Benguela upwelling region (Chapman et al., 1994). However, it is not surprising as they reported greater productivity rates and ~3 fold higher chlorophyll concentration values, indicating higher phytoplankton biomass as compared to our findings. Few studies have paid attention to the respiratory metabolism of the entire zooplankton community in this region, although recently various researchers have described the metabolic rates of the dominant species of mesozooplankton (Bode et al., 2013; Huenerlage and Buchholz, 2013). Our zooplankton respiration rates at the sediment trap stations compare well with the mean values for the different size fractions reported in Fernández-Urruzola et al. (2014) for other stations in this transition area, but they are higher than previously published values in other upwelling systems (Hernández-León et al., 2002; Isla and Anadón, 2004; Packard et al., 1974). This is likely related to the higher primary productivity in our case.

On a general level, this study is embedded in a large scale investigation of the aging process of a coastal upwelling system. On small temporal and spatial scales, like those inherent in distinct water samples or characteristics of daily sampling intervals of sediment traps, the patchiness affected our measurements much more than did the overlying general spatial pattern. In this regard, the long term development in the surface water masses after upwelling, determines what will sink out of these overlying waters in the long run. Therefore, in order to detect these consecutive stages of an aging upwelling system, more time series sampling along an Eulerian approach, integrated with more spatial coverage, would be required.

4.2. Comparing and combining the sinking POC and the F_c approaches

The comparison of conceptually different methods of estimating vertical carbon transfer in the water column in such a heterogeneous system revealed the pros and cons of each method. Whereas the sediment trap approach collects integrated amounts of sinking matter irrespective of the system interactions in the water column, the plankton respiration approach describes the system interactions with higher depth resolution. In addition, the F_c method, because of its high data acquisition rate, allows wider temporal and spatial ocean coverage than the stationary trap approach. Nonetheless, because it is a near-instantaneous measurement, it lacks the temporal integration if not performed in a highly elaborate large scale effort. Accordingly, this differs from the sediment trap approach. F_c from ETS activities are based on minute-to-hour scale changes while the C-flux from sediment traps is based on a day-to-month scale changes. Here, the POC value from the sediment trap data for the high-sed and low-sed periods comes from the average of 4–9 days, while the F_c profiles represent a snapshot of the water column characteristics at the sampling time. However, by operating on different scales of integration, the two approaches are meant to complement one another by placing recent measured fluxes into the context of the wider field of vertically resolved respiration.

When the two approaches are to be compared, one should also consider the intrinsic uncertainty of each determination. Several reviews concerning the sediment trap efficiency (Buesseler et al., 2007a; Burd et al., 2010; Gardner, 2000) pointed out that factors such as the hydrodynamic processes, the incidental presence of zooplankton swimmers, and the solubilization of labile biogenic components in the cups can bias the collection of sinking particles, specially at the shallower depths. From our results, we showed evidence of the selective solubilization process of organic phosphorus, as this element leaches from breaking cells faster than carbon, nitrogen or silica (Faul et al., 2005; Paytan et al., 2003). All things considered, the sediment trap-based carbon flux estimations vary by a factor of 3 to 10 (Buesseler, 1991). On the other hand, the uncertainty in the prediction of R_{CO2} from ETS measurements is dictated by the errors associated with all the conversion steps. Thus, the Φ has an uncertainty of ±16% (Packard et al., 1977). The recalculated CO_2/O_2 ratio from Takahashi et al. (1985) has a standard error of ±18% (Martin et al., 1987). Still, the overall variability lies in the R_{O2}/Φ ratios, namely ±12% for microplankton (Packard and Christensen, 2004) and ±23% for zooplankton (King and Packard, 1975). Considering all sources of errors during the calculations, the resultant uncertainty in the F_c determination ranges from 31 to 38% (Packard and Gómez, 2013; Packard et al., 1988).

Apart from the uncertainties in each determination, the comparison of the two approaches distinguished two different scenarios (Fig. 8). Regardless of the distance to shore, during the high-sed period, the POC flux values obtained in the sediment traps were higher than those estimated by the respiration based-F_c method, while when the sedimentation rate was lower, the value from the F_c approach was twice as high as the value from the sediment traps. This discrepancy can be explained by basic differences in the plankton community structure in the surface layer, as the phytoplankton size would directly influence their settling velocities (Boyd and Newton, 1995; Guidi et al., 2009). Thus, the high-sed scenario was dominated by large diatoms (Fig. 7A and B) that easily aggregate forming fast-sinking particles and producing a rapid flux of particulate organic matter from the surface to the deep sea, with rates that could exceed 100 m day^{-1} (see Thornton, (2002), and references therein). In addition, the relatively high presence of lithogenic material (~45%) might have contributed to this flux by the ballast effect (Armstrong et al., 2001). These rapidly settling particles are presumably

less influenced by either lateral advection or organism consumption and, therefore, the material collected in the cups is in phase with the production at the surface. During the low-sed period, in contrast, the abundance of diatoms substantially decreased while the occurrence of coccolithophorides increased. Although these organisms were also present within the cups during the high-sed period, their presence was masked by the high peak pulses of fast-sinking particles. Coccolithophorides can form aggregates that settle even faster than the diatom formed-aggregates, but they would require more time, higher cell densities and the release of coccoliths after the cell lysis (Iversen and Ploug, 2010). Contrarily, our results during this low-sed period showed a considerably low phytoplankton biomass, low contribution of lithogenic material and indicated a non-senescent community, which revealed no significant aggregate formation of these organisms. This hypothesis was strengthened by microscopic observations of the material that indicated intact coccolithophorides cells (Fig. 7C). All these data suggest that this period was dominated by slow-sinking particles with an increased probability to be consumed by zooplankton in the midwater layers. Additionally, a portion of slow-sinking particles, that originated from a previous upwelling filament could still be present in the deeper water layers and contribute to enhance respiration rates (Packard et al., 1977). Giving the observed fluctuations between the high- and low-production phases in surface waters of a few days to a week and sinking speeds of only few meters per day for slow-sinking particles, the surface production patterns and the deeper water particle inventory for this group of particles can easily be out of phase. This is different for fast-sinking aggregates and fecal pellets, which over the first few hundreds of meters in the water column are more or less synchronized with their surface production. Therefore, what we observe in deeper layers is always a mixture of particles with different production histories. Whereas the presence of light particles will enhance midwater respiration, fast-sinking particles will tend to escape this process by sinking. The persistence of slow-sinking particles in deeper layers from previous phases of high surface production and their respiration can then lead to the observed imbalance in flux rate estimations between our two methods. Besides, these particles are more susceptible to lateral transport, decreasing the collection efficiency of sediment traps. In agreement with our findings during this period, recent works have reported a greater metabolic carbon demand for the plankton community as compared to the measured vertical POC supply (Baltar et al., 2009; Steinberg et al., 2008). They recorded a contribution of slowly settling particles to the total mass flux considerably high, and hence, the consumption of this POC pool not sampled by the sediment traps could explain the mismatch (Alonso-González et al., 2010). In addition to this, considering the contribution of the dissolved organic carbon (DOC) to the microheterotroph respiration, which has been estimated to be as high as 15% for the global ocean (Arístegui et al., 2002), could help lessen the difference between the two measurements. In any case, Alonso-González et al. (2010) suggested that if the fast-sinking particles dominated the flux, the imbalance between the metabolic carbon demand and the vertical POC flux would be lower. Here, we have demonstrated that for the specific case of the high productive system of the Benguela upwelling and when the fast-sinking particles dominated in the water column, the vertical POC flux exceeded the respiration associated carbon flux. Whether this pattern holds for other productive systems and/or sinking particle characteristics needs further research. Overall, our results agree with Gust and Kozerski (2000), who asserted that particle settling velocity is a key factor controlling the hydrodynamic biases affecting sediment traps.

The F_c approach has previously been applied in waters of the Gulf of Maine (Packard and Christensen, 2004) and, more recently, the Canaries (Packard and Gómez, 2013). This method has proved to be a useful tool to determine the vertical carbon flux in these sites that are characterized by more oligotrophic waters, where the sediment respiration and carbon burial are negligible. In our case, due to the high productivity of the northern Benguela system, we might be partially underestimating total sinking carbon flux by the F_c approximation. However, the combination of this approach together with the sediment trap data serve the requirements for both integrated balanced flux estimates and layer- and size class-resolving assessments of driving forces for the particle loss in the water column. This fosters the concurrent comprehension of both quantitative and qualitative aspects of system functioning and delivers both the process-understanding and the quantitative information. Thus, assuming a mean primary productivity (PP) value of 201 mmol C m^{-2} d^{-1} for the surface waters in this transition area (Fernández-Urruzola et al., 2014), 20.2% of this PP was consumed on average from below the E_z to the sediment trap depth via plankton respiration. The mean POC value that arrived to the sediment traps during the entire sampling time was 4.7 mmol C m^{-2} d^{-1}, which represented 2.3% of the PP. This rate agrees with previous values reported for carbon accumulation on the sediments of Atlantic and Pacific continental margins (Anderson et al., 1994; Pilskaln et al., 1996; Walsh et al., 1981). The addition of both values reflected the percentage of PP that was exported at the base of the E_z, i.e. the e-ratio (Buesseler et al., 2007b), namely ~23%. These values compare reasonably well with others found in the literature for similar high productive systems (Buesseler and Boyd, 2009; Martin et al., 1987; Schlitzer, 2000).

4.3. Changes in F_c with distance to shore

The variation of POC flux with depth is commonly estimated by regression equations taken from the literature rather than by in situ measurements (Baltar et al., 2009; Sarmiento et al., 1993). One of the most used regression is that proposed by Martin et al. (1987), which relates the flux at any depth to the known flux at 100 m. However, this power law is sensitive to shallow depths and therefore, it biases the comparison of the POC flux in the upper mesopelagic waters between sites of different depths (Buesseler and Boyd, 2009; Primeau, 2006). Other published regressions related the POC flux with the PP in the surface (Betzer et al., 1984; Pace et al., 1987; Suess, 1980), although Berelson (2001) demonstrated that these models overestimated the actual POC flux when the PP > 40 mmol C m^{-2} d^{-1}. Therefore, there is still a controversy about the best model to estimate the POC flux. In our case, we have applied the best fit to model the POC flux associated with zooplankton respiration. The regression equation for the coastal and transition areas was the logarithmic function while for the oceanic area the best fit was the exponential function (Table 5). Although it seems to be in disagreement with previous applied models, we suggest that it is not. In the shallow, high productive waters of the shelf and continental slope, the zooplankton is widespread throughout the water column and so will be the POC consumption to sustain their metabolic requirements. Indeed, if we compare our results with those obtained in Martin's work for their coastal station (Fig. 2 in Martin et al., 1987) and we consider the first 400 m of their profile so as to compare with our maximum depth of the northern Benguela shelf, the shape of the curve would reasonably resemble our logarithmic curves described for the transition zone (Fig. 5). In the deep, less productive waters of the oceanic area, in turn, the zooplankton is mainly found in the upper layer of the water column and, therefore, the POC consumption will be major at surface and will decrease rapidly with depth, depicting a typical exponential curve. We propose that in the case of having more sampling depths in the mesopelagic and bathypelagic waters, the best profile might have been a power function, as it fits the data better at depth (Packard et al., 1983).

From the F_c profiles, we estimated the zooplankton associated e-ratio, T_{eff} and NRE in order to characterize the system (Table 6). Here, the e-ratio represents only the export production that sustains the zooplankton metabolism below the E_z. It does not consider the POC consumption by the microplankton and the eventual carbon accumulation in the sediments and, therefore, it falls at the low end of the range given by other trap-derived and model-based studies (Berger et al., 1989; Buesseler et al., 2007b; Schlitzer, 2000). In the oceanic area, the

Appendix

contribution of zooplankton to the POC attenuation was remarkably variable as was its distribution (Fernández-Urruzola et al., 2014). At NAM014, the zooplankton respiration was higher, which increased the POC remineralization and the NRE but decreased the T_{eff}. In contrast, the respiration values at NAM026 were lower and therefore, most of the POC was not remineralized and was transferred to the depth below 500 m, decreasing the NRE in this upper mesopelagic layer. For the stations in between, the T_{eff} stayed relatively constant, even though the e-ratio varied by a factor of 3, which suggests that most of the POC consumption occurred above 150 m in this area.

5. Conclusions

The short term assessments of vertical particle fluxes accomplished here revealed the major influence of the temporal variability rather than the effect of distance to the core of the coastal upwelling, mainly due to the important instabilities that upwelling filaments caused in this region. Two basic situations were distinguished during the study: one was influenced by mature waters of the upwelling filament, characterized by higher respiration rates of microplankton and small zooplankton as well as by high particle sedimentation rates. The predominance of diatoms during this period together with the higher contribution of lithogenic material promoted particle aggregation and led to the formation of fast-sinking particles. Thus, the remineralization by the water column plankton did not account for all the sinking POC and consequently, estimates of carbon flux from the sediment traps exceeded that of respiration-based values. The other distinct situation corresponded to a later temporal stage of the upwelled waters, with the predominance of respiration by large zooplankton, an increase of coccolitophorides and low particle sedimentation rates. In this case, the rain of POC from the surface was mainly constituted by slow sinking particles, which probably originated during a high production period and that supported asynchronously midwater respiration. Thus, in regions of oscillating surface productivity, the inventory of slow sinking particles in deeper strata from previous production peaks might have a certain compensation effect on the respiratory activities. Accordingly, the carbon flux values from the respiration-based model were larger than those from the sediment traps during this low-sed situation. In view of the results, we have shown that the previously reported mismatch in the carbon flux estimations between the sediment trap data and the metabolic carbon requirements of the organisms decreases or even disappears depending on the productivity rates, the nature of the sinking particles and, eventually, on their settling velocities. We encourage future studies to see whether this pattern holds for other highly productive systems, such as other eastern boundary currents, coastal waters or equatorial upwellings, with different community structures in the water column.

In the highly productive waters of the northern Benguela upwelling, the combination of the two approaches has served to obtain a global picture of particle fluxes. However, in oligotrophic waters, where the sediment respiration and carbon burial are negligible as compared to the water column respiration, the F_c approach itself is a useful tool to estimate the vertical carbon flux due to heterotrophic POC consumption. In the same way, the conceptual basis of the F_c approach can be applied to describe other biogeochemical processes, such as the contribution of zooplankton to the vertical PON flux attenuation, from GDH activity measurements (Fernández-Urruzola et al., 2011).

Acknowledgments

We would like to thank to R. Hansen, I. Liskow and T. Leipe for analytical work on the sediment trap material. The microphotographs were also provided by R. Hansen. We are grateful to A. Herrera for her collaboration in collecting the biological samples as well as to the anonymous reviewers for contributing valuable suggestions which notably improved the manuscript. This work was funded by a DFG cruise support, and by the BIOMBA project (CTM2012-32729/MAR) awarded to M. Gomez by the Spanish Economy and Competitiveness Ministry. N. Osma and I. Fernández-Urruzola received financial support from the Formation and Perfection of the Researcher Personal Program from the Basque Government.

References

Alonso-González, I.J., Arístegui, J., Lee, C., Sanchez-Vidal, A., Calafat, A., Fabrés, J., Sangrá, P., Masqué, P., Hernández-Guerra, A., Benítez-Barrios, V., 2010. Role of slowly settling particles in the ocean carbon cycle. Geophys. Res. Lett. 37 (13), L13608.
Altabet, M.A., Deuser, W.G., Honjo, S., Stienen, C., 1991. Seasonal and depth-related changes in the source of sinking particles in the North Atlantic. Nature 354, 1–4.
Anderson, R.F., Rowe, G.T., Kemp, P.F., Trumbores, S., Biscaye, P.E., 1994. Carbon budget for the mid-slope depocenter of the Middle Atlantic Bight. Deep-Sea Res. II 41 (2), 669–703.
Arístegui, J., Duarte, C.M., Agustí, S., Doval, M., Álvarez-Salgado, X.A., Hansell, D.A., 2002. Dissolved organic carbon support of respiration in the dark ocean. Science 298 (5600), 1967.
Armstrong, R.A., Lee, C., Hedges, J.I., Honjo, S., Wakeham, S.G., 2001. A new, mechanistic model for organic carbon fluxes in the ocean based on the quantitative association of POC with ballast minerals. Deep-Sea Res. II 49 (1–3), 219–236.
Bakun, A., Nelson, C.S., 1991. The seasonal cycle of wind-stress curl in subtropical eastern boundary current regions. J. Phys. Oceanogr. 21 (12), 1815–1834.
Baltar, F., Arístegui, J., Gasol, J.M., Sintes, E., Herndl, G.J., 2009. Evidence of prokaryotic metabolism on suspended particulate organic matter in the dark waters of the subtropical North Atlantic. Limnol. Oceanogr. 54 (1), 182–193.
Berelson, W.M., 2001. The flux of particulate organic carbon into the ocean interior: a comparison of four U.S. JGOFS regional studies. Oceanol. Acta 14 (4), 59–67.
Berger, W.H., Wefer, G., 1990. Export production: seasonality and intermittency, and paleoceanographic implications. Palaeogeogr. Palaeoclimatol. 89 (3), 245–254.
Berger, W.H., Smetacek, V.S., Wefer, G., 1989. Ocean productivity and paleoproductivity — an overview. In: Berger, W.H., Smetacek, V.S., Wefer, G. (Eds.), Productivity of the Ocean Present and Past. John Wiley & Sons Limited, pp. 1–34.
Betzer, P.R., Showers, W.J., Laws, E.A., Winn, C.D., DiTullio, G.R., Kroopnick, P.M., 1984. Primary productivity and particle fluxes on a transect of the equator at 153°W in the Pacific Ocean. Deep-Sea Res. 31 (1), 1–11.
Bode, M., Schukat, A., Hagen, W., Auel, H., 2013. Predicting metabolic rates of calanoid copepods. J. Exp. Mar. Biol. Ecol. 444, 1–7.
Boyd, P., Newton, P., 1995. Evidence of the potential influence of planktonic community structure on the interannual variability of particulate organic carbon flux. Deep-Sea Res. I 42 (5), 619–639.
Boyer, D., Cole, J., Bartholomae, C., 2000. Southwestern Africa: Northern Benguela Current region. Mar. Pollut. Bull. 41 (1–6), 123–140.
Brown, A.M., 2001. A step-by-step guide to non-linear regression analysis of experimental data using a Microsoft Excel spreadsheet. Comput. Methods Prog. Biomed. 65 (3), 191–200.
Brown, P.C., Painting, S.J., Cochrane, K.L., 1991. Estimates of phytoplankton and bacterial biomass and production in the northern and southern Benguela ecosystems. S. Afr. J. Mar. Sci. 11 (1), 537–564.
Buesseler, K.O., 1991. Do upper-ocean sediment traps provide an accurate record of particle flux? Nature 353, 420–423.
Buesseler, K.O., 1998. The decoupling of production and particulate export in the surface ocean. Global Biogeochem. Cycles 12 (2), 297–310.
Buesseler, K.O., Boyd, P.W., 2009. Shedding light on processes that control particle export and flux attenuation in the twilight zone of the open ocean. Limnol. Oceanogr. 54 (4), 1210–1232.
Buesseler, K.O., Antia, A.N., Chen, M., Fowler, S.W., Gardner, W.D., Gustafsson, O., Harada, K., Michaels, A.F., Loeff, M.R.V.D., Sarin, M., Steinberg, D.K., Trull, T., 2007a. An assessment of the use of sediment traps for estimating upper ocean particle fluxes. J. Mar. Res. 65, 345–416.
Buesseler, K.O., Lamborg, C.H., Boyd, P.W., Lam, P.J., Trull, T.W., Bidigare, R.R., Bishop, J.K.B., Casciotti, K.L., Dehairs, F., Elskens, M., Honda, M., Karl, D.M., Siegel, D.A., Silver, M.W., Steinberg, D.K., Valdes, J., Mooy, B.V., Wilson, S., 2007b. Revisiting carbon flux through the ocean's twilight zone. Science 316, 567–570 (April).
Burd, A.B., Hansell, D.A., Steinberg, D.K., Anderson, T.R., Arístegui, J., Baltar, F., Beaupré, S.R., Buesseler, K.O., Dehairs, F., Jackson, G.A., Kadko, D.C., Koppelmann, R., Lampitt, R.S., Nagata, T., Reinthaler, T., Robinson, C., Robison, B.H., Tamburini, C., Tanaka, T., 2010. Assessing the apparent imbalance between geochemical and biochemical indicators of meso- and bathypelagic biological activity: what the @$#! is wrong with present calculations of carbon budgets? Deep-Sea Res. II 57 (16), 1557–1571.
Carr, M.E., 2001. Estimation of potential productivity in eastern boundary currents using remote sensing. Deep-Sea Res. II 49 (1–3), 59–80.
Chapman, P., Mitchell-Innes, B.A., Walker, D.R., 1994. Microplankton ETS measurements as a means of assessing respiration in the Benguela ecosystem. S. Afr. J. Mar. Sci. 14, 297–312.
Dugdale, R.C., Goering, J.J., 1967. Uptake of new and regenerated forms of nitrogen in primary productivity. Limnol. Oceanogr. 12, 196–206.
Eppley, R.W., Peterson, B.J., 1979. Particulate organic matter flux and planktonic new production in the deep ocean. Nature 282, 677–680.
Estrada, M., Marrasé, C., 1987. Phytoplankton biomass and productivity off the Namibian Coast. S. Afr. J. Mar. Sci. 5 (1), 347–356.
Faul, K.L., Paytan, A., Delaney, M.L., 2005. Phosphorus distribution in sinking oceanic particulate matter. Mar. Chem. 97 (3–4), 307–333.

Fernández-Urruzola, I., Packard, T.T., Gómez, M., 2011. GDH activity and ammonium excretion in the marine mysid, *Leptomysis lingvura*: effects of age and starvation. J. Exp. Mar. Biol. Ecol. 409 (1–2), 21–29.

Fernández-Urruzola, I., Osma, N., Packard, T.T., Gómez, M., Postel, L., 2014. Distribution of zooplankton biomass and potential metabolic activities across the northern Benguela upwelling system. J. Mar. Syst. 140, 66–77.

Fisher, G., Wefer, G., 1996. Long-term observations of particle fluxes in the eastern Atlantic: seasonality, changes of flux with depth and comparison with the sediment record. In: Wefer, G., Berger, W.H., Siedler, G., Webb, D. (Eds.), The South Atlantic Ocean, Present and Past Circulation. Springer, Berlin, pp. 325–344.

Gardner, W.D., 2000. Sediment trap sampling in surface waters. In: Hanson, R.B., Ducklow, H.W., Field, J.G. (Eds.), The Changing Ocean Carbon Cycle: A Midterm Synthesis of the Joint Global Ocean Flux Study. Cambridge University Press, Cambridge, New York, pp. 240–281.

Giraudeau, J., Bailey, G.W., Pujol, C., 2000. A high-resolution time-series analyses of particle fluxes in the northern Benguela coastal upwelling system: carbonate record of changes in biogenic production and particle transfer processes. Deep-Sea Res. II 47 (9–11), 1999–2028.

González, H.E., Daneri, G., Iriarte, J.L., Yannicelli, B., Menschel, E., Barría, C., Pantoja, S., Lizárraga, L., 2009. Carbon fluxes within the epipelagic zone of the Humboldt Current system off Chile: the significance of euphausiids and diatoms as key functional groups for the biological pump. Prog. Oceanogr. 83 (1–4), 217–227.

Grasshoff, K., 1976. Methods of Seawater Analysis. Verlag Chemie, Weinheim (317 pp.).

Guidi, L., Stemmann, L., Jackson, G.A., Ibanez, F., Claustre, H., Legendre, L., Picheral, M., Gorsky, G., 2009. Effects of phytoplankton community on production, size and export of large aggregates: a world-ocean analysis. Limnol. Oceanogr. 54 (6), 1951.

Gust, G., Kozerski, H.P., 2000. In situ sinking-particle flux from collection rates of cylindrical traps. Mar. Ecol. Prog. Ser. 208 (8), 93–106.

Hansen, A., Wasmund, N., Ohde, T., 2014. Phytoplankton succession in aging upwelled waters off Namibia. J. Mar. Syst. (this volume).

Hernández-León, S., Gómez, M., 1996. Factors affecting the respiration/ETS ratio in marine zooplankton. J. Plankton Res. 18 (2), 239–255.

Hernández-León, S., Almeida, C., Portillo-Hahnefeld, A., Gómez, M., Rodríguez, J.M., Arístegui, J., 2002. Zooplankton biomass and indices of feeding and metabolism in relation to an upwelling filament off northwest Africa. J. Mar. Res. 60, 327–346.

Huenerlage, K., Buchholz, F., 2013. Krill of the northern Benguela Current and the Angola–Benguela frontal zone compared: physiological performance and short-term starvation in *Euphausia hanseni*. J. Plankton Res. 35 (2), 337–351.

Isla, J., Anadón, R., 2004. Mesozooplankton size-fractionated metabolism and feeding off NW Spain during autumn: effects of a poleward current. ICES J. Mar. Sci. 61 (4), 526–534.

Iversen, M.H., Ploug, H., 2010. Ballast minerals and the sinking carbon flux in the ocean: carbon-specific respiration rates and sinking velocity of marine snow aggregates. Biogeosciences 7 (9), 2613–2624.

King, F.D., Packard, T.T., 1975. Respiration and the activity of the respiratory electron transport system in marine zooplankton. Limnol. Oceanogr. 849–854.

Leipe, T., Knoppers, B., Marone, E., Camargo, R., 1999. Suspended matter transport in coral reef waters of the Abrolhos Bank, Brazil. Geo-Mar. Lett. 19 (3), 186–195.

Maldonado, F., Packard, T.T., Gómez, M., 2012. Understanding tetrazolium reduction and the importance of substrates in measuring respiratory electron transport activity. J. Exp. Mar. Biol. Ecol. 434–435, 110–118.

Mariotti, A., Lancelot, C., Billen, G., 1984. Natural isotopic composition of nitrogen as a tracer of origin for suspended organic matter in the Scheldt estuary. Geochim. Cosmochim. Acta 48 (3), 549–555.

Martin, J.H., Knauer, G.A., Karl, D.M., Broenkow, W.W., 1987. VERTEX: carbon cycling in the northeast Pacific. Deep-Sea Res. 34 (2), 267–285.

Mohrholz, V., Eggert, A., Junkers, T., Nausch, G., Ohde, T., Schmidt, M., 2014. Cross shelf hydrographic and hydrochemical conditions and their short term variability at the northern Benguela during a normal upwelling season. J. Mar. Syst. 140, 20–38.

Monteiro, P.M.S., Nelson, G., van der Plas, A., Mabille, E., Bailey, G.W., Klingelhoeffer, E., 2005. Internal tide–shelf topography interactions as a forcing factor governing the large-scale distribution and burial fluxes of particulate organic matter (POM) in the Benguela upwelling system. Cont. Shelf Res. 25 (15), 1864–1876.

Owens, T.G., King, F.D., 1975. The measurement of respiratory electron-transport-system activity in marine zooplankton. Mar. Biol. 30 (1), 27–36.

Pace, M.L., Knauer, G.A., Karl, D.M., Martin, J.H., 1987. Primary production, new production and vertical flux in the eastern Pacific Ocean. Nature 325 (6107), 803–804.

Packard, T.T., Christensen, J.P., 2004. Respiration and vertical carbon flux in the Gulf of Maine water column. J. Mar. Res. 62, 93–115.

Packard, T.T., Gómez, M., 2013. Modeling vertical carbon flux from zooplankton respiration. Prog. Oceanogr. 110, 59–68.

Packard, T.T., Williams, P.J.L., 1981. Rates of respiratory oxygen consumption and electron transport in surface seawater from the northwest Atlantic. Oceanol. Acta 4 (3), 351–358.

Packard, T.T., Healy, M.L., Richards, F.A., 1971. Vertical distribution of the activity of the respiratory electron transport system in marine plankton. Limnol. Oceanogr. 16 (1), 60–70.

Packard, T.T., Harmon, D., Boucher, J., 1974. Respiratory electron transport activity in plankton from upwelled waters. Tethys 6 (1–2), 213–222.

Packard, T.T., Devol, A.H., King, F.D., 1975. The effect of temperature on the respiratory electron transport system in marine plankton. Deep-Sea Res. 22, 237–249.

Packard, T.T., Minas, H.J., Owens, T.G., Devol, A.H., 1977. Deep sea metabolism in the Eastern tropical North Pacific ocean. In: Andersen, N.R., Zahuranec, B.J. (Eds.), Oceanic Sound Scattering Prediction. Plenum Press, New York, pp. 101–116.

Packard, T.T., Garfield, P.C., Codispoti, L., 1983. Oxygen consumption and denitrification below the Peruvian upwelling. NATO Conf. Ser. 147–173.

Packard, T.T., Denis, M., Rodier, M., Garfield, P., 1988. Deep-ocean metabolic CO_2 production: calculations from ETS activity. Deep-Sea Res. 35 (3), 371–382.

Paytan, A., Cade-Menun, B.J., McLaughlin, K., Faul, K.L., 2003. Selective phosphorus regeneration of sinking marine particles: evidence from ^{31}P NMR. Mar. Chem. 82 (1–2), 55–70.

Pilskaln, C.H., Paduan, J.B., Chavez, F.P., Anderson, R.Y., Berelson, W.M., 1996. Carbon export and regeneration in the coastal upwelling system of Monterey Bay, central California. J. Mar. Res. 54, 1149–1178.

Pollehne, F., Klein, B., Zeitzschel, B., 1993a. Low light adaptation and export production in the deep chlorophyll maximum layer in the northern Indian Ocean. Deep-Sea Res. II 40 (3), 737–752.

Pollehne, F., Zeitzschel, B., Peinert, R., 1993b. Short-term sedimentation patterns in the northern Indian Ocean. Deep-Sea Res. II 40 (3), 821–831.

Primeau, F., 2006. On the variability of the exponent in the power law depth dependence of POC flux estimated from sediment traps. Deep-Sea Res. I 53 (8), 1335–1343.

Romero, O., Boeckel, B., Donner, B., Lavik, G., Fischer, G., Wefer, G., 2002. Seasonal productivity dynamics in the pelagic central Benguela system inferred from the flux of carbonate and silicate organisms. J. Mar. Syst. 37, 259–278.

Sarmiento, J.L., Slater, R.D., Fasham, M., Ducklow, H.W., Toggweiler, J.R., Evans, G.T., 1993. A seasonal three dimensional ecosystem model of nitrogen cycling in the North Atlantic euphotic zone. Global Biogeochem. Cycles 7 (2), 417–450.

Schlitzer, R., 2000. Applying the adjoint method for biogeochemical modeling: export of particulate organic matter in the world ocean. In: Kasibhatla, P., Heimann, M., Rayner, P., Mahowald, N., Prinn, R.G., Hartley, D.E. (Eds.), Inverse Methods in Global Biogeochemical Cycles. American Geophysical Union, Washington, DC, pp. 107–124.

Shannon, L.V., Nelson, G., 1996. The Benguela: large scale features and processes and system variability. In: Wefer, G., Berger, W.H., Siedler, G., Webb, D. (Eds.), The South Atlantic Ocean, Present and Past Circulation. Springer, Berlin, pp. 163–210.

Shillington, F.A., Hutchings, L., Probyn, T.A., Waldron, H.N., Peterson, W.T., 1992. Filaments and the Benguela frontal zone: offshore advection or recirculating loops? S. Afr. J. Mar. Sci. 12 (1), 207–218.

Steinberg, D.K., Mooy, B.A.S.V., Buesseler, K.O., Boyd, P.W., Kobari, T., Karl, D.M., 2008. Bacterial vs. zooplankton control of sinking particle flux in the ocean's twilight zone. Limnol. Oceanogr. 53 (4), 1327–1338.

Suess, E., 1980. Particulate organic carbon flux in the oceans — surface productivity and oxygen utilization. Nature 288, 260–263.

Takahashi, T., Broecker, W.S., Langer, S., 1985. Redfield ratio based on chemical data from isopycnal surfaces. J. Geophys. Res. 90 (C4), 6907–6924.

Thornton, D.C.O., 2002. Diatom aggregation in the sea: mechanisms and ecological implications. Eur. J. Phycol. 37 (2), 149–161.

Vinogradov, M.E., Menshutkin, V.V., Shushkina, E.A., 1972. On mathematical simulation of a pelagic ecosystem in tropical waters of the ocean. Mar. Biol. 16, 261–268.

Volk, T., Hoffert, M.I., 1985. Ocean carbon pumps: analysis of relative strengths and efficiencies in ocean-driven atmospheric CO_2 changes. Geophys. Monogr. 32, 99–110.

von Bodungen, B., Wunsch, M., Fürderer, H., 1991. Sampling and analysis of suspended and sinking particles in the northern North Atlantic. Geophys. Monogr. 63 (3), 47–56.

Walsh, J.J., Rowe, G.T., Iverson, R.L., McRoy, C.P., 1981. Biological export of shelf carbon is a sink of the global CO_2 cycle. Nature 291, 196–201.

Biogeosciences, 12, 2641–2654, 2015
www.biogeosciences.net/12/2641/2015/
doi:10.5194/bg-12-2641-2015
© Author(s) 2015. CC Attribution 3.0 License.

Biogeosciences Open Access

Peruvian upwelling plankton respiration: calculations of carbon flux, nutrient retention efficiency, and heterotrophic energy production

T. T. Packard[1], N. Osma[1], I. Fernández-Urruzola[1], L. A. Codispoti[2], J. P. Christensen[3], and M. Gómez[1]

[1]Marine Ecophysiology Group (EOMAR), Universidad de Las Palmas de Gran Canaria, Campus Universitario de Tafira 35017, Las Palmas de Gran Canaria, Spain
[2]Horn Point Laboratory, University of Maryland, 21613-0775 Cambridge, MD, USA
[3]Green Eyes LLC, Easton, MD 21601, USA

Correspondence to: T. T. Packard (theodoretrainpackard@gmail.com)

Received: 22 October 2014 – Published in Biogeosciences Discuss.: 26 November 2014
Revised: 9 April 2015 – Accepted: 14 April 2015 – Published: 6 May 2015

Abstract. Oceanic depth profiles of plankton respiration are described by a power function, $R_{CO_2} = (R_{CO_2})_0(z/z_0)^b$, similar to the vertical carbon flux profile. Furthermore, because both ocean processes are closely related, conceptually and mathematically, each can be calculated from the other. The exponent b, always negative, defines the maximum curvature of the respiration–depth profile and controls the carbon flux. When $|b|$ is large, the carbon flux (F_C) from the epipelagic ocean is low and the nutrient retention efficiency (NRE) is high, allowing these waters to maintain high productivity. The opposite occurs when $|b|$ is small. This means that the attenuation of respiration in ocean water columns is critical in understanding and predicting both vertical F_C as well as the capacity of epipelagic ecosystems to retain their nutrients. The ratio of seawater R_{CO_2} to incoming F_C is the NRE, a new metric that represents nutrient regeneration in a seawater layer in reference to the nutrients introduced into that layer via F_C. A depth profile of F_C is the integral of water column respiration. This relationship facilitates calculating ocean sections of F_C from water column respiration. In an F_C section and in a NRE section across the Peruvian upwelling system we found an F_C maximum and a NRE minimum extending down to 400 m, 50 km off the Peruvian coast over the upper part of the continental slope. Finally, considering the coupling between respiratory electron transport system activity and heterotrophic oxidative phosphorylation promoted the calculation of an ocean section of heterotrophic energy production (HEP). It ranged from 250 to 500 J d^{-1} m^{-3} in the euphotic zone to less than 5 J d^{-1} m^{-3} below 200 m on this ocean section.

1 Introduction

Respiration is as ubiquitous in the ocean as the microorganisms that cause it (Seiwell, 1934; Richards, 1957; Lane, 2002). It is controlled by the respiratory electron transport (ETS) activity in eukaryotic mitochondria and prokaryotic cell membranes (Packard, 1969; Packard et al., 1971; Lane, 2005; Nelson and Cox., 2000) and is responsible for the bulk of oceanic O_2 consumption (Seiwell, 1937; Redfield et al., 1963; Packard, 1985a). It is driven by the degradation of dissolved and particulate organic carbon, generates CO_2 (Redfield et al., 1963), acidifies seawater (Harvey, 1955), and produces energy in the form of ATP (heterotrophic energy production) (Ochoa, 1943; Nelson and Cox., 2000; Madigan et al., 2000). Even in anoxic seawater, respiration degrades organic matter, produces CO_2, and generates ATP while reducing nitrogen oxides to N_2 or SO_4^- to H_2S (Richards, 1965; Madigan et al., 2000). Plankton community respiration in ocean water columns is a key variable in calculating net community productivity (Ducklow and Doney, 2013) in developing oceanic carbon models, in resolving the autotrophic–heterotrophic states of ocean ecosystems (Williams et al.,

Published by Copernicus Publications on behalf of the European Geosciences Union.

2012), and in understanding vertical ocean F_C rates (Giering et al., 2014). The research team led by Sarah Giering (Giering et al., 2014) demonstrated that, contrary to previous efforts (Burd et al., 2010) but in accord with classical oceanographic understanding (Riley, 1951; Richards, 1957; Redfield et al., 1963; Suess, 1980), zooplankton and microplankton (prokaryote and eukaryote) respiration balance vertical carbon flux (Riley, 1951; Eppley and Peterson, 1979; Packard et al., 1988). All these findings support the use of plankton respiration in assessing vertical F_C in the ocean water column. Conceptually, the reciprocal relationship between the water column respiration and the F_C, from the ocean's epipelagic zone, is clear (Suess, 1980; Martin et al., 1987). However, describing this reciprocal relationship mathematically, as a function of ocean depth in the forms,

$$R = f(z) \text{ and } F_C = \int_{z_1}^{z_2} R\,dz,$$

was delayed until the helium–tritium studies of Jenkins (Jenkins, 1982, 1984), the sediment trap studies of VERTEX program (Martin et al., 1987), and respiratory electron transport system (ETS) measurements in the Gulf of Maine (Packard and Christensen, 2004). In the latter, microplankton ETS measurements were used to build power function models of respiratory CO_2 production (R_{CO_2}) and F_C. Here, we extend this approach to calculate a microplankton respiration section across the Peruvian upwelling system ((Walsh, 1972; Barber et al., 1971) and Fig. 1a) and to model F_C on this transect. We focused our measurements on microplankton because its biomass and metabolism dominate ocean water columns (King et al., 1978; Arístegui et al., 2009; Laufkötter et al., 2013). The section was made at a time of regime change when the Peruvian upwelling system and the El Niño–Southern Oscillation (ENSO) underwent a shift (Santoso et al., 2013). Here we document some of the biological phenomenon that occurred at that time. With the F_C and the R_{CO_2} models we calculate the nutrient retention efficiency (NRE) (Packard and Gómez, 2013; Osma et al., 2014), a new metric that quantifies the ability of an ocean layer to retain its nutrients (Fig. 2c). Conceptually, the NRE is the nutrient remineralization rate within an ocean layer normalized by nutrients entering that layer via carbon flux. Below the euphotic zone, it can be calculated as the inverse of the F_C transfer efficiency (Buesseler et al., 2007; Buesseler and Boyd, 2009), but we show here that it can also be calculated from a profile of plankton respiration. In addition, using different limits to the F_C integration, we calculate the sum of the benthic respiration and carbon burial (Fig. 3a) that occurs on the sea floor. Finally, we use the respiration models and the coupling between ETS activity and oxidative phosphorylation to calculate light-independent heterotrophic energy flow (Karl, 2014). This energy is generated in the form of ATP by ATP synthase, an enzyme motor coupled to a heterotrophic respiratory process such as O_2 utilization or NO_3^- reduction (Watt et al., 2010; Ferguson, 2010). In all types of respiration, the ATP synthase senses the pH and electromotive force gradient across the membrane in which the ATP synthase is embedded (Lane et al., 2010), and when the gradient is sufficiently strong (~ 225 mV), the molecular motor that is the ATP synthase starts its rotary production of ATP (Walker, 1998). Heterotrophic ATP generation in any ecosystem is largely based on exploiting the Gibbs free energy (ΔG) released during the oxidation of different organic compounds. The biochemistry of ATP and the ETS was unknown in 1925, but even then the idea of capturing biologically useable energy from respiration was appreciated by Lotka (1925). A generation later, Odum built on this concept to describe energy flow in freshwater streams (Odum, 1956). Reviewing this earlier work, Karl recently argued that biological energy production in the ocean should be assessed to provide insight into the variability of ocean productivity (Karl, 2014). Here, we address his concern by calculating Heterotrophic energy production (HEP) in a C-line section (Fig. 2d). This HEP is the energy produced while ATP is generated by respiratory O_2 consumption (R_{O_2}) in the microplankton community composed of phytoplankton, bacteria, archaea, and protozoans in the epipelagic layer and by the R_{O_2} and NO_3^- reduction in microbial communities of bacteria, archaea, and protozoans in the meso- and bathypelagic waters of the Peruvian current upwelling system.

2 Methods

2.1 Research site

The site of this Coastal Upwelling Ecosystem Analysis (CUEA) investigation at 15° S off Pisco, Peru (Fig. 1) was chosen because the upwelling is strong, persistent, and well known (Wooster, 1961; Fernández et al., 2009). It was the focus of the R/V *Anton Bruun* cruise 15 (Ryther et al., 1970), the R/V *T.G. Thompson Pisco* expedition in 1969 (Barber et al., 1978), and others (Wyrtki, 1967; Walsh et al., 1971) before it was the focus of the CUEA–JOINT II program (Brink et al., 1981; Packard, 1981) of which the JASON Expedition was a part (King, 1981; Richards, 1981). However, in spite of the many previous expeditions to this site most of them took place in the austral fall (March–April–May). The JASON-76 expedition was unique because it took place in the late winter and austral spring (August, September, October, and November) when the southeast trade winds would be at their strongest (Wooster, 1961). In this way it was thought that the results might be more comparable with results from upwelling studies made in the Northern Hemisphere's springtime upwelling off NW Africa (Codispoti et al., 1982; Minas et al., 1982). The results presented here are from the September 10 to September 24 leg of JASON-76 on board Duke University's Oceanographic ship, R/V *Eastward*, cruise no. E-5H-67 (Packard and Jones, 1976).

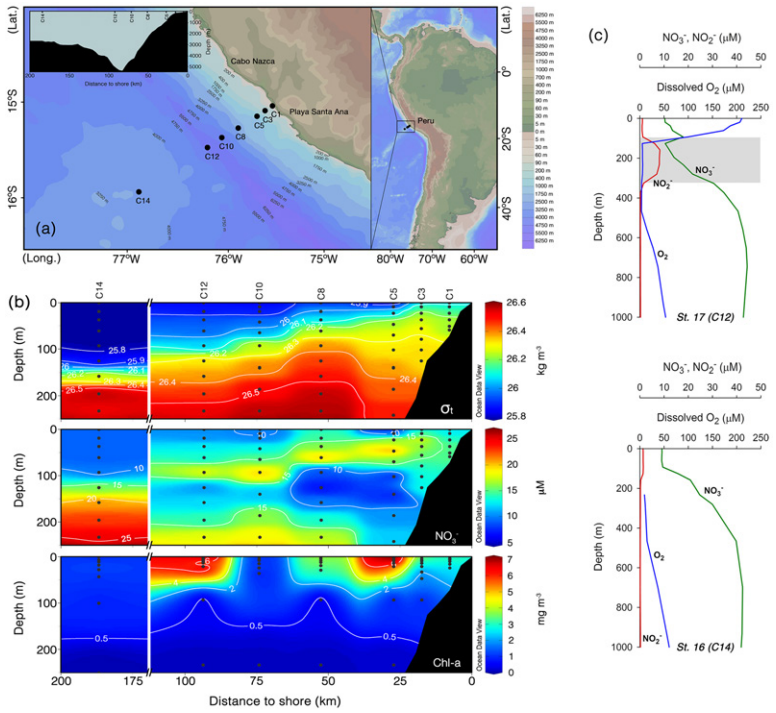

Figure 1. (a) C-line section orthogonal to the Peruvian coast at 15° S. The innermost C-line position, C1, was 2.7 km from the coast between Cabo Nazca and Punta Santa Ana. The outermost position, C14, was located west of the Peru–Chile trench 185.2 km from the coast. Depth along this transect ranged from 63 m at C1 to 4755 m at C12. C14 was in 2680 m of water on the gently rising abyssal plain seaward of the trench (inset upper left). **(b)** Density (σ_t), NO_3^- (µM) and phytoplankton chlorophyll (mg m^{-3}) sections along the C-line from C1 to C14 (top, middle and bottom panels, respectively). All sections represent the upwelling from 13 to 20 September 1976. Scale brakes avoid interpolation over a 90 km data gap. The high phytoplankton biomass over the shelf break occurs between C5 and C8, 15 to 35 km from the coast. **(c)** NO_3^-, NO_2^-, and O_2 depth profiles through the mesopelagic waters over the trench at C12 (top) and over the outermost station at C14 (bottom). The vertical plot at C12 documents the first step in denitrification (shaded area), NO_3^- reduction to NO_2^-, at the foot of the oxycline, in the oxygen minimum zone (OMZ) between 150 and 300 m. In contrast, the vertical profiles at C14, 185 km off the coast, show the absence of denitrification in mesopelagic waters.

2.2 Sampling

All sampling was conducted along the C-line (Fig. 1a) that extended seaward from the coast at position C1, just south of Cabo Nazca (Pisco), across the deep trench to position C14, 185 km offshore (Packard, 1981). Hydrographic sections were made at the beginning of the expedition (10–11 September) and again after a lapse of 10 days (20–21 September). The endpoint coordinates were from 15°3.2′ S, 75°26.0′ W to 15°55.8′ S, 75°31.4′ W (Packard and Jones, 1976; Kogelshatz et al., 1978). In addition, between 10 and 24 September, productivity stations, that focused on the biological, nutrient chemistry, and biochemical properties at depths where the light was 100, 50, 30, 15, 5, 1, and 0.1 % of the surface incident radiation (light depths), were established at C-line positions Packard and Jones (1976). These productivity stations were not made in order along the C-line section, hence the irregularity of the their numerical sequence in Tables 3–7. In addition, some locations along the C-line were occupied

Table 1. Oceanographic characteristics of Peruvian upwelling C-line stations during Duke University's JASON-76 R/V *Eastward* cruise no. E-5H-67. Ez depth is the 1 % light level. Original data are in CUEA data reports (Kogelshatz et al., 1978; Packard and Jones, 1976).

CUEA C-line position (JASON station)	Coordinates	Date in Sep 1976	Distance to coast (km)	Ocean depth (m)	Surface temperature (°C)	Surface salinity (PSU)	Euphotic zone (m)	Surface chlorophyll ($mg\,m^{-3}$)	Surface respiration ($\mu mol\,O_2\,m^{-3}\,h^{-1}$)	Surface net productivity ($mg\,C\,m^{-3}\,h^{-1}$)
C1 (22)	15°03.2′ S 75°26.0′ W	20	2.7	63	14.28	34.902	24	3.06	56.11	6.84
C3 (15)	15°05.9′ S 75°31.4′ W	12	12.9	117	14.26	–	42	2.09	24.11	3.67
C3 (21)	15°06.5′ S 75°31.0′ W	19	12.9	120	14.10	34.869	33	3.67	83.99	8.08
C5 (20)	15°09.9′ S 75°35.7′ W	18	24.7	500	15.59	34.921	21	6.96	119.13	18.24
C5 (37)	15°10.5′ S 75°36.2′ W	24	24.7	607	15.00	34.921	27	3.77	79.97	8.88
C8 (19)	15°16.9′ S 75°47.8′ W	17	49.9	1880	14.97	34.902	29	4.11	80.32	9.65
C8 (36)	15°16.9′ S 75°14.8′ W	23	49.9	2150	16.10	35.069	29	3.90	87.67	12.35
C10 (18)	15°22.0′ S 75°59.8′ W	16	70.9	4300	15.92	35.077	36	1.06	34.35	1.64
C12 (17)	15°28.0′ S 76°08.0′ W	15	92.6	4000	15.75	35.046	40	1.14	47.14	1.93
C12 (35)	15°29.0′ S 76°07.8′ W	22	92.6	4755	15.46	34.950	21	7.47	144.71	16.64
C14 (16)	15°55.8′ S 76°51.6′ W	13	185.2	2680	16.48	35.147	43	0.92	40.90	1.63

several times. For this reason, as well as to coordinate the results presented here with the results of other CUEA reports (Brink et al., 1981), both the C-line location and the station number are given through the paper. The productivity casts were made each morning before 10:00 LT with 30 L Niskin PVC bottles to six light depths (1, 5, 15, 30, 50, and 100 %). Each Niskin bottle was flushed at depth in yo-yo fashion both by the action of the ship's roll and by meter oscillations with the winch. On deck it was drained immediately, without prefiltration, into a well-rinsed carboy for subsampling and returned to depth for the next sample. The six samples were taken within 1 h. Subsamples were drawn for phytoplankton productivity, inorganic nutrient salts, (ammonium, reactive phosphorus, NO_3^-, NO_2^-, and silicate), ETS and NO_3^- reductase activities, and particulate protein (Packard and Jones, 1976). Station coordinates are given in Table 1. The inorganic nutrient salts, salinity, temperature, and O_2 can be found in CUEA data reports 38 and 45 (Hafferty et al., 1978; Kogelshatz et al., 1978). Chlorophyll and phytoplankton productivity (^{14}C uptake) are reported in CUEA data report 49 (Barber et al., 1978). The ^{14}C uptake data were calculated on an hourly basis (Table 1) from the 24 h productivity data (Kogelshatz et al., 1978). Light was measured as daily total solar radiation with an Eppley Model 8–48 pyranometer placed above the ship's bridge (Packard and Jones, 1976). Below the mesopelagic zone, the seawater was sampled for ETS activity with 30 L Niskin PVC bottles down to 2000 m, depending on the depth of the water column (Tables 2 and 3).

2.3 ETS activity, respiratory O_2 consumption, CO_2 production, and denitrification

Respiratory ETS activity in the euphotic zone (Ez) was measured according to Kenner and Ahmed (1975) as described in Packard and Williams (1981). In deeper waters it was measured according to (Packard et al., 1971) and multiplied by 3.35 to render the two data sets comparable as explained in Christensen and Packard (1979). Here, ETS activity is used as a direct measure of potential respiration and a proxy for respiration. Both potential respiration and respiration were calculated from the combined ETS data set according to Packard and Christensen (2004) and Packard and Codispoti (2007). Tables 2 and 3 explain the calculations in detail. Table 3 presents the calculations as R_{O_2} in units of $\mu mol\,O_2\,m^{-3}\,h^{-1}$ for oxic waters. Using ETS activity as a proxy for R_{O_2} requires the selection of a ratio of potential respiration (Φ) to R_{O_2}. Since direct measurements of R_{O_2} can not be made below the euphotic zone, a true calibration can not be made. The Φ to R_{O_2} ratio should be around 0.5 if Φ represents V_{max} of the ETS and standard physiological rates, governed by enzyme activities, operate close to one-half of their potential capacity (Cleland, 1967). With our methodology (Packard and Williams, 1981) and by our analysis (Packard and Christensen, 2004) we calculated a Φ to R_{O_2} ratio, 0.26 (Table 2), that successfully predicted R_{O_2} in the epipelagic and the mesopelagic waters of the Nansen Basin of the Arctic Ocean (Packard and Codispoti, 2007). In that study, R_{O_2} was a long-term average R_{O_2} calculated by the apparent oxygen utilization (AOU)–He–tritium method

Table 2. Step-by-step calculations of F_C from ETS activity at C-line position C12 (station 35). Potential R (Φ), R_{O_2}, N_2 production from denitrification (R_{N_2}) and respiratory CO_2 production (R_{CO_2}) were first determined from temperature-corrected ETS activity values. Φ is stoichiometrically related to electrons by a factor of 4 ($O_2 + 4e^- + 4H^+ \rightarrow 2H_2O$). R_{O_2} is 0.26 of Φ (Packard and Christensen, 2004). R_{N_2} relates to ETS activity according to Codispoti and Packard (1980). Here, denitrifying waters occur between 93 and 233 m (values in bold). R_{CO_2} was calculated from both R_{O_2} and R_{N_2} (see Sect. 2). Column 7 shows the modeled R_{CO_2} values below the R maximum (13 m), obtained from the depth-normalized power function ($R_{CO_2} = R_m(z/z_m)^b$) fitted to the data in Column 6. F_C was determined by integrating either to the bottom (F_{t-s}, Column 8) or to infinity (F_∞, Column 9). The first represents the C consumed by R from the Ez (21 m) to the bottom, while the second includes benthic R and C burial. The difference between F_∞ and F_{t-s} equals benthic R and the C burial rate (Column 10). Column 11 represents the C flux determined by trapezoidal approximation, which relates to F_{t-s} through the regression $F_{t-s} = 0.85 F_{c_{trap}} - 0.54$ ($r^2 = 0.99$, $p < 0.001$).

Depth z (m)	ETS Activity (neq $min^{-1} L^{-1}$)	Φ (μmol O_2 $h^{-1} m^{-3}$)	R_{O_2} (μmol O_2 $h^{-1} m^{-3}$)	R_{N_2} (μmol N_2 $h^{-1} m^{-3}$)	R_{CO_2} (μmol CO_2 $h^{-1} m^{-3}$)	R_{CO_2} modeled (μmol CO_2 $d^{-1} m^{-3}$)	F_C to bottom F_{t-s} (mmol C $d^{-1} m^{-2}$)	F_C to infinity F_∞ (mmol C $d^{-1} m^{-2}$)	Benthic respiration and burial F_∞ - F_{t-s}	C-Flux to bottom Trap Calc (mmol $Cd^{-1} m^{-2}$)
0.5	37.10	556.56	144.71	–	102.74	–	–	–	–	–
3	37.81	567.14	147.46	–	104.69	–	–	–	–	–
5	35.69	535.39	139.20	–	98.83	–	–	–	–	–
9	33.65	504.68	131.22	–	93.16	–	–	–	–	–
13	39.19	587.87	152.85	–	108.52	1629.67	–	–	–	–
21	15.34	230.16	59.84	–	42.49	707.39	19.71	20.07	0.36	25.49
31	8.79	131.81	34.27	–	24.33	359.18	14.68	15.04	0.36	20.16
93	**0.44**	–	–	**0.25**	**0.44**	53.09	6.31	6.67	0.36	7.38
233	**0.35**	–	–	**0.20**	**0.35**	10.74	3.02	3.38	0.36	3.38
465	0.05	0.75	0.19	–	0.14	3.23	1.66	2.03	0.36	1.76
698	0.01	0.14	0.04	–	0.03	1.59	1.14	1.50	0.36	1.20
930	0.02	0.23	0.06	–	0.04	0.97	0.85	1.21	0.36	0.90
1395	0.01	0.21	0.05	–	0.04	0.48	0.54	0.90	0.36	0.57
1860	0.01	0.13	0.04	–	0.02	0.29	0.36	0.73	0.36	0.40
4755	–	–	–	–	–	0.06	0	0.36	0.36	0

Table 3. R_{O_2} as μmol O_2 $h^{-1} m^{-3}$ profiles in the microplankton along the C-line section in September 1976 (roman font values). At the OMZ depths (values in bold), NO_3^- was the electron donor and N_2 was produced during denitrification (R_{N_2} as μmol N_2 $h^{-1} m^{-3}$). C-line position as well as JASON station number (in parentheses) are given. Depth (z) is in meters and R refers to either R_{O_2} or R_{N_2} depending on the font. Calculations are explained in the text.

C1 (22)		C3 (15)		C3 (21)		C5 (20)		C5 (37)		C8 (19)		C8 (36)		C10 (18)		C12 (17)		C12 (35)		C14 (16)	
$z(m)$	R	$z(m)$	R	$z(m)$	R	$z(m)$	R	$z(m)$	R	$z(m)$	R	$z(m)$	R	$z(m)$	R	$z(m)$	R	$z(m)$	R	$z(m)$	R
0.5	56.11	0.5	24.11	0.5	83.99	0.5	119.13	0.5	79.97	0.5	80.32	0.5	87.67	0.5	34.35	0.5	47.14	0.5	144.71	0.5	40.90
4	84.66	6	34.89	5	78.92	3	154.77	4	86.75	4	92.40	5	97.89	5	35.79	6	30.65	3	147.46	7	34.62
6	44.15	9	35.86	9	64.26	6	130.83	7	95.81	8	75.17	8	88.41	8	51.17	10	39.54	5	139.20	11	36.09
10	71.05	17	42.74	14	43.68	9	180.26	11	86.29	12	54.66	12	83.74	15	40.07	16	29.04	9	131.22	18	54.67
16	60.88	28	30.99	21	20.57	14	97.08	17	77.46	19	69.74	19	63.75	24	87.36	26	34.38	13	152.85	28	44.78
24	42.41	42	15.42	33	12.05	21	41.27	27	67.29	29	45.27	29	19.16	36	24.75	40	29.61	21	59.84	43	25.66
				47	**3.15**	**93**	**0.48**	40	71.55	**93**	**1.12**	44	18.08	**233**	**0.16**	**233**	**0.09**	31	34.27	100	4.51
				93	**1.80**	**233**	**0.67**			**233**	**0.48**	**93**	**0.59**	465	0.04			**93**	**0.25**	250	0.73
						465	**0.09**			465	0.62	**233**	**0.15**	1860	0.02			**233**	**0.20**	500	0.22
										930	0.36	465	0.04					465	0.19	750	0.11
										1395	0.22	698	0.03					698	0.04	1000	0.06
												930	0.05					930	0.06	2000	0.09
												1395	0.06					1395	0.05		
																		1860	0.04		

of Jenkins (1982, 1984) as used by W. Roether in Zheng et al. (1997). We have chosen to use the same Φ-to-R_{O_2} ratio of 0.26 here (Tables 2 and 3). R_{CO_2} (Fig. 2a) was then calculated from R_{O_2} using a Redfield ratio (C / O_2) of 0.71 from Takahashi et al. (1985). This is the best available way to calculate seawater respiration from our water column ETS measurements.

In waters where respiration is based on using oxides of nitrogen (NO_3^-, NO_2^-, N_2O, or NO) in place of O_2, calculations are different. Since microbial respiratory NO_3^- reduction to nitrogen gas (denitrification) occurs in the water column between 47 and 400 m between positions C3 to C12 (Garfield et al., 1979; Codispoti and Packard, 1980) (Fig. 2a), Table 3 presents denitrification rates from these depths (shaded numbers) as R_{N_2} in units of μmol N_2 m^{-3} h^{-1}. In these oxygen-deficient waters we used a Redfield ratio, C / N_2, from Gruber and Sarmiento (1997). To apply it, one first has to calculate R_{N_2} based on the fact that the ETS for R_{O_2} and R_{N_2} differ only in the terminal electron acceptor (Packard, 1969; Chen and Strous, 2013). This was done in Tables 2 and 3 according to Codispoti and Packard (1980) and Codispoti et al. (2001). The approach has recently been corroborated by Dalsgaard et al. (2012). R_{N_2} in units of μmol N_2 h^{-1} m^{-3} is calculated in Table 2, column 2, by multiplying nanoeq min^{-1} L^{-1} by 60. The product is equivalent to μmol e^- h^{-1} m^{-3}. Then, dividing this by 105 mol e^- per mol N_2 yields R_{N_2}. The

Table 4. Power functions for microplankton R (mmol CO_2 d^{-1} m^{-3}) as functions of normalized depth, $R_{CO_2} = R_m(z/z_m)^b$, where R_{CO_2} is the respiratory CO_2 production at any depth (z), R_m is the R maximum (mmol CO_2 d^{-1} m^{-3}) in the water column, z/z_m is the depth normalized by the depth at R_m, and b is the maximum curvature of the power function. Both z/z_m and b are unitless. Δz represents the depth range of the R values considered. The table includes the r^2 from the least-square regression analysis of the R models (SigmaPlot vs. 12.5) and the number of data considered (n). The significance level of the regressions is indicated by superscript letters a, b, and c. The last four columns represent the linear regression of the respiration model verification analysis. The slope, the intercept and the r^2 are given. The n value for each verification analysis is the same as the n used for each R model (column 7). These R models are based on ETS activity data taken during R/V *Eastward* JASON-76 expedition, along the C-line.

CUEA C-line position (JASON station)	Δz (m)	z_m (m)	R_m (mmol CO_2 d^{-1} m^{-3})	b	r^2	n	Modeled vs. calculated R_{CO_2} slope	intercept	r^2	n
C1 (22)	4–24	4	1.538	−0.355	0.864	4	0.975	25.24	0.878	4
C3 (15)	17–42	17	0.783	−1.109	0.929	3	1.041	20.42	0.926	3
C3 (21)	5–93	0.5	20.659	−1.080	0.972[c]	7	1.095	45.37	0.905[b]	7
C5 (20)	9–465	9	2.796	−1.655	0.951[b]	6	0.890	4.25	0.996[b]	6
C5 (37)	7–40	7	1.596	−0.192	0.873[a]	5	0.875	168.87	0.902[a]	5
C8 (19)	4–1395	4	3.247	−1.168	0.957[c]	10	1.348	129.78	0.686[a]	10
C8 (36)	5–1395	5	4.413	−1.670	0.949[c]	12	0.937	−44.14	0.808[b]	12
C10 (18)	24–1860	24	0.946	−2.051	0.962[a]	5	0.638	29.3	0.976[a]	5
C12 (17)	0.5–233	0.5	3.172	−0.720	0.497	7	2.596	−661.42	0.339	7
C12 (35)	13–1860	13	1.630	−1.740	0.948[c]	10	0.627	10.56	0.998[b]	10
C14 (16)	18–2000	18	1.183	−1.624	0.968[c]	9	1.043	−19.72	0.910[b]	9

[a] $p < 0.05$
[b] $p < 0.001$
[c] $p < 0.0001$

Table 5. Microplankton respiration in epipelagic, mesopelagic, and bathypelagic waters along the C-line across the Peruvian current upwelling system at 15° S. Calculations are based on the R models in Table 4. Shoreward of C5, the bottom limits the lower depth boundary. Note the 1000-fold shift in the rates expressed per area (columns 3–7) and per volume (columns 8–10).

CUEA C-line position (JASON station)	Ocean depth (m)	Water column R (mmol C m^{-2} d^{-1})	Benthic respiration and C burial (mmol C m^{-2} d^{-1})	Epipelagic 1–150 m (mmol C m^{-2} d^{-1})	Mesopelagic 150–1000 m (mmol C m^{-2} d^{-1})	Bathypelagic 1000 m–bottom (mmol C m^{-2} d^{-1})	Epipelagic 1–150 m (μmol C m^{-3} d^{-1})	Mesopelagic 150–1000 m (μmol C m^{-3} d^{-1})	Bathypelagic 1000 m–bottom (μmol C m^{-3} d^{-1})
C1 (22)	63	53.98	–	53.98	–	–	856.85	–	–
C3 (15)	117	80.32	99.23	80.32	–	–	686.50	–	–
C3 (21)	120	45.81	82.99	45.81	–	–	381.75	–	–
C5 (20)	550	252.48	2.60	248.99	3.49	–	1659.96	8.72	–
C5 (37)	607	507.91	–	162.98	344.93	–	1086.51	754.78	–
C8 (19)	1880	82.10	27.37	67.58	11.46	3.07	450.51	13.48	3.49
C8 (36)	2150	153.46	0.57	150.65	2.43	0.38	1004.36	2.85	0.33
C10 (18)	4300	1256.23	0.09	1262.18	2.72	0.34	8414.54	3.20	0.10
C12 (17)	4000	64.36	–	22.28	19.57	22.51	148.55	23.02	7.50
C12 (35)	4755	318.83	0.36	314.51	3.53	0.79	2096.75	4.16	0.21
C14 (16)	2680	318.14	1.50	310.56	6.30	1.28	2070.43	7.41	0.76

constant, 105 mol e^- per mol N_2, is the equivalent of the R_{N_2} / ETS ratio in Codispoti and Packard (1980), 2.4 μL O_2 $L^{-1}h^{-1}$ / (gN_2 m^{-3} yr^{-1}). The R_{CO_2} calculation is as follows. R_{CO_2} equals [106/60 mol carbon (mol N_2)$^{-1}$ × ETS activity (mol e^- h^{-1} m^{-3})] / [105 mol e^- (mol N_2)$^{-1}$]. The ratio, 106/60 mol C (mol N_2)$^{-1}$, is the Redfield ratio, mentioned above, for the carbon (as CO_2) produced during denitrification from NO_3 (Gruber and Sarmiento, 1997). Note that both R_{O_2} and R_{N_2}, from Table 3 were converted to R_{CO_2} before being used in the Ez part of Fig. 2a.

2.4 R modeling

To generate R models as depth functions (Table 4), the ETS-based R was plotted against depths (z) normalized by the depth of the R maximum (z_m) as we did in Packard and Christensen (2004). From these plots, power functions of the form $R = R_m(z/z_m)^b$ were fitted to the data using SigmaPlot (version 12.5) according to Charland (2002). Note that R_m is the depth of the respiration maximum and b, the exponent, is always negative. The exponent b represents the maximum curvature of the respiration–depth profile. Note that R in the

Table 6. Carbon flux models F_C at C-line positions deeper than 500 m in the Peruvian upwelling system in Sep 1976. From these models, F_C at four different depths were determined. NRE and F_C transfer efficiency (T_{eff}) for the upper mesopelagic waters (150–500 m) are also given. NRE was calculated as $100 \times R_{CO_2}/F_{c_{150}}$, where the R_{CO_2} represents the integrated R between 150 and 500 m; T_{eff} was calculated as $100 \times F_{C_{500}}/F_{C_{150}}$ according to Buesseler et al. (2007).

CUEA C-line position (JASON station)	Ocean depth (m)	Euphotic zone, z_e (m)	F_C models	F_C from z_e (mmol C $m^{-2} d^{-1}$)	F_C from 150 m (mmol C $m^{-2} d^{-1}$)	F_C from 500 m (mmol C $m^{-2} d^{-1}$)	F_C from 1000 m (mmol C $m^{-2} d^{-1}$)	NRE 150–500 m (%)	T_{eff} 150–500 m (%)
C5 (20)	550	21	$22.07\,(z/z_e)^{-0.655}$	22.07	6.09	2.77	–	54.6	45.4
C8 (19)	1880	29	$55.25\,(z/z_e)^{-0.168}$	55.25	41.92	34.24	30.48	18.3	81.7
C8 (36)	2150	29	$10.14\,(z/z_e)^{-0.670}$	10.14	3.37	1.51	0.95	55.4	44.6
C10 (18)	4300	36	$14.11\,(z/z_e)^{-1.051}$	14.11	3.15	0.89	0.43	71.8	28.2
C12 (35)	4755	21	$20.07\,(z/z_e)^{-0.740}$	20.07	4.68	1.92	1.15	59.0	41.0
C14 (16)	2680	43	$19.80\,(z/z_e)^{-0.624}$	19.80	5.81	2.74	1.78	52.8	47.2

Table 7. HEP as ATP production in epipelagic, mesopelagic, and bathypelagic waters of the C-line section, September 1976. Shoreward of C5 the bottom limits the lower depth boundary.

CUEA C-line Location (JASON station)	Ocean depth (m)	Epipelagic HEP 1–150 m ($J\,m^{-3}\,d^{-1}$)	Mesopelagic HEP 150–1000 m ($J\,m^{-3}\,d^{-1}$)	Bathypelagic HEP 1000 m–bottom ($J\,m^{-3}\,d^{-1}$)
C1 (22)	63	289.63	–	–
C3 (15)	117	232.05	–	–
C3 (21)	120	173.40	–	–
C5 (20)	550	977.93	1.19	–
C5 (37)	607	367.24	255.11	–
C8 (19)	1880	138.77	3.59	0.89
C8 (36)	2150	319.41	0.80	0.09
C10 (18)	4300	2609.16	0.89	0.03
C12 (17)	4000	43.60	4.56	1.23
C12 (35)	4755	535.98	1.18	0.06
C14 (16)	2680	699.88	2.51	0.26

Ez of Fig. 2a is based directly on the ETS measurements (Table 3), while the R in the mesopelagic zone of Fig. 2a is based on the R models in Table 4.

2.5 F_C, NRE, and HEP calculations

The F_C was calculated (Table 2) from depth-normalized water column R (Packard and Christensen, 2004; Packard and Gómez, 2013; Osma et al., 2014). Power functions ($R_{CO_2} = R_m\,(z/z_m)^b$) were selected over logarithmic or exponential functions because they better described the data as previous studies found (Packard and Christensen, 2004; Packard and Codispoti, 2007). Conceptually, planktonic R_{CO_2} in a seawater cube is considered equivalent to the difference between the total F_{C_1} through the top of the cube and total F_{C_2} through the bottom of the cube, where total carbon flux refers to the sum of the dissolved organic carbon (DOC) and the particulate organic carbon (POC) flux. We deduce, on the basis of Craig (1971); Carlson et al. (2010); Hansell et al. (2012), that R based on DOC and lateral POC flux, compared to the R based on the vertical flux of labile POC, is less than 30 % of the total R. Note that if organic matter, in any form, is resistant to oxidation (Arrieta et al., 2015), its flux through the water column will not be detected by respiration measurements. The flux will be transparent to our ETS measurements. However, the dissolved organic matter in the ocean, at least, appears to be oxidizable (Arrieta et al., 2015). In all cases, to a first approximation, one can express our conceptual model using the expression, $R_{CO_2} = F_{C_1} - F_{C_2}$. In other words, in the vertical, one-dimensional case, the changes in the F_C between depths in a water column are equal to the R_{CO_2} between those depths. Extrapolating this conceptual model to the deep ocean water column, using continuous mathematics, and assuming seafloor carbon burial to be small, the F_C into the top of a water column (F_{C_t}) can be calculated by integrating all the R below the top boundary (z_t) to the ocean bottom (z_s).

$$F_{C_t} = \int_{z_t}^{z_s} R_{CO_2}\,dz \quad (1)$$

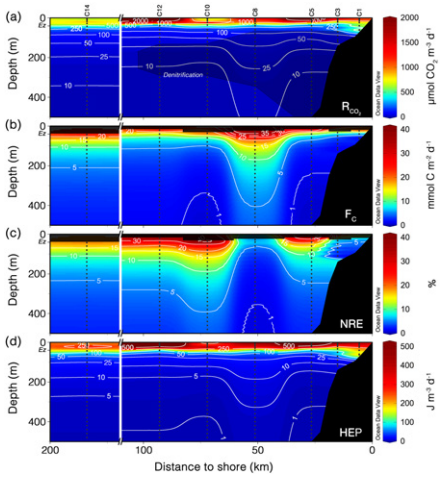

Figure 2. Sections for the upper 500 m along the C-line. **(a)** R_{CO_2}; the dark shadow delimits denitrification in the OMZ. In the Ez, R_{CO_2} is calculated directly from ETS-based R_{O_2} (Table 3). In the mesopelagic waters below, R_{CO_2} is modeled from the respiration equations in Table 4. **(b)** F_C is calculated by integration of the respiration models (Table 4) to the ocean bottom according to Eqs. (2) and (3). **(c)** NRE, as a percentage, is determined from models in Tables 4 and 6 as $100\times(R_{CO_2} / F_C)$. **(d)** HEP is either derived directly from ETS activity in the surface waters or from calculated R_{O_2} or R_{N_2} for depths below the Ez (as in Fig. 2a).

All F_C calculations here are based on depth-normalized power functions of R ($R_{CO_2} = R_m\,(z/z_m)^b$, Table 4; only if depth is normalized does the equation achieve balance with units of nmol CO_2 min^{-1} L^{-1}). For the carbon flux (F_{f-s}) through any depth layer in the water column (z_f) down to z_s, we use Eq. (2) and its integrated version in Eq. (3). Note that these carbon-flux calculations represent the flux at the time the CTD–Niskin cast was made. They are fine-scale calculations of C-Flux.

$$F_{f-s} = \int_{z_f}^{z_s} R_{CO_2}\,dz = \int_{z_f}^{z_s} R_m\,(z/z_m)^b\,dz \quad (2)$$

$$F_{f-s} = \{R_m/[(b+1)\,z_m^b]\}\,(z_s^{b+1} - z_f^{b+1}) \quad (3)$$

Note that z_f is any depth between z_t and z_s ($z_t \leqslant z_f \leqslant z_s$) and that F_{f-s} is associated with the microplankton respiration, the greater fraction of water column respiration (King et al., 1978).

The NRE is equivalent to R (mol CO_2 d^{-1} m^{-3}) within an ocean layer (Δz) divided by the F_C (mol C d^{-1} m^{-2}) into the volume of that layer expressed as a percent. Note that the calculation is $(R\times\Delta z)/F_C$. Since the Redfield N / C or P / C ratio is applied to both parts of the ratio, the C, N, or P units cancel out, leaving the ratio unitless. NRE is also related to the carbon flux transfer efficiency (Burd et al., 2010; Buesseler and Boyd, 2009; Buesseler et al., 2007) through the same layer (Packard and Gómez, 2013). For Fig. 2c, it was calculated for 20 m layers below the Ez to the ocean bottom from the R models in Table 4 and the F_C models in Table 6.

HEP (Fig. 2d, Table 6) was calculated from R_{O_2} and R_{N_2}, derived from the ETS measurements, from the modeled R_{O_2}, or from R_{N_2}. For oxic seawater HEP $= 2\times 2.5\times 48\times R_{O_2}$, where 2 represents the number of electron pairs required to reduce O_2 to $2H_2O$, 2.5 represents the ATP /$2e^-$ ratio (Ferguson, 2010), 48 is the ΔG in J per mmol of ATP (Alberty and Goldberg, 1992; Moran et al., 2012), and R_{O_2} is the respiratory O_2 consumption rate as mmol O_2 d^{-1} m^{-3}. For NO_3^-, R in anoxic waters, HEP $= 5\times 1.0\times 48\times R_{N_2}$, where 5 is the number of electron pairs required to reduce NO_3 to N_2, 1.0 is the ATP /$2e^-$ ratio (van Loosdrecht et al., 1997; Smolders et al., 1994), 48 is the ΔG as before, and R_{N_2} is the respiratory NO_3^- reduction rate as mmol N_2 d^{-1} m^{-3}.

3 Results

Oceanographic properties (Table 1) on a C-line transect at 15° S across the Peruvian current upwelling system (Fig. 1a) in mid-September of the ENSO transition year, 1976, were measured on the R/V *Eastward* during the JASON-76 cruise of the CUEA–JOINT II expedition. Classic upwelling (Smith, 1968; Packard et al., 1984; Rykaczewski and Checkley, 2008) was evident during this period. Seawater density (σ_t) and NO_3^- sloped surface-ward close to the coast (Fig. 1b). From 25 m, σ_t rose from 26.0 to 26.1, and NO_3^- rose from 12 to 16 μM. As these dense nutrient-rich waters rose, they fertilized the sunlit surface waters at the upwelling center (C3, Brink et al., 1981; MacIsaac et al., 1985), and flowed offshore towards C5 and C8, phytoplankton bloomed to 7 mg m^{-3} chlorophyll a and 18 mg carbon h^{-1} m^{-3} in productivity (Table 1 and Fig. 1b). The dynamics of this process could be seen in the variability of the Ez depth. It ranged from a low of 21 m at C5, the maximum biomass and metabolism position, to twice the depth, 43 m, at the offshore position, C14 (Table 1). Temporal variability was exemplified at the trench position (C12), where over 1 week, the Ez depth decreased from 40 to 21 m. Minimal variability occurred at position C8, where over 6 days, the Ez depth remained at 29 m (Table 1). In general, a shallow Ez is caused by high plankton biomass with a high potential for metabolism and contrary conditions associated with a deep Ez.

Sea surface R_{O_2} ranged 6-fold from a low of 24.1 μmol O_2 m^{-3} h^{-1} at the upwelling center to a high of 144.7 μmol O_2 m^{-3} h^{-1}, 93 km offshore at the trench position, C12 (Ta-

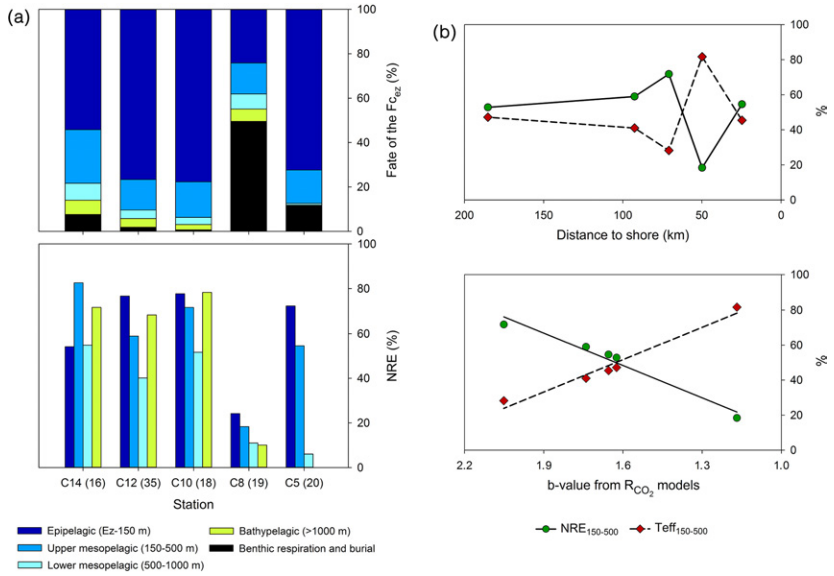

Figure 3. (a) Fate of the carbon fluxing out of the Ez (F_{cEZ}) into the water column and seafloor below (as a percent of the total flux) along the C-line (top panel). In the water column, the carbon is remineralized through R. In the benthos, part of the carbon is remineralized and returned to the water column above and part is buried. The bottom panel shows the different efficiencies with which carbon is remineralized through respiration in four different zones of the water column along the C-line. **(b)** Top panel: variability of the NRE and the T_{eff} in the upper mesopelagic waters (150–500 m) along the C-line. Bottom panel: NRE and T_{eff} as a function of the maximum curvature b (absolute value) in the R_{CO_2} models from Table 4.

ble 1). Within days, R_{O_2} could change 3-fold both inshore and offshore (Table 3). During the week between C3 stations 15 and 21, R_{O_2} rose from 24.1 to 84.0 µmol O_2 m^{-3} h^{-1} and R_{O_2} at C12 rose from 47.1 µmol O_2 m^{-3} h^{-1} (station 17) to 144.7 µmol O_2 m^{-3} h^{-1} (station 35, Table 2). This high respiration (R) at station 35, occurred in a diatom bloom of *Chaetoceros compressus* and *Ch. lorenzianus*. The documentation of such temporal variability in seawater R_{O_2} has only recently begun (Fernández-Urruzola et al., 2014; Osma et al., 2014). Similar increases were seen in the chlorophyll and net productivity at C3 and C12 (Table 1). The co-occurrence of this rise in R_{O_2}, chlorophyll and net productivity suggests seawater R_{O_2} being driven by phytoplankton. Below the immediate sea surface, microplankton R_{O_2} usually increased to a subsurface maximum within the Ez and then decreased dramatically towards the bottom of the Ez and into the dark ocean below (Tables 2 and 3). R_{CO_2} (Fig. 2a) ranged in the Ez from 0.4 mmol CO_2 m^{-3} d^{-1} in the upwelling center (C3, station 15) to 3 mmol CO_2 m^{-3} d^{-1} at C5, the shelf edge station 20. The lowest epipelagic R_{CO_2} (Table 5) compares with the R_{CO_2} range of 22–27 mmol CO_2 m^{-2} d^{-1} reported recently in eddy-upwelling in the South China Sea (Jiao et al., 2014). In the denitrifying waters, R_{CO_2} was in the µmol range from a low of 4 µmol CO_2 m^{-3} d^{-1} at C5 (station 37) to 133 µmol CO_2 m^{-3} d^{-1} at C3 (station 21). In the mesopelagic waters below 500 m (Table 5), R_{CO_2} ranged from 0.4 to 6.1 µmol CO_2 m^{-3} d^{-1} over 1 week at C-line position C8, at other locations R_{CO_2} fell in between this range. Deeper in the water column, over the trench and beyond, bathypelagic R_{CO_2} ranged from 0.3 µmol CO_2 m^{-3} d^{-1} at C10 over the trench to 3.7 µmol CO_2 m^{-3} d^{-1} at C8 over the continental slope (Table 5). Benthic R_{CO_2} and C burial (Table 5 and Fig. 3a) ranged from a high of 90 mmol CO_2 m^{-2} d^{-1} at C3, the upwelling center, to a low of 0.09 mmol CO_2 m^{-2} d^{-1} at trench position, C10, with a depth of 4300 m. The R_{CO_2} section in Fig. 2a clearly shows the strength of R and its associated remineralization in the upper 50 m of the water column and a tongue of high R descending deeper into the water column at position C8, 50 km off the coast. F_C along the C-line tran-

sect is shown in Fig. 2b. In order to include the inshore stations, F_C, in Fig. 2b, only represents that part of the C-flux that supports the water column respiration. It does not include benthic R and C burial. To scale our F_C calculations, F_C at 150 m, seaward of C8, ranging from 3 to 6 mmol $CO_2\,m^{-3}\,d^{-1}$ (Table 6) are comparable to the range of 2.5 to 6.2 mmol $CO_2\,m^{-3}\,d^{-1}$ recently measured at 100 m by Jiao et al. (2014).

As one would expect with strong F_C at C8, even at 1000 m, the carbon flux transfer efficiency (T_{eff}) at this station (19) is high and the NRE low (Table 6, Fig. 3b). T_{eff} between 150 and 500 m ($T_{eff_{500}}$) is 82 and the NRE is only 18 % (Table 6). Unexpectedly, despite the decrease in F_C throughout the water column at C8 between 17 and 23 September, $T_{eff_{500}}$ only decreased by less than a factor of 2 to 45 % (Table 6). The impact on the NRE was greater, increasing 3-fold to 55 % (Table 6). $T_{eff_{500}}$ at other locations ranged from 28 at C10 to 47 at C14 (Fig. 3b). In addition to this unique documentation of the temporal variability of F_C from Table 6, Fig. 2b demonstrates its mesoscale spatial variability. That transect shows a maxima occurring throughout the water column, 50 km from the coast at the upper slope position, C8. As Table 5 and Fig. 3a show, the benthic R and burial are also high at this location. Figure 3b highlights the importance of the maximum curvature of the respiration–depth profile. As $|b|$ increases towards 2 the NRE increases towards 70 % and the $T_{eff_{150-500}}$ decreases towards 30 %.

HEP in the Ez (Fig. 2d and Table 7) ranges from a high of $555\,J\,d^{-1}\,m^{-3}$ at the R maximum at C5 (station 20) to a low of $69\,J\,d^{-1}\,m^{-3}$ at the bottom of the Ez at C3 (station 21). It drops slightly over the continental slope, but further offshore over the trench (C12) high values of $880\,J\,d^{-1}\,m^{-3}$ can be found (Fig. 2d). In the far offshore, the Ez HEP only reaches values of $315\,J\,d^{-1}\,m^{-3}$. As an example of low HEP values, at 4755 m in the trench it decreases to $0.02\,J\,d^{-1}\,m^{-3}$. Thus the range of HEP by all the respiratory ETS and oxidative phosphorylation coupling in the microplankton of this part of the Peruvian current upwelling system spans 4 orders of magnitude from $0.02\,J\,d^{-1}\,m^{-3}$ in the abyssopelagic waters of the trench to $880\,J\,d^{-1}\,m^{-3}$ in the Ez above. This is the first time such calculations have been made. Integrating the epipelagic HEP (Table 7) over the upper 150 m yields a range from a low of 6.6×10^{-3} MJ $d^{-1}\,m^{-2}$ to a high of 0.39 MJ $d^{-1}\,m^{-2}$, averaging 0.09 MJ $d^{-1}\,m^{-2}$. This average HEP is only 0.7 % of the average solar radiation (13.5 ± 4.0 MJ $d^{-1}\,m^{-2}$) at the C-line sea surface between 12 and 24 September during the JASON-76 cruise (Packard and Jones, 1976).

4 Discussion

Here we have demonstrated the calculation of R_{CO_2}, F_C, NRE, and HEP in an ocean section from microplankton ETS activity measurements. We have previously explained how ocean water column R_{CO_2} determines F_C of labile organic matter by oxidizing sinking POC and mineralizing phosphate and nitrate (Osma et al., 2014; Packard and Codispoti, 2007). Fig. 3b shows that the maximum curvature of the respiration–depth profile determines NRE as well as F_C transfer efficiency. The offshore R_{CO_2} section (Fig. 2a) shows the variability of R with depth and location in the upwelling area. Fig. 2a also shows how seawater respiration is displaced seaward to C8 from the chlorophyll maximum at C5 (Fig. 1b). The F_C section (Fig. 2b) demonstrates the power of using R to calculate spatial variability of F_C by revealing an F_C maximum over the upper part of the continental slope. The NRE section (Fig. 2c) reveals its inverse relationship to F_C as well as its variability in the water column. This ability of the water column to retain nutrients would not have been detected without the original ETS activity profiles. The HEP section (Fig. 2d), showing the energy production by the ATPases in microbial mitochondrion and plasmalemma membranes of bacteria and archaea in the water column, is a new representation of ATP production in oceanographic analysis. Because a major purpose of all forms of respiration is to make ATP, HEP should reflect R_{CO_2} in any given section or profile. The similarity of the R_{CO_2} pattern in Fig. 2a and the HEP pattern in Fig. 2d confirms this.

Ocean R_{CO_2} filters sinking labile POC and should vary inversely with benthic R and carbon burial. However, the relationship between the two variables is more complicated (Figs. 2a and 3a). We can see this in the R maximum 50 km off the Peruvian coast at C-line position C8. One might expect low benthic R and carbon burial here (Table 5), but that is not the case (Fig. 3a). From the difference between integrating the R function (Eq. 2) to infinity and integrating it to the ocean bottom ($z = s$), we calculate a high level of benthic R and carbon burial (Fig. 3a). The minimum NRE at C-line position, C8, in Fig. 2c explains this discrepancy. The delivery of labile POC to the bottom depends not directly on F_C, but on the ratio of the water column R (Fig. 2a) to F_C (Fig. 2b). Recent studies of the organic carbon preservation on the upper parts of the Peruvian continental slope (Dale et al., 2015) support these calculations of high carbon burial (Fig. 3a.) They find high burial rates at depths between 200 and 400 m (the upper part of the Peruvian continental slope) and attribute it to the anoxia overlying these sediments. A C-line section of the T_{eff}, the difference between NRE and 1, would have revealed a T_{eff} maximum at C8. One can deduce this from Fig. 3b (lower panel).

ETS measurements can be used not only to calculate F_C, NRE, and HEP, but also to calculate biological heat production (Pamatmat et al., 1981), age, and flow rates of deep and bottom waters (Packard, 1985a). In anoxic waters, if the background chemistry (Richards, 1965) is known, ETS measurements provide proxy rate measurements for denitrification (Packard, 1969; Codispoti and Packard, 1980; Dalsgaard et al., 2012), NO_2^- production, nitrous oxide production, and sulfide production (Packard et al., 1983), and even for iron

and magnesium reduction rates (Lane et al., 2010). All of these types of microbial metabolism are different forms of R, but they are controlled by the same basic respiratory ETS with NADH dehydrogenase (Complex 1) as the common gatekeeper. Furthermore, because the energy generation of nitrification is based on a variation of this ETS, an ETS measurement is also likely a proxy for nitrification.

HEP, as ATP generation in the ocean water column, could have been calculated from R_{O_2} since 1943, the time the Nobelist Severo Ochoa first established the connection between ATP production and R (Ochoa, 1943). However, until now, calculations of biological energy production (shown in Fig. 2d), including HEP, in the ocean had not been made (Karl, 2014). Now the time is appropriate to make such calculations with recent research (Lane, 2002, 2005, 2009; Wilson et al., 2012; Chen and Strous, 2013), documenting the ubiquity of respiratory ETS in the biosphere, how it relates to R_{O_2}, to all other ocean respiratory processes, and to HEP as ATP production. As we have seen above, HEP and R_{CO_2} in the Peruvian upwelling system have similar time and space distributions (Fig. 2a and d). The small difference in the ATP $/2e^-$ relationships between oxidative phosphorylation and the rate of electron transfer in aerobic metabolism and denitrification has minimal impact. In aerobic metabolism, the ATP $/2e^-$ ratio is 2.5 and in denitrifying microbes ATP $/2e^-$ is 1.0 (van Loosdrecht et al., 1997; Smolders et al., 1994). At the rate anammox research is progressing (Dalsgaard et al., 2012), its relative contribution will soon be known, too. In any case, less ATP should be produced in anoxic waters resulting in a lower HEP. It will be interesting in the future to look for this difference by comparing HEP offshore sections made through oxic and anoxic sectors of upwelling systems.

5 Conclusions

Organic carbon fluxes are critical components of reliable carbon budgets, but they are so difficult to measure that rarely can enough measurements be amassed to construct a synoptic section of F_C. Here, from plankton respiration models, we present an original mode of calculating F_C sections as well as benthic respiration and carbon burial. We reveal the importance of plankton respiration in determining the capacity of a plankton community in retaining water column nutrients, develop the concept of NRE, and demonstrate NRE variability in an ocean section. In addition, we show that the curvature of the respiration profile (the exponent b of the power function) controls both the NRE and F_C. Finally, we use respiration to calculate the heterotrophic energy production (HEP) and the rate of ATP generated by plankton metabolism, and find an HEP maximum over the shelf break on the upper part of the Peruvian continental slope.

Acknowledgements. We thank J. Ammerman, R. T. Barber, D. Blasco, R. C. Dugdale, N. Garfield, and J. Kogelschatz for their collaboration. D. Bourgault uncovered the role of depth normalization. The suggestions from the three reviewers led to many improvements in this paper and for their diligence we are thankful. NSF (USA) grant OCE 75-23718A01 (TTP) funded JASON-76. The Basque Government (NO and I F-U), MEC (Spain) project BIOMBA, CTM2012-32729/MAR (MG), and CIE (Canary Islands): Tricontinental Atlantic Campus (TTP) funded the analysis.

Edited by: G. Herndl

References

Alberty, R. and Goldberg, R.: Standard thermodynamic formation properties of adenosie 5′-triphosphate series, Biochemistry, 31, 10610–10615, 1992.

Arístegui, J., Gasol, J., Duarte, C., and Herndl, G.: Microbial oceanography of the dark ocean's pelagic realm, Limnol. Oceanogr., 54, 1501–1529, 2009.

Arrieta, J., Mayol, E., Hansman, L., Herndl, G., Dittmar, T., and Duarte, C.: Dilution limits dissolved organic carbon utilization in the deep ocean, Science, 1258955, doi:10.1126/science.1258955, 2015.

Barber, R., Dugdale, R., MacIsaac, J., and Smith, R.: Variations in phytoplankton growth associated with the source and conditioning of upwelling water, Investig. Pesq., 35, 171–193, 1971.

Barber, R., Huntsman, S., Kogelschatz, J., Smith, W., and Jones, B.: Coastal Upwelling Ecosystems Analysis. Data Report 49. Carbon, Chlorophyll and Light Extinction from JOINT II, vol. 49, CUEA Data Rep., 1978.

Brink, K., Jones, B., Vanleer, C., Mooers, C.,Stuart, D., Stevenson, M., Dugdale, R., and Heburn, G.: Physical and biological structure and variability of the upwelling center off Peru at 15° S, during March 1977: Coastal Upwelling. Coastal and estuarine sciences 1, vol. xi–xiii, ed Richards FA (American Geophysiscal Union, Wasington DC), 473–495, 1981.

Buesseler, K. and Boyd, P.: Shedding light on precesses that control particle export and flux attenuation in the twilight zone of the open ocean, Limnol. Oceanogr., 54, 1210–1232, 2009.

Buesseler, K., Lamborg, C., Boyd, P., Lam, P., Trull, T., Bidigare, R., Bishop, J., Casciotti, K., Dehairs, F., Elskens, M., Honda, M., Karl, D., Siegel, D., Silver, M., Steinberg, D., Valdes, J., Mooy, V., B, W., and S: Revisiting carbon flux through the ocean's twilight zone, Science, 316, 567–570, 2007.

Burd, A., Hansell, D., Steinberg, D., Anderson, T., Arístegui, J., Baltar, F., Beaupré, S., Buesseler, K., Dehairs, F., Jackson, G., Kadko, D., Koppelmann, R., Lampitt, R., Nagata, T., Reinthaler, T., Robinson, C., Robison, B., Tamburini, C., and Tanaka, T.: Assessing the apparent imbalance between geochemical and biochemical indicators of meso- and bathypelagic biological activity What the @$?! is wrong with present calculations of carbon budgets?, Deep-Sea Res. II, 57, 1557–1571, 2010.

Carlson, C., Hansell, D., Nelson, N., Siegel, D., Smethie, W., Katiwala, S., Meyers, M., Halewood, E.: Dissolved organic carbon export and subsequent remineralization in the mesopelagic and bathypelagic realms of the North Atlantic basin, Deep-Sea Res. II, 57, 1433–1445, 2010.

Charland, M.: SigmaPlot 2000/2001 for Scientists, Riparian House Merrickville (Ontario), 2002.
Chen, J. and Strous, M.: Denitrification and aerobic respiration, hybrid electron transport chains and co-evolution, Biochim. Biophys. Acta, 1827, 136–144, 2013.
Christensen, J., Packard, T., Dortch, Q., Minas, H., Garfield, P., and Richez, C.: Carbon oxidation in the deep Mediterranean Sea: evidence for dissolved organic carbon source, Global Biogeochem. Cy., 3, 315–335, 1989.
Christensen, J. P. and Packard, T.: Respiratory electron transport activities in plankton: comparison of methods, Limnol. Oceanogr., 24, 576–583, 1979.
Cleland, W.: Enzyme kinetics, Ann. Rev. Biochem., 36.1, 77–112, 1967.
Codispoti, L. and Packard, T.: Denitrification rates in the Eastern tropical South Pacific, J. Mar. Res., 38, 453–477, 1980.
Codispoti, L., Dugdale, R., and Minas, A.: A comparison of the nutrient regimes off northwest Africa, Peru and Baja California, Rapp. P. Reun. Cons. Int. Explor. Mer., 180, 184–201, 1982.
Codispoti, L., Brandes, J., Christensen, J., Devol, A., Naqvi, S., Paerl, H., and Yoshinari, T.: The oceanic fixed nitrogen and nitrous oxide budhets: Moving targets as we enter the anthropocene?, Sci Mar, (Suppl. 2), 85–105, 2001.
Craig, H.: The deep metabolism: oxygen consumption in abyssal ocean water, J Geophys Res, 76, 5078–5086, 1971.
Dale, A. W., Sommer, S., Lomnitz, U., Montes, I., Treude, T., Liebetrau, V., Gier, J., Hensen, C., Dengler, M., Stolpovsky, K., Bryant, L. D., and Wallmann, K.: Organic carbon production, mineralisation and preservation on the Peruvian margin, Biogeosciences, 12, 1537–1559, doi:10.5194/bg-12-1537-2015, 2015.
Dalsgaard, T., Thamdrup, B., Farías, L., and Revsbech, N.: Anammox and denitrification in the oxygen minimum zone of the eastern South Pacific, Limnol. Oceanogr., 57, 1331–1346, 2012.
Ducklow, H. and Doney, S.: What is the metabolic state of the oligotrophic ocean? A debate, Annu. Rev. Mar. Sci., 5, 525–533, 2013.
Eppley, R. and Peterson, B.: Particulate organic matter flux and planktonic new production in the deep ocean, Nature, 282, 677–680, 1979.
Ferguson, S.: ATP synthase: From sequence to ring size to the P / O ratio, Proc. Nati. Acad. Sci. USA, 107, 16755–16756, 2010.
Fernández, C., Faría, L., and Alcaman, M.: Primary production and nitrogen regeneration processes in surface waters of the Peruvian upwelling system, Prog. Oceanogr., 83, 159–168, 2009.
Fernández-Urruzola, I., Osma, N., Packard, T., Gómez, M., and Postel, L.: Distribution of zooplankton biomass and potential metabolic activities across the northern Benguela upwelling system, J. Mar. Syst., 140, 138–149, 2014.
Garfield, P., Packard, T., and Codispoti, L.: Particulate protein in the Peru upwelling system, Deep-Sea Res., 26, 623–639, 1979.
Giering, S., Sanders, R., Lampitt, R., Anderson, T., Tamburini, C., Boutrif, M., Zubkov, M., Marsay, C., Henson, S., Saw, K., Cook, K., and Mayor, D.: Reconciliation of the carbon budget in the ocean's twilight zone, Nature, 507, 480–483, 2014.
Gruber, N. and Sarmiento, J.: Global patterns of marine nitrogen fixation and denitrification, Global Biogeochem. Cy., 11, 235–266, 1997.
Hafferty, A., Codispoti, L., and Huyer, A.: JOINT-I1 R/V Melville Legs I, I1 and IV WV Iselin Leg I1 bottle data March 1977-May 1977, 45, CUEA Data Rep., 1978.
Hansell, D., Carlson, C., and Schlitzer, R.: Net removal of major marine dissolved organic carbon fractions in the subsurface ocean, Global Biogeochem. Cy., 26, GB1016, doi:10.1029/2011GB004069, 2012.
Harvey, H.: The Chemistry and Fertility of Sea Waters. (Cambridge University Press, Cambridge), p. 224, 1955.
Jenkins, W. J.: Oxygen utilization rates in North Atlantic subtropical gyre and primary production in oligotrophic systems, Nature, 300, 246–248, 1982.
Jenkins, W. J.: The use of tracers and water masses to estimate rates of respiration, Heterotrophic Activity in the Sea, edited by: Hobbie, J. M., Williams, P. J., and Le, B., Plenum Press, New York, 391–403, 1984.
Jiao, N., Zhang, Y., Zhou, K., Li, Q., Dai, M., Liu, J., Guo, J., and Huang, B.: Revisiting the CO_2 "source" problem in upwelling areas – a comparative study on eddy upwellings in the South China Sea, Biogeosciences, 11, 2465–2475, doi:10.5194/bg-11-2465-2014, 2014.
Karl, D.M.: Solar energy capture and transformation in the sea, Elem. Sci. Anthro., 2, 1–6, 2014.
Kenner, R. and Ahmed, S.: Measurements of electron transport activity in marine phytoplankton, Mar. Biol., 33, 119–127, 1975.
King, F., Devol, A., and Packard, T.: On plankton biomass and metabolic activity from the eastern tropical North Pacific, Deep-Sea Res., 25, 689–704, 1978.
King, L.: The coastal upwelling ecosystems analysis program as an experience in international cooperation, Ocean Dev. Int., 9, 269–288, 1981.
Kogelshatz, J., Shepherd, R., Whitledge, T., Codispoti, L., and Huyer, A.: JOINT-II JASON 76 hydro data, R/V *EASTWARD* Cruises E-5F-76 through E-5L-76, International Decade of Ocean Exploration, CUEA Data Rep., vol. 38, 1978.
LaFerla, R., Azzaro, M., Civitarese, G., and Ribera d'Alcala, M.: Distribution patterns of carbon oxidation in the eastern Mediterranean Sea: evidence of changes in the remineralization processes, J. Geophys. Res., 108, 8111, doi:10.1029/2002JC001602, 2003.
Lane, N.: The Molecule that made the World, OUP (Oxford), p. 384, 2002.
Lane, N.: Power, Sex, Suicide: Mitochondria and the Meaning of Life, OUP (Oxford), p. 368, 2005.
Lane, N.: Life Ascending: The Ten Great Inventions of Evolution, OUP (Oxford), p. 352, 2009.
Lane, N., Allen, J., and Martin, W.: How did LUCA make a living? Chemiosmosis in the origin of life, BioEssays, 32, 271–280, 2010.
Laufkötter, C., Vogt, M., and Gruber, N.: Long-term trends in ocean plankton production and particle export between 1960–2006, Biogeosciences, 10, 7373–7393, doi:10.5194/bg-10-7373-2013, 2013.
Lotka, A.: Elements of physical biology, Williams and Wilkins Company, Baltimore, 495 pp., 1925.
MacIsaac, J., Dugdale, R., Barber, R., Blasco, D, and Packard, T.: Primary production cycle in an upwelling center, Deep-Sea Res., 32, 503–529, 1985.

Madigan, M., Martinko, J., and Parker, J.: Brock Biology of Microorganisms, Prentice Hall, Upper Saddle River, New Jersey, p. 991, 2000.

Martin, J. H., Knauer, G. A., Karl, D. M., and Broenkow, W. W.: VERTEX: carbon cycling in the northeast Pacific, Deep-Sea Res., 34, 267–285,1987.

Minas, J., Codispoti, L., and Dugdale, R.: Nutrients and primary production in the upwelling region off northwest Africa, Rapp. P. Reun. Cons. Int. Explor. Mer, 180, 148–183,1982.

Moran, L., Horton, R., Scrimgeour, K., and Perry, M.: Principles of Biochemistry, Prentice Hall, Saddle River, New Jersey, USA, 832 pp., 2012.

Munk, W.: Abyssal Recipes, Deep-Sea Res., 13, 707–730, 1966.

Nelson, D. and Cox, M.: Lehninger Principles of Biochemistry, Worth Publishers, New York, p. 1152, 2000.

Ochoa, S.: Efficiency of aerobic phosphorylation in cell-free heart extracts, J. Biol. Chem., 151, 493–505, 1943.

Odum, H. T.: Primary production in flowing waters, Limnol. Oceanogr., 1, 102–117, 1956.

Osma, N., Fernández-Urruzola, I., Packard, T., Postel, L., Gómez, M., and Pollehne, F.: Short-term patterns of vertical particle flux in northern Benguela: a comparison between sinking POC and respiratory carbon consumption, J. Mar. Syst., 140, 150–162, 2014.

Packard, T.: The estimation of the oxygen utilization rate in seawater from the activity of the respiration electron transport system in plankton, Ph.D. Thesis, University of Washington, Seattle, 1–115, 1969.

Packard, T.: Organizers remarks: Coastal Upwelling, in: Coastal and estuarine sciences 1, vol. xi–xiii, edited by: Richards, F. A., American Geophysiscal Union, Wasington DC, 1981.

Packard, T.: Oxygen consumption in the ocean: Measuring and mapping with enzyme analysis, in: Mapping strategies in chemical oceanography, edidet by: Zirino, A., Advances in Chemistry, American Chemical Society, Washington DC, 178–209, 1985a.

Packard, T.: Measurement of electron transport activity of marine microplankton, in: Advances in Aquatic Microbiology, edited by: Williams, L. and Jannasch, H., Academic, New York, 207–261, 1985b.

Packard, T. and Christensen, J.: Respiration and vertical carbon flux in the Gulf of Maine water column, J. Mar. Res., 62, 93–115, 2004.

Packard, T. and Codispoti, L.: Respiration, mineralization, and biochemical properties of the particulate matter in the southern Nansen Basin water column in April 1981, Deep-Sea Res. I, 54, 403–414, 2007.

Packard, T. and Gómez, M.: Modeling vertical carbon flux from zooplankton respiration, Prog. Oceanogr., 110, 59–68, 2013.

Packard, T. and Jones, V.: Biochemistry and ecology of the Peru Current: The JASON expedition to the Peru upwelling system, September 1976, CUEA Tech. Rep., 46, 129, 1976.

Packard, T. and Williams, P. LeB.: Rates of respiratory oxygen consumption and electron transport in surface seawater from the Northwest Atlantic Ocean, Oceanol. Ac., 4, 351–358, 1981.

Packard, T., Healy, M., and Richards, F.: Vertical distribution of the activity of the respiratory electron transport system in marine plankton, Limnol. Oceanogr., 16, 60–70, 1971.

Packard, T., Garfield, P., and Codispoti, L.: Oxygen consumption and denitrification below the peruvian upwelling, Coastal upwelling: Its sediment record, vol. 147–173, edited by: Suess, E. and Thiede, J., Plenum Press, New York, 147–173, 1983.

Packard, T., Blasco, D., and Dugdale, R.: Coastal Upwelling: A short summary of its physical, chemical and biological characteristics, in: Marine Geology and Oceanography of Arabian Sea and Coastal Pakistan, edited by: Haq, B. and Milliman, J., Van Nostrand Reinhold, New York, 339–350, 1984.

Packard, T., Denis, M., Rodier, M., and Garfield, P.: Deep-ocean metabolic CO_2 production: calculations from ETS activity, Deep-Sea Res. I, 35, 371–382, 1988.

Pamatmat, M., Graf, G., Bengtsson, W., and Novak, C.: Heat production, ATP concentration and electron transport activity of marine sediments, Mar. Ecol. Prog. Ser., 4, 135–143, 1981.

Redfield, A., Ketchum, B., and Richards, F.: The influence of organisms on the composition of seawater, edited by: Hill, N. M., The Seas vol. II, Interscience New York, 26–77, 1963.

Richards, F.: Oxygen in the Ocean, in: Treatise on Marine Ecology and Paleoecology, edited by: Hedgepeth, J. W., Geol. Soc. America., 67, 185–238, 1957.

Richards, F.: Anoxic Basins and Fjords, in: Chemical Oceanography, edited by: Riley, J. P. and Skirrow, G., Academic Press, New York, 611–645, 1965.

Richards, F.: Coastal upwelling, American Geophysical Union, Washington, DC, p. 529, 1981.

Riley, G.: Oxygen, phosphate, and nitrate in the Atlantic Ocean, Bingham Oceanogr. Collection Bull., 13, 1–169, 1951.

Rykaczewski, R. and Checkley, D.: Influence of ocean winds on the pelagic ecosystem in upwelling regions, PNAS, 105, 1065–1970, 2008.

Ryther, J., Menzel, D., Hulburt, E., Lorenzen, C., and Corwin, N.: Production and utilization of organic matter in the Peru Coastal Current, Anton. Brun. Rep., 4, 4.3–4.12, 1970.

Santoso, A., McGregor, S., Jin, F., Cai, W., England, M., An, S., McPhaden, M., and Guilyardi, E.: Late-twentieth-century emergence of the El Niño propagation asymmetry and future projections, Nature, 504, 126–130, 2013.

Seiwell, H.: The distribution of oxygen in the western basin of the North Atlantic, Papers in Phys. Ocean. and Meteorol, VoL. IIi, p. 1–86, 1934.

Seiwell, H.: Consumption of oxygen in seawater under controlled laboratory conditions, Nature, 140, 506–507, 1937.

Smith, R.: Upwelling, Oceanogr. Mar. Biol. Annu. Rev., 6, 11–46, 1968.

Smolders, G. J. F., van der Meij, J. , van Loosdrecht, M. C. M., and Heijnen, J. J.: Stoichiometric model of the aerobic metabolism of the biological phosphorus removal process, Biotech. Bioeng., 44, 837–848, 1994.

Suess, E.: Particulate organic carbon flux in the oceans-surface productivity and oxygen utilization, Nature, 288, 260–263, 1980.

Takahashi, T., Broecker, W., and Langer, S.: Redfield ratio based on chemical data from isopycnal surfaces, J. Geophys. Res., 90, 6907–6924, 1985.

van Loosdrecht, MCM, S., GJ, K., T, H., and JJ: Metabolism of micro-organisms responsible for enhanced biological phosphorus removal from wastewater, Antonie Leeuwenhoek, 71, 109–116, 1997.

Walker, J.: ATP synthesis by rotary catalysis, Angew. Chem. Int. Ed., 37, 2308–2319, 1998.

Walsh, J.: Implications of a systems approach to oceanography, Science, 176, 969–975, 1972.

Walsh, J., Kelly, J., Dugdale, R., and Frost, B.: Implications of a systems approach to oceanography, Gross features of the Peruvian upwelling system with special reference to possible diel variation, Invest. Pesq., 35, 25–42, 1971.

Watt, N., Montgomery, M., Runswick, M., Leslie, A., and Walker, J.: Bioenergetic cost of making an adenosine triphosphate molecule in animal mitochondria, PNAS, 107, 16823–16827, 2010.

Williams, P., Quay, P., Westberry, T., and Behrenfeld, M.: The oligotrophic ocean is autotrophic, Annu. Rev. Mar. Sci., 16.1–16.15, 2012.

Wilson, S., Kolber, Z., Tozzi, S., Zehr, J., and Karl, D.: Nitrogen fixation, hydrogen cycling, and electron transport kinetics in trichodesmium erythraeum (cyanobacteria) strain ims1011, J. Phycol. 48, 595–606, 2012.

Wooster, W.: Yearly changes in the Peru Current, Limnol. Oceanogr., 6, 222–226, 1961.

Wyrtki, K.: Circulation and water masses in the Eastern equatorial Pacific Ocean, Int. J. Oceanol. Limnol., 1, 117–147, 1967.

Zheng, Y, Schlosser, P., Swift, J., and Jones, E.: Oxygen utilization rates in the Nansen Basin, Arctic Ocean: implications for new production, Deep-Sea Res., 144, 1923–1943, 1997.

Declaration

I herewith declare that I have produced this work without the prohibited assistance of third parties and without making use of aids other than those specified; notions taken over directly or indirectly from other sources have been identified as such. This work has not previously been presented in identical or similar form to any examination board.

The dissertation work was conducted from 2010 to 2015 under the supervision of Theodore T. Packard and María M. Gómez Cabrera at the University of Las Palmas de Gran Canaria.

Las Palmas de Gran Canaria,

This dissertation was finished writing in Las Palmas de Gran Canaria on
2nd November, 2015